University of Alberta

# Adaptive Spread Spectrum OFDM
# High Throughput Cellular Data Systems

by

**Robert Novak** ©

A thesis submitted to the Faculty of Graduate Studies and Research
in partial fulfillment of the requirements for the degree of

**Doctor of Philosophy**

Department of Electrical and Computer Engineering

Edmonton, Alberta
Spring 2006

*Your file Votre référence*
*ISBN: 0-494-14023-2*
*Our file Notre référence*
*ISBN: 0-494-14023-2*

*To my parents,*

*Vlasta and Jiři.*

# Abstract

The purpose of this thesis project has been to investigate the design of spread spectrum orthogonal frequency division multiplexing (SS-OFDM) systems for the downlink of high throughput cellular data networks. The first part of this work proposes a location dependent rate assignment allocation scheme for the cellular downlink of SS-OFDM systems with small delay data transmission requirements using conventional techniques such as power control and subcarrier interleaving. The second portion, which is the major focus of the thesis, concerns the proposal and development of the downlink of a best-effort SS-OFDM packet system with two-dimensional radio resource allocation and multi-user diversity using adaptive methods such as best serving sector selection, type II hybrid ARQ, and adaptive modulation and coding. The SS-OFDM allocates radio resources in time and frequency (SS-OFDM-F/TA) in the form of time slots and sub-bands to the users with the most favourable channel conditions, while ensuring some measure of fairness for all users in the cell/sector. Adaptive formation and allocation of disjoint groups of sub-bands is proposed to facilitate transmission of large packets and exploit multi-user and frequency diversity in highly frequency selective fading channels. This method is shown to be the same or better than decreasing the packet size to

accommodate narrow sub-bands. The proposed system significantly outperforms best effort single carrier systems in frequency selective fading channels. Several asynchronous re-transmission algorithms and fast sector selection at 1 Hz are proposed for use with SS-OFDM-F/TA. Constraining the maximum re-transmission interval is proposed to reduce delays and maintain improved sector throughput using asynchronous re-transmission of packets. It is shown that fast sector selection increases throughput, fairness among users, and decreases delays. SIR quantization and the use of larger modulation constellations are examined. The final portion of the thesis proposes an interference-reducing diversity combining scheme for SS-OFDM systems, which is particularly useful in packet data systems. The analysis compares chip-level and symbol-level combining, and includes analytical and simulated BER performance comparisons. The results of the chip-level combining scheme investigation have led to the development of a novel low-complexity MMSE equalization method for partially loaded systems which is optimal in certain conditions.

# Acknowledgements

I gratefully acknowledge the following people and institutions:

- Dr. Witold A. Krzymień for providing the opportunity to pursue this research, the invaluable opportunity to be involved in instructing classes, financial support, and his supervision and extensive guidance during the course of this research.
- the external examiner and examination committee members, for taking the time to review this thesis and providing insightful suggestions.
- the current and former scientists, staff and students of TRLabs including Dr. Kay Wee Ang, Luke Chong, David D. Clegg, Dr. Matthieu Clouqueur, Dr. John Doucette, Robert Elliott, Dr. Ivan J. Fair, Chris Fields, Rhoda Hayes, Dr. Michael Leung, Dr. David Mazzarese, Dr. Bartosz Mielczarek, Dr. Roger Pederson, Glenn Rainbird, Linda Richens, Dr. Yan Xin and Dr. Fengqin Zhai for creating an enjoyable research environment through friendship, support and many informative technical discussions.
- TRLabs, the Natural Sciences and Engineering Research Council (NSERC), the Alberta Informatics Circle of Research Excellence (iCORE), the Rohit Sharma Professorship, and the University of Alberta for financial assistance.

I would also like to thank my parents Vlasta and Jiři, my sister Susan, and my close friends including Dan Taylor and Patrick Wright for their important support and counsel which was essential to the successful completion of my studies. Finally, I would like to thank Natalie Bernard for her love, support, and encouragement during the many successes and challenges of my graduate student career.

# Table of Contents

# List of Tables

# List of Figures

# List of Abbreviations

| | |
|---|---|
| 4G | fourth generation (also 2G, and 3G) |
| ACK | acknowledgement fed back to scheduler |
| ARQ | automatic repeat request |
| AWGN | additive white Gaussian noise |
| BER | bit error rate |
| BPSK | binary phase-shift keying |
| CDF | cumulative distribution function |
| CDM | code division multiplexing |
| CDMA | code division multiple access |
| CRC | cyclic redundancy check |
| CSCI | co-subcarrier interference |
| DFT | discrete Fourier transform |
| DS | direct sequence |
| FDMA | frequency division multiple access |
| FFT | fast Fourier transform |
| FH | frequency hopping |
| ICI | inter-cell interference |
| ISI | inter-symbol interference |
| IFFT | inverse fast Fourier transform |
| ISCI | inter-subcarrier interference |
| ITU | International Telecommunications Union |
| MAC | medium access control |
| MC | multicarrier |
| MT | multi-tone |
| MUD | multi-user detection |
| MMSE | minimum mean-square error |
| MRC | maximal ratio combining |
| NAK | negative acknowledgement |
| NLOS | non-line of sight |
| OFDM | orthogonal frequency division multiplexing |
| p.p. | perfect prediction |

| | |
|---|---|
| PDF | probability density function |
| PER | packet error rate |
| PHY | physical (layer) |
| PN | pseudo-random noise |
| PSD | power spectral density |
| QAM | quadrature amplitude modulation |
| QPSK | quadrature phase-shift keying |
| RTI | re-transmission interval |
| SINR | signal to interference and noise ratio |
| SS | spread spectrum |
| SS-OFDM-F/TA | SS-OFDM with frequency and time allocation |
| TDMA | time division multiple access |
| UB | upper bound |
| w.r.t | with respect to |
| WLAN | wireless local area networks |
| ZF | zero-forcing |

# List of Symbols

| | |
|---|---|
| $\mathbf{A}$ | spreading code sequence activity matrix |
| $A_{u,l}$ | equalized subcarrier gain for the $u^{th}$ mobile on the $l^{th}$ subcarrier |
| $B_{u,l}$ | power of equalization coefficient for the $u^{th}$ mobile on the $l^{th}$ subcarrier |
| $b_j$ | complex data symbol |
| $B$ | bandwidth |
| $c_{k,l}$ | element of the $\mathbf{c}_k$ spreading sequence |
| $\mathbf{C}$ | Walsh-Hadamard matrix |
| $C/B$ | maximum spectral efficiency |
| $d_{corr}$ | decorrelation distance of shadowing process |
| $d_l$ | complex spread data on the $l^{th}$ subcarrier |
| $D_{mobile}$ | distance of mobile from transmitter |
| $E_b$ | energy per bit |
| $E_s$ | energy per symbol |
| $\mathrm{Ei}[x]$ | exponential integral function |
| $f_D$ | maximum Doppler shift |
| $g_{u,l}$ | complex equalization/combining coefficient for the $u^{th}$ mobile on the $l^{th}$ subcarrier |
| $\mathbf{G}$ | equalization/combining coefficient matrix |
| $h_{u,l}$ | complex channel gain for the $u^{th}$ mobile of the $l^{th}$ subcarrier |
| $\mathbf{H}$ | complex channel gain matrix (diagonal elements) |
| $\mathbf{I}$ | identity matrix |
| $I_0$ | total interference (ICI + noise) |
| $I_{ICI}$ | interference from other cells |
| $K$ | number of active (in use) spreading codes |
| $L$ | spreading gain (and length of Walsh sequences) |
| $M$ | number of sub-bands |
| $M_{eff}$ | effective number of sub-bands after grouping of disjoint sub-bands |
| $M_g$ | number of disjoint sub-bands in a sub-band group |
| $M_n$ | total number of narrow-band sub-bands for use in sub-band grouping |

| | |
|---|---|
| $N$ | number of subcarriers |
| $N_{ave}$ | scheduler time constant |
| $N_0$ | power-spectral density of noise |
| $P_{cell}$ | total transmit power of cell |
| $P_i$ | transmit power allocated for user $i$ |
| $Q$ | $Q$ - function |
| $r$ | integer exponent needed to express system load as a power of ½ |
| $r_{face}$ | distance from centre to one the faces of a hexagonal cell region |
| $r(t)$ | received signal |
| $Rate$ | transmission format with specific structure, coding and modulation |
| $R_z$ | maximum annular zone rate |
| $R_{ave}^{(u)}(i)$ | average throughput delivered to a user |
| $s(t)$ | transmitted signal |
| $S$ | number of base station/sectors |
| $S_{sym/ACK}$ | number of symbols of packet transmitted between ACK/NAK acknowledgements |
| $S_{trans}$ | number of symbols per packet transmission |
| $E_s$ | symbol energy |
| $T$ | number of diversity replicas |
| $T_g$ | duration of cyclic prefix (or guard interval) |
| $T_p$ | partially loaded SS-OFDM symbol diversity replicas |
| $T_{slot}$ | time slot duration |
| $T_{sym}$ | duration of OFDM symbol |
| $U$ | number of users |
| $z_j$ | decision variable for the $j^{th}$ data symbol |
| | |
| $\alpha$ | mean of the squared channel gains of $L$ subcarriers |
| $\gamma_m$ | sub-band SINR |
| $\overline{\gamma}_m(U)$ | gain in the average received SINR per scheduled transmissions |
| $\Upsilon_{PL}$ | path loss exponent |
| $\delta(t)$ | unit impulse signal |
| $\Delta_u$ | power control error for the $u^{th}$ user |
| $\zeta_{u,p}$ | channel model path gain of the $p^{th}$ path received by the $u^{th}$ user |
| $\eta_l$ | sample of noise process |

| | |
|---|---|
| $\theta$ | effective number of diversity replicas due to parallel/serial transmissions and partial loading |
| $\kappa_{cell/i}$ | total transmit power divided by the power allocated to user $i$ |
| $\lambda$ | 1/ SINR per transmission replica |
| $\mu_A$ | sample mean of $A$ |
| $\xi_{u,s}$ | signal attenuation due to large-scale fading and path loss of transmissions from the $s^{th}$ transmitter, received by the $u^{th}$ user |
| $\rho_{u,s}$ | power allocated to user $u$ through power control |
| $\sigma_A^2$ | sample variance of $A$ |
| $\sigma_I^2$ | variance of interference |
| $\sigma_{shad}$ | standard deviation of shadowing process |
| $\sigma_{symbol}^2$ | variance of SS-OFDM symbol |
| $\tau_{s,p}$ | relative path delay of the $p^{th}$ path received by the $u^{th}$ user |
| $\upsilon$ | time interval over which the channel does not change |
| $\varphi$ | parameter for annular zone sizes |
| $\phi_{u,n,s,l,p}^{(i)}$ | interference due to ISCI and CSCI |
| $\psi(t)$ | channel impulse response |
| | |
| $x^*$ | complex conjugate of $x$ |
| $\mathrm{E}[x]$ | expectation of $x$ |
| $\hat{x}$ | estimate of $x$ |
| $\mathbf{X}^T$ | transpose of $\mathbf{X}$ |

# Chapter 1

# Introduction

The purpose of this thesis project is to investigate the design of spread spectrum orthogonal frequency division multiplexing (SS-OFDM) systems for the downlink of high throughput cellular data networks. The first part of this work investigates a high data rate method using conventional SS-OFDM techniques such as power control and interleaving. The second part, and the major focus of the thesis, concerns the proposal and development of a best-effort SS-OFDM packet system using adaptive techniques. The final chapter proposes an interference-reducing diversity combining scheme for SS-OFDM systems, which is particularly useful in packet data systems. The results of the combining scheme research have led to the development of a novel low-complexity MMSE equalization method for partially loaded systems that is also presented.

This introduction provides justification for pursuing this research topic by first discussing the background and requirements of the downlink of modern and future cellular systems. SS-OFDM and its supporting technologies are described, followed by a comparison of SS-OFDM to OFDM and single carrier methods. It is shown that SS-OFDM techniques are particularly well suited to future wireless mobile systems. Further discussion in this chapter illustrates the need for SS-OFDM based cellular systems that are capable of providing high data rate adaptive packet services. The purpose of this thesis is to develop high data rate SS-OFDM systems, and to improve their performance through adaptive and other innovative methods.

In Section 1.1, the advent and current state of cellular telecommunication systems is generally summarized. This section indicates how the packet data and specifically, best-effort packet data systems have became a focal point for researchers. The downlink of a cellular system is of particular importance as so many services have become asymmetric in their data rate requirements. It is also stated that future systems are expected to

continue along a similar path, but will have requirements that favour OFDM-based system implementation.

OFDM and code division multiple access (CDMA) are methods of multiplexing users' signals so that they can be detected with minimal interference at the desired receiver. In Section 1.2, multiple access and multiplexing methods are presented and discussed including the marriage CDMA and OFDM methods. The focus of this thesis is a particular variant of this combination known as spread spectrum (SS-) OFDM. The suitability of SS-OFDM for 4G systems in comparison to single carrier and pure OFDM schemes is briefly discussed. It is noted that when considering packet data, SS-OFDM can be implemented instead of OFDM without significant loss in system frequency domain adaptability, which single carrier systems do not have.

Although OFDM research is extensive and spans several decades, implementation of wireless OFDM systems was rather limited until recent years. OFDM has not been implemented for cellular systems, and further, publications that study cellular OFDM systems are relatively rare. Section 1.3 summarizes some relevant implementations of OFDM-based systems such as wireless local area networks (WLAN) and broadcast systems, as well as proposals in literature for cellular designs.

The final section of the chapter summarizes the rest of the thesis. That section briefly describes the significant research contributions of this thesis to wireless multi-carrier cellular systems.

## 1.1 Downlink Cellular Packet Data Services

### 1.1.1 Cellular Systems

Cellular communications is concerned with the transfer of information between a fixed transmission point, known as a base station, and a mobile user moving about within a localized area known as a cell. Unlike a broadcast transmission system such as commercial radio, the challenge of cellular transmission is that each mobile requires its own communications channel, as each data stream is mobile specific. Likewise, each mobile has its own data stream that must be received correctly by the base station.

Technology for cellular communications became available in the 1970's and allowed for many users in a large geographical area to be served at the same time, using a relatively small number of communication channels [85]. The subdivision of the coverage area into cells led to the development and deployment of so-called first generation cellular systems. The Nippon Telephone and Telegraph (NTT) system in 1979, Nordic

Mobile Phone (NMT) in 1981 and the North American Analog Mobile Phone System (AMPS) in 1983 are notable regional first generation systems. The systems used analog frequency modulation (FM) signalling with channel bandwidths of 30 kHz or less to provide mobile cellular voice services. Second generation systems, defined by the use of digital signalling and improved signal quality, was first developed in Europe as GSM (which was originally Groupe Special Mobile, and is now Global System for Mobile Communications) in 1992. In North America, IS-54 (and later 136) was proposed as digital system that was compatible with the AMPS systems in terms of channel structure and control channels. A more advanced and more popular 2G digital standard, IS-95 (and an update IS-95 B [99]) was proposed in 1992. IS-95 was a considerable advancement in cellular communications as it utilized fast power control, 1.25 MHz channels, antenna sectorization, spread spectrum methods, and modern coding techniques.

The common goal of first and second generation cellular communication systems was to provide reliable voice communication to mobile users in a given cell. General research problems focused on how to increase the number of users that could be served in a given cell, or improving the quality of service of each user given some received power constraint.

The evolution of 2 and 2.5 G towards third generation (3G) standards addressed packet data services as well as voice. General packet radio system (GPRS) for GSM and cdma2000 releases included special provisions for packet services. Packet services became increasing important as consumer needs began to shift towards web browsing, video-on-demand, and remote data access rather than pure voice services. In addition, the need for a high data rate downlink (from the base station to the mobile receiver) systems became clear as many services required asymmetric links as the bulk of the data transmission would go to the mobile, and comparably little data in the other direction. 3G systems such as wideband CDMA are designed to support packet and circuit switched traffic with data rates up to 2 Mb/s on the downlink.

While some 2G and all of the 3G system standards enabled packet services, it was the evolution of these systems near the turn of the millennium that marked a major shift in focus for wireless systems. As packet data for most applications are tolerant of small transmission delays, opportunistic scheduling of transmission to increase throughput replaced the continuous transmission of circuit switched data. This type of transmission results in an increased relationship between the physical (PHY) and medium access control (MAC) layers of the wireless network. The evolution cdma2000 brought about

the creation of 1x EV-DO [100], an opportunistic best-effort packet system utilizing multi-user diversity, and 1xEV-DV [101], a combined evolutionary system that allows best-effort packet data services as well as voice transmissions on the same carrier frequency.

Fourth Generation wireless networks are expected to continue along the same path of increased spectrum efficiency, but also on compatibility with other networks. Research towards 4G includes PHY/MAC layer issues of resource allocation that now includes multiple input multiple output (MIMO) links, as well as advanced coding techniques such as LDPC codes. In addition, bandwidths for 4G systems are expected to be significantly larger than 3G: with some projects proposing 100 MHz bandwidths [4]. An important issue for 4G cellular systems is compatibility with wireless local area networks (WLAN) and personal area networks (PAN) in order to allow a mobile user to use a single device to communicate in all environments. These systems will increase the burden on the downlink as many sources (PDAs, cell phones, remote headphones or terminals, etc.) require information from a centralized point.

### 1.1.2 Cellular Downlink

Data can be transferred in 2 directions: either on the *downlink* from the base station to a mobile user, or on the *uplink* from the mobile user to the base station. The terms downlink and uplink are sometimes replaced by forward link and reverse link in North America.

This thesis is concerned with increasing the performance of the downlink of multicarrier cellular wireless systems. The downlink is particularly important for emerging technologies such as internet web-browsing, remote file download, video-on-demand, and streaming applications, all of which are asymmetric as the data traffic is downlink intensive. The uplink is generally used only for the requests of these large data transfer applications.

On the downlink, all transmissions originate from the base station. The base station can also easily control when and how users' signals are transmitted. When transmissions to specific users occur is known as scheduling, and how the users' signals are arranged is known as multiplexing. Advanced scheduling and multiplexing methods are a major focus of the thesis. Optimizing downlink performance is also important, as the resources available at the mobile receiver for signal processing are limited in comparison to the base station. The mobile receiver must meet hardware complexity and power requirements that inherently limit the complexity of signal processing. Thus, the demand

for high data rate transfers on the downlink is increasing, while the resources remain limited.

## 1.2 Multicarrier and CDMA Systems

Multicarrier systems are particularly well suited to the needs of 4G systems as they allow for a high degree of adaptability on the downlink of a cellular communications system. Each subcarrier of an OFDM system can behave as a separate communication channel, and hence, the power allocation and bit loading of a subcarrier can be changed according to channel conditions and quality of service requirements. In addition, multicarrier systems are easily scalable in frequency and are ideal for wideband transmission. This sub-section discusses the various combinations of CDMA and multicarrier systems, and how SS-OFDM compares to DS-CDMA and pure OFDM methods.

### 1.2.1 Multiplexing and Multiple Access Methods

In cellular systems, several users within a cell need to send and receive information in a timely fashion. Multiple access methods allow several users to send transmissions to the base station on the uplink (mobile to base station). On the downlink, users' signals are multiplexed and transmitted throughout the cell. This is not properly multiple access as all the signals originate from a single base station. However, in general a duplex system is referred to according to the multiple access technique it uses.

Three methods of multiple access (Figure 1.1) are most common in wireless communication systems: frequency division multiple access (FDMA), time division multiple access (TDMA), and code division multiple access (CDMA). The purpose of multiple access schemes is to separate the signals from different users in a manner that will allow them to be detected at the receiver without significant interference from each other. In FDMA, the users are separated in frequency, while in TDMA; the users' signals are transmitted over the same frequencies but are separated in time. In CDMA systems, all data streams are transmitted over a given frequency band simultaneously. The signals are separated by a unique wideband spreading sequence (or spreading code) for each data stream. As the resulting signal has a much wider (or spread) bandwidth than the original narrowband data stream, code division methods are also known as spread spectrum (SS) systems. Different signals can be transmitted on the same time-frequency channel by using different spreading codes for each signal.

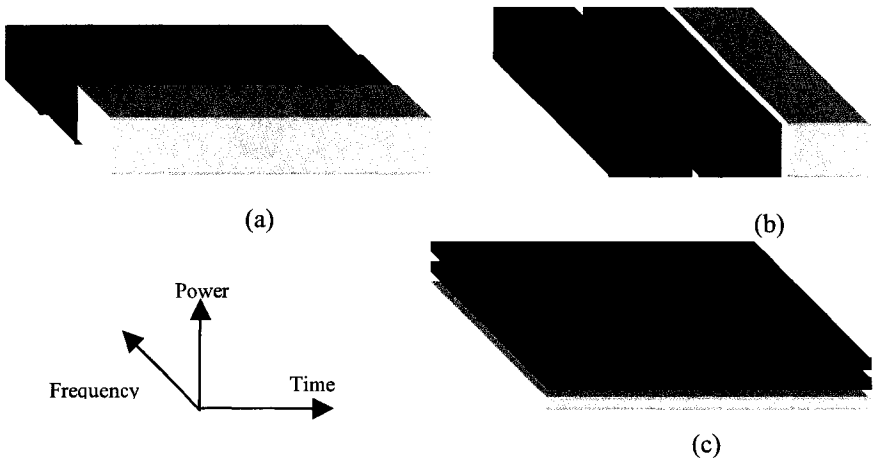


Figure 1.1. Time-frequency-power representation of FDMA (a), TDMA (b), and CDMA (c).

### 1.2.2 Multicarrier Systems

Multicarrier systems use several frequency subcarriers to send one or more streams of data in a communications system. Multicarrier modulation is inherently a form of frequency division multiplexing, although it can be used with TDM and CDM methods. Multicarrier systems have been developing continuously since the proposal of the Collins Kineplex system [22], in which bit streams are transmitted in parallel on different subcarriers.

Originally, multicarrier systems employed adjacent frequency subcarriers and proper filtering so that the spectra of the subcarriers were non-overlapping. This method required sharp filter responses, and was inherently spectrally inefficient. Chang [9][10] outlined filter criteria for a staggered QAM method that allowed for overlapping of subcarrier spectra, while still maintaining orthogonality at the receiver. This was implemented by Saltzberg [91]. In the latter scheme subcarriers are separated by $1/T_{sym}$, where $T_{sym}$ is the symbol duration, allowing for near Nyquist rate signalling [91]. This is known as frequency division orthogonal multiplexing [10] using band-limited subchannels, and is the basis for modern orthogonal frequency division multiplexing (OFDM) which general considers subcarrier spectra of the form $\sin(x)/x$ (Figure 1.2).

OFDM is a specific form of multicarrier modulation in which the subcarrier spacing is as small as possible, while still ensuring the signals can be detected without interference at the receiver. The critical element which allowed OFDM to become a practical transmission scheme was Weinstein and Ebert's work [112] on discrete Fourier transform (DFT) implementation of OFDM, eliminating the need for multiple transmit and receive filters (one per subcarrier). Later, Cioffi *et al* showed that inter-symbol interference (ISI) and inter-subcarrier interference (ISCI) could be eliminated by introducing a cyclic prefix to each OFDM symbol [11][90], making multicarrier systems ideally suited to the multipath environments which are common in wideband cellular radio communications.

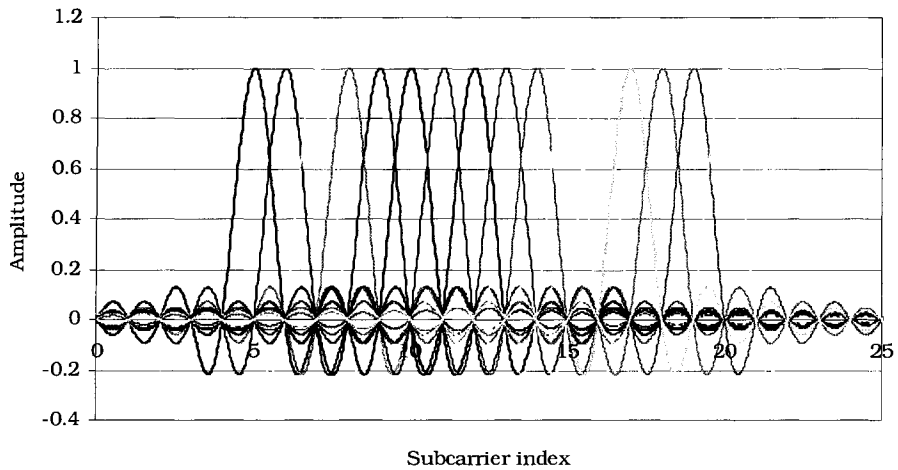


Figure 1.2. Overlapping subcarrier spectra in an OFDM based system. Rectangular pulse shaping is assumed. Note the subcarrier spectra overlap, yet at the centre frequency of a given subcarrier the other subcarriers have a null.

### 1.2.3 Single Carrier CDMA

This section and this thesis are concerned with the combination of multicarrier and spread spectrum methods for future high data rate systems. However, a very brief description of single carrier CDMA is presented for comparison. CDMA has two variants; frequency hopping (FH) or direct sequence (DS). In FH schemes, the narrowband signal of a given user is hopped between frequencies within the transmission band. Users signals are distinguished by the hopping pattern. The more common technique is DS, in which the narrowband signal is multiplied by a wideband spreading sequence creating a wideband signal. The narrowband data stream can be extracted at

the receiver by multiplying the wideband signal by the desired spreading sequence. DS-CDMA is commonly used in single carrier cellular systems. The majority of 2G and 3G systems in North America are largely based on DS-CDMA. An intuitive diagram of a DS-CDMA signal is shown in Figure 1.3a. Additional data symbols may be transmitted over the same frequencies by using different spreading sequences. By applying a spreading code in time, each data bit is spread and occupies a larger bandwidth. Because the signal is spread over a larger bandwidth, adaptability of modulation and power in the frequency domain is not possible. The use of a RAKE receiver enables good quality performance in frequency selective channels.

### 1.2.4 Multicarrier CDMA

The marriage of spread spectrum (SS), or code division multiple access methods, and OFDM has received considerable interest in wireless communications. OFDM in conjunction with CDMA has been proposed in three variants. Fettweis [116][117] and Fazel [28][30] proposed spreading in the frequency domain so that each subcarrier is modulated by one chip of the spreading sequence (Figure 1.3b). In this case, spreading of data symbols over all subcarriers does not affect the orthogonality of the subcarriers, and a cyclic guard interval can still be used to eliminate inter-symbol interference in multipath channels. This system was proposed under the acronym MC-CDMA, although to avoid confusion with the next variant, it also goes by the more descriptive name OFDM-CDMA. It is the downlink of the OFDM-CDMA variant that is considered throughout this thesis.

The two other variants proposed spreading in time, as in a direct-sequence (DS) CDMA method (Figure 1.3c). MC-DS-CDMA [21][60][95] can be seen as multiple DS-CDMA signals that overlap in frequency domain after spreading. The subcarrier spacing is the minimum separation in order to still ensure that the subcarriers are orthogonal. This is similar to OFDM-CDMA, with the exception that a data symbol is spread over several OFDM symbols, rather than across the subcarriers. A band-limited method in which spectra of subcarriers do not overlap has also been proposed [61]. In this band-limited design, the signalling is no longer OFDM and is identical to parallel band-limited DS-CDMA signals.

The third method known as multi-tone (MT) CDMA [106] spreads each subcarrier of an OFDM symbol in time, thus creating extensive overlap of subcarrier spectra. MT-CDMA can be likened to an MC-DS-CDMA signal with subcarrier spacing smaller than the width of the main lobe of a subcarrier signal. In this system, subcarriers do not

remain orthogonal after spreading, and thus any impairment of the signal due to the channel leads to significant inter-carrier interference. As significant equalization is required to control the inter-carrier interference generated, MT-CDMA is not a reliable multicarrier method for wireless communications in noisy, frequency selective fading channels.

The first of the combinations of CDMA and multicarrier methods described, OFDM-CDMA, has received the greatest attention in literature and appears to be the most promising candidate for the downlink of multicarrier cellular systems. The system experiences no ISI in multipath channels, unlike DS-CDMA and MT-CDMA, and is less susceptible to inter-symbol interference and severe inter-carrier interference in comparison to MC-DS-CDMA. A comparison of bit-error rate (BER) performance of these methods concluded that OFDM-CDMA was superior to MC-DS-CDMA, MT-CDMA, and DS-CDMA in a frequency selective environment under a heavy traffic load [37][49]. The combination multicarrier and spread spectrum known as MC-CDMA or OFDM-CDMA for the downlink is the focus of this thesis.

It should also be noted that TDMA and FDMA techniques may be used in conjunction with OFDM and OFDM-CDMA methods. Furthermore, there are multiple ways of multiplexing and interleaving signals within OFDM-CDMA schemes, which lead to hybrid schemes such as 2 dimensional spreading for OFCDM, SS-MC-MA for uplink and downlink, and various adaptive SS-OFDM schemes such as the one proposed in this thesis (see Chapter 4).

In addition, the term "multiple-access" is not exactly appropriate in this thesis as the primary concern is the downlink. As mentioned earlier, there is no "multiple-access" on the downlink; the downlink signal is simply a composite of multiplexed signals. This thesis will use terms multicarrier code division multiplexing (MC-CDM) and SS-OFDM that are more appropriate for this material than the duplex nomenclatures of MC-CDMA and OFDM-CDMA. The general nomenclature of SS-OFDM is used through the remainder of this thesis to describe the downlink schemes proposed in this thesis, all of which consider the OFDM signalling with spreading in the frequency domain as shown in Figure 1.3b.

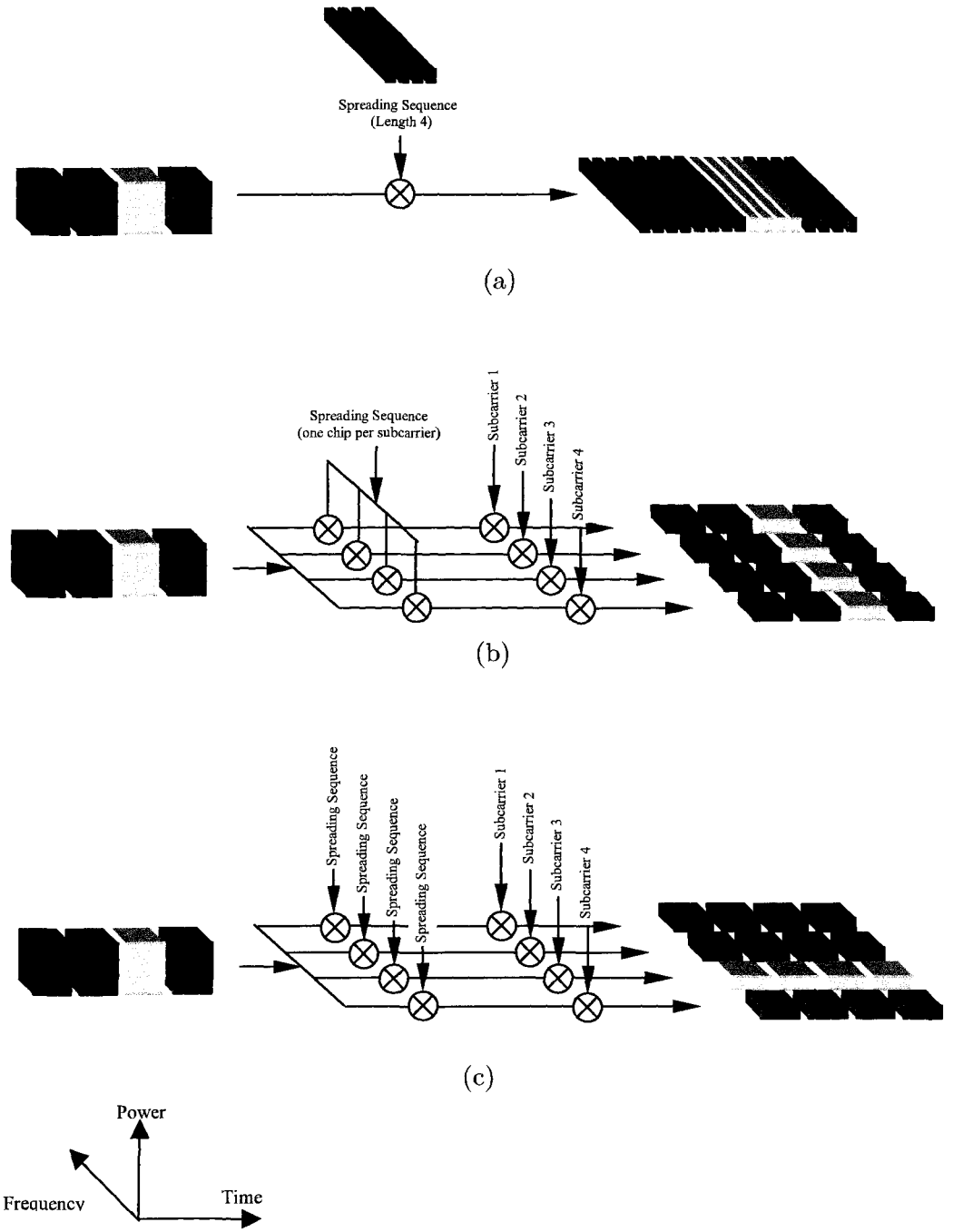


Figure 1.3. Time-frequency-power representations of DS-CDMA (a), MC-CDMA or OFDM-CDMA (b), and MC-DS-CDMA (c). The representation of MT-CDMA is the same as MC-DS-CDMA with narrower subcarrier spacing. All systems shown are nominally loaded for simplicity (one spreading sequence per time-frequency channel).

### 1.2.5 Comparison of DS-CDM and SS-OFDM

As mentioned, SS-OFDM systems were found to have better downlink BER performance than DS-CDM systems [49]. However, a general comparison of the two systems depends on the radio environment and application specifications. In general, SS-OFDM systems are better suited to high data rate applications for future systems in frequency selective channels.

SS-OFDM systems are able to eliminate any inter-code interference and ISI due to multipath channels with a cyclic prefix. The same is not true for DS-CDM, which uses a RAKE receiver for resolvable path detection, which inherently generates significant interference due to multipath. However, in cases where a single path is significantly stronger than the rest, DS-CDM has a performance advantage, as it does not suffer a loss in spectral efficiency due to the cyclic prefix.

In earlier CDMA cellular systems such as IS-95, systems were partially loaded per sector, meaning that not all spreading codes were in use. DS-CDM systems perform similarly to the more complex SS-OFDM systems when low or partially loaded, particularly at the low signal-to-noise ratios at which 2G voice systems operate. This difference is discussed further in Section 2.4. Other 2 and 2.5G features such as soft-handoff and power control pose some design complications for OFDM based systems (see Chapter 3).

Future applications of wireless systems will require higher data rates and a higher quality of service requirement. SS-OFDM is well suited for such applications as it performs significantly better when the system is fully loaded and does not experience an error floor due to inter-code interference like DS-CDM. Also, SS-OFDM is more adaptable to various parallel services through adaptive subcarrier power and modulation methods. Issues of power control, allocation and hand-off can be rectified for SS-OFDM systems when considering sophisticated adaptive transmission schemes, such as those proposed in Chapters 4 and 5.

### 1.2.6 Comparison of OFDM and SS-OFDM

In OFDM-based systems, information is transmitted on several parallel subcarriers. This inherent frequency division format allows the power and modulation scheme of each subchannel to be adjusted according to the channel conditions present at a given frequency, rather than for the entire OFDM symbol. This inherently adaptable nature of

OFDM makes it a strong choice for 4G systems. In addition, a cyclic prefix can be used to eliminate inter symbol interference in frequency selective channels; thus preventing severe degradation of signal quality in such channels.

While SS-OFDM systems retain many of the positive properties of pure OFDM systems, the use of spread spectrum results in a less adaptive system in the frequency domain. The use of spreading creates blocks of subcarriers containing spread data of the same symbol. In order to retain the orthogonality of the spreading sequences, the adaptive actions of power allocation and adaptive modulation can be performed on the block of subcarriers as a whole, but not on each subcarrier within the block. The trade-off for decreased adaptivity by using spread spectrum is increased signal reliability and mitigation of inter-cell interference.

Reliability of communications in frequency selective channels was a strong motivator in the creation of SS-OFDM. The function of spreading in SS-OFDM is to transmit each data bit over the entire wideband channel. In contrast, a pure OFDM system must employ channel coding in order to avoid losing data bits in spectral nulls. The performance of OFDM and SS-OFDM has been compared with convolutional coding under the conditions of maximum frequency diversity (i.e. fading on each subcarrier is uncorrelated). It has been shown that SS-OFDM with minimum mean square error (MMSE) equalization (see Section 2.3) and convolutional coding is similar in BER performance to that of OFDM with convolutional coding for code rates greater than ½ [48][51]. Kaiser also showed that coded SS-OFDM with maximum-likelihood sequence estimation (MLSE) detection outperforms coded OFDM at code rates ½ or greater in the same channel and under a full traffic load. In the case of a small traffic load (i.e. not all spreading sequences are used), coded SS-OFDM significantly outperforms coded OFDM even at code rates less than ½ [51].

More recently, adaptive techniques that take advantage of frequency selectivity have been developed for best-effort communication systems, so there is no need to spread over the bandwidth of the signal. In these systems, spread spectrum helps to mitigate inter-cell interference. Signals from several base stations can be identified and separated at a given mobile as each base station is assigned a distinct long pseudo-random noise (PN) sequence. The desired signal from the desired base station can therefore be received correctly in SS-OFDM systems. In pure OFDM schemes, several transmissions on the same subcarrier are indistinguishable to the mobile, making the signal reception unreliable. Cellular OFDM therefore relies on interference avoidance in which transmissions occur in a manner that limits collisions of signals on the same subcarrier.

This is less efficient than SS-OFDM as frequencies are not reused in each cell, limiting the number of available channels.

The use of spread spectrum techniques makes the system more resilient to jamming, and single subcarrier failures either at the transmitter or receiver, yet it is the mitigation of inter-cell interference that makes SS-OFDM the most promising multicarrier technique for cellular communications. As mentioned, a drawback of SS-OFDM is reduced adaptability. Even though SS-OFDM is less flexible in terms of power and bit allocation than pure OFDM, innovative methods have been proposed in this thesis (see Chapters 4 and 5) for SS-OFDM to make the performance difference in a practical packet data system negligible.

## 1.3 Selected OFDM-Based Cellular Systems and Related Research

Research on multicarrier and OFDM based systems has been ongoing for decades. OFDM has been recognized as a reliable physical layer transport mechanism for wireless LAN and broadcast applications. Historically, few cellular multicarrier systems have been proposed, and prior to the beginning of this project few multi-cell evaluations of the performance of SS-OFDM for personal communications had been published. However, due to their adaptability and suitability for high-speed downlink communications, OFDM and SS-OFDM methods have emerged as promising methods for future cellular systems.

In the late 1990's, OFDM was adopted for use in European digital audio broadcasting (DAB) [27] and terrestrial digital video broadcasting (DVB-T) [26]. OFDM is ideally suited for such applications due to its inherent parallel structure and its ability to usefully receive identical, simultaneous transmissions from multiple transmitters broadcasting on the same carrier frequency. OFDM has also been adopted for use in several wireless local area network (WLAN) standards [105], such as IEEE802.11a [40], IEEE802.11g [41] and Hiperlan II [25].

Packet access systems based on OFDM such as SONY's band-division multiple access (BDMA) [8] and AT&T's dynamic packet assignment (DPA) [14] have been proposed to be complementary to third generation (3G) systems. In these systems, frequency diversity is averaged out by slow frequency hopping over groups of subcarriers, and hence, effective use of adaptive modulation is not possible. The hopping sequences are intended to avoid intra-cell interference and limit inter-cell interference. Other systems that propose allocation of groups of subcarriers include NTT DoCoMo's

orthogonal frequency code-division multiplexing (VSF-OFCDM) system [4], and AT&T's clustered OFDM [63]. These systems, as they have been proposed, do not include adaptive allocation and modulation. It should also be noted that OFDM has been proposed for the evolution of GSM system [13].

Few multi-cell evaluations of OFDM-CDMA for personal communications have been published. In [81][103], OFDM-CDMA in its most basic form was studied extensively for 3G systems. It was shown that OFDM-CDMA required a high degree of isolation to inter-cell interference, and therefore should be considered with a frequency reuse greater than 1; spectral efficiencies of 0.06 to 0.24 bits/Hz/cell were achievable using a frequency re-use of 1/3. It was also stated that per symbol power control significantly impacted the performance in a negative manner.

An OFDM cellular system proposal with complex power control and power allocation per subcarrier was considered in [97]. Even in this complex system, significant outages were experienced even with a frequency re-use pattern of 4 and fixed BPSK modulation with rate 1/3 turbo coding.

In general, downlink OFDM methods have been considered with equal resource sharing (or equal data rate in [34]). The cell capacity and throughput of these methods are inherently limited by the performance of users with long-term poor channel conditions, either from shadowing or proximity to an interfering transmitter [1]. In this thesis, initially a location based resource allocation scheme is discussed for a multi-code OFDM-CDMA scheme for the downlink [73] (see Chapter 3). The purpose of this scheme is to allow more resources, in the form of code channels, to be allocated to users near the home base station. Spectral efficiencies of 0.3 bits/Hz/cell are achieved using fixed QPSK modulation with single frequency reuse. It should be noted that multi-user diversity is initially not exploited.

Flarion has introduced a spread-spectrum OFDM system for mobile communications [42]. This system uses spread spectrum in the form of fast frequency hopping (FH) and is called Flash-OFDM. Users are assigned different subcarrier-hopping sequences. Inter-cell interference is averaged across the bandwidth of the hopping pattern. Users within a given cell do not interfere with each other as the hopping patterns are always orthogonal, which is unlike OFDM-CDMA which requires equalization to restore the orthogonality of the spreading codes in frequency selective channels. Other then the intra-cell interference, FH-OFDM is similar to the conventional OFDM-CDMA technique discussed in the first three chapters of this thesis, and hence FH-OFDM

techniques (such as Flash-OFDM) can also be considered with the location dependent resource allocation scheme proposed in Chapter 3.

The problems of serving users with long-term poor propagation conditions and employing multi-user diversity in single carrier systems were addressed in the 1xEV-DO proposal for evolution of cdma2000 [6][100]. Proportionally fair scheduling [39] is employed to allow allocation in the time domain depending on the small-scale fading for each user. Evaluation of this system has shown that peak spectral efficiencies of approximately 1.3 bits/Hz/sector (3 sectors/cell) are attainable [86]. A similar solution for multi-carrier systems is in development [74]-[78] and is the major topic of this project (see Chapters 4 and 5). This thesis also proposes several adaptive methods to specifically improve the performance of packet data multicarrier cellular systems (see Chapters 4-6).

## 1.4 Thesis Outline and Research Contributions

### Chapter 2

This chapter is intended to give background of modern spread spectrum OFDM systems, and introduce the radio channel that is used in this thesis. The chapter discuses several equalization techniques, but focuses on MMSE equalization of the multi-carrier channel to restore orthogonality of superimposed SS-OFDM signals spread over it. The Gaussian model of inter-code interference, which was developed in [52][54], is briefly discussed in this chapter. This model is used throughout this thesis in the evaluation of link level performance. The BER of this system is shown in Rayleigh fading, and compared to DS-CDM systems.

This chapter concludes with a brief comparison of DS-CDM performance with SS-OFDM. Some previous comparisons [37][49] have compared SS-OFDM and DS-CDM systems by considering only Gold codes, and not concatenated Walsh and Gold sequences, in the spreading of the DS-CDM systems. This can lead to underestimating the performance of the DS-CDM systems in some channels. The importance of this contribution is to identify the advantage that SS-OFDM systems have over DS-CDM systems when both are fully loaded, and utilize this advantage in system design (as in Chapters 4 and 5).

# Chapter 3

This chapter discusses the basic multi-cell performance of SS-OFDM systems on the downlink, and presents a novel radio resource allocation scheme for the SS-OFDM. Inter-cell interference (ICI) is discussed, and ICI models that will be used throughout the thesis are presented. The challenges associated with SS-OFDM cellular systems with MMSE equalization are identified in this chapter. Power control for SS-OFDM systems with MMSE equalization is discussed. It is shown that the link level model for an SS-OFDM system with power control requires knowing the inter-cell to intra-cell interference ratio as well as the total inference level. This additional parameter is needed for proper MMSE equalization. Link level results for the SS-OFDM system with power control and convolutional coding are given.

A novel location-dependent rate assignment [73] is presented in the last section of the chapter. This scheme divides the cell into annular service zones and allocates code channels to users in a manner that increases the throughput of the cell without significantly increasing the transmit power at the base station. A full multi-cell simulation of this allocation scheme is completed showing a significant improvement in cell throughput. It was a significant improvement on other low-delay constrained data systems based on SS-OFDM of the time.

This chapter presents the following research contributions [73]:

- Proposal and development of a novel radio resource allocation scheme based on the mobile user's location in the cell. The premise of this scheme is the allocation of more code channels to users near the transmitter, who in general, have better average channel conditions, and therefore require less power for successful transmission, thereby reducing the interference to adjacent cells.

- Simulation of full cellular SS-OFDM system with power control, location-dependent code channel assignment and multiple mobile users. Very few SS-OFDM cellular evaluations had been done. A previous work [103] had investigated cellular SS-OFDM with poor results due to issues with per symbol power control. The "per code channel" power control implemented in [73] was a significant improvement.

# Chapter 4

After a brief discussion of adaptive bit allocation and multi-user methods for OFDM systems, this chapter proposes a 2-dimensional radio resource allocation scheme for the downlink of an SS-OFDM cellular system. The spread spectrum OFDM system with time and frequency allocation (SS-OFDM-F/TA) uses downlink scheduling to allocate rectangles in the time-frequency plane, representing sub-bands and time slots, to users with the best channel conditions. The allocation process is based on channel conditions relative to a user's average conditions to achieve some level of fairness among users in the cell (proportionally fair scheduling in two dimensions).

The system is designed to exploit the advantages, adaptability and scalability of multi-user SS-OFDM systems, while maintaining a relatively simple structure that is practical for cellular implementation and packet data services. Adaptive modulation in the form of packet format selection is used, type II hybrid ARQ, and sector selection are considered in the cellular system. Link and system level simulations are used to evaluate the cellular system's performance. The general simulation structure discussed in this chapter is also used in Chapter 5. Results for nomadic and mobile users, sectorized and omni-directional antennas, and several channel models are presented in Chapter 4. The results are compared to a best effort single carrier system.

As a feature of the SS-OFDM-F/TA system, the allocation of disjoint sub-bands for packet transmission in highly frequency selective fading channels is proposed. This method significantly increases throughput of the system by benefiting users with average (in relation to other users) channel conditions. The idea of sub-band grouping is compared to utilizing smaller packet sizes. The two ideas are compared in terms of throughput and packet delay.

This chapter contains several research contributions [74][75][76]:

- The proposal of a two-dimensional allocation scheme for OFDM-based systems with simplified power allocation and multi-user diversity. Previous systems had generally considered zero-delay constraints (allocation in frequency only) or allocation in time only. Results are nearly as good as for individual subcarrier allocation with adaptive bit and power loading for OFDM.

- Application of two-dimensional allocation system to a cellular system (SS-OFDM-F/TA packet data system). The proposed system successfully uses multi-user diversity and provides adaptability, while employing spread spectrum for ICI mitigation.

- Simplified allocation by allocating groups of adjacent subcarriers over which the fading is highly correlated. In a multi-user system, this simplifies allocation process and signalling on reverse link. In addition, spreading in frequency can then be used with minimal inter-code interference.

- Application of proportionally fair scheduling in two-dimensions. This was later suggested by other authors in [107].

- Allocation of groups of disjoint sub-bands. Important improvement to the system in highly frequency selective fading channels with large packet sizes. Increases throughput and benefits the users with average channel conditions, thereby improving fairness.

- Simple centralized decision algorithm (at the base station) for allocation of groups of sub-bands. In the worst case it requires only slightly more signalling on the uplink, but results in minimal complexity at the mobile and does not need to solve "disputes" over sub-bands requested by more than 1 user.

- Performance comparison of allocation of groups of disjoint sub-bands to using smaller packet sizes. Showed that highest throughputs were achieved by sub-band grouping method, while small packet sizes reduced packet delay.

- Cellular analysis of the system in multiple ITU channels in terms of throughputs and delays. Simulations include adaptive packet selection thresholds, and either explicit simulation of the small-scale fading of ICI sources or a model of the composite ICI from all sources, for all 57 simulated sectors. Simulations include system level simulations, and a significant number of link level simulations.

# Chapter 5

This chapter proposes some additional improvements for the SS-OFDM-F/TA system, and provides further insights into the system performance. In Section 5.1, several sets of packet formats that will be used throughout the chapter are presented. These sets have smaller transmission sizes, and exhibit different dependencies on efficient re-transmissions algorithms. The main focus of the chapter is on asynchronous re-transmission algorithms, several of which are presented. Unlike synchronous re-transmission of packets as considered in Chapter 4, the asynchronous approach delays re-transmissions of a packet until certain conditions are met. Packet may be re-transmitted over a different sub-band, or may be delayed in favour of an entirely new packet transmission. Two classes of these algorithms are considered.

Fast sector selection is also proposed in Chapter 5. The interval chosen for sector selection is shorter than the decorrelation time of the shadowing process, but long enough to average out small-scale fading. A selection interval of 1 second is chosen to satisfy these requirements, and also allow a minimal amount of time for cellular network function during the serving sector switch. The results indicate that this sector selection rate significantly increases throughput, benefiting the users with the poorest channel conditions. Fast sector selection also significantly decreases packet delays as it prevents users from experiencing very poor channel condition for extended periods, thus allowing ongoing packet transmission to be completed.

Chapter 5 also investigates using larger modulation constellations to increase throughput, and investigates adaptive termination and code-division of packets. The latter was considered in [19][20] for a single carrier system, and has been modified and adapted to the SS-OFDM-F/TA system. Quantization of the channel state information is also considered to identify the ability of the system to exploit multi-user diversity with limited feedback.

This chapter includes several research contributions [75][76][77][78]:

- Proposal of several asynchronous re-transmission algorithms. Asynchronous re-transmission was proposed before this work in [19], in which re-transmissions were withheld until the specified user was selected again by the scheduler. This work considers several options, and in addition, considers algorithms that

prioritize new packet transmission over ongoing re-transmissions to a certain user.

- Proposal of improvement for asynchronous re-transmission schemes via parallel allocation in two-dimensional allocation systems. For a given re-transmission algorithm, it is possible to further improve re-transmissions to a given user if more than one sub-band has been assigned to that user for the purpose of re-transmissions. This is shown to give higher throughputs for several of the proposed algorithms.

- Demonstration that the proposed asynchronous re-transmission scheme with the shortest packet delays, MD-ARP-PA, provides throughputs close to those of the highest throughput scheme under most conditions, and better than all schemes when the channel state information is significantly outdated.

- Proposal of constraining the maximum re-transmission interval (RTI) for a given packet. Showed that constraining the RTI can decrease asynchronous re-transmission delays to match or be similar to those of synchronous schemes, while still maintaining a significant throughput performance gain.

- Implementation of an adaptive termination and code-division multiplexing scheme for the SS-OFDM-F/TA system, similar to that proposed for single carrier schemes in [19][20].

- Proposal of fast sector selection such that the selection interval is shorter than the decorrelation time of the shadowing process, but long enough to average out small-scale fading and allow some time for the needed network signalling. Not only does fast sector improve the average throughput of the sector, but it does so by benefiting only the users with the poorest channel conditions. Fast sector selection also significantly decreases packet delays.

- Showed that best-effort packet data systems such as the proposed SS-OFDM-F/TA system can still exploit multi-user diversity even with only coarse quantization of the SIR feedback.

- Demonstrated that the proposed method of adaptive allocation and formation of groups of disjoint sub-bands can still exploit multi-user and frequency diversity even with only coarsely quantizated SIR feedback available at the transmitter.

# Chapter 6

This chapter compares diversity combining schemes for the downlink of SS-OFDM systems in frequency selective fading channels. Symbol-level combining after despreading is compared to chip-level maximal ratio combining (MRC) of signals from different diversity branches and MMSE equalization of spreading sequences. Chip-level combining combines diversity samples in an efficient manner while reducing inter-code interference that results from the loss of orthogonality of spreading sequences due to frequency selectivity. This method is shown to be superior to symbol-level combining when the diversity branches are uncorrelated, and when the branches differ only due to subcarrier interleaving. The results are relevant to antenna diversity as well as temporal diversity achieved though re-transmission within an ARQ scheme.

A MMSE equalization method with significantly reduced complexity for partially loaded systems is also presented, based on the premise of chip-level combining. The extensions of chip-level combining and low-complexity equalization of a partially loaded system to an OFDM system with 2-dimensional spreading are also shown.

This chapter includes several research contributions [79][80]:

- Equalization coefficients (for the single tap equalizer with perfect channel estimates) similar to those presented here have appeared in [5] in the context of multiple antenna systems. This thesis work is the first to show that the proposed chip-combing scheme with appropriate MMSE equalization is effective for several different scenarios including serial re-transmission, and that it is effective because it reduces inter-code interference through combining.

- Development of analytical expressions for chip-level and symbol-level combining schemes. Comparison of the two methods both analytically and by simulation.

- Development of a low-complexity equalization scheme for partially loaded systems. Results are the same as for more complex multi-user detection scheme

for certain cases, but with much simpler algorithm. In other cases of loading, the low-complexity scheme serves as an approximate solution for MMSE equalization, and is better than other sub-optimal methods.

- Extension of the proposed low-complexity equalization scheme to partially loaded systems with diversity replicas, and two-dimensional spreading with diversity replicas.

## Chapter 7

This chapter concludes the thesis and discusses possibilities for future work. The primary future research direction for the SS-OFDM methods presented in this thesis is the consideration of multiple antenna techniques with partial channel state information.

## Appendix A

This appendix discusses the channel models used in all sections of this thesis. In Appendix A.1 the ITU channel models for the indoor, pedestrian and vehicular channels are given. The channel models include a channel impulse model governing small scale fading, and path loss and shadowing parameters governing large-scale fading. Appendix A.2 discusses the generation of Rayleigh fading envelopes with accurate auto-correlation functions, while A.3 describes the method used to generate correlated shadow fading processes.

## Appendix B

The packet structures and link level simulation results for the individual packet structures are given in this section. Overhead and payload considerations are briefly discussed for the different packet structures considered in Chapters 4 and 5. Link level simulation results used in this thesis are listed in this appendix.

## Appendix C

The radiation pattern for the sectorized antennas used in Chapters 4 and 5 is shown in this appendix. The radiation pattern is from a commercially available 65° 3 dB beamwidth antenna.

## Appendix D

This appendix shows the curves for the average signal to interference and noise ratio (SINR) per scheduled transmission for the SS-OFDM-F/TA system in the indoor and pedestrian channels. The purpose of these curves is to determine the number of sub-bands required, given other SS-OFDM system parameters, in order to fully exploit the multi-user and frequency diversity of the channel. This appendix also shows the average SINR per scheduled transmission for the allocation of groups of disjoint sub-bands in the ITU Pedestrian B channel.

# Appendix E

The effect of larger quadrature amplitude modulation (QAM) constellations on the validity of the link level/system level simulation structure used in this thesis is examined. Different amplitudes within the signal constellations result in different symbol error probabilities for different symbols and also cause different levels of inter-code interference to other code channels. While different symbol amplitudes are accounted for in the link level simulations, varying inter-code interference levels due to QAM symbols on other code channels are not, and hence this approximation must be justified. A comparison of SINR curves reveals that the difference is virtually non-existent for 64 QAM signalling and the SS-OFDM-F/TA system parameters considered in this thesis.

# Appendix F

This appendix contains the derivation of the single tap per subcarrier MMSE equalization coefficient used in Chapter 6. The formula for the coefficients is found by using maximal ratio combining (MRC) of chip-level transmission replica samples, and then determining the value that minimizes the mean-square error between the transmitted and received (and MR combined) SS-OFDM symbol. A formula for the coefficient can also be found that performs both operations of MR combining and MMSE on chip level samples. This method of determining coefficients is also used in low-complexity MMSE equalization of partially loaded systems.

# Appendix G

This appendix contains a statistical significance assessment of the multi-cell simulations for Chapters 4 and 5. The reproducibility of the link and system levels is examined, and confidence intervals for the worst cases of complete multi-cell simulation reproducibility are shown.

# Chapter 2

# Spread Spectrum OFDM Systems

The purpose of this chapter is to describe the downlink of spread spectrum OFDM systems. The majority of the information presented in this chapter is intended as background information for the new work that will be presented in subsequent chapters. Radio channels used throughout this thesis are also presented in this chapter. This chapter also includes the performance comparison of SS-OFDM and DS-CDM with concatenated Walsh and Gold code sequences.

The radio channel model, and assumptions made regarding the simulation of the radio channel are presented in Section 2.1. This channel model is used throughout the thesis. Small-scale and large-scale fading assumptions are presented. In Section 2.2 the downlink of an SS-OFDM system is described. Spreading sequences and detection methods are discussed in sub-sections of Section 2.2, where the use of Walsh sequences for spreading and minimum mean-square error equalization (MMSE) for detection are of primary interest in this thesis. The chapter is concluded with the bit-error rate (BER) performance of the single cell system, and its comparison to DS-CDM systems.

## 2.1 Radio Channel

Signal distortions and time-variant attenuation due to the radio channel constitute a major challenge in wireless design. The properties of the radio channel are particularly important to multicarrier cellular communications as the wideband signal structure, orthogonal sequences, relatively long symbol durations, and long transmission distances (compared to WLAN) make the signal susceptible to small-scale and large-scale fading processes.

The channel model used is a wide-sense stationary process in that the channel changes with time and position, however the channel is static or constant over small time increments and distances. Specifically, the small-scale and large-scale fading

processes do not change over the duration of an SS-OFDM symbol. The system parameters throughout this thesis have been selected to ensure that this is an accurate assumption.

The parameters of the small and large-scale processes are governed by channel models based on ITU recommendations [24][43]. A total of 6 channel models are used in this thesis, corresponding to indoor, pedestrian, and vehicular channels, each with A and B channels. The B channel typically has a longer delay spread than the A channel. Appendix A.1 discusses the particular characteristics of each channel model.

### 2.1.1 Small-Scale Multipath Fading

Small-scale fading refers to the channel variations in time and over a frequency band due to constructive and destructive interference of signal replicas propagating over different paths from the transmitter to the receiver. This interaction results in fading that can either be flat or frequency selective. Flat fading occurs when the difference between multipath arrivals is small in comparison to the symbol/chip duration of the signal, where as frequency selective fading occurs if larger relative path delays are also present. In general, small-scale fading processes at each mobile terminal $u$ are assumed to be independent.

#### 2.1.1.1 Flat Fading

Flat fading of the signal is due the combination of unresolvable signal paths at a receiver where one or more of the transmitter, receiver, or immediate reflecting object are in motion. The paths are called unresolvable as they arrive at the receiver with relative delays much smaller than the sampling interval of signal.

Each of the unresolvable paths can be modelled a complex Gaussian process, and uniformly random phase [85]. This corresponds to the case of a non-line-of-sight (NLOS) channel. Only NLOS channels are considered in this thesis, as this is the common and limiting channel for many cellular systems. The resulting fading process due to the destructive and constructive interference of the unresolvable paths is given by a complex Gaussian random process, $\zeta(t)$. The envelope of the fading process is Rayleigh distributed. The fading process is known as flat fading as all frequencies across the signal bandwidth fade identically.

The autocorrelation function, or equivalently the power spectral density (PSD), of the flat fading process is dependent upon the speed of the moving objects, and the distribution of the arrival angles. In this thesis, the description of the spectrum of the

PSD is restricted to the spectrum shape, either *classic* or *flat*, and the maximum Doppler frequency, $f_D$. Appendix A.2 contains the details of generating the random variables and the fading autocorrelation function.

#### 2.1.1.2 Frequency Selective Fading

Frequency selective fading occurs when several signal replicas arrive at the receiver with significantly different propagation delays. The replicas are due to different signal paths from the transmitter to the receiver. The combination of delayed paths results in different channel attenuations of the signal at different frequencies. The frequency response of the channel can be modelled as either a result of a combination of a finite number of discrete transmission paths at the receiver (Section 2.1.1.2.1), or uncorrelated fading at each discrete (sampled) frequency (Section 2.1.1.2.2).

##### 2.1.1.2.1 Discrete Multipath Channel Models

As mentioned, the channel can be modelled as the arrival of several discrete signal paths at receiver. The channel impulse response in a channel with $P$ paths is given by [29][85]:

$$\psi_{multipath}(t,\tau) = \sum_{p=0}^{P-1} \zeta_{u,p}(t)\delta(\tau - \tau_p) \tag{2.1}$$

where the relative delay of the $p^{th}$ path, $\tau_p$, is measured relatively to the arrival of the first path at the receiver. $\zeta_{u,p}$ is the complex gain of the $p^{th}$ path from the transmitter to mobile user receiver $u$. Each of the $P$ paths undergoes small-scale fading. In this thesis, the complex path gains from a transmitter to a mobile user are assumed to be independent for each mobile user $u$. The corresponding time-varying frequency response of the channel is given by:

$$\Psi(f,t) = \sum_{p=0}^{P-1} \zeta_{u,p}(t)e^{-j2\pi f\tau_p} \tag{2.2}$$

If there is only 1 path, the channel is said to undergo flat fading as the magnitude of the response is the same for all frequencies, $f$. If there are multiple paths, clearly the magnitude of the channel response will change for different frequencies, and hence the channel is frequency selective. The additional frequency shift due to the Doppler shift is not included in the above equations as the Doppler shift is on the order of 5 to 200 Hz, and the frequency separation of subcarriers considered in this thesis is on the order of 10 KHz or more. The assumed net effect of the Doppler shift is a phase rotation due to the frequency offset, which is included in the complex path gain. The channel is normalized so that the expectation of the squared subchannel gains is equal to 1. This is equivalent to setting:

$$\mathrm{E}\left[\left|\Psi(t)\right|^2\right] = 1 \tag{2.3}$$

The severity of the frequency selectivity fading is dependent on the power delay profile of the channel. The power delay profile of the channel is modelled by a set of discrete paths, each with relative average power and relative delay. The six channel models used in this thesis are catalogued in Appendix A.1.

As described, frequency selective channels have different attenuations at different frequencies, and hence, the attenuation for each subcarrier of an OFDM-based symbol is different. In all cases in this thesis, it is assumed that the channel over a single narrowband subcarrier is flat, or constant. System design parameters are chosen such that the bandwidth of a subcarrier is sufficiently narrow, and ensures that this assumption is valid.

#### 2.1.1.2.2 Uncorrelated Subcarrier Fading

Uncorrelated subcarrier fading is a special case of frequency selective fading. This channel model arises from a combination of channel conditions and implementation methods. If a channel has a large number of independent paths with significantly different path delays arriving at the receiver, then the channel has a high degree of frequency diversity. If interleaving is used to separate adjacent subcarriers prior to transmission, then the fading across adjacent subcarriers will appear uncorrelated after de-interleaving at the receiver. In this case the channel can be aptly modelled as having independent fading on each subcarrier. This approximation is improved if the subcarrier frequency separation is increased by interlacing subcarriers from an unrelated transmission. This is commented on further at the end of Section 2.2.4.

### 2.1.2 Large-Scale Fading

Large–scale variations in the signal power received are due to physical attributes of the channel and physical surroundings, rather than the interaction of signal paths. The attenuation is divided into two components: shadowing and path loss. These two components are dependent on the mobiles position relative to the transmitter, and hence, are not generally included in simple single cell simulations. As majority of this thesis is concerned with multicarrier cellular systems, these radio channel properties are important to this work. The attenuation due to both factors at the $u^{th}$ mobile receiver is given by, $\xi_u(t)$, where the dependency on time relates to a mobile's position through the mobile's velocity. Each of the ITU channels has specific parameters for shadowing and path loss (see Appendix A.1). Large-scale fading is independent for each of the $U$ mobile users.

### 2.1.2.1 Shadowing

When strong or all signal paths from transmitter to the receiver are blocked by large objects such as trees, buildings, tunnels or hills, there is a sharp decrease in the received power at the mobile. The amount of attenuation due to shadowing is dependent on the mobiles position. In general, the Gundmudsen [35] log-normal correlation model is used to represent the autocorrelation function of the shadowing process with respect to changes in mobile position. This is described in detail in Appendix A.3.

### 2.1.2.2 Path Loss

Path loss models describe the rate of signal attenuation with respect to distance from the transmitter. The decay in power with respect to relative distance from the source is given by:

$$\text{Path loss} = \left( \frac{D_{mobile}}{D_0} \right)^{-\Upsilon_{PL}} \tag{2.4}$$

where $D_{mobile}$ is the distance from the transmitter to the mobile, $D_0$ is some reference distance, and $\Upsilon_{PL}$ is the path loss exponent. A value of $\Upsilon_{PL} = 2$ is free-space loss. Detailed path loss models used in this thesis are listed in Appendix A.1.

## 2.2 SS-OFDM System Description

This section describes the transmitter and receiver structures for SS-OFDM systems in a multipath frequency selective environment. Spreading sequences and equalization of spreading sequences are also discussed in this section. A simple single cell system is considered for the purposes of the section. Shadowing and path-loss attenuations are ignored so that $\xi_u(t) = 1$, for all $0 \le u \le U-1$. These large-scale fading processes will be included in following chapter where inter-cell interference (ICI) is introduced.

### 2.2.1 Transmitter

The SS-OFDM downlink transmitter is shown in Figure 2.1. $L$ spreading sequences are available for data transmission. An individual user may be allocated all, or only a subset of the $L$ codes. The length of the spreading sequence used to spread an information symbol is $L$ chips, and therefore the spreading gain is $L$. The total number of codes used for transmission during an SS-OFDM symbol is given by $K$. If all spreading sequences are used for a given SS-OFDM symbol, the system is said to be full loaded ($K = L$). In this sub-section, we will assume that the each of the $U$ users is

assigned one code channel so that $U = K$. In this system description we consider the transmission of the $k^{th}$ data stream, where $k = 0, 1, 2... K\text{-}1$. The encoded complex data symbol, $b_k$, of the $k^{th}$ data stream is spread by a spreading sequence, $\mathbf{c}_k = c_{k,0}.....c_{k,L-1}$, and is synchronously added to the other $K$-1 chip streams. The resulting sequence chip stream, $d_l$, is serial-to-parallel converted.

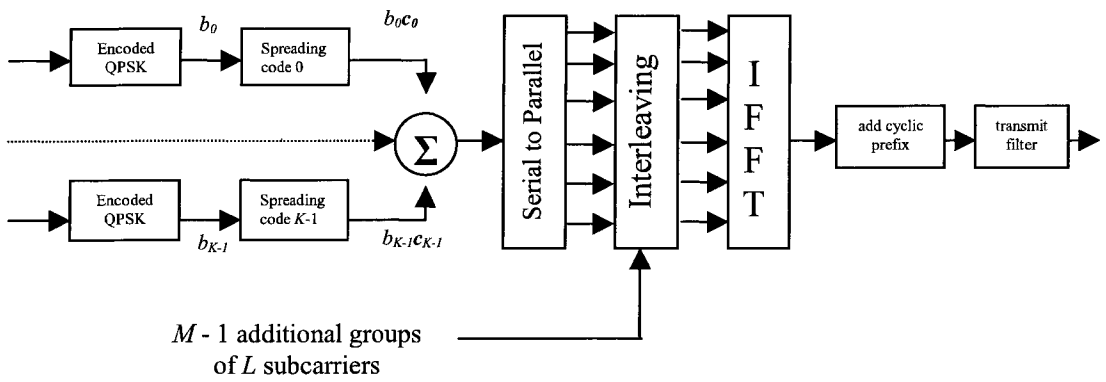


Figure 2.1. Essential operations of the SS-OFDM downlink transmitter.

The $L$ chips can be interleaved with $M - 1$ other groups of $L$ chips and mapped onto a set of $N = ML$ subcarriers via an Inverse Fast Fourier Transform (IFFT). Combining $M$ groups of spread symbols is called M&Q Modification in [52]. For now, the system with $M = 1$ is considered.

A cyclic prefix of duration $T_g$ is added to the SS-OFDM symbol [12][90]. The cyclic prefix eliminates inter-symbol interference (ISI) if its duration is greater than the maximum excess delay spread of the channel, $\tau_{\max}$. After rectangular pulse shaping, the waveform of the $i^{th}$ transmitted SS-OFDM symbol is given by:

$$s^{(i)}(t) = \sum_{l=0}^{L-1} \sum_{k=0}^{K-1} b_k^{(i)} c_{k,l} e^{j2\pi lt/T_{sym}} = \sum_{l=0}^{L-1} d_l^{(i)} e^{j2\pi lt/T_{sym}} \qquad (i-1)T_{sym} - T_g \le t \le iT_{sym} \quad (2.5)$$

where $b_k^{(i)}$ is the complex data symbol of the $k^{th}$ data stream transmitted during the $i^{th}$ SS-OFDM symbol period. The sum the $K$ spread data symbols on the $l^{th}$ subcarrier for the $i^{th}$ SS-OFDM symbol is given by $d_l^{(i)} = \sum_{k=0}^{K-1} b_k^{(i)} c_{k,l}$.

## 2.2.2 Spreading Sequences

In general, SS-OFDM uses orthogonal Walsh spreading sequences for the downlink of a wireless system. Walsh sequences are orthogonal if they are synchronous. In DS-CDM systems in multipath channels, Gold codes are used for spreading (sometimes in addition to Walsh sequences) due to advantageous asynchronous cross-correlation properties [31]

in comparison to Walsh sequences. Spreading codes on the downlink of an SS-OFDM system are inherently synchronous, and hence, the system is well suited to using orthogonal Walsh spreading sequences. The drawback of using orthogonal codes is the necessity for proper equalization in frequency selective fading channels. If the fading is not frequency selective the inter-code inference is zero. It has also been shown that these codes limit the peak-to-average power ratio (PAPR) in comparison to other orthogonal codes, particularly when the system is fully loaded ($K = L$) [71].

Walsh sequences are given by the columns of Hadamard matrix, and hence are also known as Walsh-Hadamard sequences. The $LxL$ matrix has the general recursive form (adapted from [29]):

$$\mathbf{C}_L = \frac{1}{\sqrt{2}}\begin{bmatrix} \mathbf{C}_{L/2} & \mathbf{C}_{L/2} \\ \mathbf{C}_{L/2} & -\mathbf{C}_{L/2} \end{bmatrix} = \begin{bmatrix} \mathbf{c}_0^T \cdots \mathbf{c}_{L-1}^T \end{bmatrix} \tag{2.6}$$

where $\mathbf{x}^T$ denotes the transpose of $\mathbf{x}$, $L = 2^r$, and $r$ is an integer equal to or greater than 1. In order to normalize the power of the spread sequence, the elements of the matrix are $1/\sqrt{L}$ and $-1/\sqrt{L}$.

The application of convolutional coding for the dual purpose of spreading and channel coding [108] has been proposed for SS-OFDM systems [65][96]. Maxey and Ormondroyd showed that using low-rate orthogonal convolution codes (LROCC) instead of spreading sequences for multiplexing data streams in SS-OFDM systems improves the system performance [65]. However, LROCCs can only be used for a small number of users due to the small number of codes available. This inherently limits the spectral efficiency of the system [96].

### 2.2.3 Receiver

In the simple single cell system considered, the transmitted signal is disturbed by multipath frequency selective Rayleigh fading as described in Section 2.1. The impulse response of the channel was given earlier by Equation (2.1). Additive white Gaussian noise (AWGN), $n(t)$, with a power spectral density of $N_0/2$ per dimension is also added to the signal. At the input of the $u^{th}$ receiver (Figure 2.2) the signal of the $i^{th}$ SS-OFDM symbol is given by:

$$r_{u,pre-FFT}(t) = \sum_{l=0}^{L-1} d_l e^{j2\pi lt/T_{sym}} \sum_{p=0}^{P-1} \zeta_{u,p} e^{-j2\pi l\tau_p/T_{sym}} + n(t) \tag{2.7}$$

It can be seen that the channel distortion is limited to the sum of the products of the path gains and subcarrier dependent phase shift. Hence, the net distortion due to

multipath fading can be given by a complex gain, $h_{u,l} = \sum_{p=0}^{P-1} \zeta_{u,p} e^{-j2\pi l \tau_p / T_{sym}}$, on the $l^{th}$ subcarrier at the receiver. This is because the cyclic prefix allows each of the multipath symbol replicas to span the entire receive window (Figure 2.3).

After sampling, and FFT of (2.7), the received signal can be given by:

$$r_u = \sum_{l=0}^{L-1} d_l h_{u,l} + \sum_{l=0}^{L-1} \eta_{u,l} = \sum_{l=0}^{L-1} \sum_{k=0}^{K-1} b_k c_{k,l} h_{u,l} + \sum_{l=0}^{L-1} \eta_{u,l} \tag{2.8}$$

where $\eta_{u,l}$ is the sample of the AWGN process on the $l^{th}$ subcarrier at the $u^{th}$ mobile. It has been assumed here that an ideal receiver is used; absent from phase noise, frequency offset and timing jitter. The normalization condition given by (2.3) is equivalent to $\mathrm{E}\left[\left|h_{u,l}\right|^2\right] = 1$, where the expectation is over both subcarriers and SS-OFDM symbols.

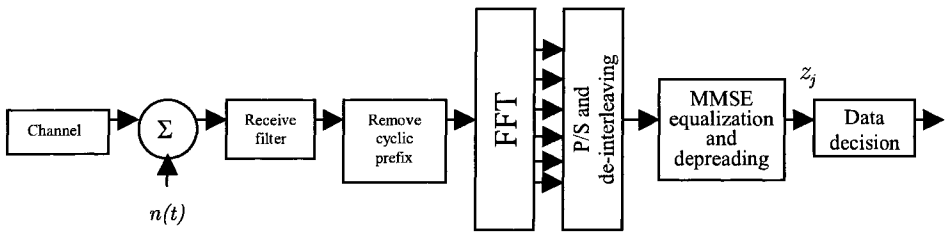


Figure 2.2 Essential operations of the SS-OFDM receiver.

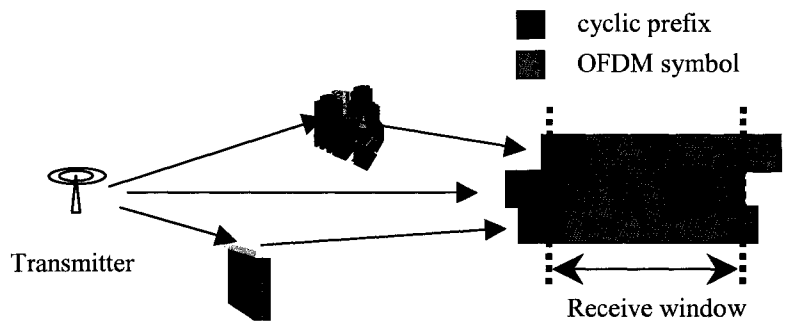


Figure 2.3. Effect of the cyclic prefix on received signal of multipath transmissions.

It can be seen that the complex subchannel coefficients, $h_{u,l} = \sum_{p=0}^{P-1} \zeta_{u,p} e^{-j2\pi l \tau_p / T_{sym}}$, are correlated in the frequency domain. The correlation is dependent on the relative path delays compared to the symbol duration $\tau_p / T_{sym}$. Note that the symbol duration, $T_{sym}$, is the inverse of the subcarrier spacing. For channels with sufficient frequency diversity, the correlation of complex subcarrier gains, $h_{u,l}$, is low. If $M>>1$ and interleaving is used, the distance between adjacent subcarriers of the same spreading sequence is further

increased, thus reducing the correlation further. In this instance, using a channel model of only independent complex channel gains such as described in Section 2.1.1.2.2 is valid.

### 2.2.4 Detection Strategies for SS-OFDM

In OFDM based systems, there is no need for frequency equalization of a given subcarrier as the fading over the bandwidth of a subcarrier is flat. In SS-OFDM systems, frequency equalization of subcarriers modulated by the same data bit is necessary to maintain orthogonality of the Walsh spreading sequences. Maintaining the orthogonality or the codes becomes increasingly important when considering systems in which all possible spreading sequences are being used (i.e. fully loaded). Zero forcing (ZF) and minimum-mean squared error (MMSE) equalization have been considered. ZF fully restores the orthogonality of the spreading sequences, however inversion of spectral nulls causes the noise to be greatly amplified prior to detection. MMSE equalization balances the inter-code interference with the amplification of noise. It has been shown [37][50][102] that MMSE has the best BER performance of the simple single-tap equalization methods, and hence, it is the equalization techniques considered throughout this work.

MMSE equalization is accomplished by minimizing the mean square error between the transmitted SS-OFDM symbol and the equalized SS-OFDM symbol. The MMSE equalization coefficient is given by [29][50][102]:

$$g_{u,l} = \frac{\hat{h}^*_{u,l}}{\left|\hat{h}_{u,l}\right|^2 + \lambda} \tag{2.9}$$

$x^*$ is the complex conjugate of $x$, and $\hat{h}_{u,l}$ is the estimate of the $l^{th}$ channel gain at the $u^{th}$ receiver. The derivation of (2.9) is discussed in Appendix F in the context of equalizing multiple signal replicas. $1/\lambda$ is the signal-to-noise ratio (SNR) of the of the entire SS-OFDM symbol. In single cell systems, $\lambda$ is given by[29][50]:

$$\lambda = \frac{\sigma^2_{noise}}{\sigma^2_{symbol}} = \frac{N_0}{(E_s K / L)} \tag{2.10}$$

where $E_s$ is the data symbol energy and $K/L$ is the system load. It can be shown that for zero-forcing equalization, $\lambda$ is equal to zero.

Note that this equalization coefficient is also valid for partially loaded systems ($K < L$), however it is not optimal. A multi-user detection (MUD) and MMSE equalization method [38], which is superior to this approach, is presented in Chapter 6 of this thesis. A simple, novel form of this MUD method and its analysis is a contribution of this thesis [79][80].

The equalized signal is given by:

$$r_{u,equalized} = \sum_{l=0}^{L-1} \sum_{k=0}^{K-1} b_k c_{k,l} h_{u,l} g_{u,l} + \sum_{l=0}^{L-1} \eta_{u,l} g_{u,l} \tag{2.11}$$

After equalization, the SS-OFDM signal is despread. Despreading the $j^{th}$ data symbol occurs by multiplying the signal by the $j^{th}$ spreading code, and summing over all subcarriers. The decision variable for the $j^{th}$ data symbol at the $u^{th}$ receiver is given by:

$$z_{u,j} = b_j \frac{1}{L} \sum_{l=0}^{L-1} h_{u,l} g_{u,l} + \sum_{l=0}^{L-1} h_{u,l} g_{u,l} \sum_{\substack{k=0 \\ k \neq j}}^{K-1} b_k c_{k,l} c_{j,l} + \sum_{l=0}^{L-1} g_{u,l} c_{j,l} n_{u,l} \tag{2.12}$$

The first term of (2.12) is the desired data symbol, the second term is the inter-code interference, and the third term is the noise. Note that if zero-forcing equalization were used and perfect channel estimation was assumed, the first term would just be $b_j$, and the second term would be zero. The use of MMSE equalization does not completely restore the orthogonality of the spreading sequences, however, it does prevent the noise term from being highly amplified when $h_{u,l}$ is very small.

Maximum ratio combining (MRC) and equal gain combining (EGC) have also been considered in literature [50], but have poorer performance than the equalization techniques simply because the orthogonality of the codes is not restored. Kaiser [52][54] showed that more complex techniques such as maximum likelihood symbol by symbol estimation (MLSSE) and sequence estimation (MLSE) give better performance, however, the performance gain of ML methods is less than 1 dB over MMSE in convolutional coded systems over realistic channels. Joint detection [46][47] and interference cancellation [53] methods have also been proposed.

## 2.3 BER Performance of SS-OFDM

The SINR of the SS-OFDM signal at a given mobile $u$ can be found from (2.12), and is given by [54]:

$$SINR_u = \frac{|b_j|^2 \frac{1}{L^2} \left| \sum_{l=0}^{L-1} h_{u,l} g_{u,l} \right|^2}{\sum_{\substack{k=0 \\ k \neq j}}^{K-1} |b_k|^2 \left( \frac{1}{L^2} \sum_{l=0}^{L-1} \left| h_{u,l} g_{u,l} - \mathrm{E}\left[ h_{u,l} g_{u,l} \right] \right|^2 \right) + N_0 \frac{1}{L} \sum_{l=0}^{L-1} |g_{u,l}|^2} \tag{2.13}$$

If all data symbols are transmitted with the same energy, $|b_k|^2 = E_s$, and the channel gain estimates are perfect, with some simplification of the expression the SINR can be given by:

$$SINR_u = \frac{\mu_{A_{u,l}}^2}{\sigma_{A_{u,l}}^2 \frac{K-1}{L} + \frac{N_0}{E_s} \mu_{B_{u,l}}} \tag{2.14}$$

in which $\mu_{A_{u,l}}$ and $\mu_{B_{u,l}}$ are the sample means of the random variables $A_{u,l}$ and $B_{u,l}$, respectively, and $\sigma^2_{A_{u,l}}$ is the sample variance of $A_{u,l}$. $A_{u,l}$ and $B_{u,l}$ are given by:

$$A_{u,l} = \frac{\left|h_{u,l}\right|^2}{\left|h_{u,l}\right|^2 + \lambda} \tag{2.15}$$

and

$$B_{u,l} = \frac{\left|h_{u,l}\right|^2}{\left(\left|h_{u,l}\right|^2 + \lambda\right)^2} \tag{2.16}$$

for $l = 0,1,2,\ldots,L\text{-}1$.

The conditional bit error rate (BER) can be found simply if the inter-code interference is assumed to be Gaussian distributed. The assumption of a Gaussian distribution is reasonable for large spreading sequences [54] due to the central limit theorem. This is because the inter-code interference is the sample variance of the $L$ equalized subcarriers gains, each of which is multiplied by a chip-sum that is itself the sum of $K$ binomial random variables (BPSK modulation). Hence, when $L$ is large the central limit theorem can be applied.

The conditional bit error rate (BER) assuming QPSK signalling is given by [84]:

$$P_b\left(error \middle| \left|h_{u,l}\right|^2\right) = \mathrm{Q}\left(\sqrt{SINR}\right) \tag{2.17}$$

using the Q-function (which is the area under the right tail of a normalized Gaussian distribution).

Equation (2.17) well approximates the performance of a SS-OFDM system with QPSK modulation in a multipath channel (ITU Indoor B), as shown in Figure 2.4. For QPSK modulation, the energy per bit $E_b$ is half of the symbol energy $E_s$. The analytical results agree with the ones from simulation for full and partial loading cases of the system.

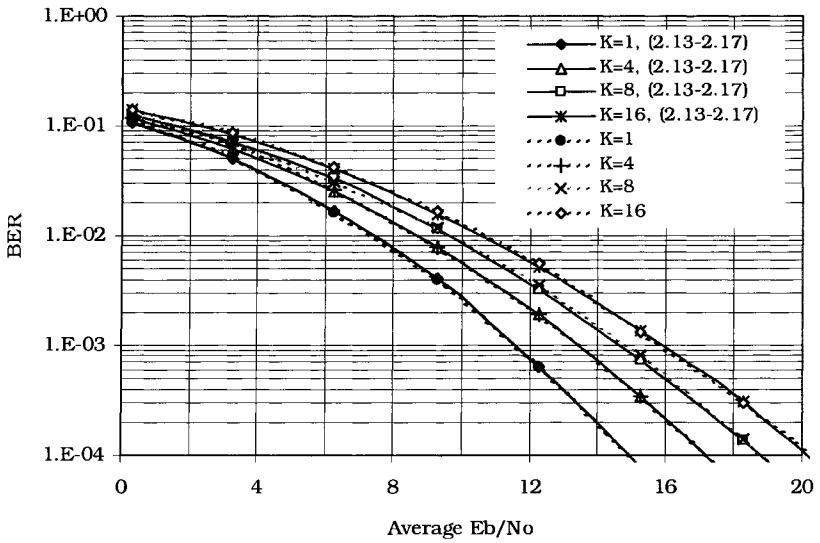


Figure 2.4. Uncoded SS-OFDM BER performance in the ITU Indoor B channel. $N$=256 subcarriers, $L$=16, $M$ = 16, $T_{sym}$= 15.625 $\mu$s, and $T_g$=1 $\mu$s. Additional energy for the cyclic prefix is included in abscissa. QPSK modulation.

## 2.4 Comparison to DS-CDM

As single carrier DS-CDM systems have dominated North American cellular standards through the present, it is worthwhile to compare SS-OFDM to this technique in some fundamental ways. As described in Chapter 1, SS-OFDM has a better BER performance than DS-CDM for fully loaded systems in multipath channels at high SINR. However for low loads and low SNR, the BERs of the two systems are quite similar. Also, previous comparisons [38][49] were pessimistic when considering the performance of DS-CDM by considering spreading with only Gold codes.

DS-CDM systems use a RAKE receiver to combine resolvable signal paths at the receiver using MRC. As each RAKE finger receives the desired signal as well as interference from the other asynchronous paths, multipath interference is introduced. A Gold code concatenated with orthogonal Walsh sequences is used for spreading to mitigate this interference. The low cross-correlation properties of the sector specific Gold code minimize the interference due to multipath. Walsh spreading sequences incident at the receiver from a single path remain orthogonal, as channel is static during the transmission of a single data symbol and the codes channels are received synchronously. In previous comparisons such as [38][49], only Gold codes are considered for spreading, which results in inter-code interference between synchronous sequences arriving at the receiver on a given transmission path.

Figure 2.5 shows the BER of a DS-CDM system found through simulation and analysis from [31] for the Indoor B channel with a 4-finger RAKE receiver. The system parameters for the SS-OFDM (as used in Figure 2.4) and DS-CDM systems are given in Table 2.1. The DS-CDM chip duration has been chosen so that all paths (given by the channel models in Appendix A.1) are resolvable by the RAKE receiver.

Previous work concluded that SS-OFDM systems out perform DS-CDM systems [37]. From the figures it can be seen that this is only true for a system with significant loading and/or high SINR. Figure 2.5 shows that the performance of DS-CDM is very similar with low loads; particularly for higher BERs. This was noted previously in [49]. Thus for low-rate coded voice systems with relatively low loading per sector, such as IS-95 systems, DS-CDM systems can may be advantageous.

For comparison a flat fading channel is considered (Figure 2.6). The SS-OFDM system has a slightly higher BER (i.e., poorer performance) than DS-CDM system due to the additional energy required for the cyclic prefix. Note that if only Gold codes are used for spreading in the DS-CDM system, irreducible inter-code interference is introduced and it maybe incorrectly concluded that DS-CDM systems perform significantly worse than SS-OFDM systems in flat fading with full loads.

The result of this comparison is the realization that the advantages of SS-OFDM are best exploited when the systems are fully loaded, and the system SINR is as high as possible (low interference). Chapters 3, 4 and 5 examine SS-OFDM system structures and algorithms to achieve these goals. This comparison also demonstrates the need for improving detection of partially loaded SS-OFDM systems. It had been shown that the performance of partially loaded SS-OFDM systems can be improved (except $K$=1) by using a multi-user detection method, of which a low-complexity version is developed in Chapter 6.

Table 2.1. DS-CDM and SS-OFDM system parameters for BER comparison

| | *DS-CDM* | *SS-OFDM* |
|---|---|---|
| Chip duration ($T_{chip}$) | 61.035 ns | N/A |
| Spreading gain ($L$) | 16 | 16 |
| Subcarriers ($N$) | 1 | 256 |
| Symbol duration ($T_{sym}$) | 9765.625 ns | 15625 ns |
| Cyclic prefix ($T_g$) | 0 | 1000 ns |
| Maximum data rate | 16.384 Mb/s | 15.398 Mb/s |

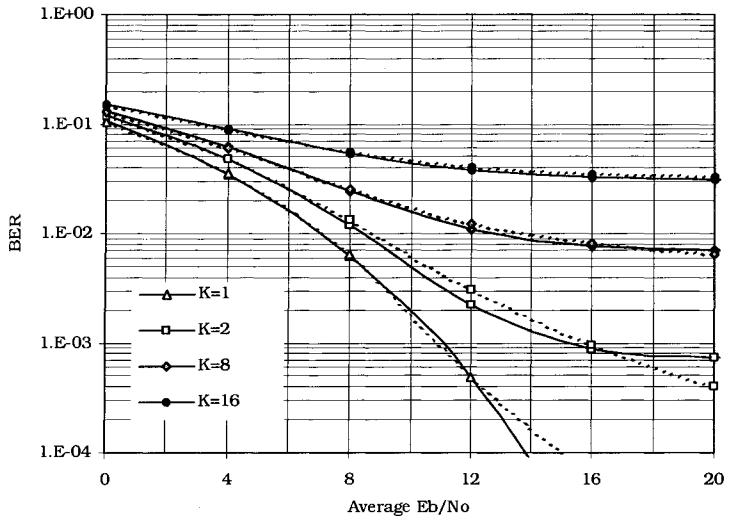


Figure 2.5. Uncoded DS-CDM BER using Gold codes concatenated with Walsh codes from simulations (dotted lines) and analytical approximation [31] (solid lines).

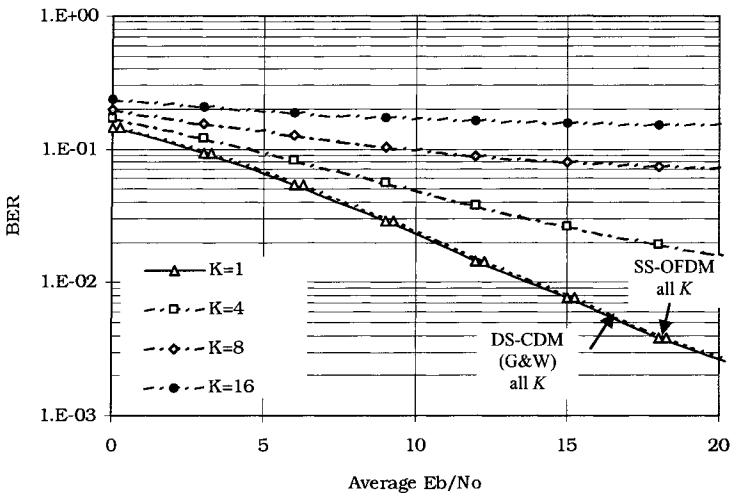


Figure 2.6. The BER of DS-CDM systems with Gold codes only (dash-dot lines), Gold codes concatenated with Walsh sequences (solid line), and an SS-OFDM system (dotted line) with QPSK signalling in a flat fading channel.

# Chapter 3

# Location Dependent Data Rate Allocation for Cellular SS-OFDM Systems

This chapter describes a new radio resource allocation algorithm for cellular SS-OFDM systems. The purpose of this scheme is to allow users near to the transmitter to receive a higher data rate. The data rate transmitted to a given user is increased by allocating additional code channels (spreading codes) to that user. This has the effect of increasing the total data throughput of the cell while only requiring only a minimal amount of additional transmit power. This algorithm is intended for delay intolerant systems such as voice communications as each user in the cell receives transmission during each SS-OFDM symbol. It also ensures a minimum average data rate for all users in the cell. This system was originally presented in [73] as a method to increase the cell throughput of SS-OFDM systems without sacrificing delay or fairness to users. Concepts used and discovered during this investigation also served as a motivation for the best-effort system described in Chapters 4 and 5.

Prior to presenting the location dependent rate assignment scheme, the first three sections give a brief discussion of the specific techniques and the difficulties involved in cellular SS-OFDM communications. Section 3.1 discusses some specific details of SS-OFDM cellular systems, including some parameters and assumptions made in the cellular model in this thesis. Section 3.2 describes inter-cell interference (ICI), which can occur from either synchronous or asynchronous interfering base station transmissions. The two models of ICI with small-scale fading used throughout this thesis, namely *explicit simulation of ICI* sources and a *composite ICI model* are then presented. This section is followed by a brief discussion of power control for SS-OFDM systems (Section

3.3), and some simple results of conventional SS-OFDM performance (Section 3.4). In Section 3.5, the location dependent rate assignment scheme for cellular SS-OFDM is presented, and analyzed in terms of throughput performance.

## 3.1 SS-OFDM Cellular Systems

Cellular systems are designed to serve mobile users in a small area or cell. The signalling to mobile users in a cell is seen as interference in neighbouring cells. In most cases this inter-cell interference (ICI) is significantly larger than the thermal noise, and hence, cellular systems are interference limited.

Typical cellular areas are irregularly shaped to properly serve specific areas within a city or along populated corridor. In rural areas with good line-of sight, macro-cells can be used to cover large areas without the cost of many transmitters. In cities, micro and pico-cells are more common, with the latter being used to service local smaller busy areas that are somewhat shadowed from the surrounding micro-cells. Even smaller hot-spots transmitters can be considered for specific sites such as bus stops or coffee shops, although WLAN connections are being considered for many of these rather than cellular services.

As this chapter considers general robust design of cellular systems, a generic and regular cell layout is considered (Figure 3.1). Each cell is hexagonal in shape, and interfering cells are immediately adjacent to the 'home' cell on all six sides. Two tiers of interfering cells are included in the model. Unlike physical layout models, no specific building or hill locations are considered as shadowing objects. Shadowing is considered a random process that changes with location as discussed in Section 2.1.2.1, and is assumed to be non-directional from the home transmitter. Uniform distribution of the users across the entire area is assumed in all cells, and in all cases, all cells are assumed to have the same average channel conditions, transmission scheme, and average transmit power.

The consequence of the last assumption is that an increase in transmit power directly translates to an increase in interference power. The schemes presented and investigated in this thesis focus on methods to make better use of the transmit power received, and to avoid ICI from adjacent cells as much as possible.

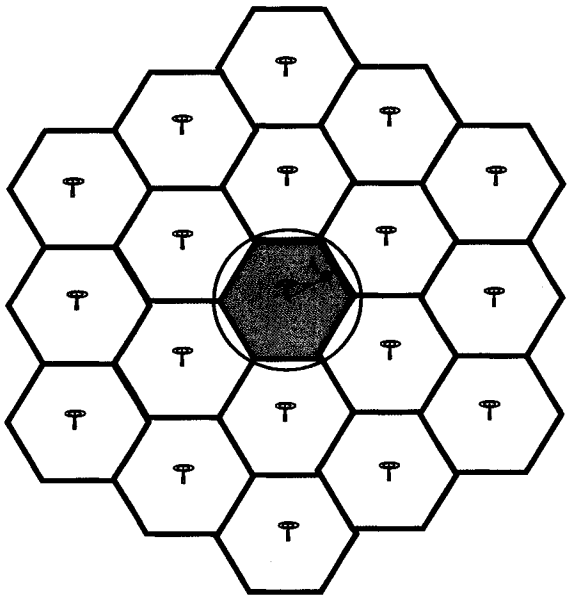

Figure 3.1. A 19-cell hexagonal cell model used in multi-cell simulations in this chapter. Each cell is centred on a base station transmitter

Transmissions from each base station are distinguished at the mobile by the use of a base station-specific pseudo-random noise (PN) sequence. These PN sequences are concatenated with the Walsh sequences, which are common to every cell. The result is that the ICI will have nearly a Gaussian distribution after despreading provided $L$ is sufficiently large, even if the desired Walsh sequence code channel is also in use in the interfering SS-OFDM symbol (see Section 3.2.1). As the same PN sequence is applied to all Walsh codes within a cell, the Walsh spreading sequences from the same transmitter remain orthogonal to each other.

The 2 and 2.5G cellular systems use soft hand-off techniques for users near the cell boundary. Unlike DS-CDMA systems that can receive transmissions from several transmitters using a RAKE receiver, special provisions must be made to allow this in SS-OFDM systems. Either the signals from the desired base stations must be strictly synchronous as described in Section 3.2.2, or two complete receiver front-ends are required to receive transmissions simultaneously from 2 transmitters. The former is similar to broadcast systems such as DVB [26], however long system durations are general assumed to facilitate synchronization, while the latter, represents a worst-case scenario as extra equipment is required. In this chapter, it is assumed that a system must transmit to all users in the cell without the aid of either soft-handoff or a second

receiver. The novel system presented in Chapters 4 and 5 overcomes this difficulty with so-called hard hand-offs appropriate for packet data using slow and fast sector selection.

## 3.2 Inter-Cell Interference (ICI)

Due to the large number of subcarriers, simulating inter-cell interference in SS-OFDM systems can be very complex. For these reasons, few cellular studies on OFDM systems have been published. In this sub-section, ICI is described for synchronous and asynchronous systems. While the form of interference is different for these two cases, both are derived assuming small-scale multipath fading for generality. In the final sub-section, small-scale fading ICI models for practical SS-OFDM simulations are described. Specifically, an explicit model that includes the simulation of small-scale fading of each ICI source and a composite ICI model are presented, along with the conditions for which they are valid. The importance of the ICI model depends upon the specific features on the system. The impacts of the models on systems considered in this thesis will be discussed in their respective chapters.

In the downlink of a SS-OFDM system, the $u^{th}$ mobile receives the desired signal given by (2.8), and also interference from $S$ - 1 other base station transmitters. Each of these interfering signals undergoes small-scale fading due to the $P$-path channel, and large-scale fading of shadowing and path loss given by $\xi_{u,s}$. The impact of the assumption that the same channel model can be applied to each interfering transmitter is discussed in the ICI model section (see Section 3.2.3). In general, the latter portion of the $(i\text{-}1)^{th}$ SS-OFDM symbol and the beginning of the $i^{th}$ SS-OFDM from the $s^{th}$ transmitter are received during the receive window of the desired signal at the mobile (Figure 3.2). The general expression for the desired signal plus interference and noise at the $u^{th}$ mobile receiver is given by [73]:

$$\begin{aligned} r_u(t) = {} & \xi_{u,0}\sum_{l=0}^{L-1} d_l h_{u,l} e^{j2\pi lt/T_{sym}} \\ & + \sum_{s=1}^{S-1} \xi_{u,s} \sum_{p=0}^{P-1} \zeta_{u,p,s} \left[ \sum_{n=0}^{L-1} d_{n,s}^{(i-1)} e^{j2\pi(t+T_{sym}-(\tau_{u,s,p}-T_g))(f_{u,p,s}+\frac{n}{T_{sym}})} + \sum_{n=0}^{L-1} d_{n,s}^{(i)} e^{j2\pi(t-\tau_{u,s,p})(f_{u,p,s}+\frac{n}{T_{sym}})} \right] \\ & + n(t) \end{aligned} \quad (3.1)$$

where $f_{u,p,s}$ is the frequency offset of the signal, and $\tau_{u,s,p}$ is the path delay relative to the receive window for the desired signal, at the $u^{th}$ receiver originating from the $s^{th}$ base station on the $p^{th}$ path. This frequency offset is due to oscillator drift or offset relative to the transmission from the desired base station. Additional frequency offset can also occur from the Doppler shift of channel as mentioned in Section 2.1.1.2.1. The corresponding

phase shifts are accounted for in the complex path gains. The value of the relative delay of the transmission from the $s^{th}$ base station of the $p^{th}$ path is bounded by $0 \le \tau_{u,s,p} \le T_{sym} + T_g$ (see Figure 3.2). The spread data is given by $d_{l,s} = \sum_{k=0}^{K-1} b_{k,s} c_{k,l,s}$, where the spreading sequence $\mathbf{c}_{k,l,s}$ is the $k^{th}$ Walsh sequence concatenated with the $s^{th}$ base station-specific PN sequence.

At the receiver, the actions of sampling and FFT subcarrier demapping are performed. MMSE equalization is used as before, however the value $\lambda$ also accounts for ICI. For equalization at the $u^{th}$ receiver, $\lambda_u$ is given by:

$$\lambda_u = \frac{\sigma_{u,I}^2 + \sigma_{noise}^2}{\sigma_{symbol}^2} = \frac{\sigma_{u,I}^2 + N_0}{\left|\xi_{u,0}\right|^2 E_s K / L} \tag{3.2}$$

where $\sigma_{u,I}^2$ is the variance of the ICI.

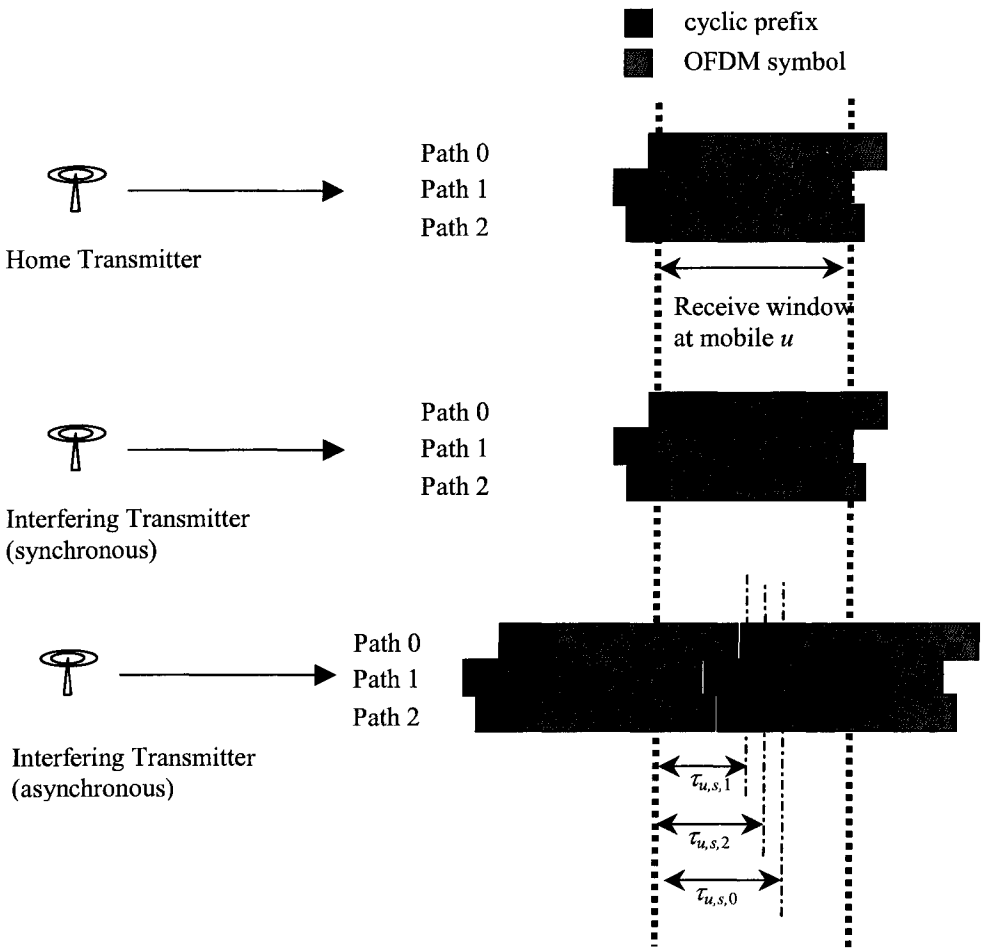


Figure 3.2. General representation of inter-cell interference.

In order to clearly express the form of the inter-cell interference, an $L$ tone filter bank is considered instead of the digital implementation (i.e., FFT operation) for subcarrier demodulation at the receiver. Given the received signal in Equation (3.1), the received signal on the $l^{th}$ subcarrier, after subcarrier demodulation can be given by:

$$\begin{aligned} r_{u,l,filtered} &= \frac{1}{T_{sym}} \int_0^{T_{sym}} r_u(t) e^{-j2\pi lt/T_{sym}} dt \\ &= \xi_{u,0} \sum_{k=0}^{K-1} b_k c_{k,l} h_{u,l} \\ &+ \frac{1}{T_{sym}} \int_0^{T_{sym}} \sum_{s=1}^{S-1} \xi_{u,s} \sum_{p=0}^{P-1} \zeta_{u,p,s} \left[ \sum_{n=0}^{L-1} d_{n,s}^{(i-1)} e^{j2\pi(t+T_{sym}-(\tau_{u,s,p}-T_g))(f_{u,p,s}+\frac{n}{T_{sym}})} + \sum_{n=0}^{L-1} d_{n,s}^{(i)} e^{j2\pi(t-\tau_{u,s,p})(f_{u,p,s}+\frac{n}{T_{sym}})} \right] dt \\ &+ \eta_{u,l} \end{aligned} \tag{3.3}$$

After equalization by $g_{u,l}$, and despreading by $\mathbf{c}_{j,l}$, the decision variable of the $j^{th}$ information bit is given by:

$$\begin{aligned} z_{u,j} &= \xi_{u,0} b_j \frac{1}{L} \sum_{l=0}^{L-1} h_{u,l} g_{u,l} + \xi_{u,0} \sum_{\substack{k=0 \\ k \neq j}}^{K-1} b_k \sum_{l=0}^{L-1} h_{u,l} g_{u,l} c_{k,l} c_{j,l} \\ &+ \sum_{l=0}^{L-1} g_{u,l} c_{j,l} \sum_{s=1}^{S-1} \xi_{u,s} \sum_{p=0}^{P-1} \zeta_{u,s,p} \left( \sum_{n=0}^{L-1} d_{n,s}^{(i-1)} \phi_{u,n,s,l,p}^{(i-1)} + \sum_{n=0}^{L-1} d_{n,s}^{(i)} \phi_{u,n,s,l,p}^{(i)} \right) \\ &+ \sum_{l=0}^{L-1} g_{u,l} c_{j,l} \eta_{u,l} \end{aligned} \tag{3.4}$$

where $\phi_{u,n,s,l,p}^{(i-1)}$ is the interference at the $u^{th}$ mobile due to the $(i\text{-}1)^{th}$ interfering symbol transmitted on the $n^{th}$ subcarrier from the $s^{th}$ base station on the $p^{th}$ path, received on the $l^{th}$ subchannel. This interference can be given by the integral:

$$\begin{aligned} \phi_{u,n,s,l,p}^{(i-1)} &= \frac{1}{T_{sym}} \int_0^{\tau_{u,s,p}-T_g} e^{j2\pi(t+T_{sym}+T_g-\tau_{u,s,p})(f_{u,p,s}+n/T_{sym})} e^{-j2\pi tl/T_{sym}} dt \\ &= \frac{e^{j2\pi(T_{sym}+T_g-\tau_{u,s,p})(f_{u,p,s}+n/T_{sym})}}{T_{sym}} \int_0^{\tau_{u,s,p}-T_g} e^{j2\pi t(n-l+f_{u,p,s}T_{sym})/T_{sym}} dt \end{aligned} \tag{3.5}$$

The interference from the $i^{th}$ interfering symbol is given by $\phi_{u,n,s,l,p}^{(i)}$, where:

$$\begin{aligned} \phi_{u,n,s,l,p}^{(i)} &= \frac{1}{T_{sym}} \int_{\tau_{u,s,p}-T_g}^{T_{sym}} e^{j2\pi(t-\tau_{u,s,p})(f_{u,p,s}+n/T_{sym})} e^{-j2\pi tl/T_{sym}} dt \\ &= \frac{e^{-j2\pi\tau_{u,s,p}(f_{u,p,s}+n/T_{sym})}}{T_{sym}} \int_{\tau_{u,s,p}-T_g}^{T_{sym}} e^{j2\pi t(n-l+f_{u,p,s}T_{sym})/T_{sym}} dt \end{aligned} \tag{3.6}$$

The exact formula for the ICI depends on whether or not the interfering signals are received synchronously (see Figure 3.2).

The decision variable given by (3.4) can also be written in the simpler form:

$$z_{u,j} = \xi_{u,0} b_j \frac{1}{L} \sum_{l=0}^{L-1} h_{u,l} g_{u,l} + \xi_{u,0} \sum_{\substack{k=0 \\ k \neq j}}^{K-1} b_k \sum_{l=0}^{L-1} h_{u,l} g_{u,l} c_{k,l} c_{j,l} + \sum_{l=0}^{L-1} g_{u,l} c_{j,l} \sum_{s=1}^{S-1} \xi_{u,s} I_{u,l,s} + \sum_{l=0}^{L-1} g_{u,l} c_{j,l} \eta_{u,l} \tag{3.7}$$

where $I_{u,l,s} = \sum_{p=0}^{P-1} \zeta_{u,s,p} \left( \sum_{n=0}^{L-1} d_{n,s}^{(i-1)} \phi_{u,n,s,l,p}^{(i-1)} + \sum_{n=0}^{L-1} d_{n,s}^{(i)} \phi_{u,n,s,l,p}^{(i)} \right)$ is the ICI received on the $l^{th}$ subchannel from $s^{th}$ transmitter, over the $P$-path channel.

### 3.2.1 Synchronous Signal Reception

Synchronous signal reception occurs when interfering signals from all base stations are received synchronously at the mobile (Figure 3.2). This implies that the propagation delay from the $s^{th}$ transmitter plus the maximum delay spread on the channel is less than the cyclic prefix duration $T_g$. In this case only the $i^{th}$ interfering SS-OFDM symbol is present in the receive window (see Figure 3.2). Furthermore, it is assumed that there is no frequency offset between the base stations so that $f_{p,s} = 0$ for all $s$ and $p$. From Equation (3.6), $\phi_{u,n,s,l,p}^{(i-1)} = 0$, and:

$$\phi_{u,n,s,l,p}^{(i)} = e^{-j2\pi\tau_{u,s,p} n / T_{sym}} \frac{e^{j2\pi(n-l)} - 1}{j2\pi(n-l)} = \begin{cases} e^{-j2\pi\tau_{u,s,p} n / T_{sym}} & \text{for } n = l \\ 0 & \text{for } n \neq l \end{cases} \tag{3.8}$$

The expression in Equation (3.4) can be simplified as only co-subcarrier interference (CSCI) appears from the interfering symbol. The simplified expression is given by [78]:

$$\begin{aligned} z_{u,j} &= \xi_{u,0} b_j \frac{1}{L} \sum_{l=0}^{L-1} h_{u,l} g_{u,l} + \xi_{u,0} \sum_{\substack{k=0 \\ k \neq j}}^{K-1} b_k \sum_{l=0}^{L-1} h_{u,l} g_{u,l} c_{k,l} c_{j,l} \\ &\quad + \sum_{l=0}^{L-1} g_{u,l} c_{j,l} \sum_{s=1}^{S-1} \xi_{u,s} \sum_{p=0}^{P-1} \sum_{n=0}^{L-1} d_{n,s}^{(i)} \zeta_{u,s,p} \phi_{u,n,s,l,p}^{(i)} + \sum_{l=0}^{L-1} g_{u,l} c_{j,l} \eta_{u,l} \\ &= \xi_{u,0} b_j \frac{1}{L} \sum_{l=0}^{L-1} h_{u,l} g_{u,l} + \xi_{u,0} \sum_{\substack{k=0 \\ k \neq j}}^{K-1} b_k \sum_{l=0}^{L-1} h_{u,l} g_{u,l} c_{k,l} c_{j,l} \\ &\quad + \sum_{l=0}^{L-1} g_{u,l} c_{j,l} \sum_{s=1}^{S-1} \xi_{u,s} d_{l,s}^{(i)} h_{u,l,s} + \sum_{l=0}^{L-1} g_{u,l} c_{j,l} \eta_{u,l} \end{aligned} \tag{3.9}$$

where the complex channel gain of the interfering signal at the $u^{th}$ mobile, from the $s^{th}$ base station on the $l^{th}$ subcarrier (using the result of Equation (3.8)) is $h_{u,l,s} = \sum_{p=0}^{P-1} \zeta_{u,s,p} \phi_{u,n,s,l,p}^{(i)} = \sum_{p=0}^{P-1} \zeta_{u,s,p} e^{-j2\pi\tau_{u,s,p} l / T_{sym}}$. The implication of this result is that the power of the ICI at the receiver is different for each subcarrier for a given channel realization (i.e. set of $h_{u,l,s}$). The power of the ICI differs significantly for different subcarriers due to small-scale frequency selective fading of the interfering signal. As

channel changes due to motion of the mobile user, the values of the complex channel gains $h_{u,l,s}$ will also change. The long-term average (i.e., very many channel realizations) of the ICI is the same for each subcarrier.

It should be noted that the interfering data symbols on each subcarrier are distorted by only the complex gain of the channel (different for each transmitter) and the attenuation due to shadowing and path loss at time $t$. Over small frequency bands in which the correlation of the subcarriers gains is high, it is possible to use codes orthogonal to one another for different transmitters. In these cases, the set of $L$ orthogonal sequences used for transmission is divided among a group of transmitters or base stations. Code sharing between transmitters can be used to significantly reduce ICI in special cases.

The importance of using specific long PN sequences for base station identification as discussed in Section 3.1 can also be seen in this case. If the desired Walsh code channel is also in use in the interfering signal, it will also be despread at the transmitter and substantially impair reception. In fact, it would be difficult to determine which transmission is the desired one.

### 3.2.2 Asynchronous Reception of Interfering Signals

Synchronous base station operation is an idealized assumption that assumes perfect frequency synchronization of interfering signals, as well as synchronization of interfering signals in time. If the ICI is not received synchronously, inter-subcarrier interference (ISCI) is introduced in addition to CSCI. The ISCI and the CSCI from the $(i\text{-}1)^{th}$ interfering symbol are given by [73][78]:

$$\phi_{u,n,s,l,p}^{(i-1)} = \frac{e^{j2\pi(T_{sym}+T_g-\tau_{u,s,p})(f_{u,p,s}+n/T_{sym})}}{T_{sym}} \int_0^{\tau_{u,s,p}-T_g} e^{j2\pi t(n-l+f_{u,p,s}T_{sym})/T_{sym}} dt$$

$$= \begin{cases} \dfrac{e^{j2\pi(T_{sym}+T_g-\tau_{u,s,p})(f_{u,p,s}+\frac{n}{T_{sym}})}}{e^{-j\pi(\tau_{u,s,p}-T_{sym})\frac{(n-l+f_{u,p,s}T_{sym})}{T_{sym}}}} \dfrac{\sin\left(\pi(\tau_{u,s,p}-T_g)\dfrac{(n-l+f_{u,p,s}T_{sym})}{T_{sym}}\right)}{\pi(n-l+f_{u,p,s}T_{sym})}, & n \neq l,\ \tau_{u,s,p} > T_g \\ e^{j2\pi(T_{sym}+T_g-\tau_{u,s,p})(f_{u,p,s}+n/T_{sym})} e^{j\pi(\tau_{u,s,p}-T_g)f_{u,p,s}} \dfrac{\sin(\pi f_{u,p,s}(\tau_{u,s,p}-T_g))}{\pi f_{u,p,s}T_{sym}}, & n = l,\ \tau_{u,s,p} > T_g \\ 0 & n \neq l,\ \tau_{u,s,p} \leq T_g \\ 0 & n = l,\ \tau_{u,s,p} \leq T_g \end{cases} \quad (3.10)$$

If $f_{u,p,s}$=0, then the $n=l,\ \tau_{u,s,p} > T_g$ case becomes $e^{j2\pi(T_{sym}+T_g-\tau_{u,s,p})(n/T_{sym})}(\tau_{u,s,p}-T_g)/T_{sym}$. Similarly, the ISCI and CSCI from $i^{th}$ interfering symbol are:

$$\phi^{(i)}_{u,n,s,l,p} = \frac{e^{-j2\pi\tau_{u,s,p}(f_{u,p,s}+n/T_{sym})}}{T_{sym}} \int_{\tau_{u,s,p}-T_g}^{T_{sym}} e^{j2\pi t(n-l+f_{u,p,s}T_{sym})/T_{sym}} dt$$

$$= \begin{cases} e^{-j2\pi\tau_{u,s,p}(f_{u,p,s}+\frac{n}{T_{sym}})} \left[ \dfrac{e^{j\pi(n-l+T_{sym}f_{u,p,s})}\sin(\pi(n-l+f_{u,p,s}T_{sym}))}{\pi(n-l+f_{u,p,s}T_{sym})} - \dfrac{e^{j\pi(\tau_{u,s,p}-T_g)\frac{(n-l+f_{u,p,s}T_{sym})}{T_{sym}}}\sin(\pi(\tau_{u,s,p}-T_g)(n-l+f_{u,p,s}T_{sym})/T_{sym})}{\pi(n-l+f_{u,p,s}T_{sym})} \right] & n \neq l,\ \tau_{u,s,p} > T_g \\ e^{-j2\pi\tau_{u,s,p}(f_{u,p,s}+\frac{n}{T_{sym}})} \left[ \dfrac{e^{j\pi T_{sym}f_{u,s,p}}\sin(\pi f_{u,p,s}T_{sym})}{\pi f_{u,p,s}T_{sym}} - \dfrac{e^{j\pi(\tau_{u,s,p}-T_g)f_{u,s,p}}\sin(\pi f_{u,p,s}(\tau_{u,s,p}-T_g))}{\pi f_{u,p,s}T_{sym}} \right] & n = l,\ \tau_{u,s,p} > T_g \\ 0 & n \neq l,\ \tau_{u,s,p} \leq T_g \\ 1 & n = l,\ \tau_{u,s,p} \leq T_g \end{cases} \tag{3.11}$$

If $f_{u,p,s}$=0, then the $n=l,\ \tau_{u,s,p} > T_g$ case becomes $e^{-j2\pi\tau_{u,s,p}\frac{n}{T_{sym}}}(T_{sym}+T_g-\tau_{u,s,p})/T_{sym}$.

It is useful to examine the interference of a signal from the $s^{th}$ transmitter on the $p^{th}$ path alone. The contribution of the ISCI and CSCI to the total interference for a given subcarrier is shown in Figure 3.3. It can be seen that the maximum contribution of the ISCI is 50% of the total interference power on any given subcarrier. Further, from (3.10) and (3.11) it can be seen that the interference power dispersed onto the other subchannel decreases rapidly with value of $|l\text{-}n|$. While subcarrier data may be spread over several subchannels at the receiver due to asynchronous reception, the power of the ICI may still differ significantly for different subcarriers due to the frequency selective fading channel for a single channel realization (i.e. set of $\zeta_{u,s,p}$ and $\tau_{u,s,p}$), provided that relative path delays and frequency offsets do not change fast (relative to the frame duration).

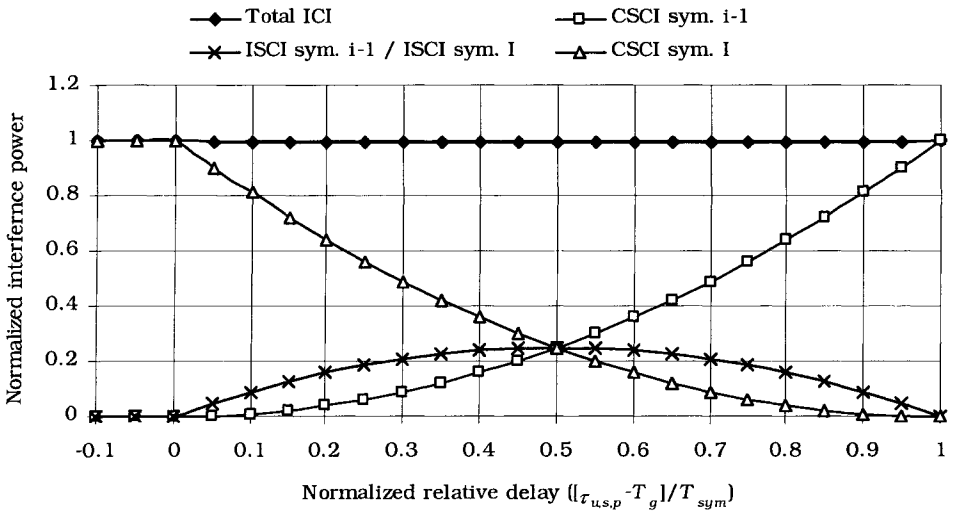


Figure 3.3. The relative contributions of co-subcarrier and inter-subcarrier interference from the $i^{th}$ and $(i\text{-}1)^{th}$ interfering symbols. $N$=256, and the cyclic prefix is $T_g$=0.1$T_{sym}$.

### 3.2.3 Small-Scale Fading ICI Models

Two models are considered for the frequency spectrum and fading of the inter-cell interference at a given mobile receiver: one in which the ICI components arriving at the mobile receiver from all interfering transmitters are simulated *explicitly*, and another that approximates the *composite* ICI from all interfering sources. In either case, it should be noted that these models refer to the ICI received on each subcarrier in the presence of small-scale fading only. Shadowing and path loss of each interfering signal are accurately modelled based on the position and change of position of the mobile as described in Section 2.1.2. In addition, regardless of the small-scale assumptions for the fading envelope of the ICI, the underlying interfering data symbols after despreading of the desired signal are assumed to be Gaussian distributed due to the effect of the symbol modulation and concatenated spreading sequences, in the same manner that inter-code interference is assumed to be Gaussian distributed (see Section 2.3).

When the first ICI model is applied, the ICI components are explicitly simulated as received from several interfering sources over statistically identical and independent frequency selective multipath fading channels. For a given ICI source, the received ICI may be different for different subcarriers due to the recombination of signal replicas from different paths with different relative delays at the receiver, which results in frequency selective fading of the ICI. In this ICI model, it is also assumed that the channel from each interfering transmitter is statistically the same as the channel for the desired signal

in the home cell/sector. The ICI is only different for each subcarrier when observed over short time intervals (SS-OFDM symbol or time slot) during which the channel varies only slightly. This ICI model assumes small-scale fading on each interfering channel, from each interfering transmitter, and hence the model is referred to as the *explicit simulation of the ICI* to clearly separate it from the other ICI model. As was shown, both synchronous and asynchronous ICI scenarios can lead (over short time intervals) to ICI received with different powers for different subcarriers. However it is most convenient to use a portion of the result in (3.9) to describe the interference. It is useful to view the channel during a short time interval $\upsilon$, which is short enough so that the channel does not change. The ICI at some time index $\upsilon$ on the $l^{th}$ subcarrier is given by a Gaussian distributed random variable (due to modulation and spreading of the interfering signal) with variance:

$$\sigma^2_{ICI-\text{explicit}}(\upsilon, l) = \sum_{s=0}^{S-1} \frac{P_{cell,s}}{L} \left|\xi_{u,s}(\upsilon)\right|^2 \left|h_{u,l,s}(\upsilon)\right|^2 \tag{3.12}$$

where (similar to Section 3.2.1) $h_{u,l,s}(\upsilon) = \sum_{p=0}^{P-1} \zeta_{u,s,p}(\upsilon) e^{-j2\pi\tau_{u,s,p} l / T_{sym}}$ is the complex channel gain on the signal from the $s^{th}$ transmitter at the $u^{th}$ receiver, received on the $l^{th}$ subcarrier at some time interval $\upsilon$. The factor of $1/L$ arises from the spreading gain of the signal as

$$\sigma^2_{d^{(i)}_{l,s}} = \underset{-\infty \le i \le \infty}{\mathrm{E}} \left[ \left| d^{(i)}_{l,s} \right|^2 \right] = \underset{-\infty \le i \le \infty}{\mathrm{E}} \left[ \left| \sum_{k=0}^{K-1} b^{(i)}_{k,s} c_{k,l,s} \right|^2 \right] = \frac{P_{cell,s}}{L} \tag{3.13}$$

where the transmit power of the $s^{th}$ base station has been denoted as $\sum_{k=0}^{K-1} \left| b^{(i)}_{k,s} \right|^2 = P_{cell,s}$. Note that $\xi_{u,s}(\upsilon)$ and $h_{u,s,p}(\upsilon)$ do not change during $\upsilon^{th}$ time interval. The complex path gains $\zeta_{u,s,p}(\upsilon)$ change for different time intervals $\upsilon$, and are complex Gaussian processes as discussed in Section 2.1.1, while $\xi_{u,s}(\upsilon)$ is a sample of the large-scale fading process (see Section 2.1.2). Clearly, the short-term power spectrum of the ICI changes for different $\upsilon$ due to frequency selective fading on paths from the $s^{th}$ transmitter to the $u^{th}$ receiver.

The second model approximates the sum of all ICI components from all interfering sources, and hence is called the *composite ICI model.* The composite ICI model assumes that the sum of all ICI components from all interfering sources can be modelled as a single white Gaussian process, with average power equal to the sum of the average powers of all ICI components. This model can be used to approximate the case of many independent ICI sources, received over frequency selective or flat fading channels, when average received powers are similar. Large-scale fading processes from each interfering

source are still applied in this model. For this model, the ICI at some time index $\upsilon$ on the $l^{th}$ subcarrier is given by a Gaussian distributed random variable with variance:

$$\sigma^2_{ICI-\text{composite}}(\upsilon, l) = \sum_{s=0}^{S-1} \frac{P_{cell,s}}{L} \left|\xi_{u,s}(\upsilon)\right|^2 \tag{3.14}$$

Clearly, the process has the same power for each subcarrier (even during the interval $\upsilon$) as there is no dependence on $l$.

In Chapters 3, 4, and 5, inter-cell interference is generally modelled by the *composite ICI model*, affected by large-scale fading processes. Explicit simulation of the ICI from each source with small-scale frequency selective fading is also used for comparison in Chapter 4 and 5. It is shown that using the approximate composite ICI model represents the worst-case scenario in terms of throughput for the opportunistic scheduling system considered in Chapters 4 and 5.

## 3.3 Power Control

The objective of power control is to mitigate the effect of channel fading on the received signal power at a given mobile. Without power control, successful transmissions to a mobile user during a deep fade may be very difficult, and hence it is necessary for reliable circuit switched data transmissions such as voice calls. Power control is of critical importance on the uplink of CDMA cellular systems, but also improves the performance on the downlink. The goal of power control on the downlink is to allocate only enough power to a given user/code channel to ensure a target $\text{SINR}_t$ at the receiver. Power control functions by allocating enough power to reach the target $\text{SINR}_t$ in order to ensure a given quality of service, and reducing the power allocated if the target $\text{SINR}_t$ is exceeded in order to minimize the transmit power, and hence interference to surrounding cells. Fast and slow power control are considered in this chapter.

Slow power control on the downlink adjusts the transmit power to a given user so that the average SINR is kept at a constant level given some quality of service constraints. While the reasons for keeping the SINR from falling below a certain level are obvious, the power level should be lowered if the SINR is higher than required to conserve the transmit power so that the interference to adjacent cells is limited. Power can also be distributed to another user whose received SINR is below its required SINR. Slow power control combats the effect of large-scale fading, namely shadowing and path loss.

Fast power control is intended to mitigate the effects of small scale fading. The SINR is frequently measured at the mobile to determine whether more power is required. If so,

a request for more power is issued to the transmitter. Decreasing the transmit power to a mobile is the default operation for the transmitter during each update cycle. Note that even with fast power control, subcarrier fading still occurs (as given by the complex channel gain) $h_{u,l}$, however the average of the squared channel gains in each symbol, $\alpha_{u,t} = \frac{1}{L}\sum_{l=0}^{L=1}\left|h_{u,l}\right|^2$, is equal to one. Hence, the operation of fast power control for SS-OFDM symbols is for the whole SS-OFDM, and not per subcarrier.

The size of the power control increments is important to the functionality of fast power control. Small increments will not be able to properly track fading at increased mobile speeds, while larger increments cause significant volatility in the signal power and increase the error in cases where the power control command is in error, or is out-dated. Increments of 0.5 dB or 1 dB have been found to be appropriate for most applications [2][94][109]. The frequency of the fast power control commands is as high as 800 Hz for second-generation (2G) systems [99].

In ideal cases, power control is assumed perfect and the effects of the channel are eliminated, with the exception of frequency-selective fading (in OFDM systems), leaving only noise. In practice, this assumption is optimistic and some error is assumed. The error is measured as the difference between the received SINR and the target $SINR_t$, which is set by some quality of service requirement. The error in dB is assumed to have a log-normal distribution [2][109]. Figure 3.4 shows the distribution of the received SIR error due to power control errors for the simulation of an SS-OFDM system in the ITU Indoor B channel (Rayleigh fading) with a 5 Hz maximum Doppler shift. Fast power control is used and perfect SIR and channel estimation are assumed. The distribution of the error in the received SIR around the target SIR is log-normal for a small power control increment of 0.25 dB, however, for larger increments (0.5 dB and 1.0 dB) the error approaches a log-uniform distribution. Power control in this example performs very well as all the estimates are perfect, the frequency of the power control commands is high and the maximum Doppler shift is low. Shadowing is also not considered. In more realistic investigations with imperfect signal estimation, shadowing and higher mobile speeds, the performance of slow and fast power control systems combined is significantly worse. The standard deviation of the distribution has been estimated at 1.5 to 2.1 dB [109], which is supported by experimentally measured values for the standard deviation of 1.5 to 2.5 [109][110[111].

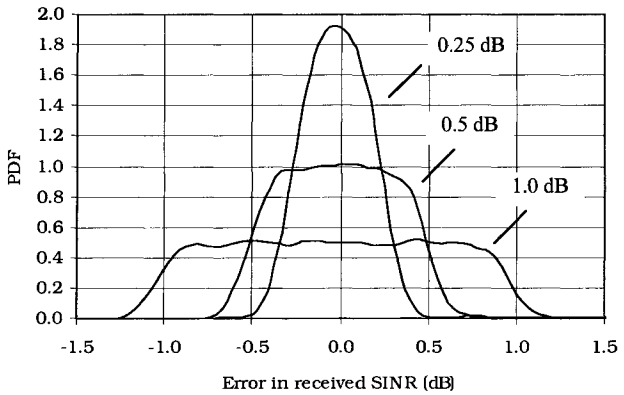


Figure 3.4. Error in received SINR for a 5 Hz Doppler shift channel with 800 Hz fast power control with different increments.

The per user power control gain for the $u^{th}$ user from the $s^{th}$ base station is defined as $\rho_{u,s}$. Power control for a given ($u^{th}$) user compensates for the losses due to the estimated large-scale fading (which is path loss and shadowing) and average subchannel gains such that $\rho_{u,s} = 1/(\hat{\alpha}_{u,s}\hat{\xi}_{u,s})$, where $\hat{\alpha}_{u,s}$ is the estimate of the average subchannel gain of a signal from the $s^{th}$ transmitter for the $u^{th}$ user. As $\alpha$ and $\xi$ change with time, the error in power control for a given SS-OFDM symbol is $\Delta_u = \rho_{u,s}(\alpha_{u,s}\xi_{u,s})$. The decision variable (which was originally given in (3.4)) for the $j^{th}$ spreading code channel received by the $u^{th}$ user for a given symbol can be re-written as:

$$\begin{aligned} z_{u,j} = {} & \frac{\Delta_u}{\alpha_u} b_j \frac{1}{L} \sum_{l=0}^{L-1} h_{u,l} g_{u,l} + \xi_{u,0} \sum_{\substack{k=0 \\ k \neq j}}^{K-1} \rho_u b_k \sum_{l=0}^{L-1} h_{u,l} g_{u,l} c_{k,l} c_{j,l} \\ & + \sum_{l=0}^{L-1} g_{u,l} c_{j,l} \sum_{s=1}^{S-1} \xi_{u,s} \sum_{p=0}^{P-1} \zeta_{u,s,p} \left( \sum_{n=0}^{L-1} \sum_{k=0}^{K-1} \rho_{k,s} c_{k,s} b_{k,s}^{(i-1)} \phi_{u,n,s,l,p}^{(i-1)} + \sum_{n=0}^{L-1} \sum_{k=0}^{K-1} \rho_{k,s} c_{k,s} b_{k,s}^{(i)} \phi_{u,n,s,l,p}^{(i)} \right) \\ & + \sum_{l=0}^{L-1} g_{u,l} c_{j,l} \eta_{u,l} \end{aligned} \tag{3.15}$$

where the large-scale fading of the desired signal has been replaced by the power control error. In this case it has been assumed that each user is assigned a single code channel, so that information to the $u^{th}$ user is transmitted on the $j^{th}$ Walsh sequence. In addition, the denominator of the MMSE equalization coefficient must also take into account the total symbol power including the various powers of each spreading code in use in the symbol, and hence, equation (3.2) becomes

$$\lambda_u = \frac{\sigma_I^2 + \sigma_{noise}^2}{\sigma_{symbol}^2} = \frac{\sigma_I^2 + N_0}{\left|\xi_u\right|^2 \sum_{k=0}^{K-1} \rho_u{}^2 \left|b_k\right|^2 / L} \tag{3.16}$$

## 3.4 Conventional Cellular SS-OFDM Performance

In the original SS-OFDM design [28][116[117], the use of spreading is intended for diversity across the entire transmission bandwidth. In addition, it is assumed that all users must receive transmission in each SS-OFDM symbol due to delay sensitive data. In this thesis, this is referred to as a conventional SS-OFDM system. Multiplexing the users' signals is done solely by code-division. The primarily limiting factor with such conventional systems on the downlink is the mobile with the worst average channel conditions. This mobile is located on or near the cell boundary.

In order to demonstrate the difficulties in achieving high spectral efficiencies with this system, it is useful to develop a highly simplified model for approximate performance measures. Perfect power control, simple white Gaussian ICI, no shadowing, and no thermal noise are assumed, and only the SINR of the $i^{th}$ code channel (a specific Walsh sequence) is examined. The SINR for the $i^{th}$ code channel transmitted to the $u^{th}$ user can be expressed as (using the previous results from:

$$SINR_{u,i} = \frac{P_i \mu_{A_{u,l}}^2}{\sigma_{A_{u,l}}^2 \frac{P_{cell} - P_i}{L} + \mu_{B_{u,l}} \frac{I_{u,ICI}}{L\xi_{u,0}^2}} = \frac{P_i \mu_{A_{u,l}}^2}{\sigma_{A_{u,l}}^2 \frac{P_{cell} - P_i}{L} + \mu_{B_{u,l}} P_{cell} \frac{\sum_{s=1}^{18} \xi_{u,s}^2}{L\xi_{u,0}^2}} \tag{3.17}$$

where, as in Chapter 2, $\mu_{A_{u,l}}$ and $\mu_{B_{u,l}}$ are the sample means of the random variables $A_{u,l}$ and $B_{u,l}$, respectively, and $\sigma_{A_{u,l}}^2$ is the sample variance of $A_{u,l}$. $A_{u,l}$ and $B_{u,l}$ are given by (2.15) and (2.16). In this simple model, $\lambda = \sigma_{ICI}^2 / \sigma_{sym}^2 = I_{u,ICI} / \left(\xi_{u,0}^2 P_{cell}\right)$, and $\frac{1}{L}\sum_{l=0}^{L-1} \left|h_{u,l}\right|^2 = 1$ for each SS-OFDM symbol due to perfect power control. Each cell transmits the same average power, $P_{cell,s} = \sum_{k=0}^{K-1} \rho_{k,s} \left|b_{k,s}\right|^2$. The value of $I_{u,ICI}$ is the sum of the 18 interfering cell transmit powers $P_{cell}$, each attenuated by path loss over the distance from the interfering transmitter to the $u^{th}$ mobile

$$I_{u,ICI} = \frac{P_{cell}}{L}[\xi_{u,1}^2 + \xi_{u,2}^2 \cdots \xi_{u,18}^2] \tag{3.18}$$

where the factor of $1/L$ arises from the spreading gain of the signal (as in (3.13)).

The transmit power on the $i^{th}$ code channel to the $u^{th}$ user, $P_i$, changes due to fast power control, however, in this highly simplified model it is assumed that these changes in $P_i$ are very small relative to the average value of $P_i$ transmitted to a mobile location near the cell boundary (where path loss and inter-cell interference are large). The approximation of only small relative changes in $P_i$ due to fast power control is more

reasonable in channels with a large degree of frequency diversity. Thus for simplicity, for the results given in Figure 3.5 it is assumed that the fraction of the total transmit power allocated to the $i^{th}$ code channel $P_i/P_{cell}$ remains relatively constant. This approximation, along with the absence of shadowing, result in this model giving BER values that can be very optimistic. QPSK signalling, uncorrelated subcarrier fading, and a path loss exponent of 3 are used in Figure 3.5

Figure 3.5 shows the BER of a QPSK system for a user at different distances from the transmitter on a path that is perpendicular to one of the cell faces (see point A, Figure 3.1). The processing gain in this system is assumed to be $N = L = 32$ subcarriers, and the inter-code interference is assumed to be Gaussian distributed in all cases. The 4 curves show the performance for different portions of the cell power being allocated to the $i^{th}$ code channel, $P_f = P_i / P_{cell}$, whereas the remaining power is allocated to other code channels in the cell. It can be seen that it is exceedingly difficult to transmit to users near the cell boundary. In particular, a user must receive 25 % of the cell power over a single code channel to achieve an average BER of $10^{-2}$ at the cell boundary, even in this simple highly optimistic model. As another example, if a single user at 80% of the distance to the cell boundary requires the resources of 20 code channel data streams, a BER of only $10^{-2}$ is possible, and leaves no resources for other user in the cell. Clearly, transmitting reliably to a user at or near the cell boundary requires significant cell resources. It should also be noted that transmitting reliably to a user a distance 0.5 $r_{face}$ from the transmitter requires very little power resources. This property is exploited in a more complete cellular model in Section 3.5.

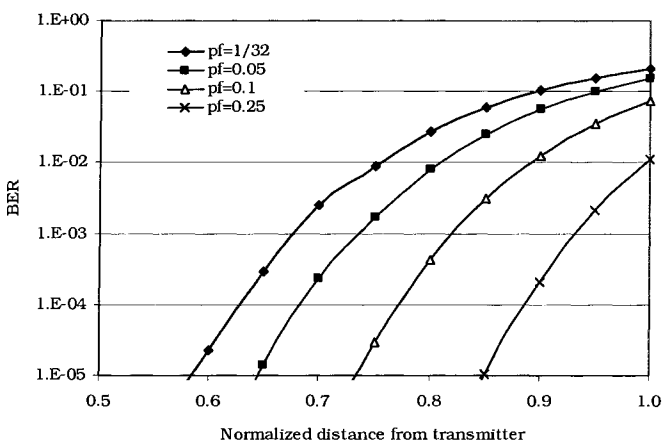


Figure 3.5. The BER of the $i^{th}$ code channel that has been allocated a portion of the total transmit power, $P_f = P_i/P_{cell}$, at the $u^{th}$ user terminal located various normalized distances from the home transmitter.

## 3.5 Location Dependent Rate Assignment

This section proposes a location-dependent rate assignment scheme for SS-OFDM as the downlink of an OFDM-CDMA cellular system [73]. The purpose of the scheme is to allow users near the base station a larger share of the possible code channels, and limit users near the cell boundary to only a few code channels. In this multi-code system, a user may be allocated 1 or more code channels, and hence $U \leq K$. In general, transmissions to users close to the base station are more power efficient due to their proximity to the desired transmitter and distance from interfering transmitters. By using less power to transmit bits to nearby users rather than distant users, the total transmit power, and therefore the inter-cell interference (ICI) generated, is decreased. The goal of this scheme is to increase the overall cell throughput.

### 3.5.1 Annular Service Zones

The cell is divided into $Z$ annular service zones in which the maximum data rates assigned decrease with distance from the transmitter. Intuitively, the ideal zone data rate assignment would be directly related to the ratio of power received by a mobile (for a fixed transmit power) to the average ICI at the mobile's location. This decreases with distance to a power slightly greater then the path loss exponent, and hence the disparity between transmission rates of users in the cell becomes extreme. Annular zone structures are designed with the goal of maximizing the data rate, while ensuring reasonable fairness to users in the cell.

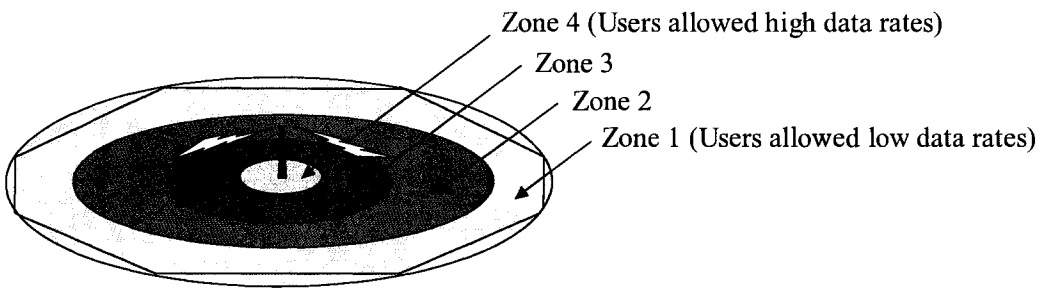


Figure 3.6. Annular zone layout (1 cell). The maximum data rate in each zone is fixed.

In the zoning schemes, the cell area is dived into concentric annular rings, each of different thickness. Maximum data rate in each ring is set, with the innermost annulus having the maximum data rate and the outermost one having the lowest maximum data rate. Figure 3.6 illustrates the annular ring layout. As mentioned, the purpose of the zones is to increase the data throughput of the cell in a manner that causes the total average transmit power to increase the least. The solution to this is to increase the data rate to nearest user. This location-dependent solution is valid as the average SINR of the mobiles decreases monotonically with distance from the transmitter.

As mentioned, this is a multi-code system in which each user is assigned 1 or more spreading code channels. Data rates to a given user are increased and decreased by assigning more or less code channels to the user. By constraining the maximum rate, or equivalently the number of codes, of the outmost zone some radio resources are reserved for other users near the cell. This set-up allows users far away from the transmitter to still receive transmissions, but allow those users to have a monopoly of the radio resources. Those users near the cell are also assigned a maximum data rate, as it would be possible to serve only these users by assigning all the codes channels to them. In this system, all users must receive data on at least 1 code channel.

In order to compare zoning schemes fairly, the following conditions are set for annular ring design:

1. The average of the maximum data rate per cell per user, given by (3.19), assuming a uniform user distribution, must be the same for all schemes.

$$\bar{R}_{cell} = \sum_{z=1}^{Z} R_z \left[ \left( \frac{z}{Z} \right)^{2\varphi} - \left( \frac{z-1}{Z} \right)^{2\varphi} \right] \tag{3.19}$$

   The zone-rate relationship in (3.19) is discussed later in this section, and illustrated in Figures 3.7 and 3.8.

2. The maximum data rate of the outer-most annulus is the same for all annular zone structures.

The first condition ensures that if no inter-cell interference or noise was present so that the maximum rates could be assigned to each user in their respective zones, then the average data throughput for all schemes would be the same. Hence, the difference between the schemes is due to the way in which the transmit power and code channels are allocated. Note that $R_Z$ is the *maximum* zone data rate, and in general the data rate delivered to a user in that zone will be less than this value due to channel conditions, and transmit power limitations.

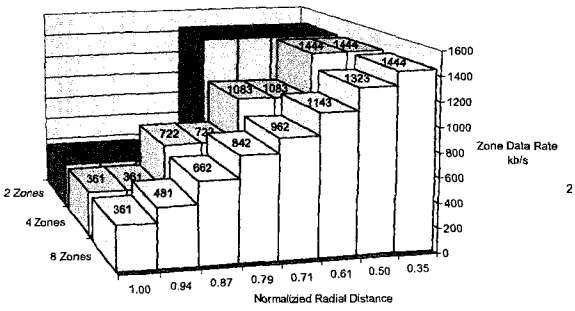


Figure 3.7a. Indoor system zone layout for $\varphi = 1/2$.

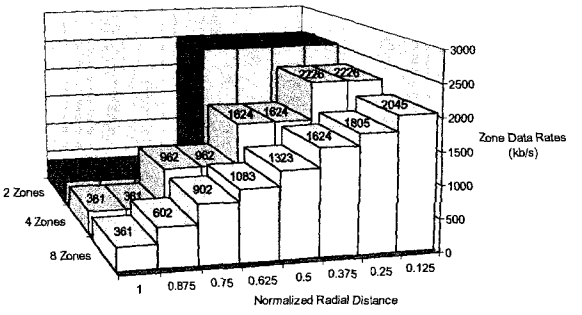


Figure 3.7b. Indoor system zone layout for $\varphi = 1$.

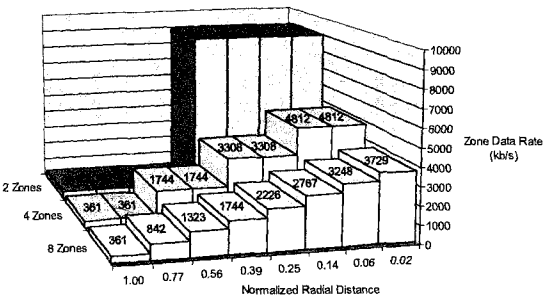


Figure 3.7c. Indoor system zone layout for $\varphi = 2$.

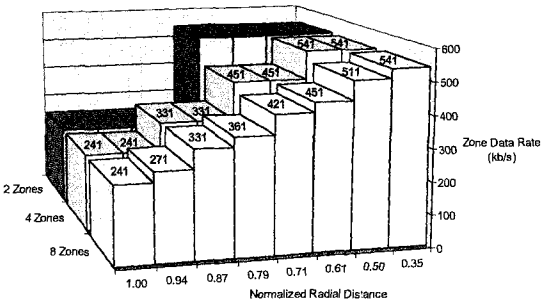


Figure 3.8a. Pedestrian system zone layout for $\varphi = 1/2$.

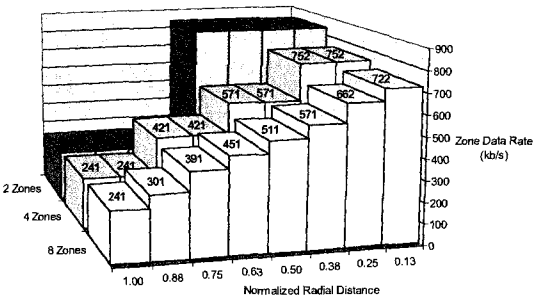


Figure 3.8b. Pedestrian system zone layout for $\varphi = 1$.

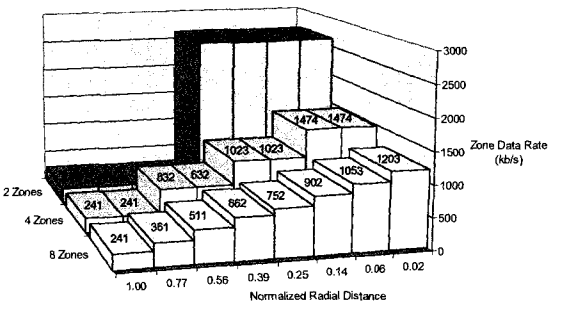


Figure 3.8c. Pedestrian system zone layout for $\varphi = 2$.

According to Condition 2, the outer-most zone data rate, $R_Z$, is the same for all annular structures. The second condition sets the minimum service level offered within a cell the same for all schemes.

The zone-rate relationship is designed so that the allocated maximum data rates decrease linearly with zone number $z$, while the boundaries of the annular zones are chosen to be $r_{cell}(z/Z)^{\varphi}$, where $r_{cell}$ is the cell radius, $z$ is the zone index and $Z$ is the total number of zones. For a given number of zones $Z$, increasing the value of $\varphi$ results in an increased maximum rate in the inner zones, but a decrease in their size. This work considers values of $\varphi$ = ½, 1, and 2, with the cell partitioned into $Z$ = 2, 4, and 8 annular zones. Annular zone structures indicating the maximum data rates are shown in Figures 3.7a-c and 3.8a-c for the ITU Indoor B channel and ITU Pedestrian B channel, respectively.

### 3.5.2 Power Control and Allocation

Fast power control at approximately 800 Hz is assumed for each mobile to combat the Rayleigh fading in the channel. Power is controlled on a per user basis and is applied to the entire spreading code(s) assigned to that user as described in Section 3.3.

In addition to fast power control, slow power control is used to maintain a BER of less than $10^{-4}$, however the total transmit power is fixed which means that not all requests for increased power can be met. A simple power allocation algorithm is implemented for this purpose. Maximum data rates for each zone are transmitted as long as the total transmit power is less than the maximum. If a user requires additional power to maintain a BER less than $10^{-4}$ and the maximum transmit power of the base station has been reached, the user's data rate is lowered (by means of assigning fewer code channels) to meet the BER constraint for that user.

### 3.5.3 Simulation Parameters

Two cellular environments are considered: pico-cell indoor office and micro-cell pedestrian. The simulation parameters for each environment are given in Table 3.1. When applicable, the values reflect recommendations and link budget parameters from [24][43]. Maximum powers and modest cell sizes are chosen such that maximum data rates are physically realizable. Convolutional coding of rate ½, constraint length 7, is implemented with generator polynomials (171,133) used in the DVB-T standard [26]. Each user's signal undergoes independent log-normal shadowing, and independent Rayleigh fading. Fast power control is used to combat Rayleigh fading. Fast power

control errors are modelled by a log-normal distribution of the received SINR with standard deviation of 2 dB. Perfect channel estimation and SINR estimation for MMSE coefficients are assumed. The additional power required for the cyclic prefix is included in the simulations.

Table 3.1. Simulation Parameters

| *ITU Channel Model* | *Indoor Office B* | *Pedestrian B* |
|---|---|---|
| Nominal bandwidth | 20 MHz | 10 MHz |
| Main lobe bandwidth | 16.4 MHz | 8.2 MHz |
| Cell radius | 100 m | 500 m |
| Maximum transmit tower | 2 W | 20 W |
| Log-normal shadowing (std. dev). | 12 dB | 10 dB |
| Subcarriers | 256 | 512 |
| Mobile speed | 3 km/h | 3 km/h |
| Walsh code length | 256 | 256 |
| Thermal noise | 3.98E-21 W/Hz | 3.98E-21 W/Hz |
| Channel coding | Convolutional coding, R=1/2, 64 states | Convolutional coding, R=1/2, 64 states |
| SS-OFDM symbol duration | 15.625 μs | 62.5 μs |
| Cyclic prefix duration | 1 μs | 4 μs |
| Minimum data rate | 60.1504 kb/s | 15.0376 x 2 kb/s |

### 3.5.4 Link and System Level Simulations

The simulation of this system consists of two parts; link level simulations for SS-OFDM in log-normal fading and an iterative simulation to determine the outage of a system given a specific system load. The link level simulations determine the average SINR required for a BER of $P_b^{(cc,tpc)} = 10^{-4}$ for the SS-OFDM system after fast transmitter power control (tpc) and convolutional encoding (cc) in the multipath channels. The SS-OFDM link with QPSK modulation and convolutional coding is simulated in a Rayleigh channel with fast power control in the manner described in Section 3.3. In the link level simulation, the performance of the convolutionally encoded SS-OFDM system is measured in the presence of a log-normal distribution of the received signal power with standard deviation of 2 dB due to power control errors. In general, the probability of error given coding and power control parameters, $P_b^{(cc,tcp)}$, is dependent on the

distribution of the SINR. The SINR at the $\upsilon^{th}$ time interval for the $u^{th}$ user and the $i^{th}$ code channel in the link level model is given by:

$$SINR_{u,i}(\upsilon) = \frac{\xi_{u,0}^2 P_i \mu_{A_{u,l}}^2}{\sigma_{A_{u,l}}^2 \xi_{u,0}^2 \frac{P_{cell} - P_i}{L} + \mu_{B_{u,l}} I_{u,ICI} + \mu_{B_{u,l}} N_0} \tag{3.20}$$

where $A_{u,l}$ and $B_{u,l}$ are as given in Section 2.3, and $\lambda$ is given by (3.16). By expressing the total cell transmit power in terms of the power allocated to the $i^{th}$ code channel, $P_{cell} = \kappa_{cell/i} P_i$, and the SINR can be expressed as:

$$SINR_{u,i}(\upsilon) = \frac{\mu_{A_{u,l}}^2}{\sigma_{A_{u,l}}^2 \frac{\kappa_{cell/i} - 1}{L} + \mu_{B_{u,l}} \frac{I_{u,ICI} + N_0}{\xi_{u,0}^2 P_i}} = \frac{\mu_{A_{u,l}}^2}{\sigma_{A_{u,l}}^2 \frac{\kappa_{cell/i} - 1}{L} + \mu_{B_{u,l}} \frac{I_{u,0}}{P_{u,i,0}}} \tag{3.21}$$

where $P_{u,i,0} = \xi_{u,0}^2 P_i$. Note that all code channel sent to the $u^{th}$ user are transmitted with the same power on over the same channel so that $P_{u,i,0} = P_{u,0}$. It can therefore be seen that the average bit error rate of the system over some interval is dependent only on the values of $\kappa_{cell/i}$ and $P_{u,0}/I_{u,0}$, such that it can be expressed as $P_b^{(cc,tpc)}(\kappa_{cell/i}, P_{u,0}/I_{u,0}) = 10^{-4}$. The link level curves in Figure 3.9 show the values of $\kappa_{cell/i}$ and $P_{u,0}/I_{u,0}$ required to achieve a BER of $10^{-4}$ for the given system parameters and channel models. During each link level run, the parameters of $\kappa_{cell/i}$ and $P_{u,0}/I_{u,0}$ are held constant while small-scale fading, and the counter action of power control with power control errors, are simulated throughout the run. The curves are different for the pedestrian and indoor channels due to a different spreading gain and the differences in the multipath amplitudes and delays. These curves are used in the system level simulations.

The system level simulations model a 19-cell system as shown in Figure 3.1, but focus only on the mobiles in the home cell. All cells are of equal size and contain an identical number of users. The composite ICI model is used (see Section 3.2.3) with proper large-scale fading for each interfering transmitter. The main loop of the simulation consists of 100 runs of 10 seconds each. For each loop, new user positions and shadowing values are created. During the simulation run, small-scale and large-scale fading, along with the counter action of power control, are accurately modelled to determine the power requirements of a given user throughout the simulation run. Power allocation and code channel allocation are managed as described in Section 3.5.2. If a user cannot support the minimum data rate (1 or 2 code channel in indoor and pedestrian channels, respectively) an outage is recorded.

After the 100 10-second runs, the average transmit power of the cell is recorded, and used as the transmit power value for each of the 18 interfering transmitters in the next 100 runs. This iterative loop continues until the average transmit power for a set of 100 runs converges to the value of the previous iteration. A minimum of 5 iterations are completed.

The load of the system is increased by introducing additional users to the system. The iterative process is carried out for several different numbers of users. As mentioned, an outage is recorded when a user is unable to receive transmission at the required BER. For each simulation, the average throughput and outage (percentage of total time) are recorded for the final 100-run iteration.

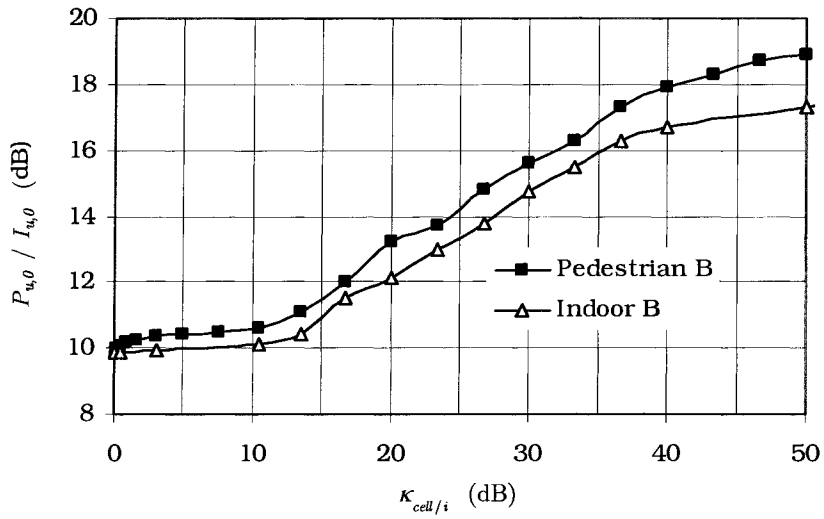


Figure 3.9. Link level simulations that show the values of $\kappa_{cell/i}$ and $P_{u,0}/I_{u,0}$ that are needed in order to achieve a BER of $10^{-4}$ given the system coding, system and channel parameters.

### 3.5.5 Simulation Results

The spectral efficiency of the indoor office and pedestrian systems is summarized in Table 3.2 for outages of 5% and 10%, and $\Upsilon_{PL} = 3$. The annular zoning performance worsens as the number of zones increases. The performance of the zoning schemes depends largely on the maximum bit rate assigned to users near the cell boundary. In 4- and 8-zone structures, zone data rates are gradually increased from the outer to inner zones. In 2-zone structures, the increase is abrupt and hence, a larger number of users operate in the outer-most (minimum bit rate) zone. For both the indoor and pedestrian

systems considered, $\varphi$ =2 structures showed the highest throughputs as the outer zones are larger than in the $\varphi$ =1 and $\varphi$ =1/2 structures, for the same number of zones. Conversely, the $\varphi$ =1/2 case showed the smallest performance benefit of the multi-zone structures for this reason. Only a slight performance benefit was observed for the 2-zone $\varphi$ =1/2 system over the 4- and 8-zone systems as the inner annular ring extended to 70.71% of radius, where transmission conditions are less favourable to those very near the transmitter.

Table 3.2. Spectral efficiency of SS-OFDM annular zone systems.

| *Indoor Office B* ($\Upsilon_{PL}$ = 3) | | *5% outage (b/s/Hz/cell)* | *10% outage (b/s/Hz/cell)* | *Pedestrian B* ($\Upsilon_{PL}$ = 3) | | *5% outage (b/s/Hz/cell)* | *10% outage (b/s/Hz/cell)* |
|---|---|---|---|---|---|---|---|
| 1 zone | | 0.13 | 0.24 | 1 zone | | 0.17 | 0.23 |
| $\varphi$ =1/2 | 2 zones | 0.16 | 0.27 | $\varphi$ =1/2 | 2 zones | 0.19 | 0.26 |
| | 4 zones | 0.15 | 0.27 | | 4 zones | 0.19 | 0.26 |
| | 8 zones | 0.15 | 0.26 | | 8 zones | 0.18 | 0.26 |
| $\varphi$ =1 | 2 zones | 0.18 | 0.31 | $\varphi$ =1 | 2 zones | 0.20 | 0.29 |
| | 4 zones | 0.16 | 0.28 | | 4 zones | 0.19 | 0.27 |
| | 8 zones | 0.16 | 0.28 | | 8 zones | 0.19 | 0.27 |
| $\varphi$ =2 | 2 zones | 0.22 | 0.37 | $\varphi$ =2 | 2 zones | 0.22 | 0.33 |
| | 4 zones | 0.18 | 0.31 | | 4 zones | 0.20 | 0.29 |
| | 8 zones | 0.16 | 0.29 | | 8 zones | 0.20 | 0.28 |

Table 3.3 Outage for SS-OFDM systems with different path loss exponents $\Upsilon_{PL}$

| *Indoor Office B* | | *Outage (%) at 0.2 Mb/s/MHz/cell* | | | *Pedestrian B* | | *Outage (%) at 0.15 Mb/s/MHz/cell* | | |
|---|---|---|---|---|---|---|---|---|---|
| $\Upsilon_{PL}$ | | 2 | 3 | 4 | $\Upsilon_{PL}$ | | 2 | 3 | 4 |
| 1 zone | | 18.0 | 8.2 | 5.1 | 1 zone | | 12.6 | 4.1 | 2.2 |
| $\varphi$ =1/2 | 2 zones | 16.0 | 6.7 | 3.7 | $\varphi$ =1/2 | 2 zones | 10.8 | 3.4 | 1.7 |
| $\varphi$ =1 | 2 zones | 14.5 | 5.6 | 3.0 | $\varphi$ =1 | 2 zones | 9.9 | 2.8 | 1.4 |
| $\varphi$ =2 | 2 zones | 12.2 | 4.6 | 2.6 | $\varphi$ =2 | 2 zones | 8.2 | 2.5 | 1.2 |

The division of the cell into rate-specific zones provides a higher cell throughput as it allocates a larger portion of the resources (code channels) to users near the base station. Transmitting to users near the base station is inherently more efficient than transmitting to users near the cell boundary. The system requires a small amount of feedback from each mobile: a fast power control command and the mobiles distance from the base station (or equivalently in this model, the long term average SIR of the user).

### 3.5.6 Shortcomings of the SS-OFDM Location Dependent Rate Assignment Cellular System

As mentioned, the limiting factor is the large number of code channels afforded to users near the cell boundary. In fact, the system sacrifices a significant amount of throughput to ensure reasonable fairness, which is measured in terms of code channels. Higher throughputs can be achieved in this system if 8 PSK and 16 QAM constellations were used in addition to QPSK. One can imagine higher throughputs could be achieved if resource allocation was based on small scale fading, rather than a user's position in the cell. The portion of the total cell power consumed by distant users is still magnitudes larger than power allocated to users near the transmitter (see Figure 3.10). Furthermore, fairness in this system is relative to a mobile's distance from the transmitter, and therefore does not take a mobile's shadowing conditions in consideration. Unfortunately, the system stills suffers from a large probability of outages, particularly for users near the cell boundary and no provisions are made for soft hand-offs. All of the issues raised in this paragraph are addressed in the development of the cellular system in Chapter 4.

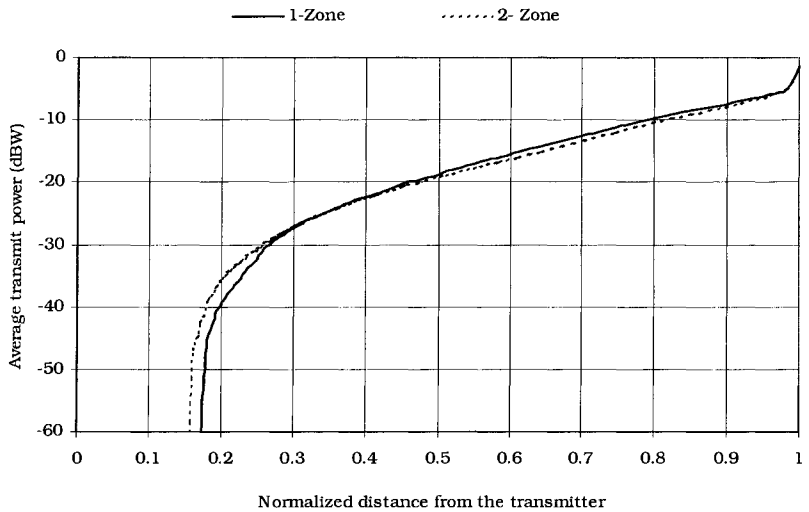


Figure 3.10. Relative average power needed for transmission to mobiles at normalized distances from the base station (centre of cell); $\varphi = 1$.

# Chapter 4

# Efficient 2-Dimensional Allocation of Radio Resources for Multi-user Multicarrier Systems

This chapter presents a new scheme to allocate radio resources in an efficient manner for multi-user multi-carrier systems. The system is designed to accommodate data packet communication and the use of spread spectrum techniques, while still exploiting the advantages of adaptive subcarrier modulation and multi-user diversity. The system is designed for use in a practical cellular system, and successfully addresses the failures of the location dependent rate assignment scheme outlined in Section 3.5.6.

Since the first proposal of this multi-user diversity SS-OFDM system in 2001 [74], similar systems have been proposed from other sources. Specifically, in spring 2003 Motorola proposed a similar scheme based on adaptive allocation of sub-bands in an OFDM system [16]. A recent proposal by a consortium of Swedish universities has a similar focus [98]. NTT DoCoMo has suggested the use of adaptive multi-user scheduling methods [93] with their VSF-OFCDM system. Samsung has also investigated a similar OFDM scheme [36]. It is envisioned that an OFDM-based system that employs multi-user diversity and adaptive allocation techniques in multiple dimensions will be selected for future high-speed cellular systems.

This chapter begins by discussing specific theoretical and practical system designs for multi-carrier systems to provide a basis for the rest of the chapter. Adaptive modulation for multicarrier systems, as well as multi-user techniques will be presented in Section 4.1. The basic physical layer of the proposed spread spectrum orthogonal frequency division multiplexing with frequency and time allocation (SS-OFDM-F/TA) system is presented in Section 4.2. This system allocates resources by dividing the time frequency-time plane

into small rectangles denoted by sub-bands and time slots, and then allocating these sub-bands appropriately to users with superior channel conditions. It is shown how the proposed system provides robust data service to all users in a realistic cellular environment. The multi-cell simulation model used to evaluate the SS-OFDM-F/TA system is presented in Section 4.3. Basic cellular performance results of average throughput per sector and packet delays are discussed in Section 4.4. Section 4.5 presents an adaptive sub-band grouping and allocation which facilities the exploitation of multi-user diversity in highly frequency selective environments. In Section 4.6, the system performance is compared to that of a best-effort packet data service in a cellular channel. The final section of this chapter discusses proper packet structure transmission and design for high data rate transmission in doubly selectively channels, and in particular, vehicular channels. The trade-off between using larger packet sizes together with the allocation of disjoint groups of sub-bands (as proposed in Section 4.5), and the use of smaller packets transmitted in a single sub-band is examined in terms of throughput and delay.

## 4.1 Adaptive Single-user and Multi-user OFDM Systems

The frequency dimension of OFDM-based systems allows for power and bit adaptation to the frequency selectivity of the channel. Kalet originally developed the optimum multicarrier power spectrum [55] that maximizes the channel capacity, which is very similar to the classical "water-pouring" (also known as water-filling) solution [32]. Assuming the capacity of the channel can be achieved through ideal coding and modulation, the spectral efficiency of the multi-tone system is given by:

$$C/B = \sum_{l=0}^{N-1} \log_2(1 + P_l \gamma_l) \tag{4.1}$$

where $C$ is the channel capacity, $B$ is the total bandwidth, $\gamma_l$ is the signal-to-noise (SNR) ratio of the $l^{th}$ subcarrier, and $P_l$ is the power allocated to the $l^{th}$ subcarrier. Given a total power constraint of $P_{total} = \sum_{l=0}^{N-1} P_l$, the maximum throughput of the system is achieved by using the allocation strategy:

$$P_l = \begin{cases} \frac{1}{\gamma_{thres}} - \frac{1}{\gamma_l} & \gamma_l \geq \gamma_{thres} \\ 0 & \text{otherwise} \end{cases} \tag{4.2}$$

This solution maximizes the throughput for an $N$-channel system given a total power constraint in frequency selective fading. In comparison to uniform distribution, additional power is allocated to subchannels with higher SNR's, and only to subchannels where the SNR is a above a given SNR threshold $\gamma_{thres}$. Kalet's solution is for a general multi-tone system without interference between subchannels, and hence it can be applied to subcarriers in an OFDM system.

Several authors have also provided solutions for M-QAM or M-PSK modulation with a target bit or symbol error rates [15][55] for all subchannels. Chow *et al* have completed similar investigations for asymmetric digital subscriber lines (ADSL) [11][12]. Willink and Wittke later investigated optimal multicarrier bit and power allocation with individual subcarrier bit and symbol error constraints [114] for OFDM systems. Finally, an algorithm for adaptive loading for multicarrier systems considering a discrete modulation constellation was also developed [7]. Joint optimization of power allocation in time and frequency has also been studied for multicarrier systems [15]

Practical application and analysis of these principles for OFDM systems echoed these theoretical findings. Czylwik showed the performance improvement of adaptive multicarrier modulation techniques over similar single carrier systems [18]. In the context of a single user OFDM system, Keller and Hanzo demonstrated the performance improvement of adaptively modulating each subcarrier with a specific constellation size, dependent of the channel gains of the subcarriers [56]-[58]. Further, it was shown that higher throughputs were achievable if deeply faded sub-bands, or groups of subcarriers, were not used in favour of transmitting with a higher power over sub-bands with better channel conditions [58].

The investigation of multi-user diversity has led to further increases in spectral efficiency. Multi-user diversity can be exploited by scheduling transmissions to users in a manner that exploits the independence of their channels conditions. In 1997, Tse determined that the maximum throughput in a multi-user, $N$ independent parallel channel system is achieved by transmitting to the user with the best channel conditions in each parallel channel, and then performing water-filling across the channels [104]. This can be seen as a similar result for broadcast channels in the frequency domain as was found for multiple access channels in the time domain by Knopp and Humblet [59].

Multi-user diversity is exploited by adaptive OFDM-FDMA employing an adaptive subcarrier allocation scheme in a practical system in [89]. A more complex algorithm that includes adaptive power and bit allocation, while minimizing the transmit power under the constraint of transmitting to each user during every OFDM symbol, has been

introduced for OFDM by Wong *et al* [115]. The allocation of subchannels in an adaptive manner to maximize the minimum user data rate by exploiting multi-user diversity is considered in [87]. A recent interesting proposal by Costa et al [17], considers the adaptive grouping of users, and adaptive selection of subcarriers within a sub-band to maximize the overall capacity of the OFDM-based system. It should be noted that adapting power and bit allocation based on the channel gains in a frequency selective environments is a significant departure from traditional methods of interleaving, coding and spreading over the frequency band of the channel.

## 4.2 The SS-OFDM-F/TA System

A method of allocating radio resources in time and frequency dimensions is introduced and analyzed in this section. This method employs multi-user diversity, and does not require transmission to every user in each OFDM symbol. The system is designed to provide high throughputs in a cellular environment, while ensuring some fairness among the users. The objective is to develop a multicarrier based solution for the downlink of a high data rate wireless communications system that is significantly superior to comparable single carrier systems.

Figure 4.1 shows the variation in time and frequency of the received signal to noise ratio (SIR) (due to small scale fading) at a selected mobile. The fading is independent for each user, and hence, multi-user diversity can be achieved by dividing the time-frequency plane into rectangles. These rectangles can then be individually allocated for packet transmission to the user with the best channel conditions.

For this purpose, this thesis proposes an adaptive spread spectrum OFDM system using frequency and time allocation (SS-OFDM-F/TA) as a multi-carrier solution for future best effort packet data wireless access systems [74]. The SS-OFDM-F/TA system exploits multi-user diversity and temporal variations of the radio channel by transmitting to the mobile experiencing the best propagation conditions in a given sub-band and time slot, where a sub-band is a group of adjacent subcarriers. Sub-bands are chosen narrow enough so that almost all multi-user and frequency diversity of the channel can be exploited. In addition, spectral nulls present in the transmission band are avoided by transmitting to a mobile with a relatively high signal-to-interference ratio (SIR) over a given frequency sub-band. In this manner, the system implements allocation of radio resources in time and frequency domains to increase the average cell throughput. The system performs adaptive sub-band allocation and adaptive modulation/coding in each time slot using channel state information (CSI) fed back from the mobile. High

data throughputs have been shown in low-mobility [75][77][78] and high-mobility [76] cellular environments using best sector selection and type II hybrid Automatic Repeat reQuest (ARQ) [113].

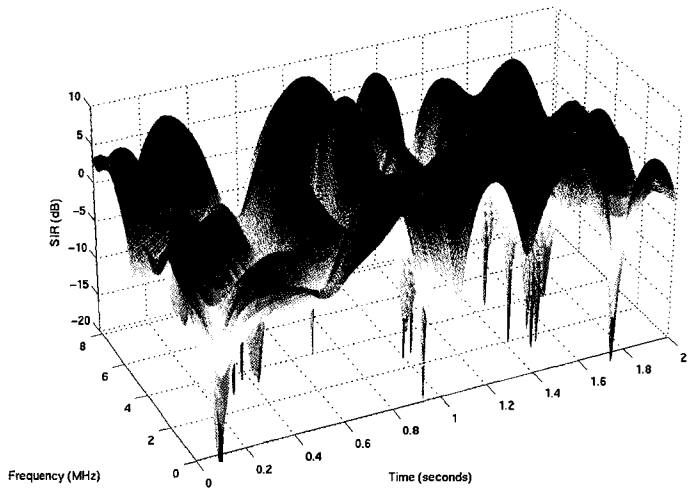


Figure 4.1. Signal to interference ratio mesh for a single mobile user in an OFDM system in a frequency selective fading environment.

This proposal differs significantly from the practical adaptive multi-user schemes described in the previous section, which generally assumes that every user receives at least some transmission during a given OFDM symbol. That constraint is used in order to ensure a certain quality of service, and also for some measure of fairness among users. As the present scheme is intended for packet-based services, the data service can tolerate some delay. This feature of packet services allows for adaptive radio resource allocation in time as well as frequency. Fairness in a cellular system is achieved by proportionally fair scheduling, and is discussed in Section 4.2.3.1.

In addition, previous schemes generally avoided the use of spread spectrum techniques as they limit the adaptability of the system; however the use of spread spectrum is desirable in cellular systems for the purposes of inter-cell interference mitigation and signal identification. In Section 4.2.1, it will be shown that the performance loss due to the use of spread spectrum in the SS-OFDM-F/TA system is negligible.

In this section the basic elements of the SS-OFDM-F/TA system are described. The premise behind two-dimensional resource allocation is examined. Results of SIR gain during scheduled transmissions are presented, and supported with some simple analytical results. The remainder of this section will deal with the design and evaluation of features

specifically related to packet transmission and their implementation in a variety of channel conditions.

### 4.2.1 Two-Dimensional Allocation

The transmission bandwidth occupied by $N$ subcarriers is equally divided into $M$ sub-bands, each containing of $L=N/M$ subcarriers. Each of the $M$ frequency sub-bands operates as an independent communications channel. A data symbol is spread across the subcarriers of a sub-band by a Walsh sequence of length $L$, and hence this system is similar to the SS-OFDM scheme described in Section 2.2 with a value of $M>1$. However, it should be noted that in the SS-OFDM-F/TA scheme there is no interleaving of subcarriers. By modifying (2.14) and assuming perfect channel estimation and a fully loaded system ($K=L$), the SINR in the $m^{th}$ sub-band at the $u^{th}$ mobile user is given by [74][75]:

$$\gamma_m^{(u)} = \frac{\mu_{A_{u,l,m}}^2}{\sigma_{A_{u,l,m}}^2 \frac{L-1}{L} + \frac{N_0}{E_s}\mu_{B_{u,l,m}}} \tag{4.3}$$

in which $\mu_{A_{u,l,m}}$ and $\mu_{B_{u,l,m}}$ are the sample means of the random variables $A_{u,l,m}$ and $B_{u,l,m}$ in the $m^{th}$ sub-band, respectively, and $\sigma_{A_{u,l,m}}^2$ is the sample variance of $A_{u,l,m}$. $A_{u,l,m}$ and $B_{u,l,m}$ are given by

$$A_{u,l,m} = \frac{\left|h_{u,l,m}\right|^2}{\left|h_{u,l,m}\right|^2 + \lambda} \tag{4.4}$$

and

$$B_{u,l,m} = \frac{\left|h_{u,l,m}\right|^2}{\left(\left|h_{u,l.m}\right|^2 + \lambda\right)^2} \tag{4.5}$$

for $l = 0,1,2,\ldots,L\text{-}1$.

#### 4.2.1.1 Multi-User Diversity Gain with Sub-Band Allocation

In order to exploit multi-user diversity, only the user with the highest SINR in a given sub-band will receive transmission in that sub-band. In this fashion, only a maximum of $M$ of possible $U$ users receive transmission during a given time slot. A user will only receive transmission in the sub-band/time slot when its channel conditions are better than that of the other $U$-1 users.

The average received SINR during scheduled transmissions, $\overline{\gamma}$, is useful in showing the performance benefit gained from exploiting the multi-user diversity. This performance measure records the SINR of the user with the best channel conditions in each sub-band. The average received SINR during scheduled transmissions for a system with $M$ sub-bands and $U$ users is given by:

$$\overline{\gamma}(U,M) = \mathrm{E}\left[\frac{1}{M}\sum_{m=0}^{M-1}\max_{0\le u<U}\gamma_m^{(u)}\right] \tag{4.6}$$

where E[$X$] denotes the expectation of $X$.

It may be perceived that significant loss in adaptability would occur as sub-bands are being allocated and adaptively modulated rather than individual subcarriers; however with proper system design the loss is negligible. For the purpose of demonstration, we consider the simple case of $U$ mobiles with identical average $E_s/N_0$= 0 dB. Channel variations are due to Rayleigh fading only. ITU indoor B channel is considered. An SS-OFDM symbol of $N$=256 subcarriers and a duration of $T_{sym}$=27.008 μs with a $T_g$=1 μs cyclic prefix is used. A 10 MHz transmission bandwidth is assumed.

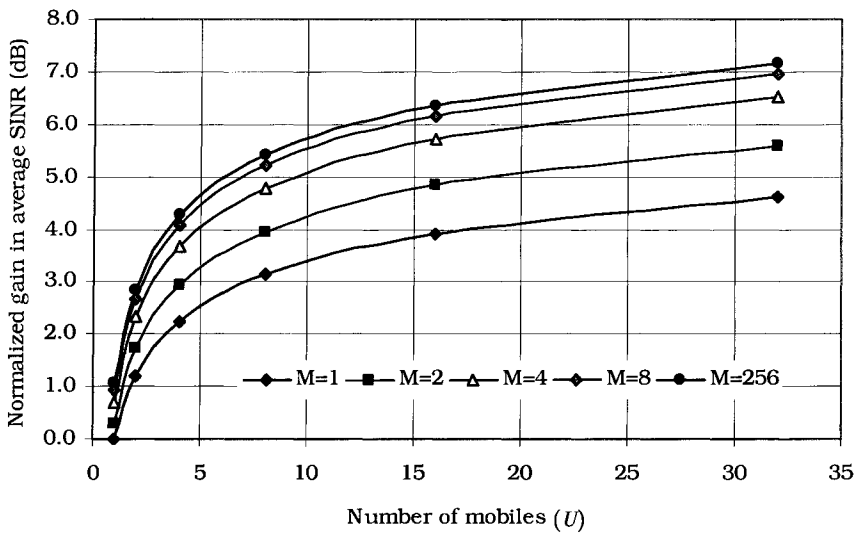


Figure 4.2. Average received SINR during scheduled transmissions, $\overline{\gamma}$. Average SINR gain is normalized to the average SINR of the $M$=1, $U$=1 system. A 10 MHz ITU Indoor B channel is assumed.

In each sub-band, the scheduler chooses the user with the highest SINR, from the set of $U$ users as given by (4.6), to receive transmission. This is repeated for each of $M$ sub-bands, and subsequently for each time slot (i.e. a different set of channel gains $h_{u,l,m}$ for each time slot). Note that a user may be chosen in more than one sub-band, or may not be chosen at all in a given time slot. It can be seen that the average received SIR during

scheduled transmissions as given by (4.6), increases with an increasing number of users, as the scheduler has a greater number of users (each with independent channel conditions) from which to choose. Hence, the average channel conditions (or SIR) during transmissions based on these scheduler selections improves with the number of users $U$. In addition, division of the band into sub-bands significantly improves the performance (Figure 4.2) as frequency diversity is also exploited. Note that for the case of a single Rayleigh fading channel, the increase in the average received SIR during scheduled transmissions due to multi-user diversity is approximately proportional to $\ln(U)$ for large values of $U$. Figure 4.2 illustrates similar behaviour.

Employing $M$=8 sub-bands is sufficient to exploit the multi-user diversity in the frequency selective channel, due to the high correlation of adjacent subchannel gains. As there is a small performance difference between the OFDM ($M$=$N$=256 sub-bands) system and the $M$=8, it can be seen that the fading is not completely flat across each of the $M$=8 sub-bands and inter-code interference is introduced due to the loss of orthogonality of the spreading sequences. However, this performance difference between the more complex OFDM independent subcarrier allocation ($M$=$N$=256 sub-bands) system and the $M$=8 system is not significant. Further, using $M = 8$ instead of $M = 256$ sub-bands decreases the demand on channel state information feedback by a factor of 32. It can be noted that conventional SS-OFDM as described in Section 2.2 is represented by the $M$=1, $U$=1 point as a data symbol in the conventional system is spread over all sub-carriers in an SS-OFDM symbol, and each user receives transmission during every SS-OFDM symbol.

A simple analytical evaluation for the bit error rate (BER) of the system with QPSK modulation is possible if we assume (for the purpose of this derivation) that each sub-band is much narrower than the coherence bandwidth of the channel. With this simplification, all the channel gains, $h_{u,l,m}$, are identical within a sub-band so that $h_{u,l,m} = h_{u,j,m}$ for $j,l \in [0, L-1]$. The SINR for a given sub-band in (4.3) then simplifies to a chi-squared random variable with 2 degrees of freedom (using $E_s = 2E_b$ for QPSK):

$$\gamma_m^{(u)} \approx \left|h_{u,l}\right|^2 \frac{2E_b}{N_0} \tag{4.7}$$

Using order statistics from [3], the cumulative distribution function (CDF) of the highest sample out of $U$ samples of chi-squared random variables is given by:

$$F_{\max\limits_{0\le u<U} \gamma_m^{(u)}}(x) = (1 - e^{-x/\overline{\gamma}_b})^U \tag{4.8}$$

where the average (bit) signal to noise ratio (SNR) is $\overline{\gamma}_b = E_b / N_0$.

If we further assume that each sub-band is statistically identical, the average received SINR during scheduled transmissions can be shown to be:

$$\overline{\gamma}(U,M) = \overline{\gamma}_m(U) = \frac{2E_b}{N_0}\left(\sum_{i=1}^{U} 1/i\right) \tag{4.9}$$

where we have used the expression for the mean values of order statistics of an exponential distribution from [3]. A similar result is given in [39] in the context of a single carrier system.

It can be seen that there is no dependence in (4.9) on the number of sub-bands. In other words assuming the same bandwidth $B$ and number of users $U$, multi-user diversity gain of a multiple sub-band system in a frequency selective environment is the same as the multi-user diversity gain of a single sub-band system in a flat fading channel.

Using (4.8) and the results from [83, Equation 14-4-14], the bit error rate (BER) of the system with $U$ users and QPSK modulation can be shown to be:

$$P_b = \sum_{j=0}^{U-1}\binom{U-1}{j}(-1)^j \frac{U}{2(j+1)}\left(1-\sqrt{\frac{\overline{\gamma}_b}{\overline{\gamma}_b + j + 1}}\right) \tag{4.10}$$

This is clearly the same as the expression for a selection combining system with $U$ branches, as also observed in a slightly different context in [59]. The results of (4.10) are compared with simulation results for the BER of an SS-OFDM system with the same system parameters used to generate the curves of Figure 4.2. These results are shown in Figure 4.3.

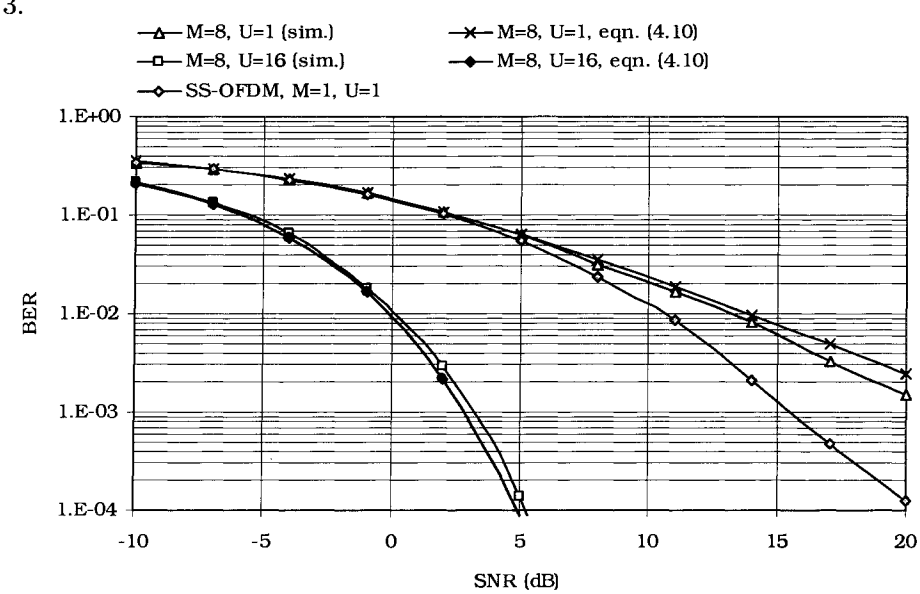


Figure 4.3. BER performance of SS-OFDM, where the user with the best channel conditions will receive transmission in each sub-band/time slot. ITU Indoor B, 10 MHz channel, $N$=256 subcarriers, $T_{sym}$=27.008 μs, and 1 μs cyclic prefix.

In addition to validating the analytical expressions given in this section, the curves show the benefit of multi-user diversity and two-dimensional allocation. Figure 4.3 also indicates that in the absence of multi-user diversity ($U$=1 cases), the sub-band/time slot structure purposed in here in Chapter 4 for SS-OFDM performs worse (in terms of uncoded BER) than conventional SS-OFDM systems using full bandwidth spreading and/or subcarrier interleaving discussed in Chapter 2.

#### 4.2.1.2 Capacity Comparison to OFDM

As discussed in Section 1.2.6, the use of spread spectrum is beneficial in cellular systems, however a drawback in the proposed design is the inter-code interference generated due to frequency selective fading. Comparing the proposed sub-band allocation scheme to an OFDM system with per subcarrier allocation can quantify this loss. This section assumes uniform power allocation across subcarriers for comparison, while optimal power allocation is considered in the following sub-section.

The maximum spectral efficiency of the system, $C/B$, is useful in showing the performance benefit gained from exploiting the multi-user diversity using sub-band allocation, and loss due to inter-code interference. The maximum spectral efficiency for this system with $M$ sub-bands and $U$ users and uniform power distribution across subcarriers is given by:

$$C/B = E\left[\frac{1}{M}\sum_{m=0}^{M-1}\log_2\left(1+\max_{0\le u<U}\gamma_m^{(u)}\right)\right] \tag{4.11}$$

where it is assumed that long-term fading statistics in each sub-band are identical.

Using the same parameters for the SS-OFDM and OFDM systems considered in the previous section in the ITU Indoor B channel, the spectral efficiency of OFDM and SS-OFDM systems are plotted in Figure 4.4. In this comparison, transmission bandwidth-division into sub-bands for the purpose of user selection is also considered for OFDM.

As in the previous section, it can be seen that the maximum spectral efficiency increases with increasing number of users (Figure 4.4). In addition, division of the channel bandwidth into sub-bands significantly improves the performance by exploiting the frequency diversity of the channel.

The maximum spectral efficiency of the OFDM system is slightly higher than that of SS-OFDM for the single sub-band case ($M = 1$) due to the loss of orthogonality of the spreading sequences on a frequency-selective channel, but approaches that of SS-OFDM as the number of sub-bands is increased. When $M = 8$ sub-bands are used, the use of

spread spectrum needed for inter-cell interference mitigation results in a negligible performance loss in comparison to OFDM without spreading.

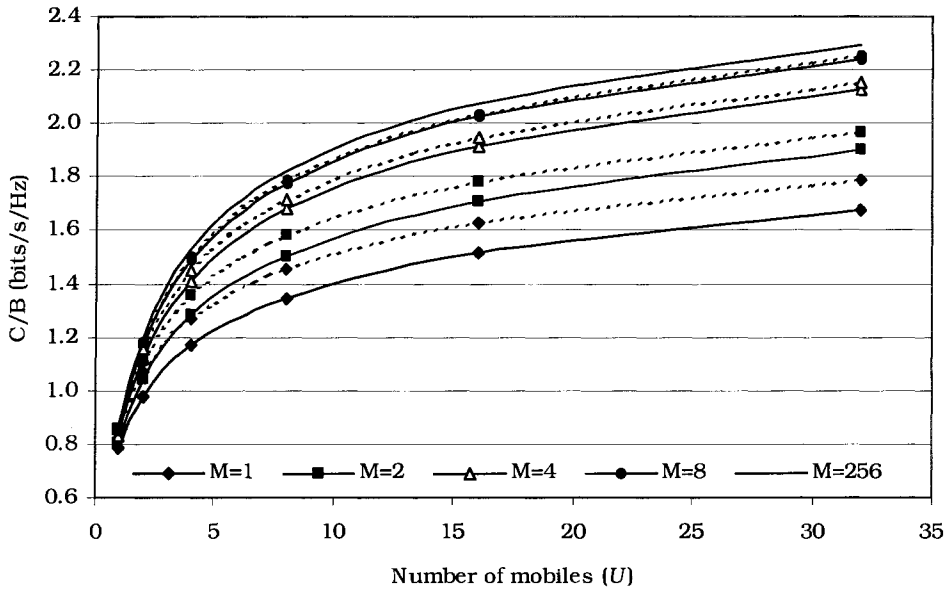


Figure 4.4. Maximum spectral efficiency of SS-OFDM (solid lines) and OFDM (dashed lines) for different numbers of sub-bands ($M$) and $N = 256$ subcarriers.

An analytical representation is possible for the maximum spectral efficiency of an OFDM, and serves as the performance upper bound for an SS-OFDM system in the limit when there is no inter-code interference in a given sub-band. The probability density function (PDF) of the SIR for the best 1 out of $U$ users is given by:

$$f_{\max\limits_{0\le u<U}\gamma_m^{(u)}}(x) = U\frac{e^{-x/\bar{\gamma}_m}}{\bar{\gamma}_m}(1-e^{-x/\bar{\gamma}_m})^{U-1} \tag{4.12}$$

where order statistic properties from [3] have been used. The maximum spectral efficiency for $U$ user system, assuming no inter-code interference, can be found by:

$$\begin{aligned} C/B &= \int_0^\infty \log_2(1+x) f_{\max\limits_{0\le u<U}\gamma_m^{(u)}}(x)dx = \int_0^\infty \log_2(1+x) U\frac{e^{-x/\bar{\gamma}_m}}{\bar{\gamma}_m}(1-e^{-x/\bar{\gamma}_m})^{U-1}dx \\ &= \int_0^\infty \log_2(1+x)\frac{U}{\bar{\gamma}_m}\sum_{i=0}^{U-1}\binom{U-1}{i}(-1)^i e^{-x(i+1)/\bar{\gamma}_m}dx \\ &= U\sum_{i=0}^{U-1}\binom{U-1}{i}(-1)^{i+1}\frac{e^{(i+1)/\bar{\gamma}_m}\,\mathrm{Ei}(-(i+1)/\bar{\gamma}_m)}{(i+1)\ln(2)} \end{aligned} \tag{4.13}$$

where $\mathrm{Ei}(-x) = -\int_x^\infty \frac{e^{-t}}{t}dt$ is the exponential integral function.

#### 4.2.1.3 Bit and Power Allocation with Multi-User Diversity and Sub-Bands

Adaptive bit loading and proper power allocation per subcarrier are important features of OFDM transmission, as they allow for high throughputs in frequency selective channels. In this section it is demonstrated that allocating sub-bands rather than subcarriers in a SS-OFDM as described early does not significantly decreases the maximum throughput of the system with multi-user diversity in common physical channels. Bit loading in this section is achieved by assuming capacity achieving modulation and coding for given power allocation.

Again the maximum spectral efficiency of the proposed SS-OFDM system with and without sub-band power allocation can be compared (Figure 4.5). The simulation and system parameters are identical to those described in the previous sub-sections (see Figure 4.4). Note that the $M$=256 sub-band system represents an OFDM with per subcarrier bit loading and power allocation. Equal power allocation to each sub-band is assumed for the proposed SS-OFDM sub-band allocation scheme, while water-filling power allocation (in frequency only) according to (4.2) is used for SS-OFDM system with power allocation. It should be noted that this power allocation is not optimal in a system using spread spectrum due to the presence of inter-code interference. Equation (4.2) is optimal for cases where a $X$ dB increase in transmit power results in a $X$ dB gain in SNR, and this is not the case for $M$=1 or 2 sub-bands due to loss of orthogonality of the spreading codes in frequency selective fading sub-bands. This allocation strategy is nearly optimal for $M$=8 as the fading across a given sub-band is nearly flat, and is optimal for the $M$=256 system which is an OFDM system.

Optimal power allocation across sub-bands provides up to a 13% (for $U = 1$) increase in throughput in comparison to uniform power allocation when $M$=8 sub-bands are considered (Figure 4.5). The largest gain due to water-filling is found when there is only one user, and decreases quickly with multi-user diversity. The gain in capacity is less than 0.6% for $U = 8$ active users or greater with $M = 8$ sub-bands. In comparison to the OFDM system ($M = 256$) with optimal power allocation, the SS-OFDM system with $M = 8$ sub-bands has a spectral efficiency that is 4.4 % lower with $U = 4$ users, and is within 3 % for cases of $U = 16$ users or more. From the results, it is clear that gain due to appropriate power allocation becomes significantly less important to system performance in the presence of multi-user diversity. This was the assumption in the original SS-OFDM-F/TA system proposal in reference [74], and was later suggested to be

the case in [107], and was finally shown explicitly for OFDM systems in [44] for independent subcarrier fading. It is noteworthy to point out that a benefit of using equal power allocation across all sub-bands, in addition to decreased complexity at the transmitter, is that the system provides a constant transmit power making interference level estimation in adjoining cells significantly easier and more reliable. It should also be noted that the performance gain of the water-filling power allocation method over the uniform power allocation schemes increases significantly at lower SINRs.

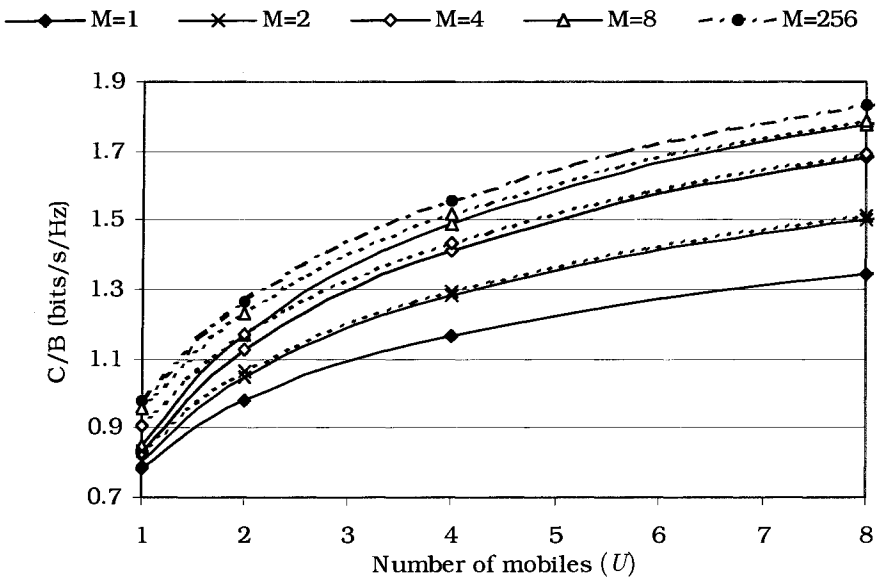


Figure 4.5. Maximum spectral efficiency of SS-OFDM with uniform power allocation (solid lines) and water-filling power allocation according to (4.2) (dashed lines) for different numbers of sub-bands ($M$) and $N = 256$ subcarriers. $M = 256$ is an OFDM system (without the spread spectrum component) with optimal power allocation.

### 4.2.2 SS-OFDM-F/TA Packet Data System

As SS-OFDM with two-dimensional allocation requires delay tolerant traffic to perform effectively, it is most useful to enable very high throughput for best-effort packet data access. In [74], a multi-carrier system with frequency and time allocation (SS-OFDM-F/TA) proposed as a solution for future best effort delay tolerant wireless access systems. This system uses equal sub-band power allocation as described earlier to reduce complexity and channel state information feedback. This system also considers a form of frequency and time proportionally fair scheduling [39] that allows for fairness in cellular systems, while still exploiting multi-user diversity.

The SS-OFDM transmitter is shown in Figure 4.6. The structure is similar to that given in Section 2.2, without subcarrier interleaving. The transmission bandwidth occupied by $N$ subcarriers is equally divided into $M$ sub-bands, each containing $L=N/M$ subcarriers. Each of the $M$ frequency sub-bands operates as an independent communication channel. Individual packets are assigned to each sub-band for transmission based on SIR estimates fed back by the mobiles. The SIR estimates are also used for the purpose of adaptive modulation and coding of each packet given a required quality of service.

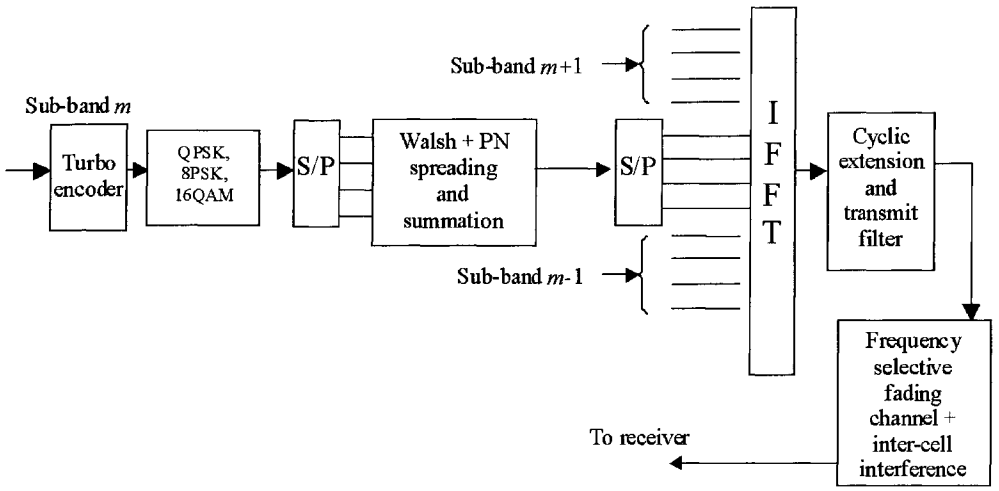


Figure 4.6. SS-OFDM-F/TA downlink transmitter.

The $m^{th}$ stream of encoded data symbols, $b_{0,m}, b_{1,m}, \cdots, b_{k,m}, \cdots, b_{L-1,m}$, is serial to parallel converted to form $L$ parallel symbol streams. The $K=L$ streams are code division multiplexed (CDM). Each stream is spread by an orthogonal Walsh code of length $L$ concatenated with a serving sector specific pseudo-noise (PN) sequence, $\mathbf{c}_k = \left\{c_{k,0}, c_{k,1}, \cdots c_{k,L-1}\right\}$, and $c_{k,l} \in \left\{-1/\sqrt{L}, 1/\sqrt{L}\right\}$. As all of the $L$ spreading codes are used in each sub-band, the system is fully loaded ($K=L$). The $L$ spread streams are synchronously summed to form a single chip stream. The chip stream is serial-to-parallel converted to form $L$ parallel chip streams, $d_{l,m} = \sum_{k=0}^{L-1} b_{k,m} c_{k,l}$. The $L$ chip streams are mapped onto adjacent subcarriers along with the chip streams from the other $M$-1 sub-bands to form the $N = ML$ subcarrier SS-OFDM symbol of duration $T_{sym}$.

$$s(t) = \sum_{m=0}^{M-1} \sum_{l=0}^{L-1} \sum_{k=0}^{L-1} b_{k,m} c_{k,l} e^{j2\pi(l+mL)t/T_{sym}} = \sum_{m=0}^{M-1} \sum_{l=0}^{L-1} d_{l,m} e^{j2\pi(l+mL)t/T_{sym}}, \quad \text{for } -T_g \le t \le T_{sym} \tag{4.14}$$

As in Section 2.2, a guard interval containing a cyclic prefix of duration $T_g$ is added to each SS-OFDM symbol to prevent inter-symbol interference (ISI). The transmitted signal is disturbed by frequency selective fading, and large-scale channel propagation conditions of path loss and log-normal shadowing. Transmissions from $S$ - 1 interfering base stations further degrade the desired signal, introducing inter-cell interference (ICI) at the receiver. As the multi-cell system is interference limited, the performance loss due to additive white Gaussian noise is ignored throughout the discussion and analysis of this system.

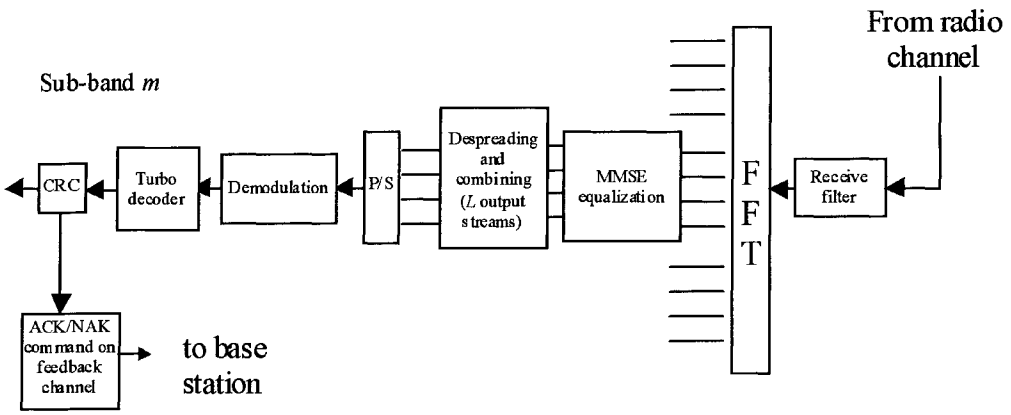


Figure 4.7. Essential operations of the SS-OFDM –F/TA receiver.

This cellular system has been designed to operate with a frequency re-use factor equal to one to maximize spectral efficiency. The ICI in the system is mitigated through the application of spread-spectrum techniques. Concatenated spreading sequences obtained by superposition of orthogonal Walsh codes with sector-specific long PN sequences are used as in Chapter 3. The long PN sequences ensure suppression of the ICI by a factor equal to the spreading gain, and allow the mobile to distinguish transmission from different sectors.

The mobile user demodulates and decodes only signals on the sub-band(s) assigned to it (Figure 4.7). The mobile receiver performs minimum mean squared error (MMSE) equalization [29] to partially restore the orthogonality between parallel chip streams while minimizing ICI amplification. The MMSE equalization coefficient is given by $g_{u,l,m} = h^*_{u,l,m} \Big/ \left( \left| h_{u,n,m} \right|^2 + \sigma^2_{I_{u,m}} / \sigma^2_{sym} \right)$, where $h^*_{u,n,m}$ is the complex conjugate of the channel gain at receiver $u$ on the $n^{th}$ sub-carrier in the $m^{th}$ sub-band, and $\sigma^2_{I_{u,m}} / \sigma^2_{sym}$ is the ratio of the variances of inter-cell interference and transmitted symbols. In the same manner

that (3.7) was derived, it can be shown that the decision variable at the $u^{th}$ receiver corresponding to the $i^{th}$ information symbol on the $m^{th}$ sub-band during a given SS-OFDM symbol is [78]:

$$z_{u,m,i} = \xi_{u,0} b_{i,m} \frac{1}{L} \sum_{l=0}^{L-1} h_{u,l,m} g_{u,l,m} + \xi_{u,0} \sum_{l=0}^{L-1} h_{u,l,m} g_{u,l,m} \sum_{\substack{k=0 \\ k \neq i}}^{L-1} c_{i,l} c_{k,l} b_{k,m} + \sum_{s=1}^{S-1} \xi_{u,s} \sum_{l=0}^{L-1} c_{i,l} g_{u,l,m} I_{u,l,m,s} \tag{4.15}$$

where $I_{u,l,m,s}$ is the ICI received on the $l^{th}$ subcarrier of the $m^{th}$ sub-band, from the $s^{th}$ interfering base station. The signal-to-interference ratio (SIR) in the $m^{th}$ sub-band at the $u^{th}$ receiver is given by [78]:

$$\gamma_m^{(u)} = \frac{\left[\frac{1}{L}\sum_{l=0}^{L-1} A_{u,l,m}\right]^2}{\left(\frac{1}{L}\sum_{l=0}^{L-1} A_{u,l,m}^2 - \left[\frac{1}{L}\sum_{l=0}^{L-1} A_{u.l,m}\right]^2\right)\frac{L-1}{L} + \frac{\sigma_{I_{u,m}}^2}{L\sigma_{sym}^2}\sum_{l=0}^{L-1} B_{u,l,m}} = \frac{\mu_{A_{u,l,m}}^2}{\sigma_{A_{u,l,m}}^2 \frac{L-1}{L} + \mu_{B_{u,l,m}} \frac{\sigma_{I_{u,m}}^2}{\sigma_{sym}^2}} \tag{4.16}$$

where $\sigma_{I_{u,m}}^2 = \frac{1}{L}\sum_{s=1}^{S-1} \left|\xi_{u,s}\right|^2 \sum_{l=0}^{L-1} \left|I_{u,l,m,s}\right|^2$ is the variance of the inter-cell interference, $\sigma_{sym}^2 = \left|\xi_{u,0}\right|^2 E_s$ is the variance of the symbol transmitted from the desired base station, $E_s$ is the information symbol energy, and $\mu_{A_{u,l,m}}$ and $\sigma_{A_{u,l,m}}^2$ are the sample mean and sample variance of $A_{u,l,m}$ and $B_{u,l,m}$. The variables $A_{u,l,m}$ and $B_{u,l,m}$ are given by:

$$A_{u,l,m} = \frac{\left|h_{u,l,m}\right|^2}{\left|h_{u,l,m}\right|^2 + \frac{\sigma_{I_{u,m}}^2}{\sigma_{sym}^2}}, \quad \text{for } l = 0,1,\ldots,L-1 \tag{4.17}$$

$$B_{u,l,m} = \frac{\left|h_{u,l,m}\right|^2}{\left(\left|h_{u,l,m}\right|^2 + \frac{\sigma_{I_{u,m}}^2}{\sigma_{sym}^2}\right)^2}, \quad \text{for } l = 0,1,\ldots,L-1 \tag{4.18}$$

Perfect channel estimation has been assumed in (4.17) and (4.18).

After equalization, despreading and demodulation, the packet is turbo decoded and a cyclic redundancy check (CRC) is performed to verify successful packet transmission. Either an acknowledgement (ACK) or negative acknowledgement (NAK) of successful packet reception is transmitted on the feedback channel for use in the hybrid ARQ scheme (see Section 4.2.4).

### 4.2.3 Adaptive Transmission and Single Sub-Band Allocation

Using pilot symbols embedded in each time-frequency frame, each mobile estimates the received signal to interference ratio (SIR) in each sub-band. These SIR estimates, $\hat{\gamma}_m^{(u)}$, are transmitted to the base station by the mobile on the reverse link. For each mobile, the SIR estimates are compared to the minimum required SIR values contained in a look-up table of possible transmission formats (Table 4.1). Details on packet structure and the PER curves are given in Appendix B.1. As a result of this comparison a modulation size, code rate and other parameters (Tables 4.1) suitable for the channel conditions of the sub-band seen by the mobile are chosen for possible packet transmission. Each of the sub-bands is allocated to a single user by the downlink scheduler (described later in this sub-section), based on the channel conditions experienced by each user in that sub-band. The delay between the channel estimation at the mobile and the beginning of the packet transmission is assumed to be 3 time slots (one slot is approximately 1.79 ms long in this section) to account for propagation and processing delays.

Table 4.1. Packet transmission formats

| *Maximum no. of slots* | *Packet Size (bits)* | *Turbo code rate* | *Modulation constellation* | *Data rate per sub-band (kb/s)* | *Ec/No at PER of 1%* |
|---|---|---|---|---|---|
| 16 | 1024 | 1/5 | QPSK | 35.70 | -13.5 |
| 8 | 1024 | 1/5 | QPSK | 71.41 | -10.5 |
| 4 | 1024 | 1/5 | QPSK | 142.82 | -7.4 |
| 2 | 1024 | 1/5 | QPSK | 285.63 | -4.3 |
| 1 | 1024 | 1/3 | QPSK | 571.27 | -1.0 |
| 1 | 2048 | 2/3 | QPSK | 1142.53 | 3.7 |
| 2 | 3072 | 1/3 | 8PSK | 856.90 | 1.5 |
| 1 | 3072 | 2/3 | 8PSK | 1713.80 | 7.1 |
| 1 | 4096 | 2/3 | 16QAM | 2285.06 | 9.2 |

Three time slots is the minimum time required to acquire an SIR estimate, send an SIR estimate to the base station, and schedule the next transmission. A half-slot offset of uplink and downlink signalling facilitates efficient feedback from the mobile to the base station.

It should be noted that the estimated supportable data rate can be based on out-dated channel information (SIR at the time of request) or channel prediction may be used to

predict the channel conditions 3 slots ahead. Adaptive margins are added to the SIR thresholds given in Table 4.1 to account for imperfect channel state estimation and prediction. The implementation of adaptive format selection thresholds is discussed with other simulation methods, in Section 4.3.3. Hybrid ARQ, to be discussed in Section 4.2.4, also mitigates the effects of these imperfections.

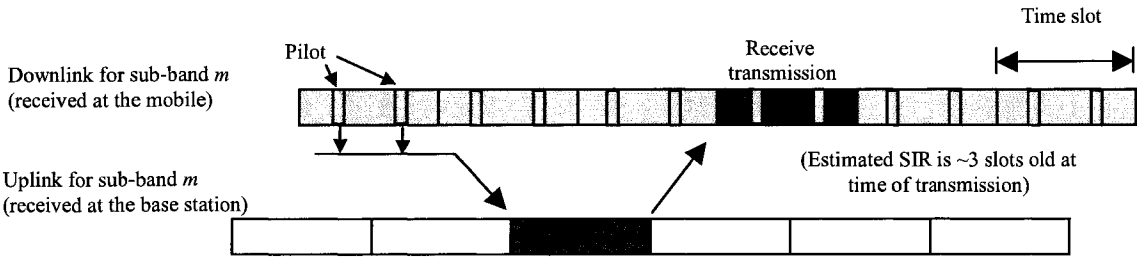


Figure 4.8. SIR estimation feedback to the base station on the uplink.

### 4.2.3.1 Scheduling of Transmissions

#### 4.2.3.1.1 Proportionally fair scheduling

Proportionally fair scheduling was first proposed by Holtzman [39] for use in single carrier cellular systems. This scheduling mechanism allows for efficient use of radio resources by scheduling transmissions to the user with the best channel conditions, compared to the user's average channel conditions.

If all users in a system undergo statistically identical fading and the window over which the user's average channel conditions are measured is sufficiently long, the system is identical to maximum SIR scheduling as the user with the best channel conditions is chosen in each time interval. This selection procedure achieves the maximum throughput of the system, and every user is allocated the same amount of resources on average.

In cellular applications, the operation of proportionally fair scheduling is significantly different from maximum SIR scheduling. The ratio of the instantaneous SIRs to the average SIR of each user is compared. In this manner, users are scheduled according to small-scale fading conditions, while long-term average SIR of the users varies with large-scale fading such as path loss and shadowing. As the small-scale fading statistics are generally the same for all users, each user receives equal radio resources in the long-term. This is significantly different from maximum SIR implementation in a cellular environment, which would result in users very near the transmitter receiving the vast majority, if not all, transmissions. The window of the average SIR must be large enough

such that small-scale fading is averaged-out, but short enough to change with varying shadowing and path loss due to mobile user movement.

#### 4.2.3.1.2 Implementation of proportionally fair scheduling

In the proposed SS-OFDM-F/TA packet data system, allocation is in two dimensions and there are only a finite number of modulation and coding schemes in a given system. Allocation in two-dimensions is accomplished by treating and allocating each sub-band independently, while maintaining a single average condition value for each user. As there are only a finite number of modulation schemes, comparing the ratio of instantaneous to average SIRs is not fair to users whose channel conditions cannot support one of the modulation schemes available. To this end, average and instantaneous throughputs are used to ensure proportionally fair scheduling with a limited number of modulation schemes. The allocation process is described below.

The allocation of transmit sub-bands to users in the $i^{th}$ time slot is dependent upon the ratio of the estimated supportable data rate, $\hat{R}_m^{(u)}(i)$, to the average data rate of packets delivered to a user, $R_{ave}^{(u)}(i)$, over a suitably chosen averaging interval. This ratio is calculated at the base station for every user in each sub-band. The mobile with the highest ratio will receive transmission at the rate $R_m^{(u)}(i) = \hat{R}_m^{(u)}(i)$ in the sub-band and time slot under consideration. The value of the average bit rate delivered to each user is updated using a low pass filter with a time constant $N_{ave}$ ($N_{ave}$ = 1000 time slots is assumed in our simulations). The average bit rate can be updated per sub-band as follows:

$$R_{ave,0}^{(u)}(i+1) = \left(1 - \frac{1}{MN_{ave}}\right) R_{ave,M}^{(u)}(i) + \left(\frac{1}{MN_{ave}}\right) R_M^{(u)}(i) \tag{4.19}$$

$$R_{ave,m+1}^{(u)}(i) = \left(1 - \frac{1}{MN_{ave}}\right) R_{ave,m}^{(u)}(i) + \left(\frac{1}{MN_{ave}}\right) R_m^{(u)}(i); \qquad m = 0,1,\ldots,M \tag{4.20}$$

where $m = 0,1,\ldots,M-1$. Alternatively, the average bit rate may be updated once per time slot $i$:

$$R_{ave}^{(u)}(i+1) \approx \left(1 - \frac{1}{N_{ave}}\right) R_{ave}^{(u)}(i) + \left(\frac{1}{N_{ave}}\right) \frac{1}{M} \sum_{m=0}^{M-1} R_m^{(u)}(i) \tag{4.21}$$

which is equivalent to the approach described by (4.19) and (4.20) when $N_{ave}$ is large. Average rate of users not selected to receive transmission in the $m^{th}$ sub-band are updated by $R_m^{(u)} = 0$.

The process takes advantage of multi-user diversity, as channel conditions are practically independent for different mobiles. The evaluation and allocation process is completed for every sub-band. Allocation of sub-bands is done on a per packet basis,

and hence, after a packet has been transmitted the sub-band is reallocated (except in the synchronous re-transmission case) according to the scheduling algorithm. Furthermore, a mobile may receive transmission on one or more sub-bands, whereas another mobile may not receive any transmission at all during a given time slot.

It is worthwhile to note that this scheduling algorithm has some similarities to the location dependent resource allocation scheme described in Chapter 3. Conventional SS-OFDM systems do not allocate resources between users based on small scale fading (with the exception of fast power control), However a greater amount of radio resources (in the form of slow power control) are allocated to users that are further from the transmitter. The location dependent resource allocation scheme attempts to equalize the average power allocated to each user by assigning more power (in the form of code channels) to those users near the transmitter. In the proportionally fair scheduling scheme described here, all users receive the same power, but are simply scheduled one at a time when the channel conditions are favourable. Note that equal power assignment was not possible in the system described in Chapter 3 as distant users would not have sufficient SIR to receive reliable zero-delay transmissions.

### 4.2.4 Type II Hybrid ARQ

The SS-OFDM-F/TA system employs stop-and-wait type II hybrid ARQ with incremental redundancy and soft packet combing [45][113]. Multi-slot transmission is terminated early if a packet is correctly decoded and an acknowledgement (ACK) is received by the base station over a feedback channel. The sub-band is then reallocated according the scheduling algorithm (Section 4.2.3) and transmission of a new packet (possibly to a different mobile) begins. If a negative acknowledgement (NAK) is received from the mobile, re-transmissions of the original packet continue. Re-transmissions occur at least 4 slots apart in order to receive positive or negative packet acknowledgement from the receiver. Time domain interlacing of independent multi-slot packet transmissions is applied to improve spectral efficiency of the stop-and-wait ARQ scheme used. Re-transmission modes other than stop-and-wait (go-back-N or selective repeat) are not considered, because in conjunction with soft packet combining they would lead to unmanageable complexity of the mobile receivers.

This thesis considers asynchronous and synchronous re-transmission methods. Synchronous re-transmission is used in the IS-856 high bit rate packet data system (1xEV-DO) [45][100]. After a packet transmission is scheduled to a user, re-transmissions occur every 4 slots regardless of the channel conditions until the packet is successfully

delivered (i.e., early termination occurs) or the maximum allowed number of re-transmissions is reached. Provided the channel changes very slowly, using synchronous re-transmissions results in low packet delay, minimal signalling overhead and high throughput. Transmission of a single packet can take from 1 to 16 time slots, depending on the data rate selected (see Table 4.1, Section 4.2.3).

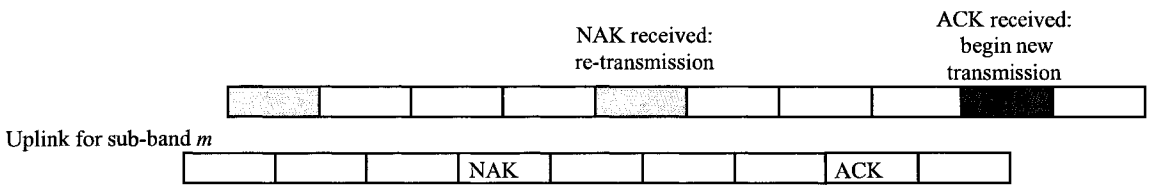


Figure 4.9. Operation of ACK/NAK feedback for early re-transmission termination in the hybrid ARQ scheme.

Asynchronous re-transmission is desirable at higher mobile speeds as synchronous re-transmission does not fully exploit multi-user diversity due to significant changes in the channel between re-transmissions. Asynchronous re-transmission options are discussed thoroughly in Chapter 5. In this chapter, a simple asynchronous re-transmission option is considered in Section 4.7 in which re-transmissions within the ARQ scheme are delayed until transmission conditions to a given mobile are favourable once again in order to ensure a proper analysis of packet structures.

## 4.3 Evaluation of Multi-Cell Performance

The simulations of the multi-cell system are partitioned into link level and system level simulations. The process of using the link level results in the system level simulation is common throughout the systems considered in Chapters 4 and 5. The system level simulations are generally the same for all sections of Chapters 4 and 5, while the link level packet configurations may be different. The cellular and channel parameters given in this section are used throughout the thesis, unless otherwise indicated. In general, this thesis considers mobile users receiving transmission from sectorized antennae. Results of the multi-cell simulation for the basic cellular performance are given at the end of this section. The reproducibility of these simulations is discussed in Appendix G.

### 4.3.1 Link Level Simulations

In the link level simulations, curves of the packet error rate (PER) in additive white Gaussian noise (AWGN) are generated for all the transmission formats given in Table 4.1, accounting also for early terminations. The PER curves corresponding to all possible formats and early terminations are employed in the system level simulations to determine success or failure of packet transmissions. Note that PER curves are used rather than a hard threshold to determine success or failure. For each packet decision, the SIR of the packet (including soft-combining of previous re-transmissions) is compared to the PER curve for that format and number of re-transmissions. The PER for the packet is estimated by interpolation (with a simulation point every 0.2 dB), and compared to a uniform random variable between 0 and 1 to determine success or failure.

Employing the AWGN results in the system level simulations is reasonable, since each sub-band is practically time-invariant during each packet time slot, and each information symbol is spread across the entire sub-band or group of sub-bands (i.e., each symbol experiences the same SIR).

Several packet format sets are considered in this thesis, and hence the link level results used are different in the various sections of Chapter 4 and 5. Encoding and packet structures are given in Appendix B.1 for Chapter 4 configurations, and in Appendix B.2 for Chapter 5 configurations. Link level curves for all packet formats considered are listed in Appendix B. Link level results for the formats listed in Table 4.1 which are used in Sections 4.4 to 4.6, are given in Appendix B.1.

### 4.3.2 System Level Simulations

The simulation is organized into 30-second runs. At the beginning of each run, users are dropped into an embedded sector. During the simulation run, shadowing and frequency selective Rayleigh fading vary depending on the mobile's velocity. Path loss is assumed constant during each run. 100 runs are completed for each case, with each run considering a different set of user locations. Results are recorded for each user of the 100 runs. Users are distributed uniformly over the area of the sector. Prior to each of the 30-second simulation runs, a 10-second window for system initialization time is simulated so the results are applicable to a "steady-state" system, and not the case of $U$ users accessing the system for the first time. The values of average bit rate delivered (for proportionally fair scheduling in Section 4.2.3.2.1) and adaptive packet format selection thresholds are initialized during this period, along with generating ongoing transmissions

to users. No results are recorded during these 10 seconds of "set-up" time. The packet selection thresholds are also primed by running 5 non-recorded 30-second simulation runs prior to the 100 recorded runs.

A 19-cell cluster, either with omni-directional antennas or sectored cells (3 hexagonal sectors per cell) is considered. Unless otherwise stated, this thesis considers sectorized cells. The sector layout is shown in Figure 4.10, and is slightly different from the layout in Chapter 3 (Figure 3.1). A horizontal radiation pattern from a typical commercial antenna with a 65° 3 dB beamwidth is used (see Appendix C) in all simulations in this thesis for all 57 sectors in the simulated model. It is assumed that the number of users communicating with each sector transmitter is constant during a given simulation run.

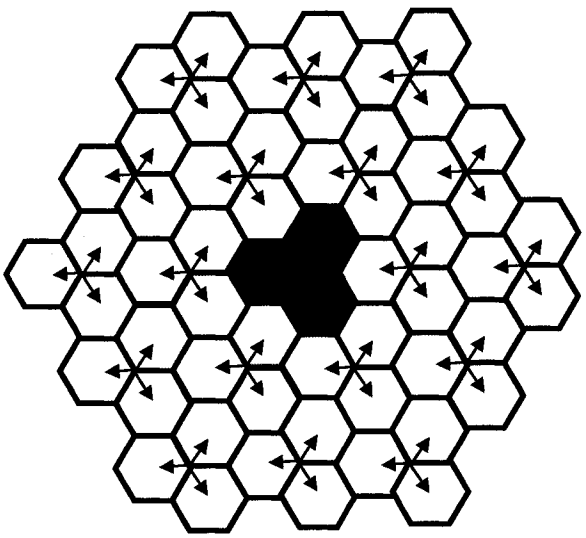

Figure 4.10. The 19-cell (57 sector) layout of the multi-cell simulation model. The arrows indicate the centre of the directional main lobe for each sector antenna. In the case of omni-directional antennas, the cell is comprised of the 3 composite sectors (shown by 3 red sectors).

Path loss and fading models are taken from ITU recommendations [43] for the Indoor Office A and B, and the Pedestrian A and B channels (see Appendix A.1). Vehicular applications will be studied exclusively in Section 4.7. Unless otherwise stated, the maximum Doppler shift assumed is $f_D = 5$ Hz which corresponds to a mobile speed of approximately 3km/h at a carrier frequency of 2 GHz. The Rayleigh fading process is generated by the means described in Appendix A.2. Spatial autocorrelation of shadowing

is exponential [35] (see Appendix A.3), with a decorrelation distance of 5 metres. Cross-correlation of the shadowing from sector antennas of the same cell is assumed equal to 1, and 0.5 between different base station sites. The standard deviations of the log-normal shadowing processes are 12 dB and 10 dB in the indoor and pedestrian environments, respectively [43]. While these are the ITU recommended values for the standard deviation of the shadowing processes, they are relatively high in comparison to other suggestions. The impact of this is briefly discussed in Section 4.4.3. This chapter uses the *composite ICI model* for small-scale fading of the ICI as described in Section 3.2.3 unless otherwise stated. Time-varying shadowing processes for each of the 56 ICI sources are simulated accurately by the method given in Appendix A.3.

Slow cell/sector selection is considered in this chapter. The best serving sector or antenna is selected for each user at the beginning of each 30-second simulation run based on the path loss and shadowing values of the beginning of the simulation time, after the 10-second initialization period. Sector selection issues are discussed in greater detail in Section 5.2. Slow sector selection has previously been considered for IS-856 [100], and was proposed for SS-OFDM-F/TA in the fall of 2001 [74].

In all sections of Chapter 4 and 5, 21.875% of each time slot/sub-band are reserved for pilot and MAC layer signalling. In the packet formats given in Table 4.1 each packet transmission over a sub-band, during a given time slot consists of 2048 complex valued chips, 1600 of which carry data, and 448 are reserved for pilot and MAC layer signalling. Packet format structures are discussed further in Appendix B.

### 4.3.3 Adaptive Packet Format Selection Thresholds

Adaptive margins at SIR thresholds for data rate selection are used to ensure a packet error rate of approximately 1% in each run, for each rate. The method used in this simulation is intended to be realistically viable. The SIR thresholds are raised and lowered based on the average packet error rate observed for a given data rate. The average data rate is updated after each time slot using a low pass filter approach, similar to that for the average data rate user in the proportionally fair scheduler (see Section 4.2.3). The time constant for average packet error rate is 1000 sub-band/time-slots, and the SIR threshold increment is 1.00005 (0.000217 dB). The initial values are chosen to be 1 to 2 dB higher than the SIR thresholds required to achieve a 1% PER in a static channel.

In order to ensure that the thresholds are at the proper levels at the start of the simulation, the values are primed by running the simulation for 5 complete 30-second

simulation sets with the appropriate number of users so that the initial thresholds are near the steady-state values for the specified number of mobiles. In addition, 10 seconds of simulated time prior to recording the performance measures of throughput, delay, etc for each of the recorded 100 30-second runs.

### 4.3.4 Nomadic Users and Mobile Users

Nomadic and mobile users are two possible categories of users for this system. Nomadic users are those that change locations, however they are relatively stationary while receiving transmissions. This model applies to office workers, or workers using wireless inspection equipment, both of which change locations throughout the day but are not generally interfacing with the wireless network and moving at the same time. In order to model these users, the attenuation due to shadowing does not change throughout the 30-second run. Small-scale fading still occurs as signal reflections can occur of moving objects resulting in the same effect as if the user was in motion.

This thesis considers mobile users unless otherwise specified. Mobile users are those that can be assumed to be in motion while receiving transmission. These user maybe in a vehicle (i.e., taxi or forklift) or may simply be walking. It should be noted that a user does not have to be actively interfacing with wireless equipment in order to require transmission. For example, a user may request a large portion of information or an ongoing-buffered stream of information such as music or video, and then proceed to change locations that would require transmission to a mobile in motion. In this more general case of mobile users, the value of shadowing process changes throughout the 30-second simulation run with an exponential correlation in distance (related to time through mobile velocity) as discussed in Appendix A.3.

## 4.4 Basic Multi-Cell Performance

### 4.4.1 System Parameters

The system parameters used in this section are intended to facilitate comparisons to single carrier systems. For this reason, the packet format set from IS-856 [100] is used. These formats are given in Table 4.1. The packet transmission is 2048 symbols, including overhead (21.875 %). As the IS-856 system was intended to be compatible with the 1.25 MHz 2 and 3G North American channel bandwidths allowing for channel chip rates of 1.2288 Mchip/s, a direct comparison is made with an SS-OFDM-F/TA with similar time-slot durations and equivalent sub-band chip rates. This configuration results in

relatively large sub-band bandwidths, but it is shown in Appendix D that this configuration is satisfactory in terms of frequency resolution of sub-bands for the Indoor and Pedestrian A channels, while this has already been shown for the Indoor B channel in Section 4.2. The Pedestrian B channel requires narrower sub-bands for optimal performance; a problem that is solved by the proposal of allocating disjoint groups of sub-bands in Section 4.5. Vehicular configurations are discussed in Section 4.7. The main lobe bandwidth of the SS-OFDM signal occupies approximately 95 % of the channel bandwidth, which is the same as for DVB systems [26], and less than the 98.3 % value for IS-856.

The system parameters are given in Table 4.2. The parameters are different for the indoor and pedestrian channels as it is envisioned that the system would operate in different modes depending on the physical qualities of the cell. The system parameters are all different by factors equal to powers of 2, so that a mobile receiver could use the same hardware and processing configurations with only factor of 2 multiples of clock timing or array sizes. The configurations are the same for the A and B channel of each environment as it is assumed that they each occur with some probability.

Table 4.2. System parameters for the indoor and pedestrian channels.

| | *Indoor* | *Pedestrian* |
|---|---|---|
| $N$ (subcarriers) | 256 | 512 |
| $M$ (sub-bands) | 8 | 4 |
| Bandwidth | 10 MHz | 5 MHz |
| Main lobe bandwidth | 9.5157 MHz | 4.7486 MHz |
| $T_{sym}$ (SS-OFDM symbol duration) | 27.008 μs | 108.032 μs |
| $T_g$ (cyclic prefix duration) | 1 μs | 4 μs |
| Time slot length | 1.7925 ms | 1.7925 ms |

### 4.4.2 Common Performance Measures

In Chapters 4 and 5, the cellular systems are evaluated through the average throughput per cell/sector and packet delays. This sub-section describes the basic performance measures used often throughout the cellular examination. Other performance measures that are used less frequently are described as needed.

The *average throughput per sector/cell* is the average amount of information in bits successfully transmitted to all users in a given sector or cell per second. Note that the average throughput is the average over all 100 30-second runs, and therefore considers

100 sets of $U$ mobile locations and shadowing processes. The packet sizes as given on Table 4.1 indicate the number of data bits sent (e.g., 1024, 2048, etc), however, 6 bits per packet are appended 'tail' bits, add by the turbo encoder and do not carry data. These 6 bits per packet are not included in the average throughput of the system. This performance measure shows the overall performance of system and its ability to exploit multi-user diversity; however, it says nothing about how the transmitted information had been divided amongst the users. The *cumulative distribution function* (CDF) *of the average throughput per user* is the CDF of average throughputs across all locations. For example, if the simulation considers 32 users per cell, then after the simulation we have 3200 average throughputs each corresponding to a 30-second span at a given location. The CDF of these 3200 values can then be plotted. The distribution can be considered a measure of fairness among the users. A CDF with a very steep slope would indicate a large degree of fairness, as many users would have similar average throughputs, whereas a lower slope would indicate a greater spread in the average throughputs per user.

*Packet delays* are an important measure in this best effort system as the throughput of the system has been increased by allowing longer packet delays through scheduling. The *head-of-queue packet delay* is measured from the start of the transmission of the $(i+1)^{th}$ packet transmission of the $u^{th}$ user, to the start of the $i^{th}$ packet transmission of the $u^{th}$ user. A head-of-queue packet delay of zero time slots can occur as there are multiple parallel channels (i.e., sub-bands) in the system. The *transmission delay of a packet* is the number slots from the first transmission to the completion of the packet transmission. Unless one of the previous 2 component delays are specifically mentioned, the term *packet delay* refers to the *total delay* of the packet from the start of the $(i+1)^{th}$ packet transmission of the $u^{th}$ user, to the end of the $i^{th}$ packet transmission of the $u^{th}$ user. Showing the CDF of the delays is the most effective way of displaying the delay results, although occasionally the average of this distribution will be given. Packet delay statistics can be measured for all users and every packet, or the *average packet delay per user* can be measured. The average packet delay per user is found by determining the average packet delay for each of the $U$ users in each of the 100 simulations, and then plotting the distribution of these averages.

### 4.4.3 Simulation Results

The average throughput per sector in the indoor channels is shown in Figure 4.11 for the cases of omni-directional antennas and sectorized antennas, and mobile and nomadic users. The results in Figure 4.11 are for the Indoor B channel, as the results for the Indoor A channel are nearly identical. It can be seen that as the number of users is increased, the average throughput of the cell/sector increases. This is because with increased multi-user diversity, the scheduler has more mobiles from which to choose, and therefore it is more likely that the channel conditions for each transmission will be highly favourable. Because the shadowing conditions do not change during a given simulation run for nomadic users, the nomadic users are always receiving transmission from the best possible serving sector, and therefore the throughput is the highest for these users. As mentioned, this thesis generally assumes the case of mobile users. Comparing omni-directional and sectorized antennas shows that the throughput per cell is increased by 178 % by using 3 sector antennas for the mobile user case.

Figure 4.11 also shows the performance difference between using the composite ICI model and the explicit simulation of the ICI sources. Clearly, the throughput is significantly higher with the explicit ICI model. The additional fluctuations in the ICI in time and across sub-bands in this model result in increased fluctuations in the received SIR of users signals. Provided there is multi-user diversity ($U > 1$), the increased SIR fluctuations are exploited by the scheduler by transmitting to the user with the most favourable channel conditions. This thesis uses the more general composite ICI model, which can be seen as the 'worst-case' model for the ICI for this system and hence the results can be considered slightly pessimistic.

Figure 4.12 shows the throughput of the Pedestrian A and B channels, using both the ICI models. The throughput for the pedestrian channels is somewhat higher than the indoor channels because there is more sector isolation due to a larger path loss exponent (4 compared to 3) for the pedestrian channels. In additional, the standard deviation of the shadowing process is slightly lower in the pedestrian channel (10 compared to 12). The throughput is lower in the Pedestrian B channel as the channel is very frequency-selective, and 4 sub-bands are not sufficient to exploit the frequency diversity of each sub-band. This problem is addressed in Section 4.5. Figure 4.12 also shows that explicitly simulating the ICI sources results in significantly higher average throughputs in the Pedestrian channels, in comparison to using the composite ICI model.

The CDF of the user throughputs is a critical measure in determining how the data is distributed among the users. From Figure 4.13 it can be seen that fairness among users is slightly better in the pedestrian channel, whereas in the 10 MHz indoor channels more than 50% of users in the sector have throughputs less than 250 kb/s when there are $U = 32$ users in the sector.

The packet delay for the Indoor B and Pedestrian A channels is shown in Figure 4.14a and b for $U$=32 per sector for the default parameters of shadowing, mobile users, and sectorized antennas as given in Section 4.3. The total packet delay is less than or equal to 10 time slots (~17 ms) for 90% of the packets. The average packet delay per user with $U = 32$ users per sector provides a clearer picture of the distribution of packet delays (Figures 4.15 and 4.16). The average packet delays are shorter in the Indoor B channel, as there are more parallel channels in the system (8 sub-bands compared to 4). This is supported by noting that the transmission delays in both channels are similar, while the head-of-queue packet delays in the pedestrian are nearly twice as long. Comparing the average packet delays per user to the packet delays given in Figure 4.13, the average packet delay per user are much longer and hence, the relatively long packet delays corresponding to transmission with poorer or average channel conditions makes up a very small portion of the total number of packet transmissions.

As mentioned earlier, increased multi-user means that the scheduler is more likely to be able to select a mobile with favourable channel condition to transmit. This is clearly visible in the histograms of the selected packet formats in Figure 4.17. It shows that 48% of packet format selections resulted in outage for $U$=1 as the channel conditions were too poor. For $U$=32 users per sector the probability of not being able to select a suitable packet format is 0.4 %. As different packet formats have different numbers of allowable re-transmissions, it is useful to also examine the portion of time a given packet transmission is being used (Figure 4.18). In this case it can be seen that for $U$=1 user, a given sub-band/time slot is in outage 36 % of the time. This is not surprising considering the results of the conventional system in Chapter 3. The outage drops to 3.4 % for $U$=4 users, and 0.3 % for $U$=32 users. At the far right-hand side of the histogram it can be seen that the highest data rate available is in use 34.5 % of the time, which corresponds to 44.6 % of all packet format sections for $U$=32 users per sector.

ITU recommendations for the standard deviation of the shadowing processes for the indoor and pedestrian channels of 12 dB and 10 dB [43], respectively, are used in this thesis. As mentioned, these are somewhat higher than recommended by other sources [85] and higher than other similar best-effort investigations [23]. It is of interest to see

how this selection of severe shadowing conditions affects the system performance. Figure 4.19 shows the increase in throughput if a standard deviation of 6.5 dB for the shadowing process is used instead of the ITU recommended values. The throughput gain is up to 89% for $U$=32 users. It is important to note that the throughput increase due to considering a less significant shadowing process benefits the users with the poorest channel conditions the most. It can be seen from Figure 4.13 that users with the lowest throughputs have significant better average throughputs with a lower shadowing standard deviation, where as the users with high throughput are relatively unaffected, or slightly drop in average throughput. It is also evident from Figure 4.20 that a lower standard deviation for the shadowing process decreases packet delays. This is the case because users are less likely to have prolonged very poor channel conditions that would prevent the completion of a packet transmission when the shadowing process is less significant. Summarizing Figures 4.13, 4.19, and 4.20, it is clear that if lower standard deviation values for the shadowing process were chosen the results would be higher average throughput per sector, increased fairness in user throughputs and average packet delays, and lower overall packet delays. Clearly the high ITU shadowing parameters used give a 'worst case' performance of the system.

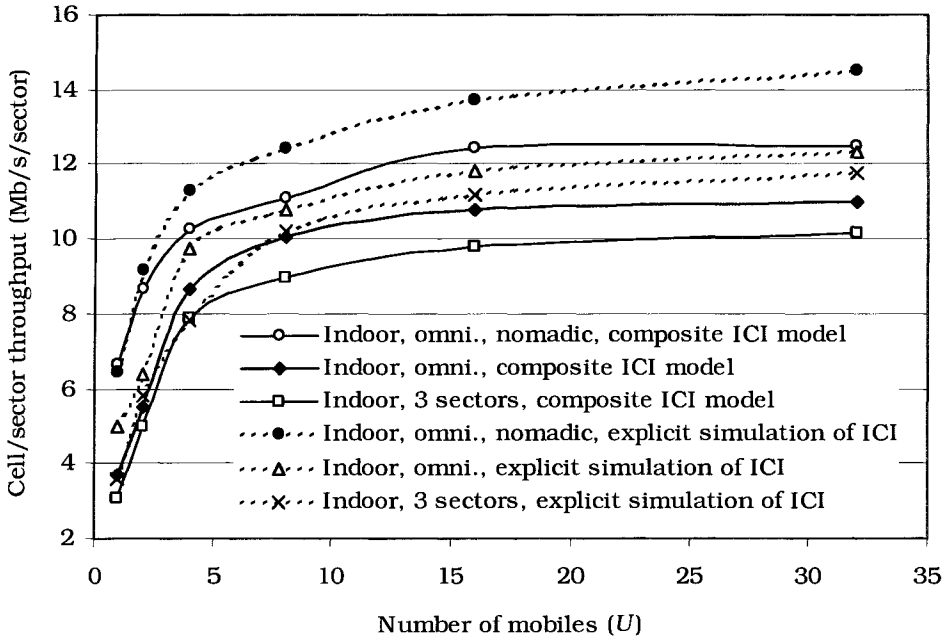


Figure 4.11. The average throughput per cell/sector in the indoor channels for omni-directional or sectorized antennas, nomadic or mobile users, and the 2 different ICI models; 10 MHz bandwidth.

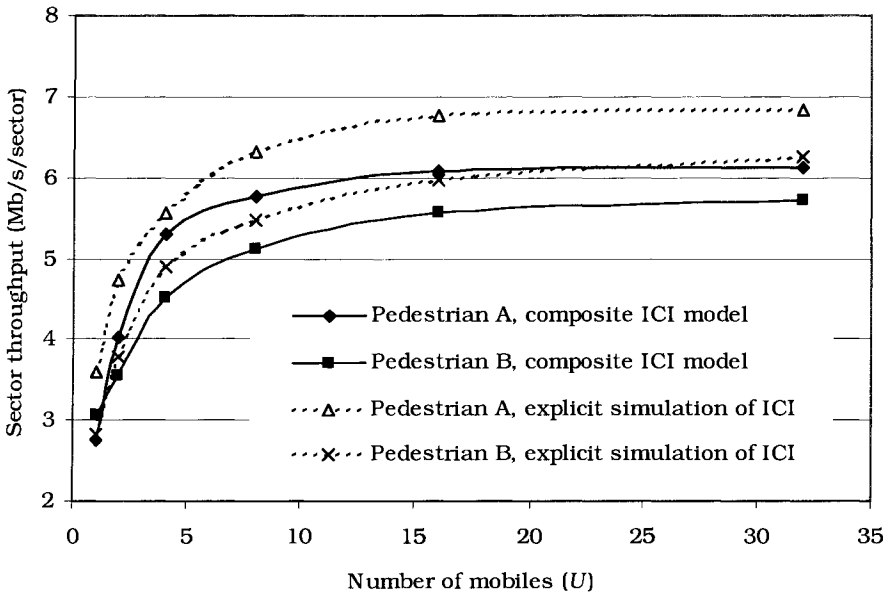


Figure 4.12. The average throughput per cell/sector in the pedestrian channels for the 2 different ICI models; 5 MHz bandwidth. The composite ICI model is used in this thesis, unless otherwise stated.

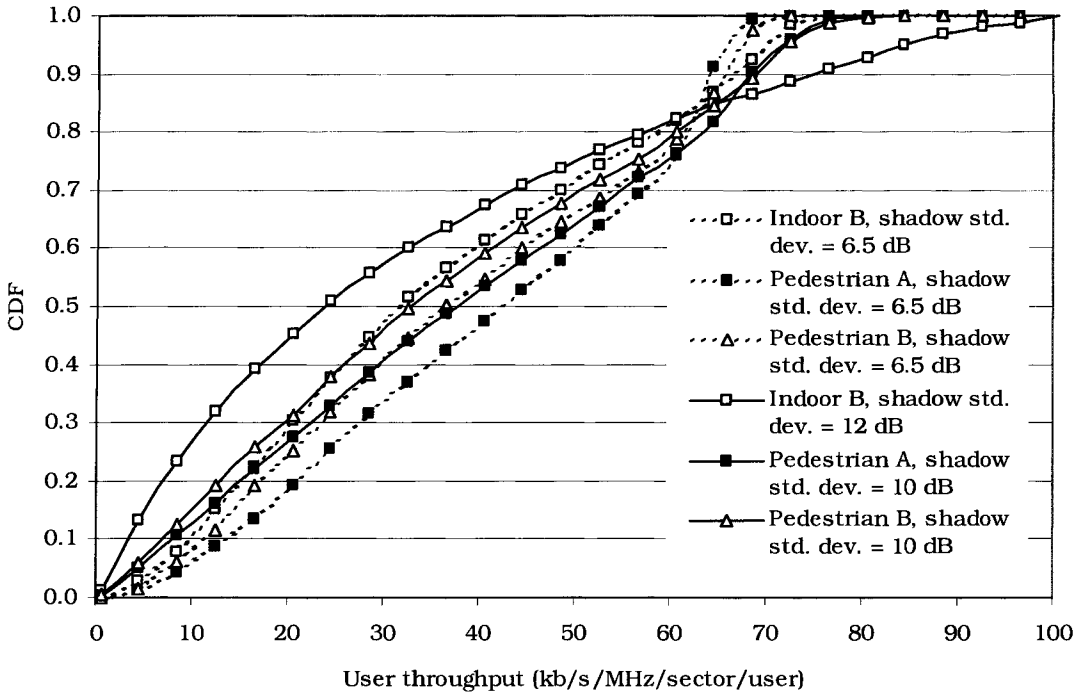


Figure 4.13. The CDF of user throughputs for the 10 MHz indoor channel and the 5 MHz pedestrian channels; sectorized antennas, mobile users, and composite ICI model; $U = 32$ users.

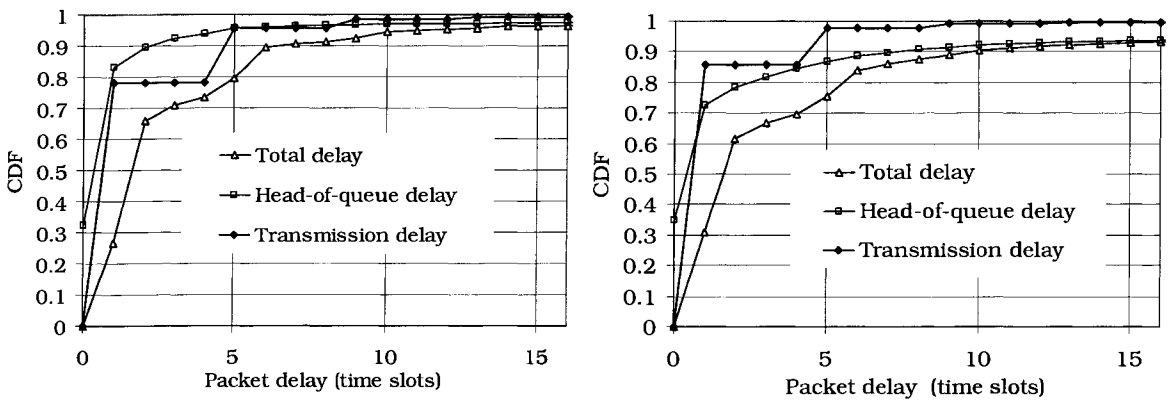


Figure 4.14. The CDF of the packet delays for the Indoor B channel (a) and the Pedestrian A channel (b) with $U$=32 users per sector.

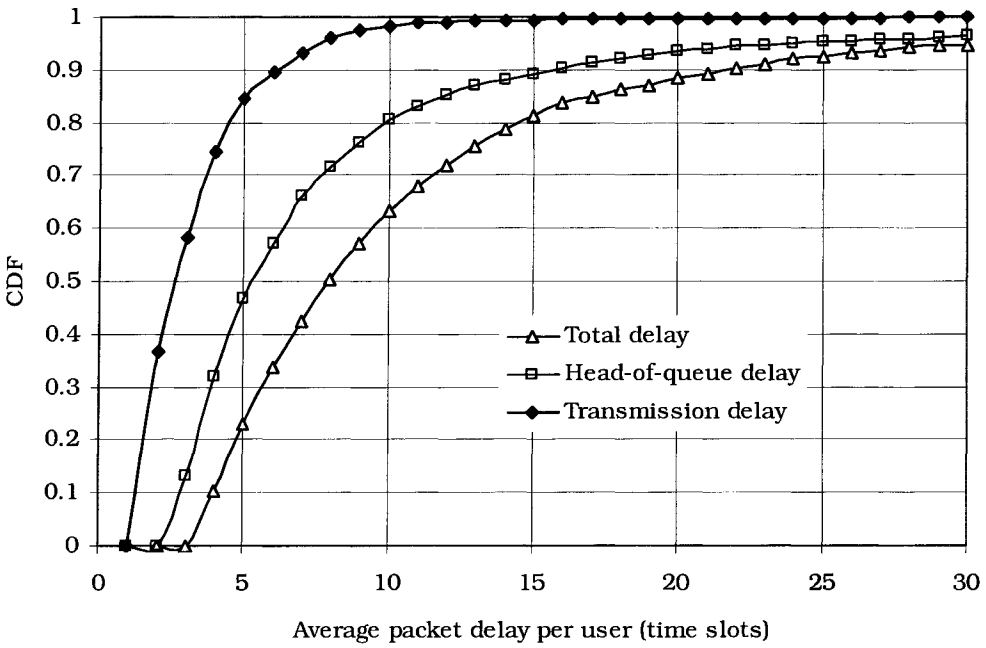


Figure 4.15. The CDF of the average packet delays per user for the Indoor B channel with $U$=32 user per sector.

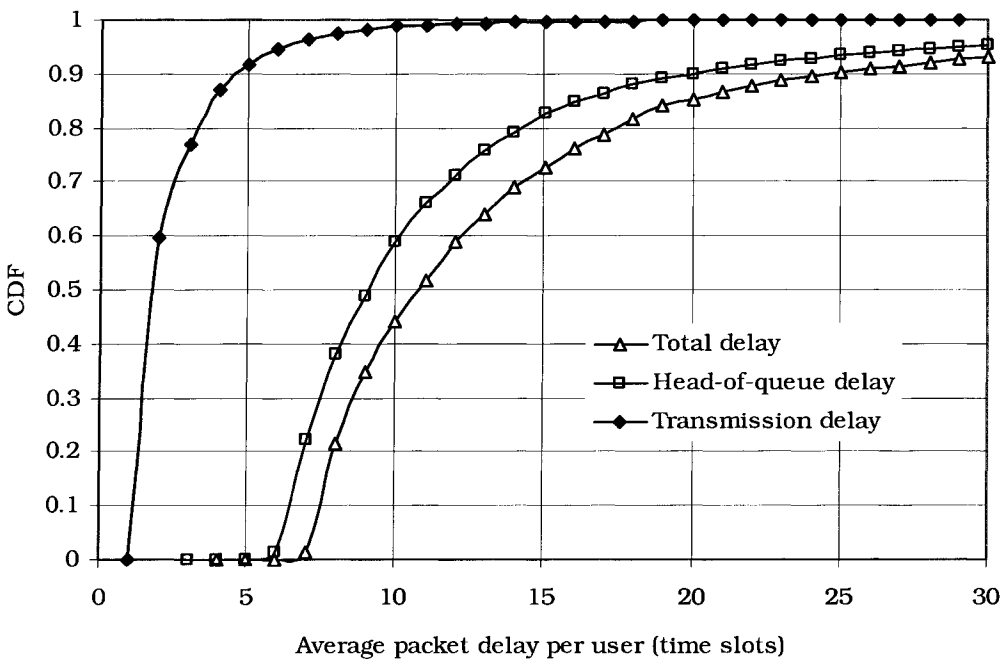


Figure 4.16. The CDF of the average packet delays per user for the Pedestrian A channel with $U$=32 user per sector.

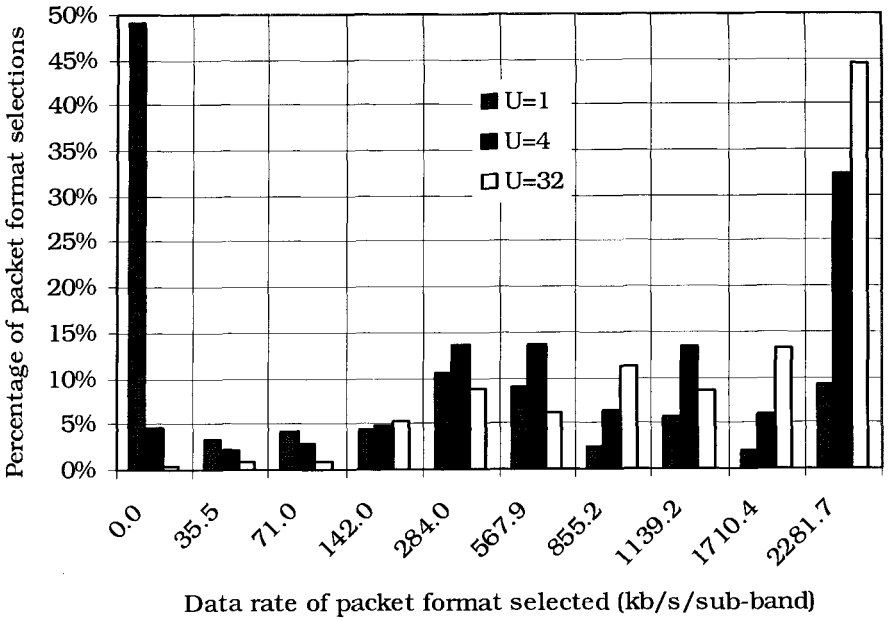


Figure 4.17. The percent of the total packet format selections that a given packet format was selected for the Indoor B channel.

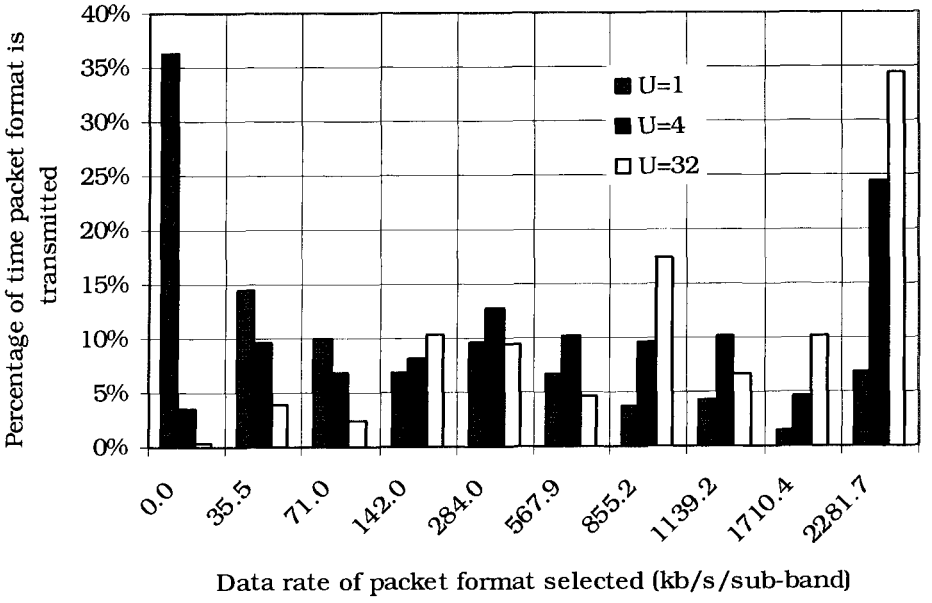


Figure 4.18. The percent of all sub-band/time-slots that a given packet format is being transmitted for the Indoor B channel.

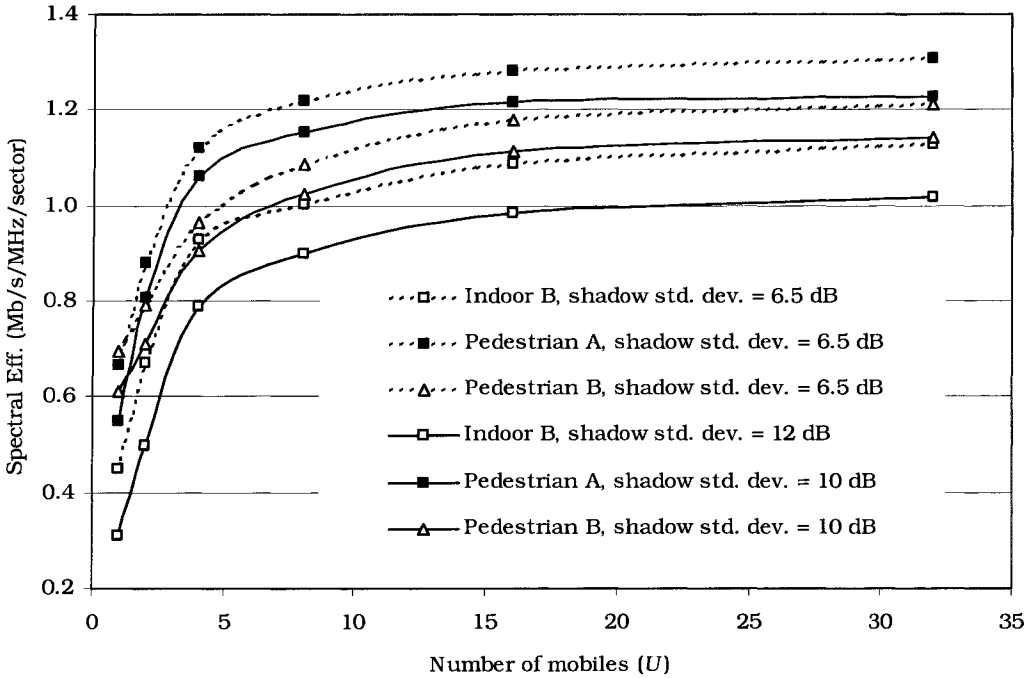


Figure 4.19. The average throughput per sector for the Indoor B and pedestrian channels with different standard deviations of the shadowing process.

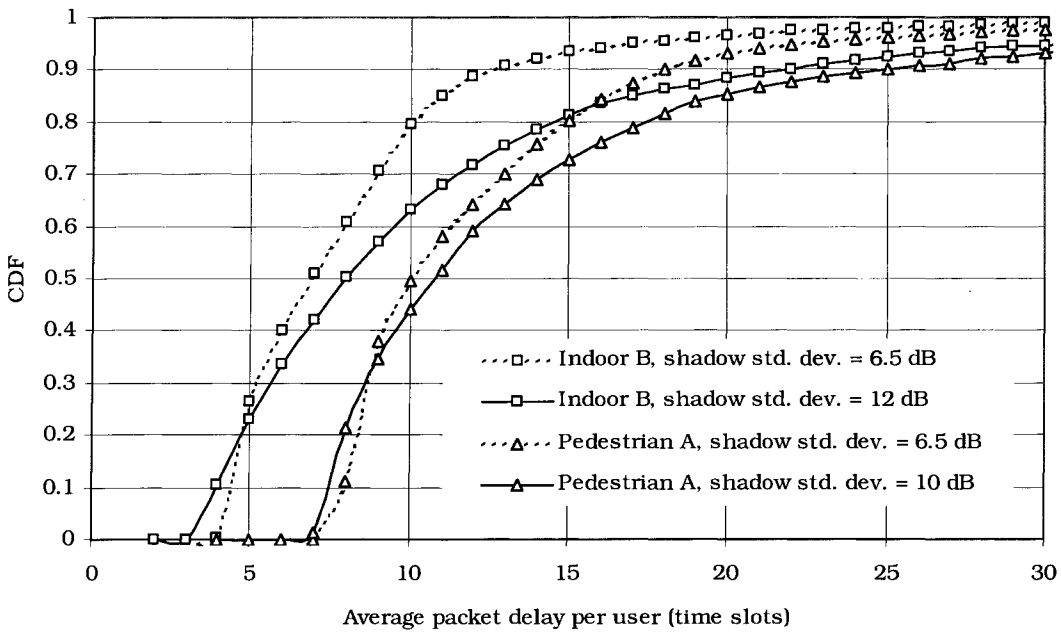


Figure 4.20. The CDF of the average packet delays per user for the Indoor B and Pedestrian A channel with $U$=32 user, considering different values for the standard deviation of the shadowing process.

## 4.5 Allocation of Groups of Disjoint Sub-bands

In highly frequency selective environments, a large number of sub-bands is required to fully take advantage of the diversity in the system. In addition, the time slots need to be sufficiently short to ensure the channel does not change significantly during transmission. These time-frequency constraints may lead to very small packet sizes, which are undesirable. Sufficiently large packet sizes can be maintained by allowing several disjoint sub-bands to be allocated jointly [75] (see Figure 4.21). This section considers allocation of several disjoint sub-bands to a user in sets of $M_g = M_n / M_{eff}$, where $M_n$ is the number of narrow frequency-flat sub-bands in the wideband channel. $M_{eff}$ is the number of sub-band groups, and hence, $M_{eff}$ is the effective number of parallel channels to be allocated. $M_{eff}$ replaces $M$ in (4.14)-(4.21). A packet transmission is spread over the $M_g$ sub-bands allocated to it.

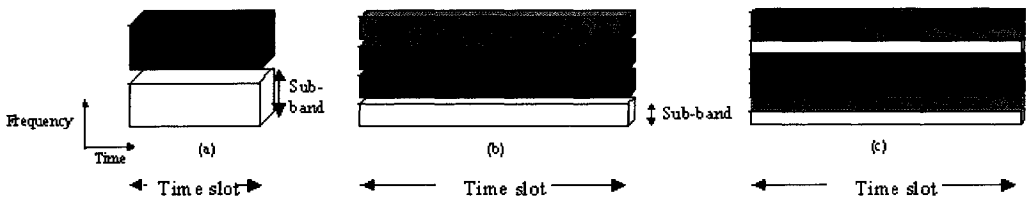


Figure 4.21. Increasing the number of sub-bands increases the time slot duration (if all other parameters are held constant). Allocation of groups of disjoint sub-bands (shown by the same colours in (c)) allows for a larger number of sub-bands without changing the time slot duration.

The formation, as well as the allocation, of the groups of disjoint sub-bands is adaptive. The best group formation and allocation with proportionally fair scheduling maximizes the ratio of the delivered throughput to average throughput during the $i^{th}$ time slot, $\sum_{g=0}^{M_{eff}} R_g^{(u_g)}(i) / R_{ave}^{(u_g)}(i)$, where $R_g^{(u_g)}(i)$ is the data rate delivered to the $u_g{}^{th}$ user over the $g^{th}$ group of sub-bands, and $u_g$ is the user selected by scheduler to receive transmission over the $g^{th}$ group of sub-bands. The best group formation and allocation scheme requires calculating the estimated SIR $\hat{\gamma}_g^{(u)}$, over each possible group of $M_g$ sub-bands for each of the $U$ users. There are $\binom{M_n}{M_g}$ possible ways of selecting $M_g$ sub-bands from $M_n$ sub-bands. For each of these cases, the user with the highest ratio of $\hat{R}_g^{(u)}(i) / R_{ave}^{(u)}(i)$ is determined, where $\hat{R}_g^{(u)}(i)$ is the estimated supportable data rate found

from $\hat{\gamma}_g^{(u)}$. The scheduler must then select which one of the possible $G_{total} = \prod_{m=0}^{M_{eff}-1} \binom{M_n - mM_g}{M_g} / M_{eff}!$ distinct sub-band configurations results in the highest value of $\sum_{g=0}^{M_{eff}} \hat{R}_g^{(u_g)}(i) / R_{ave}^{(u_g)}(i)$ for use in the $i^{th}$ time slot. This can be an overly complex procedure that would be difficult to implement for large numbers of users and sub-bands.

A simple algorithm is proposed to allocate and form groups of disjoint sub-bands that requires only the feedback of sub-band SIRs from each user to the base station. For each user, the $M_g$ sub-bands with the highest SIRs are grouped together. The SIR over the group of sub-bands, $\hat{\gamma}_g^{(u)}$, is compared to the data rate thresholds. The user with the highest estimated supportable to average bit rate ratio (proportionally fair scheduling) will receive packet transmission as described for single sub-band allocation in Section 4.2.3.1. The process is repeated for the remaining $M_n$-$M_g$ sub-bands, again with all $U$ users, until all sub-bands have been allocated.

In order to properly select the packet format best suited to the channel conditions of the $g^{th}$ group of sub-bands, the group SIR $\hat{\gamma}_g^{(u)}$ must be known at the base station. The value of $\hat{\gamma}_g^{(u)}$ can be well approximated from the values of the sub-band SIRs assigned to the $g^{th}$ group, $\hat{\gamma}_{m_g}^{(u)}$, $m_g$=0,1,...,$M_g$-1. Provided each sub-band is narrow compared to the coherence bandwidth of the channel (which is generally true by design), the SIR of the $m^{th}$ sub-band can be approximated from (4.16) as $\hat{\gamma}_m^{(u)} \approx \left|h_{u,m}\right|^2 \left(\sigma_{sym}^2 / \sigma_{I_{u,m}}^2\right)$, where we have assumed for simplification in the analysis that $h_{u,n,m} = h_{u,l,m}$, for $n, l \in [0, L-1]$. Using this result, the SIR of the $g^{th}$ group of sub-bands for the $u^{th}$ user can be well approximated by [75]

$$\hat{\gamma}_g^{(u)} \approx \frac{\mu_{A_{u,m_g}}^2}{\sigma_{A_{u,m_g}}^2 \frac{N - M_{eff}}{N} + \mu_{B_{u,m_g}}} \tag{4.22}$$

where $A_m$ and $B_m$ are defined by:

$$A_{u,m_g} = \frac{\hat{\gamma}_{m_g}^{(u)}}{\hat{\gamma}_{m_g}^{(u)} + 1} \quad \text{for } m_g = 0,1,...,M_g - 1 \tag{4.23}$$

$$B_{u,m_g} = \frac{\hat{\gamma}_{m_g}^{(u)}}{\left(\hat{\gamma}_{m_g}^{(u)} + 1\right)^2} \quad \text{for } m_g = 0,1,...,M_g - 1 \tag{4.24}$$

### 4.5.1 Simple Model Analysis

As in Section 4.2.1.1, the average received SINR during scheduled transmission in a simplified system with AWGN instead of inter-cell interference is useful in showing the effectiveness of this technique. The average received SINR during scheduled transmissions for a system with $M_n$ sub-bands allocated in groups of $M_g$ sub-bands, and $U$ users in the system, is given by:

$$\overline{\gamma}_g(U, M_n, M_g) = E\left[\frac{1}{M_{eff}}\sum_{g=0}^{M_{eff}} \gamma_g^{(u_g)}\right] \tag{4.25}$$

where $\gamma_g^{(u_g)}$ is the received SIR over the $g^{th}$ group of $M_g$ sub-bands which have been allocated to the $u_g^{th}$ user according to the algorithm described earlier in this section. The simple case of all users having an average $E_s/N_0 = 0$ dB in the Pedestrian B channel, and channel variations due to Rayleigh fading only, is examined in this sub-section. An SS-OFDM symbol with $N$=512 subcarriers, a duration of $T_{sym} = 108.032$ $\mu$s and a cyclic prefix of duration 4 $\mu$s is used.

The average received SINR during scheduled transmissions is shown in Figure 4.22 for cases of single sub-bands allocation with various numbers of sub-bands $M$, and in Figure 4.23 for various cases of sub-band grouping with the configurations ($M_n$, $M_g$). Clearly, 32 sub-bands are required to fully exploit the multi-user and frequency diversity in this system. Given the time slot duration of 1.7925 ms from Section 4.3 and the packet sizes of Table 4.1, only a maximum of $M = M_{eff} = M_n/M_g = 4$ sub-bands is possible in the 5 MHz Pedestrian B channel, and hence the (16,4) and (32,8) sub-band systems are shown in comparison to the (4,1) or $M$=4 single sub-band allocation case. It is clear that the ($M_n$,$M_g$)=(32,8) configuration is significantly better than the ($M_n$,$M_g$)=(4,1), even though both have $M_{eff} = 4$ parallel channels. It can also be noted, that the (32,8) configuration still incurs a performance loss due to lack of frequency resolution in comparison to the $M$=512 system.

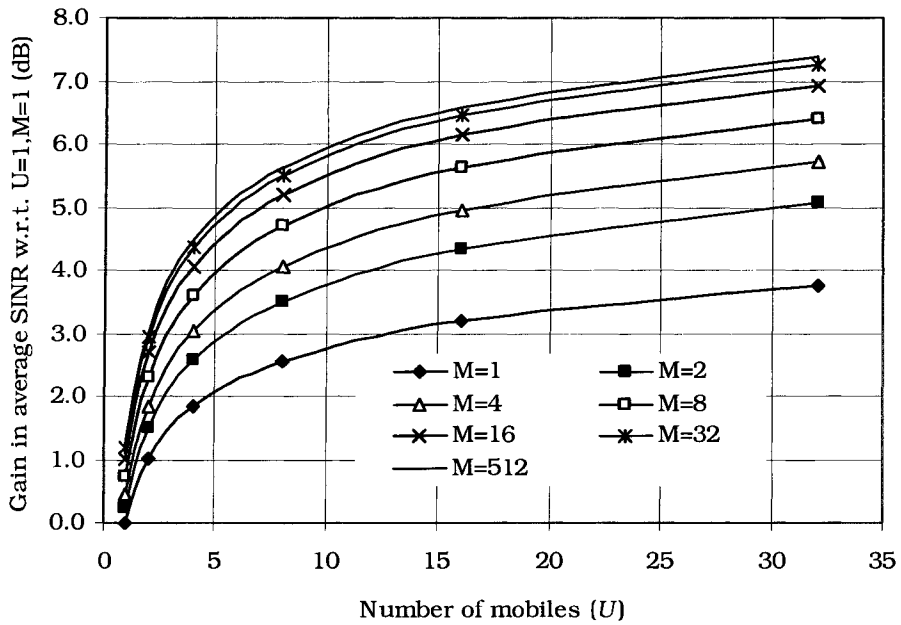


Figure 4.22. The normalized gain in average SINR for the Pedestrian B channel.

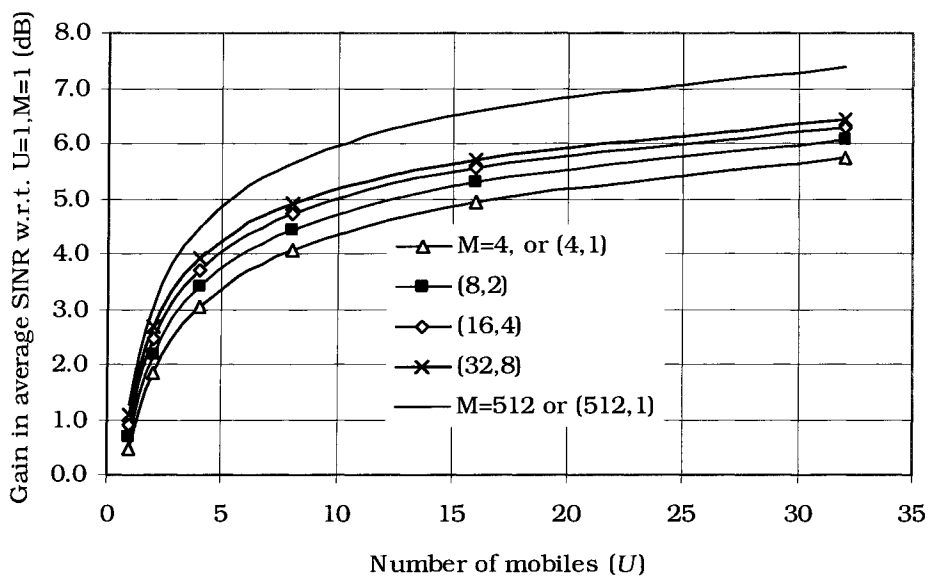


Figure 4.23. The normalized gain in average SINR for the Pedestrian B channel with grouping of disjoint sub-bands. Sub-band grouping configurations are given in the format $(M_n, M_g)$.

### 4.5.2 Cellular System Results

In the Pedestrian B channel, the case exists where the packet size and time slot duration dictate the use of relatively wide sub-band that are significantly greater than the coherence bandwidth of the channel. As was shown in the previous section, $M_n$=32 sub-bands are sufficient to properly take advantage of the frequency diversity of the channel. In Figure 4.24, the performance of the system in the Pedestrian B channel with and without the grouping of disjoint sub-bands is shown. The multi-cell simulations use the simulation structure and system parameters given in Sections 4.3 and 4.4 for sectorized cells and mobile users. Clearly, this method of sub-band grouping is highly effective as it raises the average throughput per sector by 8% with $U$=32 users. More significant is the observation that the benefit in terms of user throughputs is to user with average channel conditions; between the $20^{th}$ and $80^{th}$ percentiles (Figure 4.25). Note that user around the $50^{th}$ percentile experience a throughput gain of approximately 15%. The effect of perfect channel prediction is also evident from Figure 4.24. Perfect channel prediction refers to knowing the SIR estimates exactly, rather than using SIR estimate that are out-dated by 3 time slots (see Figure 4.8). One might expect that as the adaptive formation and allocation of sub-band groups use only SIR estimates, that perfect (3 slots ahead) prediction of these estimates may significantly improve the throughput results, however, only small increases in the average throughput per sector are observed for systems with and without sub-band grouping. The use of sub-band grouping and out-dated and perfect estimates are discussed in Chapter 5 in the context of asynchronous re-transmission algorithms.

It was stated in Section 4.4 that the same basic system is used in both Pedestrian A and B channels, however the Pedestrian B channel is highly frequency selective and the Pedestrian A channel is nearly flat (see Appendix D). Note that the use of sub-band grouping in general in the Pedestrian channels does not change the lower performance of the system in the Pedestrian A channel, as there is no loss associated with sub-band grouping in non-selective channels. Allocation of $M = 4$ single sub-bands can be seen as a special case of the (32,8) sub-band grouping configuration in which 4 groups of 8 adjacent sub-bands are allocated. Hence, the $M$= 4 system gives the worst-case performance for the (32,8) sub-band grouping configuration in the Pedestrian A channel, as the formation of sub-band groups is fixed (4 groups of 8 adjacent sub-bands) and not adaptive. In general, this thesis assumes (32,8) sub-band grouping in the Pedestrian B channel, and to show the worst case performance, the single $M$=4 sub-band allocation is

considered in the Pedestrian A channel. Note that both systems have 4 parallel channels, $N$=512 sub carriers, and identical SS-OFDM symbol parameters so it is envisioned that the configurations would be compatible.

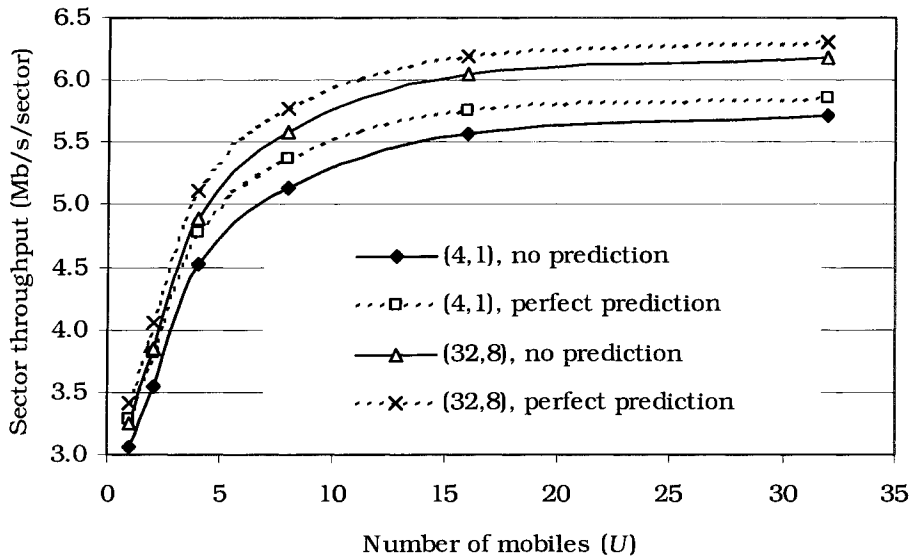


Figure 4.24. The average throughput per sector for the Pedestrian B channel with and without the grouping of disjoint sub-bands where the sub-band configuration is given in the format ($M_n$, $M_g$). Perfect channel prediction is also considered.

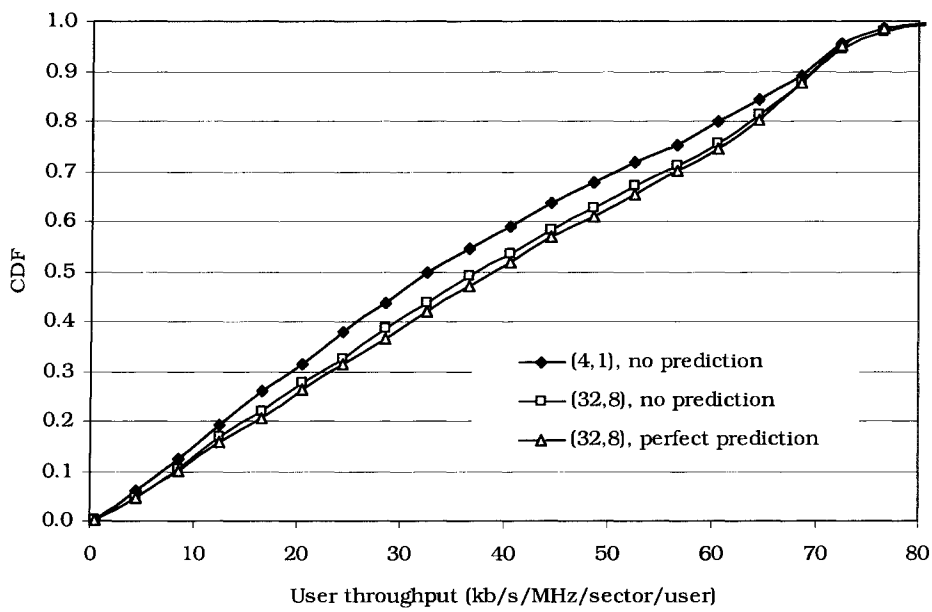


Figure 4.25. The CDF of the use throughputs for the Pedestrian B channel with and without the grouping of disjoint sub-bands where the sub-band configuration is given in the format ($M_n$, $M_g$); $U$=32 user per sector.

## 4.6 Comparison to Single Carrier Systems

As discussed in Chapter 1, some single carrier best-effort packet data systems have been proposed. It is of great interest to examine the relative performance difference between this OFDM-based system and a single carrier option.

As the basic packet structures and hybrid ARQ scheme used in this chapter are identical to those proposed for 1xEV-DO, a rough comparison in performance can be made. The average data throughput per sector for the 1xEV-DO system and SS-OFDM-F/TA system are presented in Figure 4.26 with a standard deviation of shadowing fading of 6.5 dB, and a path loss exponent of $\Upsilon_{PL} = 3.8$. The single carrier system slightly outperforms the multi-carrier system in the Pedestrian A channel, which is nearly a flat fading channel. The decorrelation distance used in the EV-DO simulations is 10 m instead of the 5 m used for the SS-OFDM-F/TA simulations, resulting in optimistic performance estimates for the EV-DO system. When significant multipath is introduced (Pedestrian B), the single carrier system suffers from self-interference. The performance advantage of the SS-OFDM-F/TA system is increased to approximately 35% when the allocation of disjoint sub-bands in groups is considered, as proposed in the previous section. It can also be noted that as the multi-carrier system is easily scalable in frequency, increasing the bandwidth of the system easily attains increased multi-user diversity. In general, the use of large IS-856 packet sizes is too constricting for the SS-OFDM-F/TA system to take full advantage of the frequency and multi-user diversity with $M_{eff} = 4$ sub-bands (see Appendix D) given a time slot of 1.7925 ms, and hence sub-grouping is needed. If the 1xEV-DO and SS-OFDM-F/TA systems were compared with longer time slot durations in low mobility environments, the performance advantage for SS-OFDM-F/TA would be even larger.

In practical applications of this system with low user mobility, there is some time constraint applied so that a user will not go without transmission for very long periods of time (~1000 slots in this system). This is particularly significant when the number of users becomes large because the number of times favourable signalling conditions occur in a given time window is limited, and a given user would have a decreasing probability of being selected during these times as the number of users increases. It is intuitive to assume that having a larger number of sub-bands from which to choose would be advantageous. The comparison of a single sub-band, 1.25 MHz system and a 4 sub-band, 5 MHz system indicates this performance difference.

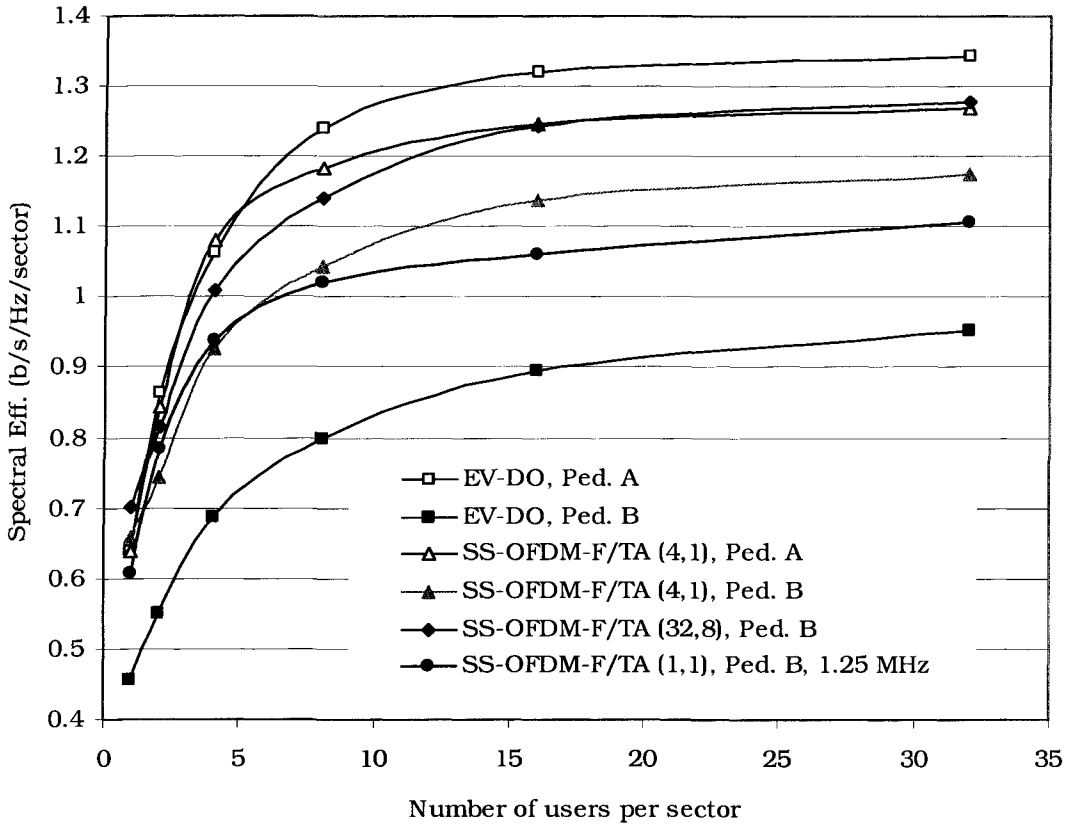


Figure 4.26. Comparison of spectral efficiencies of SS-OFDM-F/TA and 1xEV-DO. 1xEV-DO results are estimated from [24]. The sub-band structure for the SS-OFDM-F/TA is given by the notation ($M_n$, $M_g$).

## 4.7 System Structure for Vehicular Channels

Vehicular channels are characterized by relatively long delay spreads and high Doppler shifts. In order to take full advantage of multi-user diversity in vehicular channels, the fading over each sub-band must be essentially flat and the channel must be almost constant during each time slot, and hence, relatively small transmission sizes (narrow sub-bands and short time slots) are required. This section considers small packet sizes (turbo code block sizes), sub-band grouping and division of packets into smaller sub-packets as possible methods to achieve relatively small transmission sizes, and ultimately allow for a large number of sub-bands to be employed given a fixed time slot duration [76].

### 4.7.1 Appropriate Configurations for Vehicular Channels

The appropriate system configurations determined in this section are used in the multi-cell simulations in the following sections. Appropriate system configurations are determined from the simulation of the average received SINR during scheduled transmissions. As in Section 4.2, the average of the recorded SINRs indicates the relative performance of various system configurations due to multi-user diversity and bandwidth partitioning into sub-bands. Multiple samples per sub-band/time slot are taken to account for channel variations during a time slot, or due to the frequency selective nature of the channel.

In this sub-section, all users are assumed to have an average $E_s/N_0$ of 0 dB. Channel variations are due to Rayleigh fading only. ITU Vehicular A and B channels [43] (see Appendix A.1) and a transmission bandwidth of 5 MHz are considered. An SS-OFDM symbol of $N$=1024 subcarriers and a duration of $T_{sym}$= 216.064 μs with a $T_g$=20 μs cyclic prefix is used. Each system configuration assumes a given transmission size $S_{trans}$ to be transmitted per sub-band/time slot. The duration of the time slot is given as:

$$T_{slot} = \frac{M(S_{trans})}{N}(T_{sym} + T_g) \tag{4.26}$$

It can be seen that for a given $S_{trans}$ an increase in the number of sub-bands results in a proportional increase in the time slot duration.

The results are presented as relative gains in the average received SINR in comparison to a single sub-band system. All configurations assume $U = 32$ users in the system. Figure 4.27 shows the gain in the received SINR for several transmission sizes at a maximum Doppler shift of 100 Hz. As the number of sub-bands in each configuration

is increased, the average received SINR increases until the time slot duration becomes excessively long. An infinitesimally small transmission (which is found from instantaneous SINR values) is also considered to show the maximum possible SINR gain available and is denoted by "INST.". Approximately $M$=32 sub-bands are required to take full advantage of the multi-user diversity in the Vehicular A channel. At a maximum Doppler shift of 100 Hz, a maximum transmission size of $S_{trans}$=128 in each sub-band can be accommodated with negligible loss in performance at $M$=32. It can be noted that the curves are dependent only on the product of the transmission size and the maximum Doppler shift. Hence, the performance of a system with $S_{trans}$=128 at 200 Hz, is the same as that of $S_{trans}$=256 at 100 Hz. In this fashion, it can be seen that the system performance for $S_{trans}$=128 deteriorates only slightly at a maximum Doppler shift of 200 Hz for $M = 32$.

In the Vehicular B channel, more than 500 sub-bands are needed to fully take advantage of multi-user diversity (Figure 4.28). However, a very large number of sub-bands is impractical as the corresponding time/frequency slots would only contain a few symbols each. The use of $M = 8$ sub-bands provides significant SINR gain, and only a small loss in comparison to using 64 sub-bands. A transmission of size of $S_{trans}$=512 symbols is the largest that can be accommodated with $M$=8 sub-bands.

Table 4.3. Gain in received SINR by allocation of groups of sub-bands relative to single sub-band ($M$=1) case.

| | $M_n$=32, $M_g$=16 | $M_n$=32, $M_g$=4 |
|---|---|---|
| Vehicular A | 1.67 dB | 2.54 dB |
| Vehicular B | 1.37 dB | 1.83 dB |

The benefit of allocating groups of sub-bands can also be seen from the gain in average received SINR. The SINR gain of allocating $M_n$=32 in groups of $M_g$=16 and $M_g$=4 are shown in Table 4.3. Allocation in groups of 4 results in a higher performance in terms of SINR gain, but requires the use of smaller packet sizes.

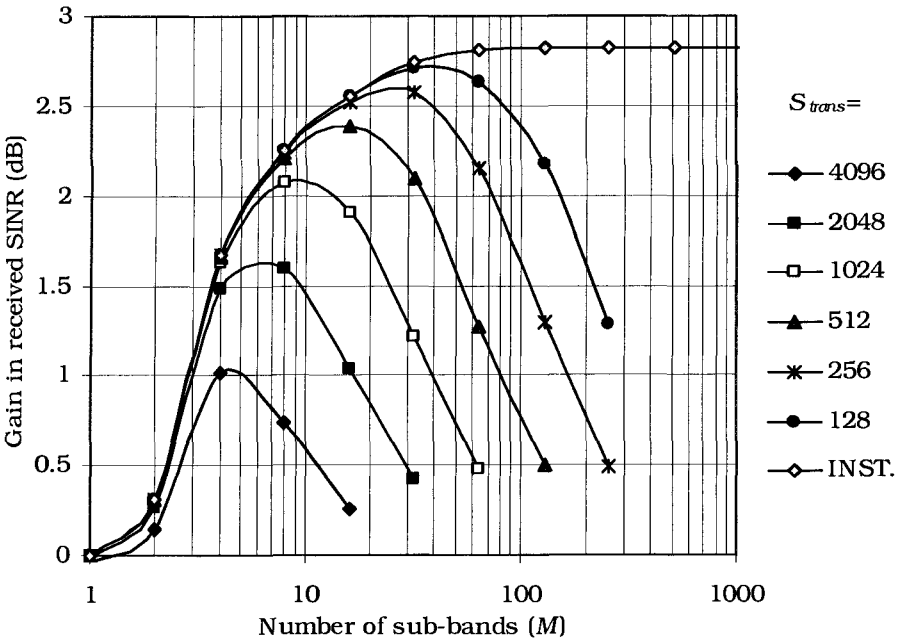


Figure 4.27. Gain in received SINR relative to single sub-band results in Vehicular A channel. $U$=32 users.

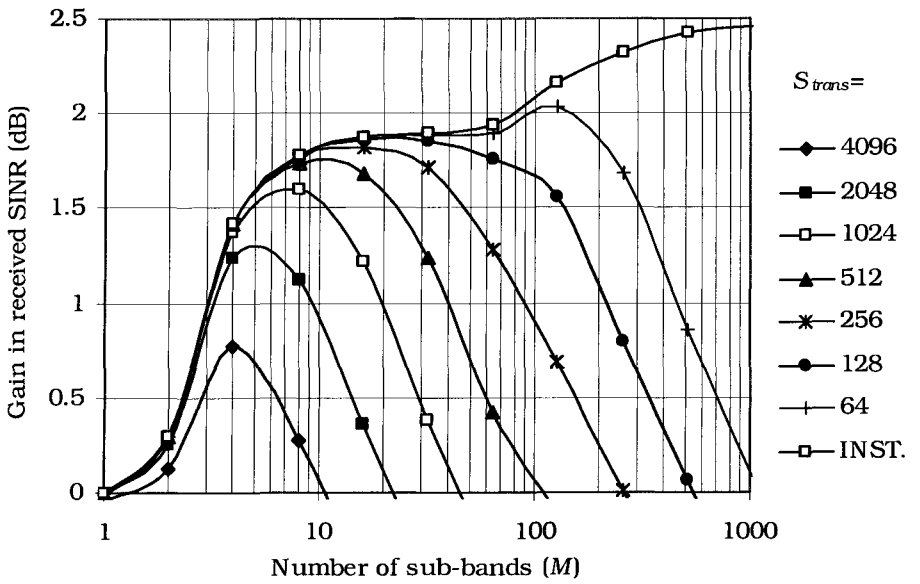


Figure 4.28. Gain in received SINR relative to single sub-band results in Vehicular B channel. $U$=32 users.

### 4.7.2 Appropriate Packet Formats

In this section, 3 packet format sets are considered. For the set of transmission formats containing the longest packets each full transmission consists of $S_{trans}$ =$S_{sym/ACK}$ =2048 symbols, 448 of which are reserved for pilot symbols and MAC overhead. This set is the same as the one considered in Sections 4.2 to 4.6 (with additional format variants), and is identical that suggested for IS-856 [100].

It is important to clarify the terminology in this section as both *packet transmission sizes* and *packet sizes* are discussed. Packet transmission size is the number of complex symbols transmitted in a single burst of 1 sub-band/time-slot, as discussed in the previous section. The packet size is equivalent to the turbo code block size, and refers to the number of bits that are being transmitted with 1 or more re-transmissions using a given packet format.

In order to allow a large number of sub-bands and relatively short time slot duration as required in vehicular channels, the packet transmission size must be made smaller. An obvious approach is simply to employ smaller packet sizes, as given by the packet format sets $S_{trans}$= 512, and 128. For small packet sizes, the data payload, pilot, MAC and preamble are all proportionally scaled down by a factor of 4 or 16. In all cases, 21.875 % of the packet is reserved for pilot and overhead considerations. The details of payload, MAC and preamble for these packet formats are given in Appendix B.1.

The packet size, or turbo code block length, has a significant impact on the performance of the turbo decoding process. Decreasing the packet sizes from 1024, 2048, 3072, and 4096 bits to 256, 512, 768, and 1024 bits results in an average ~0.4 dB loss (see Table 4.4) in performance at a packet error rate (PER) of 1%. A further four times decrease in the packet sizes decreases the relative performance an additional ~0.7 dB (see Table 4.4). These values are determined from link level curves given in Appendix B.1.2.

An alternate method to decreasing the packet size is to divide the packet transmission into a series of smaller sub-packet transmissions. The packet size (or turbo code block length) remains unchanged. Decoding attempts and ACK/NAK acknowledgements for multi-slot transmissions occur only after all sub-packets are received at the mobile. In this special case, the packet format set is related to the number of symbols transmitted per sub-packet by $S_{sym/ACK} = S_{trans} N_{sub-packet}$.

It must be noted that using link level results in system level simulations does not properly represent this case, as the SIR performance of the turbo codes is unclear when each sub-packet has been received with significantly different SIRs. The upper bound

(UB) decoding performance is estimated by comparing the linear average of the SIRs of the sub-packet transmissions to the PER curves for the equivalent transmission of the full packet.

Table 4.4. Transmission formats [76].

| | | | | $S_{sym/ACK}$ =2048 | | | $S_{sym/ACK}$= 512 | | | $S_{sym/ACK}$= 128 | | |
|---|---|---|---|---|---|---|---|---|---|---|---|---|
| *Rate* | *Maximum no. of slots* | *Modulation* | *Code Rate* | *Packet Size (bits)* | *Data Rate (kb/s)* | *SIR (dB) at 1% PER* | *Packet Size (bits)* | *Data Rate (kb/s)* | *SIR (dB) at 1% PER* | *Packet Size (bits)* | *Data Rate (kb/s)* | *SIR (dB) at 1% PER* |
| 1 | 16 | QPSK | 1/5 | 1024 | 67.4 | -13.5 | 256 | 16.5 | -13.0 | 64 | 3.8 | -12.2 |
| 2 | 8 | QPSK | 1/5 | 1024 | 134.8 | -10.5 | 256 | 33.1 | -10.0 | 64 | 7.7 | -9.2 |
| 3 | 4 | QPSK | 1/5 | 1024 | 269.5 | -7.4 | 256 | 66.2 | -6.9 | 64 | 15.4 | -6.2 |
| 4 | 2 | QPSK | 1/5 | 1024 | 539.0 | -4.3 | 256 | 132.4 | -3.9 | 64 | 30.7 | -3.1 |
| 5 | 1 | QPSK | 1/3 | 1024 | 1078.1 | -1.0 | 256 | 264.8 | -0.5 | 64 | 61.4 | 0.2 |
| 6 | 4 | QPSK | 2/3 | 2048 | 540.6 | -4.4 | 512 | 134.0 | -4.0 | 128 | 32.3 | -3.3 |
| 7 | 2 | QPSK | 1/3 | 2048 | 1081.3 | -1.1 | 512 | 267.9 | -0.8 | 128 | 64.6 | -0.2 |
| 8 | 1 | QPSK | 2/3 | 2048 | 2162.5 | 3.4 | 512 | 535.9 | 3.8 | 128 | 129.2 | 4.4 |
| 9 | 2 | 8PSK | 1/3 | 3072 | 1623.5 | 1.5 | 768 | 403.5 | 1.8 | 192 | 98.5 | 2.4 |
| 10 | 1 | 8PSK | 2/3 | 3072 | 3247.0 | 7.1 | 768 | 807.0 | 7.6 | 192 | 197.0 | 8.1 |
| 11 | 2 | 16QAM | 1/3 | 4096 | 2165.7 | 3.3 | 1024 | 539.0 | 3.7 | 256 | 132.4 | 4.3 |
| 12 | 1 | 16QAM | 2/3 | 4096 | 4331.5 | 9.1 | 1024 | 1078.1 | 9.4 | 256 | 264.8 | 10.1 |

### 4.7.3 Cellular Throughput and Delay Analysis

#### 4.7.3.1 Simulation Parameters

Cellular performance is evaluated by link and system level simulations as those described in Section 4.3, with the exception that only 60 simulation runs were completed due to the larger number of subcarriers considered, and hence, increased simulation durations. The packet format sets are given in Table 4.4, along with the tabulated values of the SIR for a PER of 1%. These values are determined from link level graphs given in Appendix B.1.2. All system configurations consider an SS-OFDM symbol with $N$=1024 subcarriers and of a duration of $T_{sym}$= 216.064 μs with a $T_g$=20 μs cyclic prefix. The loss in spectral efficiency due to the cyclic prefix is 9.26%. The time slot length for each configuration is 0.944 ms, and the transmission bandwidth is 5 MHz (4.74 MHz main lobe width). All system configurations consider the same number of MAC and pilot symbols per time slot (i.e., same overhead symbol rate). A maximum Doppler shift of 100 Hz is assumed. Shadowing with a 10 dB standard deviation and decorrleation

distance of 20 metres are considered. The Vehicular channel models are described in detail in Appendix A.1.

As mentioned in Section 4.2.4, this section considers asynchronous re-transmissions of packet (and sub-packets). This is necessary here in order to compare sub-band grouping and smaller packet formats as asynchronous re-transmission ensures proper selection of users and modulation scheme for each transmission and re-transmission. Asynchronous re-transmission schemes are discussed in detail in Section 5.2. In this section, asynchronous re-transmission is considered such that a given mobile must be selected by the downlink scheduler (as described in Section 4.2.3.1) for each transmission and re-transmission of packets. In addition for a given selected user, re-transmission of a packet occurs only when the mobile requests a packet of the same transmission format (based on channel conditions), or if the mobile buffer is full and no new packets can be started. If the selected user has more than one packet awaiting re-transmission, the packet that has gone without re-transmission the longest will be given priority. If the mobile buffer is full, the packet that is of a transmission format closest to format requested by the mobile will be transmitted. This scheme is similar to the SF-RP algorithm discussed in Section 5.2.

#### 4.7.3.2 System Configurations

Seven system configurations are considered in the simulations using the 3 packet format sets given in Table 4.4. The configurations are listed in Table 4.5. Configurations I, II, and III consider single sub-band allocation and the three different packet transmission format sets. Configurations IV and V consider the allocation of groups of disjoint sub-bands (see Section 4.5) with two different packet format sets. Configuration VI considers the upper bound performance of transmitting sub-packets, and is only used for comparison. Perfect prediction of the SIR in each sub-band/time slot is assumed for configurations I through VI. For these configurations, rates 6, 7, and 11 are omitted from the packet format sets as rates 4, 5, and 8 are nearly identical but require fewer re-transmissions.

Configuration VII is a special case that considers no channel prediction for comparison. In this configuration only, sub-band allocation and rate selection are based on path loss and showing only, as small-scale fading changes too rapidly. Synchronous re-transmission of packet is used with this scheme as proper allocation is difficult without channel prediction. In addition, subcarrier interleaving is performed across the

entire transmission bandwidth and rates 6, 7, and 11 are used instead of 4, 5, and 8 in order to achieve additional frequency and time diversity.

The mobile buffer for Configurations I-V, and VII is the same size, and is the minimum needed to allow proper operation of the re-transmission procedure. For configurations using the largest transmission formats ($S_{sym/ACK}$=2048 in Table 4.4), soft information for 8 packets can be stored, while soft information for 128 packets can be stored for Configuration III, which uses the smallest set of transmission formats ($S_{sym/ACK}$=128). Configuration VI requires a larger buffer of $8N_{sub\text{-}packet}$ to ensure proper operation.

Table 4.5. System configurations [76].

| | *Configuration* | | | | | | |
|---|---|---|---|---|---|---|---|
| | *I* | *II* | *III* | *IV* | *V* | *VI-UB* | *VII* |
| Sub-bands ($M$) | 2 | 8 | 32 | 32 | 32 | 8 | 2[a] |
| Sub-bands per group ($M_g$) | 1 | 1 | 1 | 16 | 4 | 1 | 1 |
| Transmission format set ($S_{sym/ACK}$) | 2048 | 512 | 128 | 2048 | 512 | 2048 | 2048 |
| Sub-packets ($N_{sub\text{-}packet}$) | 1 | 1 | 1 | 1 | 1 | 4 | 1 |
| Packets per time slot | 2 | 8 | 32 | 2 | 8 | 8(1/4) | 2 |
| Rate request / SIR (bits per time slot) | 8 | 32 | 128 | 128 | 128 | 32 | 8 |
| Packet ID (bits per time slot) | 6 | 40 | 224 | 6 | 40 | 56 | n/a |
| User ID (bits per time slot) | 10 | 40 | 160 | 10 | 40 | 40 | 10 |
| Group ID (bits per time slot) | 0 | 0 | 0 | 32 | 96 | 0 | 0 |

a. The subcarriers of the two sub-bands are interleaved.

#### 4.7.3.3 Multi-Cell Simulation Results

The average data throughputs per sector for the various configurations of the Vehicular A and B channels are shown in Figures 4.29 and 4.30, respectively. The best performance in both channels is given by the upper bound of using 4 sub-packets per transmission (Configuration VI (UB)). The next highest throughput is achieved by using sub-band grouping. Configuration V generally outperforms configuration IV as 4-times as many groups of sub-bands are allocated. Configuration V represents a 6 to 15 % gain in throughput over Configuration II in the Vehicular A and B channels for more than four users per sector.

Configurations I, II and III represent the trend of increasing the number of sub-bands by decreasing the packet sizes. It can be seen that in both channels, increasing the number of sub-bands from 2 to 8 improves the performance. Direct comparison of Configuration II and Configuration IV shows that the increase in throughput due to allocation of groups of disjoint sub-band is nearly the same as decreasing packet size by 4. However, decreasing the packet size further (Configuration III) results in a turbo code performance loss that is larger than the multi-user diversity gain, whereas applying sub-band grouping (Configuration V) provides some small increase in the average data throughput.

It should be noted that the sub-band grouping method is more versatile as the throughputs are the same as or better than smaller packet size configurations, and if the systems were tested in a relatively frequency non-selective fading channel, the only difference in throughput between the two would be the performance loss of the system with smaller packet sizes due to poorer turbo code performance (i.e., smaller interleaver size).

The throughput without the use of channel prediction (Configuration VII) is about half of that when prediction and proper allocation are used. Very little multi-user diversity is available in this case.

With the exception of the transmission of sub-packets (Configuration VI (UB)) that incurs the longest delays, the packet delays decrease with the number of independent parallel channels in the Vehicular A channel (Figure 4.31). For Configurations II, III and V, the $90^{\text{th}}$ percentile packet delays are less than 20 slots with $U$=32 users.

The distribution of packet delays averaged per user (Figure 4.32) shows that the transmission of sub-packets (Configuration VI) results in 20% of users having average packet delays of 350 slots or greater. The lowest average packet delay is observed in the special case of Configuration VII, where re-transmissions of packets occur every 4 slots, if needed, and are therefore completed quickly. The average delay per user is drastically reduced by the use of 8 independent parallel channels as in Configuration II (101 slots) and V (89 slots), in comparison to Configurations I (193 slots) and IV (153 slots), which transmit only 2 packets in parallel. The distributions of delays for the Vehicular B channel are similar (not shown).

Figure 4.33 shows the distribution of average throughputs per user in the Vehicular A channel for Configurations I, III, V, and VII. Clearly the gain in average throughput for configurations V and III over I and VII are shared by all users in the system. It should also be noted that best-effort transmission that is used in Configurations I, III,

and V provides a higher throughput for all users in the system than Configuration VII, which due to lack of prediction is similar to a round-robin scheduled scheme.

### 4.7.4 Reverse Link and MAC Considerations

Increasing the number of sub-bands increases the demand on the reverse link. The last 4 rows of Table 4.5 list the bits per time slot that need to be transmitted on the reverse link for proper operation of adaptive allocation at the base station. Allocating groups of sub-bands (as in Configurations IV and V) requires significant signalling on the reverse link as the SIR estimate in each sub-band must be sent to the base station. Sending only the 4-bit rate requests in each sub-band represents a coarse form of SIR quantization; however it is all that is required in the single sub-band allocation configurations. Coarse quantization feedback for sub-band grouping and adaptive rate selection is discussed further in Section 5.5.

The total downlink overhead per time slot is assumed to be the same for all configurations in this Section for simplicity. However, the actual overhead requirements may be different for different configurations. An example is the packet identifier (PID) that is necessary for asynchronous packet re-transmissions. The costs in bits of the PID fields are listed in Table 4.5. The configurations that use transmission of sub-packets (Configuration VI), and those that send small packets (Configurations II, III, and IV) require a larger portion of the fixed overhead for this purpose. In addition, this section assumed that the preamble was proportionally reduced with the transmission size. This is unlikely, and makes the very small packet sizes less desirable to larger relative loss in payload capacity per transmission.

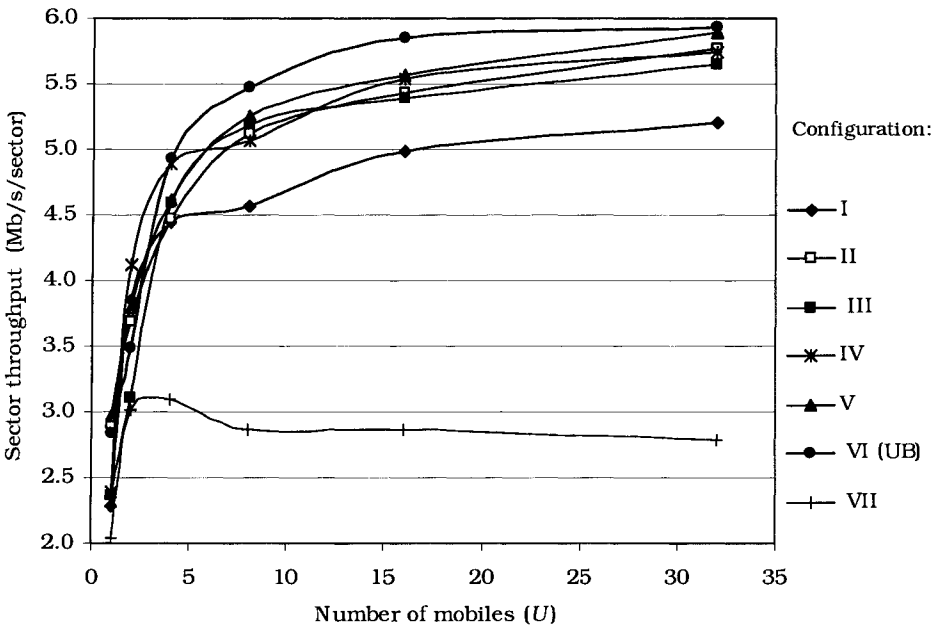


Figure 4.29. The average throughput per sector in the 5 MHz Vehicular A channel.

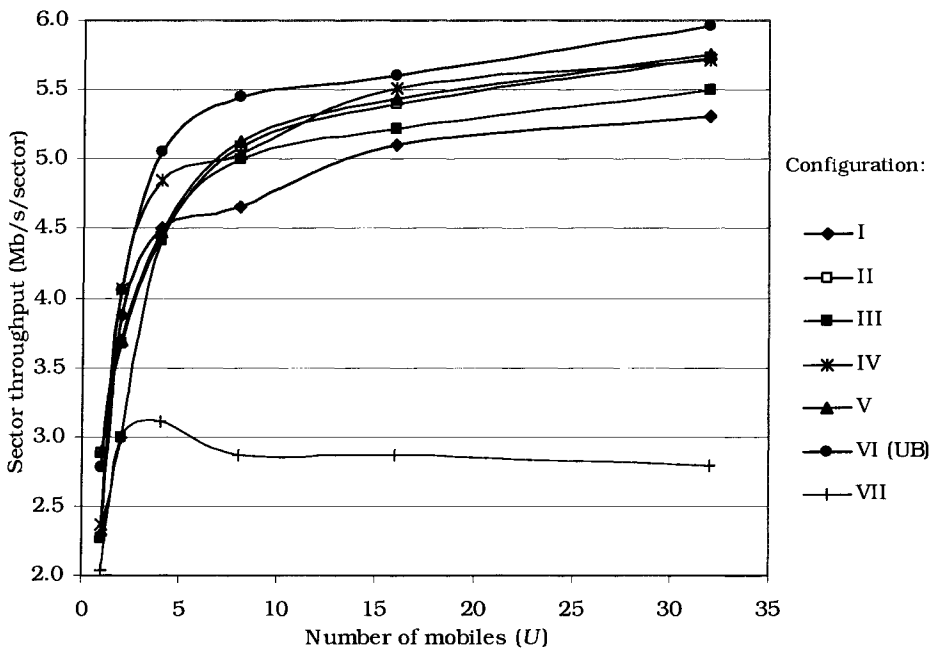


Figure 4.30. The average throughput per sector in the 5 MHz Vehicular B channel.

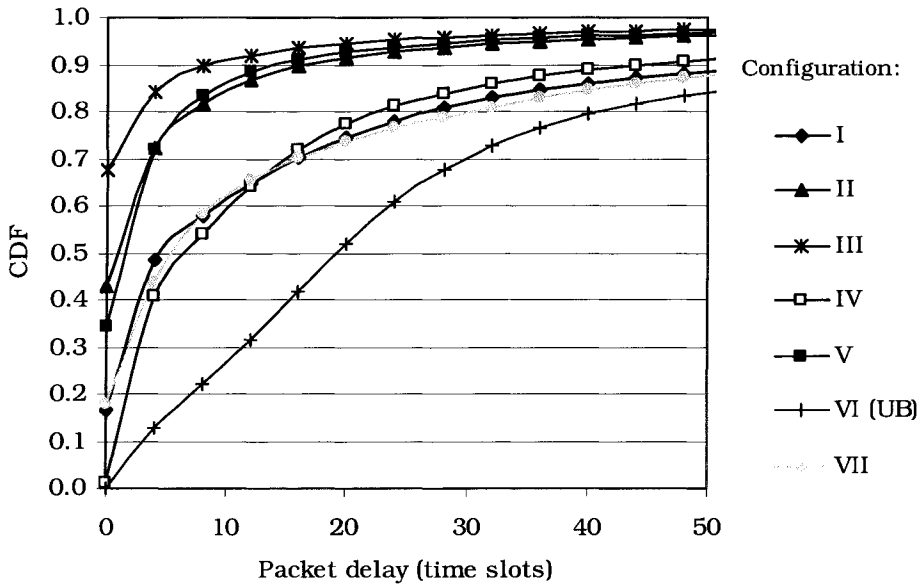


Figure 4.31. Distribution of packet delays in Vehicular A channel and $U$=32 users per sector.

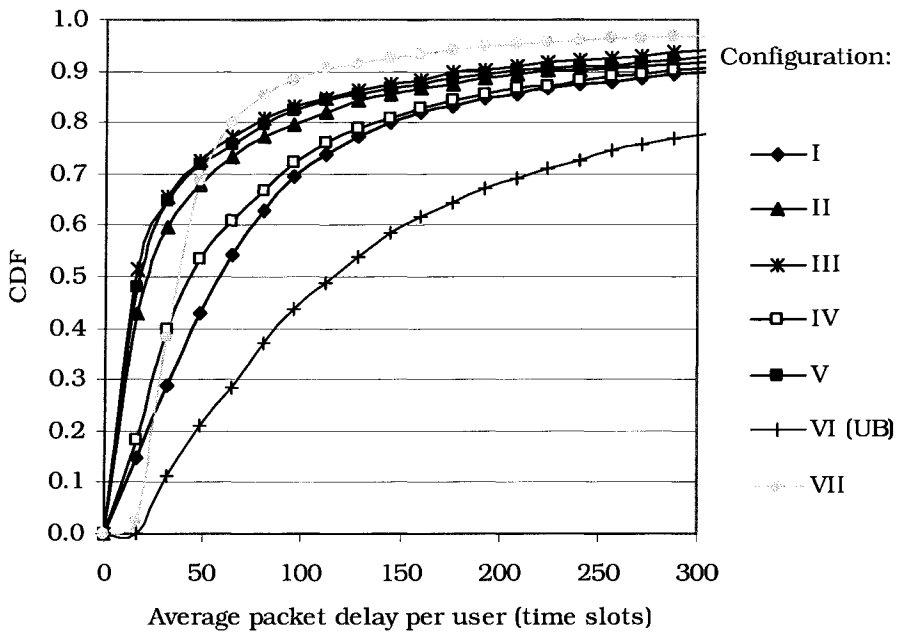


Figure 4.32. Distribution of packet delays averaged per user in Vehicular A channel and $U$=32 users per sector.

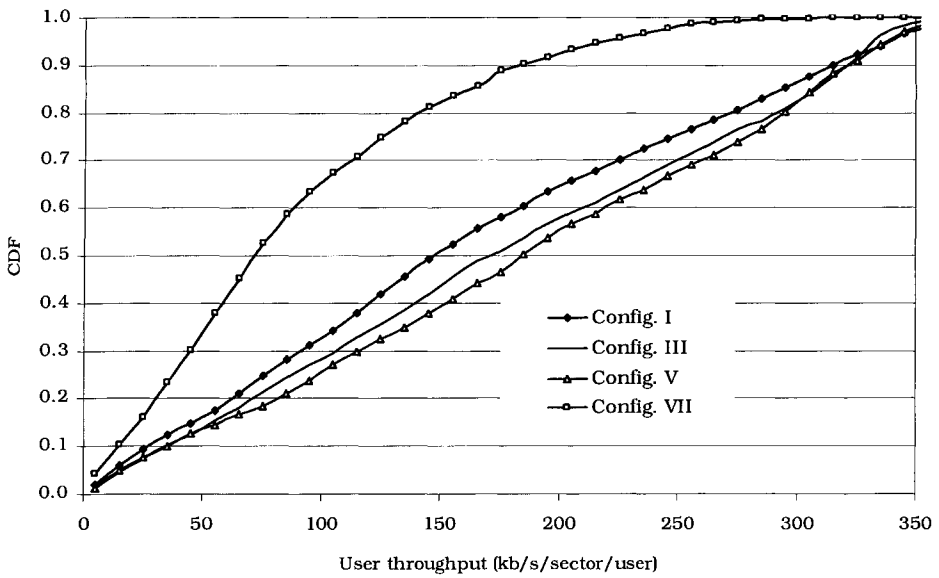


Figure 4.33. Distribution of the average throughput per sector per user in the Vehicular A channel. $U$=32 users per sector.

# Chapter 5

# Improvements and Analysis of the SS-OFDM-F/TA Packet Data System

This chapter presents and discusses improvements to some of the features of the SS-OFDM-F/TA system presented in Chapter 4. First, the packet transmission structures used in this chapter is presented, along with general system parameters. The packet transmissions size is smaller than those general used in Section 4.4, in part due to results of Section 4.7, and are based on packet structures for cdma2000 [101]. Four sets of packet configurations with varying amounts of dependence on re-transmissions are considered in this examination so that system performance can be measured with and without extensive use of type II ARQ. Asynchronous packet re-transmission options with the type II hybrid ARQ will be presented in Section 5.2 for the SS-OFDM-F/TA system. Several novel asynchronous re-transmissions schemes are proposed and analyzed. The asynchronous re-transmission options are compared assuming different mobile velocities, and different numbers of allowable re-transmissions. Asynchronous re-transmission inherently results in longer packet transmission delays, and hence, placing a constraint on the re-transmission interval (RTI) is proposed. In Section 5.3, slow and fast best sector selections are discussed and analyzed considering different shadowing conditions. It is shown that fast sector selection increases throughput and decreases delays. In the final 3 sections of this chapter, the use of larger modulation constellations, adaptive termination and code-division multiplexing of packets, and the quantization of SIR feedback to the transmitter will be discussed. The impact of these 3 factors on system performance will be shown.

## 5.1 Packet Formats for Re-transmission Options and Improvements

The basic packet structure considered in this chapter is smaller than that used for IS-856 (used in Chapter 4), and hence the time slot duration is appropriately shortened from 1.79 ms to 1.34 ms. The changes in packet structure and parameters are indicative of some of the results from Chapter 4. The shorter time slot and smaller packet transmissions size reduce the delays as suggested in Section 4.7. In addition, short time slots increase the performance in cases of high mobile speeds through more accurate CSI estimation. Delays are also reduced by setting the smallest packet size to 408 bits, which is less than half of the smallest packet size considered in Chapter 4, and reducing the number of allowable re-transmission from 16 to 8. The sub-band bandwidths are the same as for the basic configurations in Chapter 4, as the indoor channels and the Pedestrian A channel do not require narrower sub-bands (see Appendix D), and the Pedestrian B channel can be serviced using sub-band grouping (see Section 4.5). Note that using even smaller packet sizes to decrease the sub-band bandwidths would result in overall performance loss in less frequency selectively channels (see Section 4.7). The encoding, packet sizes and packet transmissions sizes are based on that given in cdma2000 revision D for the downlink [101]. Each packet transmission over a sub-band, or group of sub-bands, during a given time slot consists of 1536 complex valued chips, 1200 of which carry data, and 336 are reserved for pilot and MAC layer signalling (21.875%). As before, adaptive margins at SIR thresholds for bit rate selection are used to ensure a packet error rate of approximately 1% in each run, for each rate. Packet structure specific are given in Appendix B.2.1.

A significant factor in the throughput and delay performance of the SS-OFDM-F/TA system is the number of allowed re-transmissions for a given packet. For example, if the SIR estimate is not reliable it may be advantageous to use a packet size of 792 bits over 8 slots, rather than a 408 bit packet over 4 slots. Four data packet format sets are used: $A$, $B$, $C$ and $D$, with set $A$ allowing the fewest transmissions (Table 5.1) of a packet and $D$ allowing the most.

Table 5.1. Packet format sets.

| *Packet format set* ***A*** | | | *Packet format set* ***B*** | | | *Packet format set* ***C*** | | | *Packet format set* ***D*** | | |
|---|---|---|---|---|---|---|---|---|---|---|---|
| *Max. no. of slots* | *Packet size (bits)* | *SIR at 1% PER (dB)* | *Max. no. of slots* | *Packet size (bits)* | *SIR at 1% PER (dB)* | *Max. no. of slots* | *Packet size (bits)* | *SIR at 1% PER (dB)* | *Max. no. of slots* | *Packet size (bits)* | *SIR at 1% PER (dB)* |
| 8 | 408 | -13.1 | 8 | 408 | -13.1 | 8 | 408 | -13.1 | 8 | 408 | -13.1 |
| 4 | 408 | -10.0 | 4 | 408 | -10.0 | 4 | 408 | -10.0 | 8 | 792 | -10.5 |
| 2 | 408 | -6.9 | 2 | 408 | -6.9 | 4 | 792 | -7.3 | 8 | 1560 | -7.5 |
| 1 | 408 | -3.7 | 2 | 792 | -4.0 | 4 | 1560 | -4.3 | 8 | 2328 | -5.0 |
| 1 | 792 | -0.7 | 2 | 1560 | -1.0 | 4 | 3096 | 0.3 | 8 | 3864 | -2.0 |
| 2 | 2328 | 1.7 | 2 | 2328 | 1.7 | 2 | 3096 | 3.7 | 4 | 3096 | 0.3 |
| 1 | 1560 | 5.0 | 2 | 3096 | 3.7 | 2 | 3864 | 5.9 | 2 | 3096 | 3.7 |
| 1 | 2328 | 8.3 | 2 | 3864 | 5.9 | 1 | 2328 | 8.3 | 2 | 3864 | 5.9 |
| 1 | 3096 | 10.5 | 1 | 2328 | 8.3 | 1 | 3096 | 10.5 | 1 | 2328 | 8.3 |
| 1 | 3864 | 13.7 | 1 | 3096 | 10.5 | 1 | 3864 | 13.7 | 1 | 3096 | 10.5 |
| | | | 1 | 3864 | 13.7 | | | | 1 | 3864 | 13.7 |

Table 5.2. The modulation constellations used with different packet sizes.

| *Modulation constellation* | *Packet sizes (bits)* |
|---|---|
| QPSK | 408, 792, 1560 |
| 8 PSK | 2328 |
| 16 QAM | 3096, 3864 |

### 5.1.1 Simulation, System and Channel Parameters

The structures for link and system level simulations are the same as given in Chapter 4. The curves of the link level results for the packet format given in Table 5.1 are shown in Appendix B.2, as well as details of the packet structures. As mentioned, the simulation parameters such as time slot duration are different than previous sections as smaller packet sizes are being used. The simulation parameters are listed in Table 5.3. In the Pedestrian B channel, the disjoint sub-band grouping is $(M_n,M_g)$ = (32,8) unless otherwise noted. The system is simulated with single sub-band allocation and 4 sub-bands, $(M_n,M_g)$ =(4,1), in the Pedestrian A channel. In cases where perfect channel prediction is used, it is assumed that the SIR estimate of the first transmission slot is known as in Section 4.5, not further. For cases without perfect channel prediction, the formation and allocation of groups of disjoint sub-bands is completed with only out-dated SIR estimates.

Table 5.3. System parameters.

| | *Indoor* | *Pedestrian* |
|---|---|---|
| $N$ (subcarriers) | 256 | 512 |
| $M_n$, $M_g$ | 8, 1 | 32, 8 *or* 4,1 |
| $M = M_{eff}$ | 8 | 4 |
| Bandwidth | 10 MHz | 5 MHz |
| Subcarrier spacing | 37.026 kHz | 9.2565 kHz |
| $T_{sym}$ (SS-OFDM symbol duration) | 27.008 μs | 108.032 μs |
| $T_g$ (cyclic prefix) | 1 μs | 4 μs |
| Time slot length | 1.344384 ms | 1.344384 ms |

As in previous sections, the channel parameters for the indoor and pedestrian environments are listed in Appendix A.1. In this section, mobiles in outdoor pedestrian environments are primarily considered. These mobiles may be moving very slowly, or at low vehicular speeds. Therefore the Pedestrian B channel with maximum Doppler shifts from 5 Hz to 100 Hz, corresponding to mobile speeds of up to approximately 55 km/h at a carrier frequency of ~2 GHz is considered. It can be noted that the ITU Pedestrian B channel is very similar to the ITU Vehicular A channel. Only the pedestrian channel is considered in this section so that a comparison of system performance with different Doppler shifts can be readily made. As before, the standard deviation for the shadowing processes in the Indoor and Pedestrian channels is 12 dB and 10 dB respectively.

## 5.2 Re-Transmission Options

### 5.2.1 Synchronous and Asynchronous Re-Transmission

As introduced in Section 4.2.4, the SS-OFDM-F/TA system employs stop-and-wait type II hybrid ARQ with incremental redundancy and soft packet combining [100][113]. In this scheme re-transmission of a packet continues until the packet is successfully received, or the maximum number of re-transmissions for the given packet format has been reached. Re-transmissions can either be synchronous or asynchronous. In synchronous re-transmission systems [45], packets are re-transmitted every 4 time lots until successfully received, regardless of user channel conditions. In asynchronous re-transmission schemes, re-transmission occurs only when the user is scheduled again. Scheduling each re-transmission ensures that multi-user diversity is exploited for all

transmissions to users. The decision of user selection by the scheduler is not based on proportionally fair scheduling for all asynchronous algorithms considered in this section.

The concept of asynchronous re-transmissions was originally proposed in [19][20]. In this proposal re-transmissions were withheld until the user was selected to receive re-transmissions once again by the best-effort scheduler. As a single carrier systems was considered, there are generally very few simultaneous ongoing packet re-transmission to a single user so there is little need for devising options for selections of which packet to re-transmit at any given time.

In this section, several proposals for asynchronous re-transmission algorithms are presented. The algorithms vary by setting different criteria for which of the packets awaiting re-transmission to a given user will be transmitted. In addition, algorithms are also proposed which allow for starting a new packet transmission even though there are packets awaiting re-transmission to a user. An option for user/re-transmission scheduling, that does not base user selection on the proportionally fair scheduler is also considered.

The asynchronous re-transmissions can occur in any sub-band [75]. Due to the parallel structure of the system, there may be several partially transmitted packets to choose from for each user. In this section, we consider a mobile buffer memory size of $4M_{eff}$ packets. This is the minimum memory size for SS-OFDM-F/TA with stop-and-wait ARQ as it is the number of new packet transmissions that can occur before an ACK/NAK is received at the base station. The following algorithms are used to select a packet, $P_{RT}$, for re-transmission or start a new packet transmission.

#### 5.2.1.1 Asynchronous Re-Transmission Methods

This section considers two categories of asynchronous re-transmission methods. In the *first category*, asynchronous re-transmissions occur only when the user is selected by the scheduler (in the same manner as for new packet transmissions), whereas in the *second category*, a packet is re-transmitted when the channel conditions are as good as, or better than when the packet was initially transmitted with no consideration of the channel conditions of other users. This section considers re-transmission of the $\nu^{th}$ packet awaiting re-transmission, $P_\nu$, with the properties of delay, $D(P_\nu)$, since last re-transmission and the minimum data rate achievable with the selected transmission format $R(P_\nu)$. This value is given by $R(P_\nu) = \text{packet size}/[(\text{max. no. of slots})(1.344 \text{ ms})]$. The re-transmission methods belonging to the *first category* considered are discussed next.

*Minimum delay, absolute re-transmit priority (MD-ARP)*: The packet that has gone without re-transmission the longest, $P_{RT} = P_{\nu_{\max}}$ where $\nu_{\max} = \arg\max_{\nu \in 4M_{eff}} D(P_\nu)$, is selected for re-transmission.

*Same format re-transmit priority (SF-RP)*: The packet of exactly the format appropriate for the channel condition is selected for re-transmission, hence $R(P_{RT}) = \hat{R}_m^{(u)}$. If more than one packet satisfies this constraint, the packet that has been awaiting re-transmission the longest is selected. If no such packet is awaiting re-transmission, a new packet transmission is started.

*Minimum delay with supportable format, re-transmit priority (MDSF-RP)*: The packet that has gone without re-transmission the longest, and is of a format that can be supported by the current channel conditions, is selected for re-transmission. This is expressed as:

$$P_{RT} = P_{\nu_{\max}}, \text{ where } \nu_{\max} = \arg\max_{\nu \in Z} D(P_\nu) \tag{5.1}$$

and Z is defined such that

$$Z = \{\forall \nu'\}, \text{ and } \nu' \text{ satisfies } R(P_{\nu'}) \le \hat{R}_m^{(u)} \tag{5.2}$$

If no such packet is awaiting re-transmission, a new packet transmission is started.

*Minimum delay, absolute re-transmit priority with parallel allocation (MD-ARP-PA)*: Let the number of sub-bands (or groups of sub-bands) assigned to the $u^{th}$ user in a given time slot be $M_u$. As with MD-ARP, select the $M_u$ packets that have been waiting the longest for transmission. Of these $M_u$ packets, assign the one with the lowest transmission format to the sub-band (or group of sub-bands) with the lowest SIR. Continue this process for the next $M_u - 1$ packets.

*Minimum delay, with supportable format, re-transmission priority with parallel allocation (MDSF-RP-PA)*: Find all the packets that meet the MDSF-RP criterion in (5.2), and rank them according to (5.1). Select the top $M_u$ packets for re-transmission, where $M_u$ is as defined in the previous algorithm. Of these $M_u$ packets, assign the one with the lowest transmission format to the sub-band (or group of sub-bands) with the lowest SIR. Continue this process for the next $M_u - 1$ packets. If less than $M_u$ packets meet the criterion, start new packet transmissions.

One asynchronous re-transmission algorithm belonging to the *second category* is considered. It is a distinct alternative to the forgoing algorithms as the algorithm determines which mobile will receive transmission, as well as which packet (if any) will be re-transmitted.

*Minimum delay with supportable format channel state information based (MDSF-CSIB)*: For all users, find the packets that require re-transmission and of a format that can be supported by the current channel conditions, namely $Z = \{\forall(\nu', u')\}$ for which $R(P_{\nu'}^{(u')}) \leq \hat{R}_m^{(u)}$. If the allocation of disjoint sub-bands is used, the channel conditions for all possible relevant sub-band groups are examined. Of the packets that can be supported in the current time slot, transmit the packet that has been waiting the longest, $P_{RT} = P_{\nu'_{\max}}^{(k'_{\max})}$, where $\{\nu'_{\max}, u'_{\max}\} = \arg\max_{\nu', u' \in Z} D(P_{\nu'}^{(u')})$. If no such packet exists, transmit a packet to the user selected by the proportionally fair scheduler.

### 5.2.2 Comparison of Re-Transmission Schemes

The re-transmission options described in Section 5.2.1 have been simulated extensively over the Pedestrian B channel. Asynchronous re-transmission of packets provides a higher average data throughput per sector than using synchronous re-transmission in most cases (Figures 5.1 and 5.2). Asynchronous re-transmission is particularly useful in the cases of a maximum Doppler shift of 30 Hz with no channel prediction (14% throughput gain, with $U = 32$ users and packet format set $D$), 50 Hz with no channel prediction (7% throughput gain), and 100 Hz with channel prediction (10% throughput gain). A maximum of 3.9 Mb/s per sector has been achieved at 100 Hz and with no prediction (not shown). Unless otherwise stated, asynchronous re-transmissions in this section are assumed under the MD-ARP-PA algorithm.

All asynchronous re-transmission schemes examined in this section provide relatively the same average throughput per sector (Figure 5.3). Nevertheless, the SF-RP and MD-ARP-PA algorithms perform the best, with the exception of the case of a 30 Hz maximum Doppler shift, in which the SF-RP algorithm is ineffective. The algorithms employing parallel allocation (MD-ARP-PA, MDSF-RP-PA) perform slightly better than those without it (MD-ARP, MDSF-RP). This is particularly noticeable in the cases of only a few users per sector, as there is a high probability that multiple sub-bands will be assigned to a single user in a given time slot. For example, the MD-ARP-PA scheme outperforms the MD-ARP scheme by 10.3 % with $U = 4$ users, and by 19.9 % with $U = 2$ users.

Packet delays are significantly different between different asynchronous re-transmission algorithms. The distribution of packet delays (Figure 5.4) and average packet delays per user (Figure 5.5) reveal large delays associated with the SF-RP algorithm, and small delays for the MD-ARP-PA algorithm. Delays associated with the synchronous system are shorter than for all the asynchronous options, and hence,

employing asynchronous re-transmissions trades off higher throughputs (in most cases) for longer packet delays. The MDSF-CSIB algorithm also results in low packet delays; however the sector throughput with this scheme is among the lowest of the algorithms examined.

After each re-transmission, the soft samples of the packet are stored at the mobile in a packet buffer. As mentioned earlier, it is assumed that each mobile is capable of storing $4M_{eff}$, or 16 packets in the Pedestrian B channel configuration. Figure 5.6 and 5.7 show the probabilities of packet buffer loading per user for the system in the Pedestrian B channel with 5 Hz and 50 Hz maximum Doppler shifts, respectively, with $U$=32 users per sector. Clearly the synchronous re-transmission method results in the lowest level of packet buffer loading, while the asynchronous SF-RP system results in a user having the most ongoing packet transmissions on average. The case of a maximum Doppler shift of 50 Hz results in more packets being in a state of re-transmission at any given time due to the poor channel state estimates, and reliance on packet formats with a larger number of re-transmissions.

Aside from providing a higher average throughput, asynchronous re-transmissions improve fairness by benefiting users with poorer channel conditions. For example, the average data throughput delivered to the $20^{th}$ to $50^{th}$ percentile users is increased by 17% over that for synchronous re-transmissions in a 100 Hz Doppler channel with perfect prediction (Figure 5.8). The relative increase in average data throughput delivered is even greater for the case of a 30 Hz maximum Doppler shift.

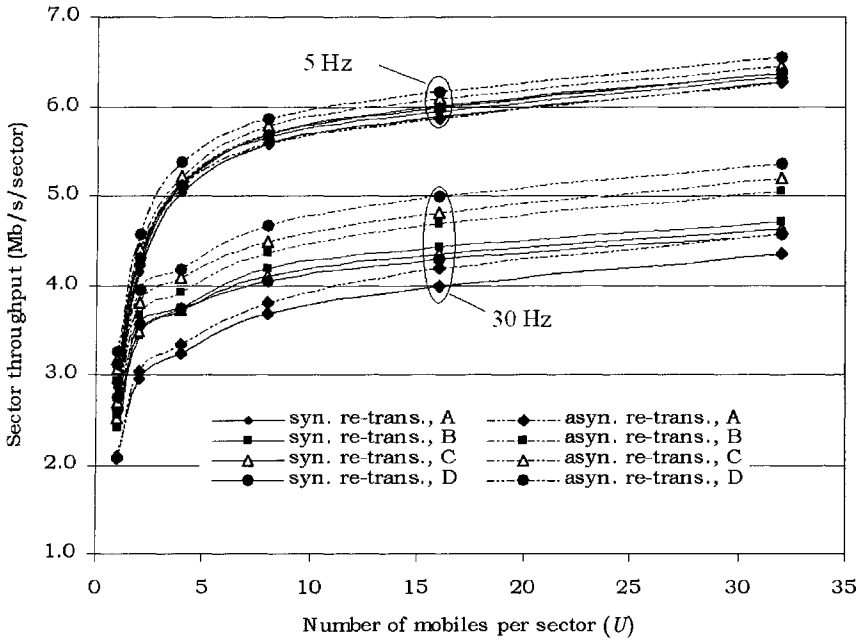


Figure 5.1. Average throughput per sector with synchronous and asynchronous retransmission of packets with different packet format sets. 5 Hz and 30 Hz maximum Doppler shifts.

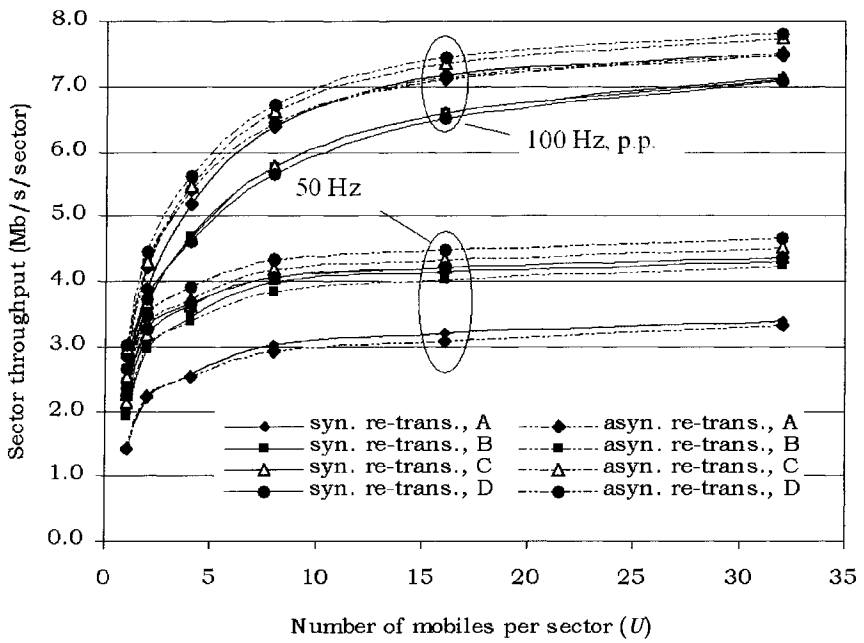


Figure 5.2. Average throughput per sector with synchronous and asynchronous retransmission of packets with different packet format sets. 50 Hz and 100 Hz maximum Doppler shifts; perfect prediction (p.p.) applied in the 100 Hz case.

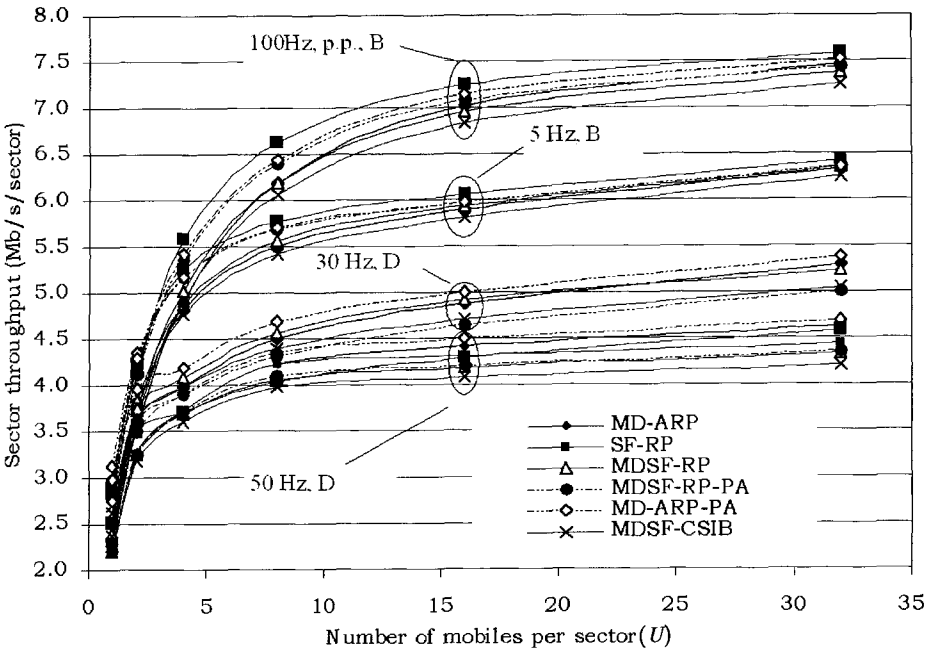


Figure 5.3. Average throughput per sector for asynchronous re-transmission algorithms in the ITU Pedestrian B channel.

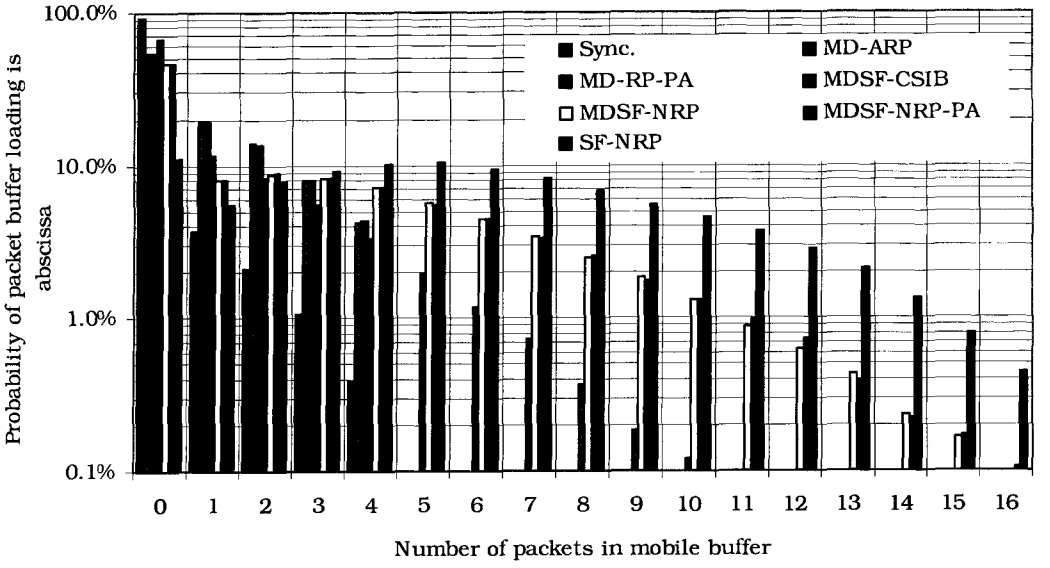


Figure 5.4. The average mobile packet buffer occupancy for synchronous and asynchronous re-transmission schemes in the pedestrian B channel with 5 Hz Doppler shift and $U$=32 users.

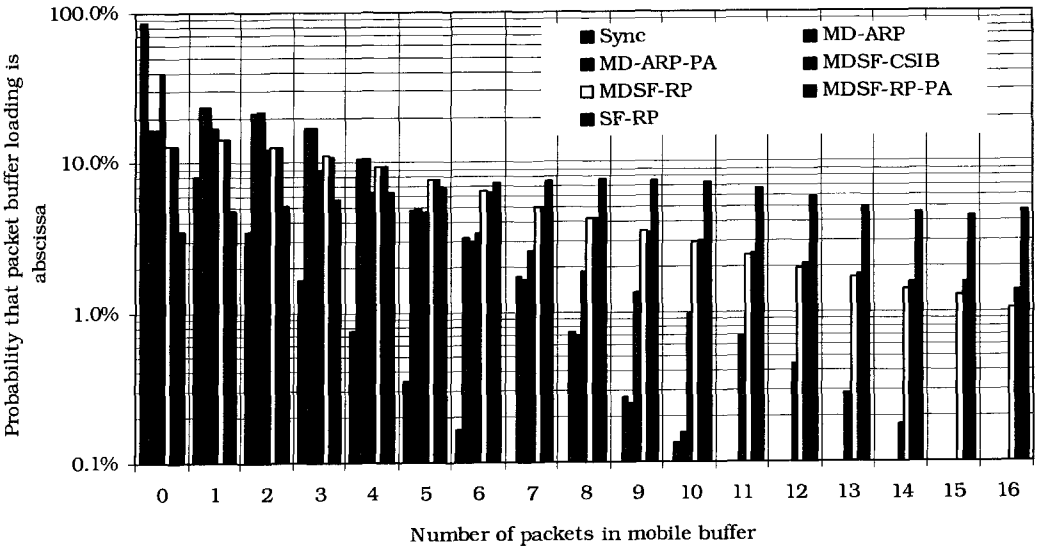


Figure 5.5. The average mobile packet buffer occupancy for synchronous and asynchronous re-transmission schemes in the pedestrian B channel with 50 Hz Doppler shift and $U$=32 users.

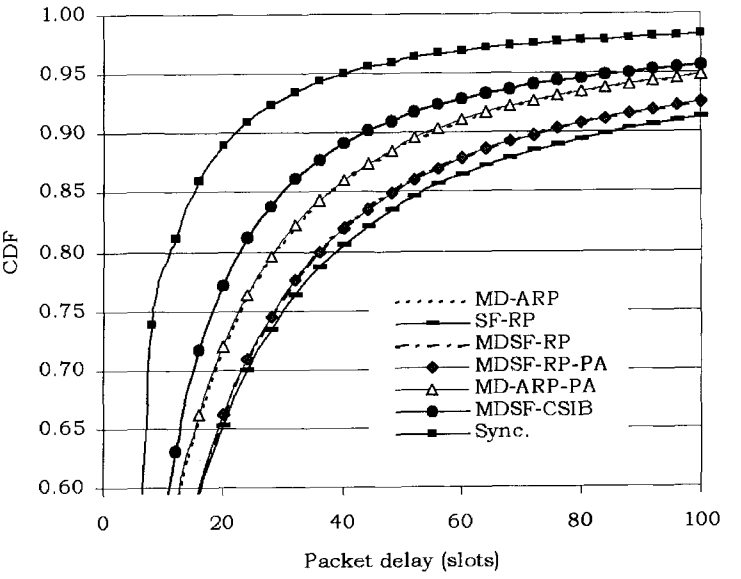


Figure 5.6. Distribution of packet delays in ITU Pedestrian B channel at 50 Hz maximum Doppler shift and packet format $B$; $U = 32$ users per sector.

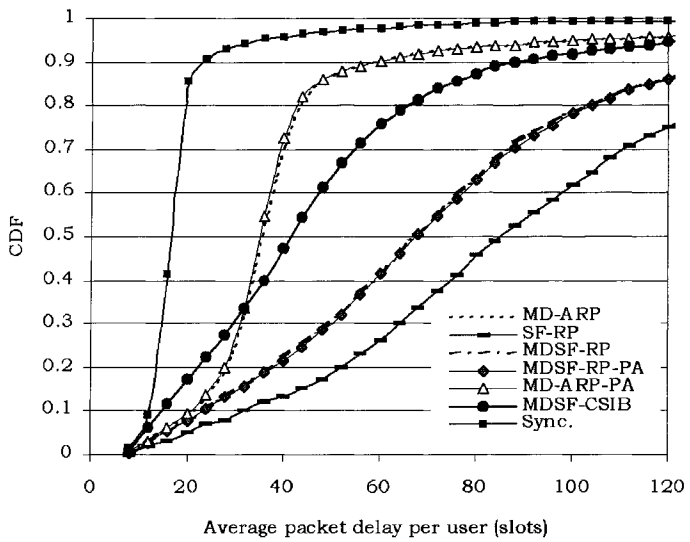


Figure 5.7. Distribution of average packet delays per user in ITU Pedestrian B channel at 50 Hz maximum Doppler shift and packet format $B$; $U$=32 users per sector.

### 5.2.3 Maximum Re-Transmission Interval

Aside from maximizing the average throughput per sector, re-transmission schemes that minimize the packet delay are desirable. In this section, we impose limits on the maximum delay between re-transmissions of a given packet to ensure an acceptable packet delay. If a packet has been awaiting re-transmission longer than the maximum re-transmission interval, then re-transmission of the packet to the given user is immediately scheduled, regardless of channel conditions. Note that in the case of the allocation of disjoint sub-bands as described in Section 2.4, the sub-bands are re-allocated to offer the best possible channel conditions for the forced re-transmission.

Imposing a maximum on the duration of re-transmission intervals reduces the delay associated with asynchronous re-transmission. With a Doppler shift of 30 Hz, forcing a re-transmission every 40 slots reduces the packet delay per user (Figure 5.9) by nearly half with a negligible loss in the average throughput per sector (Figure 5.8). A significant throughput gain is still achieved if the $RTI$ is further constrained to only 10 slots. In the case of perfect prediction and 100 Hz maximum Doppler shift, a maximum $RTI = 10$ slots results in nearly the same delay as the synchronous re-transmission scheme. It can be noted that in the system with the smallest re-transmission interval constraint possible, $RTI = 4$ slots, there is still significant throughput gain due to the adaptive re-

formation and re-allocation of sub-band groups. In summary, asynchronous re-transmission with a constrained maximum RTI can increase the overall throughput of the system by significantly increasing throughput to users with "average" conditions in the cell in comparison to synchronous schemes. This throughput increase is gained while also limiting the packet delays to nearly those of synchronous systems.

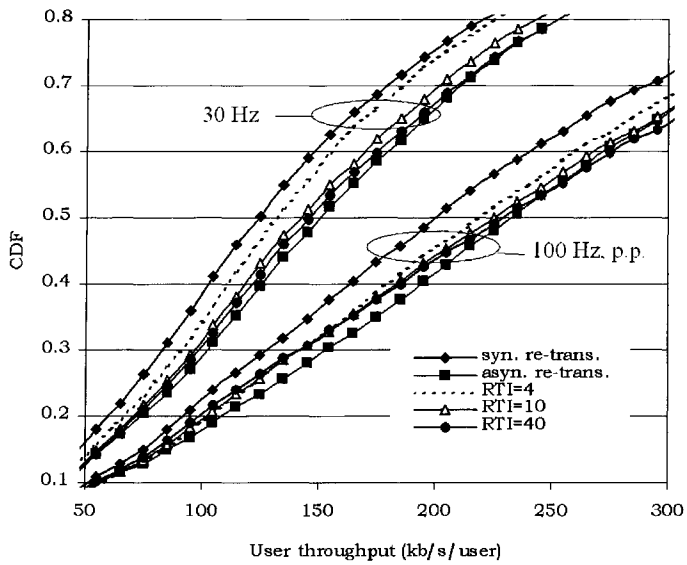


Figure 5.8. Distribution of user throughputs with asynchronous re-transmission of packets and a constraint on the maximum re-transmission interval ($RTI$); packet format $D$ and $U = 32$ users per sector.

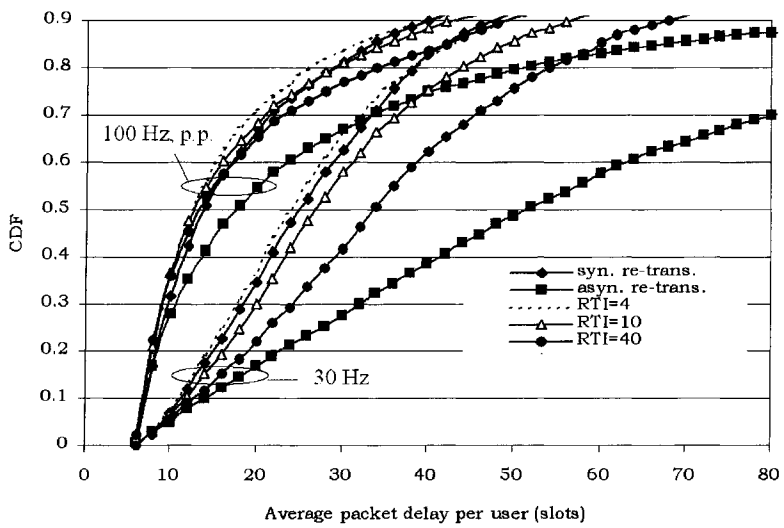


Figure 5.9. Distribution of average packet delays per user with asynchronous re-transmission of packets and a constraint on the maximum re-transmission interval ($RTI$); packet format $D$ and $U = 32$ users per sector.

## 5.3 Best Sector Selection

Best sector selection is a significant feature in best-effort wireless packet data systems. Best sector selection periodically ensures that the strongest possible signal is received at the mobile. The pilot signals transmitted from every base station sector during each time slot (see Fig 4.8) allow the mobile to determine from which sector it receives the strongest signal. Base station transmissions are distinguished by a sector specific pseudo-random noise (PN) sequence, which is concatenated with the Walsh sequences. For the purpose of best sector selection the pilot signal power is estimated within a time window sufficiently long to average out the small scale fading. Thus, only path loss and shadowing are accounted for in the best sector selection process.

In Chapter 4, the SS-OFDM-F/TA best-effort packet data system was introduced using slow sector selection [74]-[76]. As mentioned in Chapter 4, for slow sector selection the best transmitter is selected for each user every 30 seconds. The interval of slow sector selection (30 s) is 5 times the correlation time of the shadowing process at mobile velocity of about 3 km/h, and hence, a user is not always receiving transmission from the best sector antenna. The thesis work has also investigated implementation of fast sector selection [76]-[78]. A selection interval time of 1 second was chosen to be significantly less than the correlation time of the shadowing process, but long enough to average out temporal variations in the channel due to small-scale fading. Note that sector selection based on out-dated small-scale variations may negatively affect the system performance. The selection interval must also be long enough to allow for necessary network signalling between base stations for each serving sector change. Other works have also briefly investigated sector selection using intervals on the order of milliseconds [69], however sector selection at this rate may be too challenging to implement. Fast sector selection can be seen as selection based on large scale fading; that is both shadowing and path loss as the selection interval is somewhat less than the decorrelation time in low mobility applications. In comparison, slow sector selection is largely dependent on path loss, and only somewhat dependent on the shadowing fading process. In a parallel study [120][121], adaptive cell selection is also considered in which the selection is based on instantaneous samples of shadowing and path loss without regard for other system channel parameters. In the following section it is shown that fast sector selection on the order of 1 second significantly increases the throughput of the sector, improves fairness among users in terms of throughputs, and lowers the average packet delay.

### 5.3.1 Multi-Cell Simulation and Results

In this section, the average throughput per sector, packet delays and some switching statistics are presented for slow and fast best sector selection options. The choice of a sector is based on values of path loss and shadowing prior to the beginning of each 30 s simulation run. Fast sector selection occurs every second and is based on a running average of path loss and shadowing values with a time constant of 1 second. All simulations in this section assume asynchronous re-transmission of packets using the MD-ARP-PA algorithm described in Section 5.2.1.1.

In order for the proportionally fair scheduler to accurate estimate the average data rate delivered to a user, $R_{ave}^{(k)}(i)$, and properly schedule transmissions, data rate information must be tracked for longer than 1 second. Hence, for fast sector selection, it is assumed that the value of $R_{ave}^{(k)}(i)$ transferred the next serving sector station in the cases where a different serving sector has been selected.

Figure 5.10 shows the significant throughput increase in indoor channels, as low sector isolation and severe shadowing conditions caused a high probability of outage with slow sector selection. Figure 5.11 shows the performance gain in the Pedestrian A channel for two different packet format sets ($A$ and $D$) and models of ICI (see Section 3.2.3). As before, the packet format set that allows more re-transmissions ($D$) results in a higher sector throughput. Explicit simulation of each ICI source increases the average sector throughput, as the ICI is more variable than it is using the composite ICI model, thus improving the possible multi-user gain due to scheduling. The pessimistic small-scale composite ICI model is used unless otherwise stated.

Figure 5.12 shows the performance again with fast sector selection applies to system with and without allocation of disjoint sub-bands in the Pedestrian B channel. The throughput improvement due to fast sector selection is also clear at different mobile speeds (Figure 5.13) with and without channel prediction. This is significant as it indicates that fast sector selection at a rate of 1 Hz still provides a performance gain in cases when the correlation time of the shadowing process is ~0.3 s (as in the 100 Hz case). Fast sector selection provides throughput gains of up to 22% (Figures 5.10-5.13) with $U = 32$ users.

More significant than the average throughput gain is the distribution of user throughputs in the system (Figure 5.14). With fast sector selection, the throughput delivered to the users with the poorest channel conditions is increased, thereby increasing the fairness in the system [75]. Moreover, the minimum user throughput of the system

with $U$=32 users per sector is increased from nearly 0 to ~ 13 kb/s/MHz/sector/user. The CDFs in Figure 7 are for the case of MD-ARP-PA asynchronous re-transmission, and packet format set $D$.

Fast sector selection also ensures that users are not in severely degraded channel conditions for extended periods, and hence the packet delays are shorter. Figure 5.15 shows the distribution of the average packet delays per user with slow and fast sector selection in the ITU Pedestrian B channel.

The results shown in this section clearly indicate that using fast sector selection at 1 Hz significantly increases the performance of the system. Fast sector selection increases the throughput, decreases the packet delays significantly, and increases fairness among users in terms of both throughput and delays.

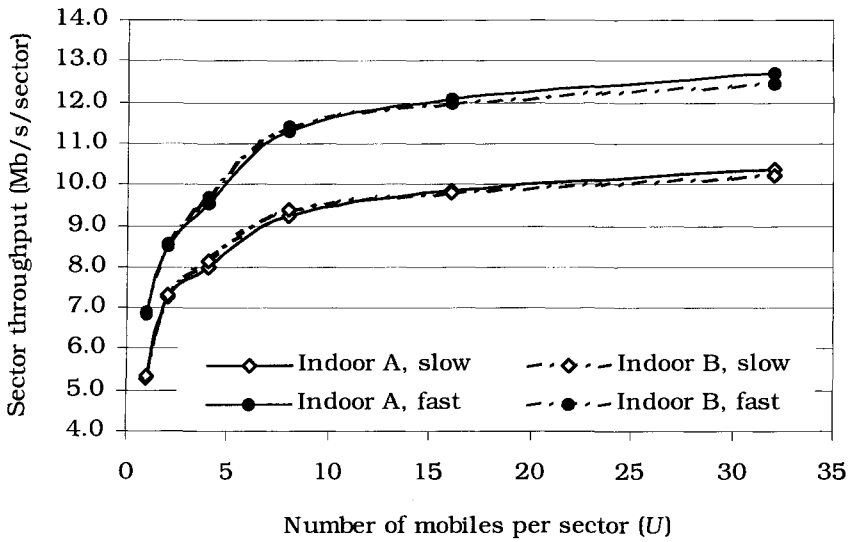


Figure 5.10. Average throughput per sector in the Indoor A and B channels with slow and fast sector selection. Packet format set *D*.

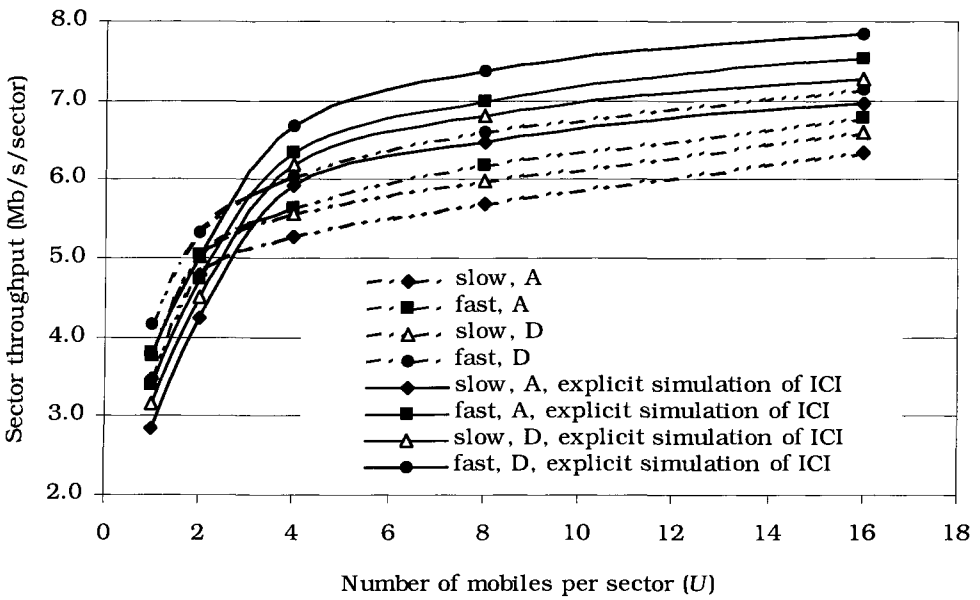


Figure 5.11. Average throughput per sector for ITU Pedestrian A channel, with slow and fast sector selection; packet format sets *A* and *D*, and composite ICI model (no label) and explicit simulation of ICI sources.

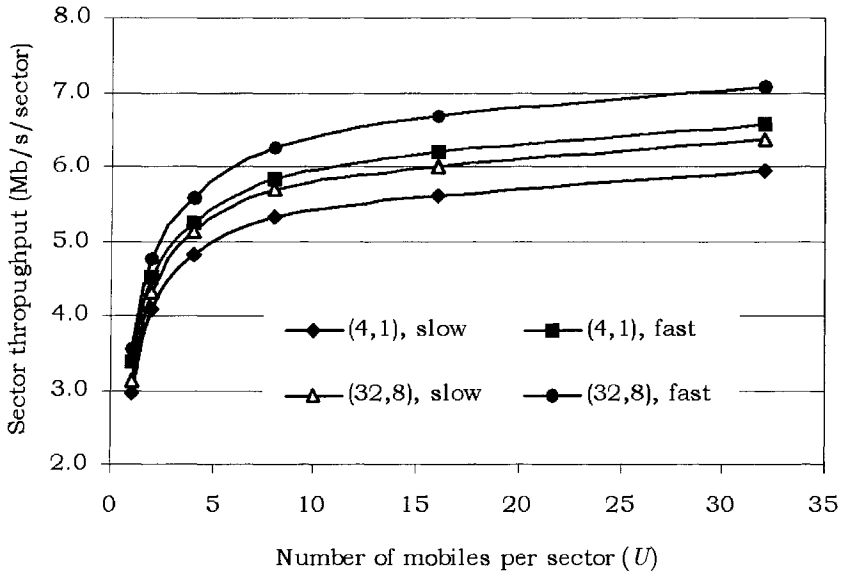


Figure 5.12. Average throughput per sector with allocation of disjoint sub-bands, ($M_n$, $M_g$), with slow and fast sector selection in the Pedestrian B channel. Packet format set $D$ is used.

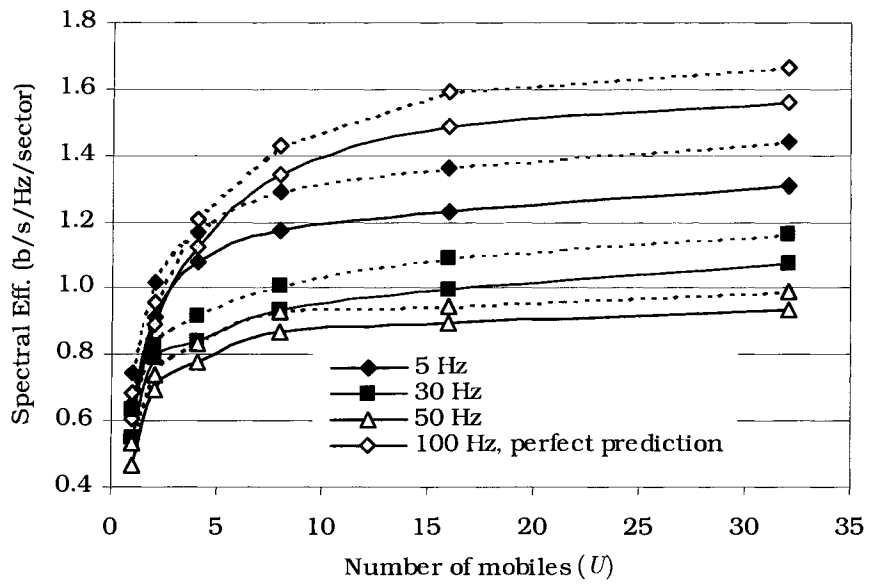


Figure 5.13. The average throughput per sector for the Pedestrian B channel with 5, 30, 50 and 100 HZ maximum Doppler shifts with slow (solid lines) and fast (dashed lines) sector selection. Only the 100 Hz case assumes channel prediction. Packet format set $D$ is used.

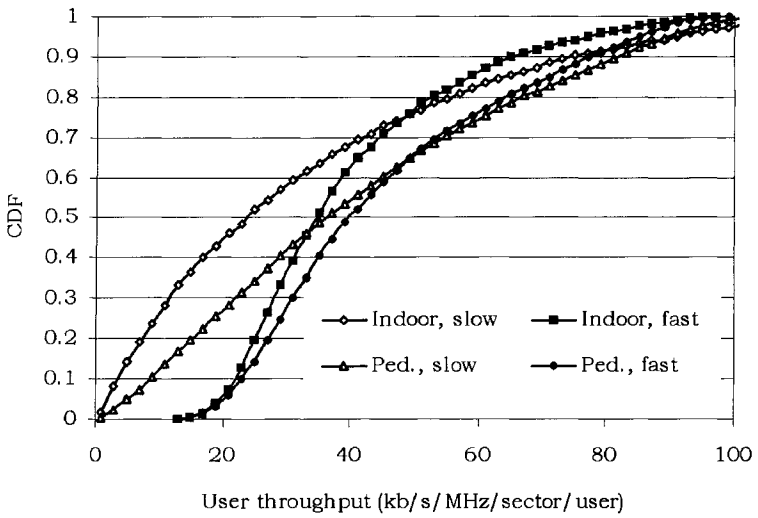


Figure 5.14. User throughput distributions for the ITU Pedestrian B and Indoor B channels with slow and fast sector selection; $U$=32 users per sector.

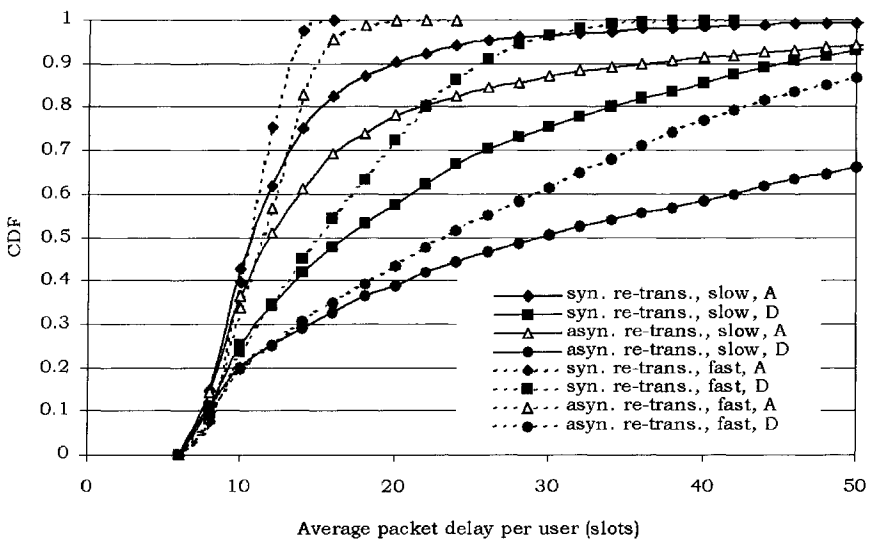


Figure 5.15. Distribution of average packet delay per user with synchronous and asynchronous re-transmission of packets, slow and fast sector selection, and packet format sets $A$ and $D$; $U$=32 users per sector.

### 5.3.2 Sector Switching Statistics

As shown in the previous sub-section, fast sector selection provides a significant improvement in throughput, as well as user fairness, and lowers packet delays. The cost of fast sector selection is increased demand on the serving network, and therefore it is of interest to examine properties of sector selection such as distribution of selected serving sectors, average switching probabilities, and delay in sector switching due to packet re-transmissions.

Figures 5.16 and 5.17 show the probability of a mobile receiving transmission from one of the 57 simulated serving sectors for the indoor and pedestrian models, respectively. The probabilities are the portion of time a mobile in the home sector receives transmissions from each one of the sector antennas. Probabilities less than 0.1% are not shown on the figures. The values were generated from cellular system simulations as described in Section 4.3, which gives 31 sector switching decisions from 3200 mobile positions (for the $U$=32 simulations) in the home sector. Clearly, the majority of the time mobiles receive transmission from the home sector. In the indoor channel, nearly 28% of the time mobiles in the home sector receive transmission from an adjacent sector belonging to one of three other base stations. In general, the mobiles in the home sector will receive transmissions at least 1% of the time from one of 11 sector antennas, which correspond to 9 separate base stations. Sector selection is somewhat more geographically limited in the pedestrian channel. This is because the sectors are more isolated in the pedestrian channel due to a higher path loss exponent (4 instead of 3, in the indoor model). In addition, large-scale fading is more significant for the indoor channel due to a higher standard deviation of the shadowing process. Only five sectors in the pedestrian model have a selection probability of greater than 1%. The five sectors correspond to 4 different base stations, including the home sector. There is little difference in the switching statistics for the Indoor A and B channels, or the Pedestrian A and B channels, respectively, as the parameters of the long-term fading processes are the same for the A and B channels of each category.

Figure 5.18 shows the distribution of the average sector switching probabilities per user. The distribution indicates that about 18% of users in the indoor channel and between 34 and 40% of users in the pedestrian channels do not switch sectors during the 30-second (31 sector selection decisions) window. Users in the indoor channel are likely to switch sectors more frequently (12.7% switching probability average) than users in the pedestrian channel at low mobile speeds corresponding to maximum Doppler shift of 5

Hz (7.1% switching probability average). At higher mobile speeds, the long-term channel fading values change more quickly, which can result in a higher number of decisions to switch sectors (11.2 and 11.3% for 30 Hz and 50 Hz, respectively), either due to greater variability in average signal powers from sector antennae or increased incorrect sector switching decisions as the information may be outdated (and incorrect) at the switching instant. For all pedestrian cases and the indoor channel case, the maximum probability of sector switching recorded for a single user is approximately 50% (not shown on the figure).

Multiple packet re-transmissions in the hybrid Type II ARQ scheme can cause delays in the switching of sectors. Ongoing re-transmissions during sector selection can be handled by either seamlessly continuing re-transmissions from the next sector, or by completing all re-transmissions of a packet to a user before switching sectors. The former requires that considerable information be sent to the next serving sector before the next scheduled transmission. This scheme is justified in cases where there is sufficient time between re-transmission such as asynchronous re-transmissions of packets with a sufficient larger re-transmission interval (RTI) constraint. For synchronous re-transmissions it is more practical to complete all existing packet transmission before switching sectors; however this process will cause delays in sector switching.

Assuming synchronous re-transmission of packets with the packet format set $D$ (see Table 5.1) which supports the most amount of re-transmissions (8 maximum), the maximum delay in waiting for an ongoing transmission to finish is 28 slots in which we have assumed that a sector change can occur only every $4^{\text{th}}$ slot to correspond with the 4 inter-laced time division multiplexed channels inherent in this system (see Figure 4.9). For $U$= 32 users, it can be seen from Figure 5.19 that at least 92% of the time there is no delay associated with fast sector selection at 1 Hz. The maximum delay of 28 time slots corresponds to only 3.8% of the sector selection interval, and occurs only rarely so that this delay is not significant for fast sector selection at 1 Hz. Systems that use asynchronous re-transmissions and wait for ongoing packet transmission completion before sector switching are more likely to incur longer delays. The delay itself will depend largely on the selected re-transmission interval (RTI) constraint.

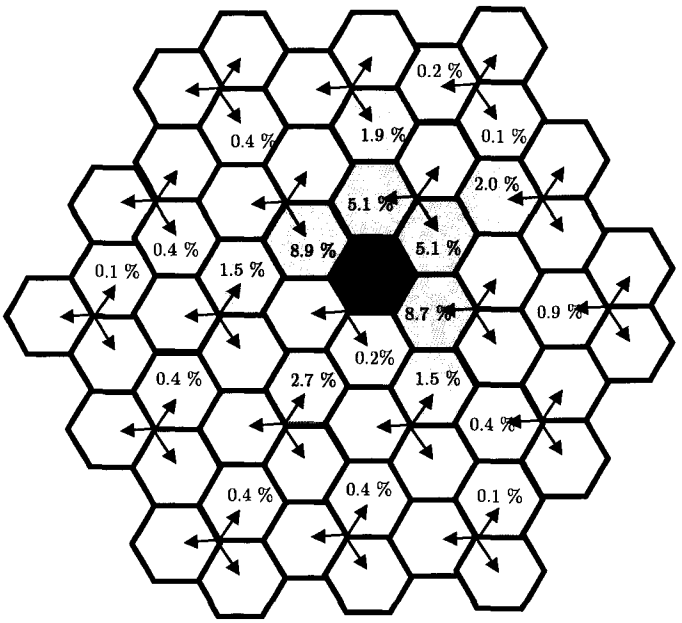


Figure 5.16. The average probability of receiving transmission from each of the 57-sector antennae for a user in the home sector. The indoor channel model is assumed.

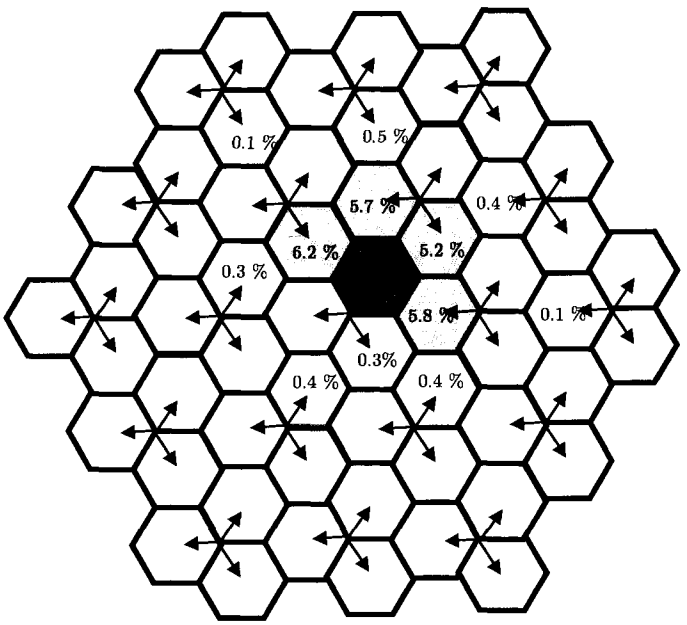


Figure 5.17. The average probability of receiving transmission from each of the 57-sector antennae for a user in the home sector. The pedestrian channel model is assumed.

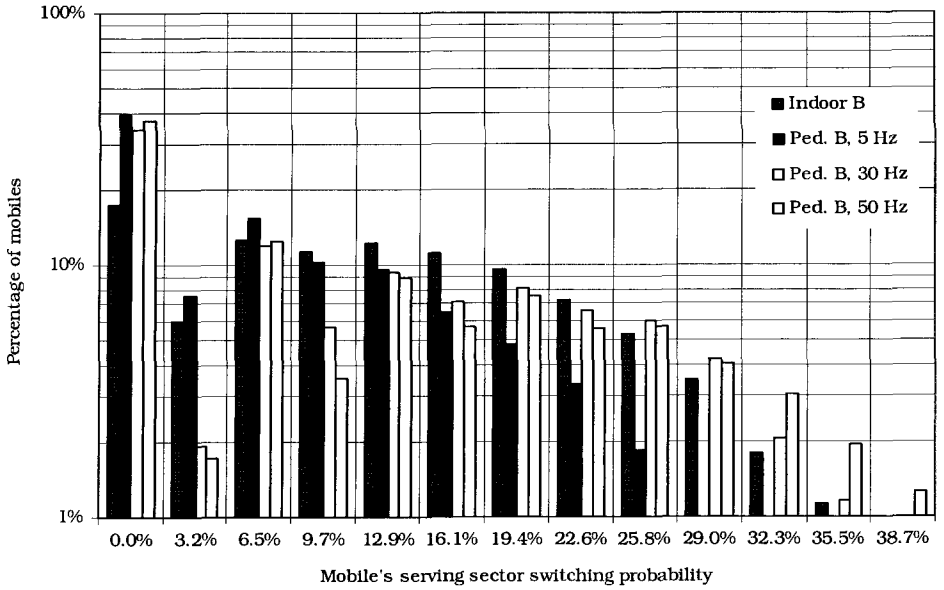


Figure 5.18. The average probability of a mobile switching serving sectors at a given sector selection interval.

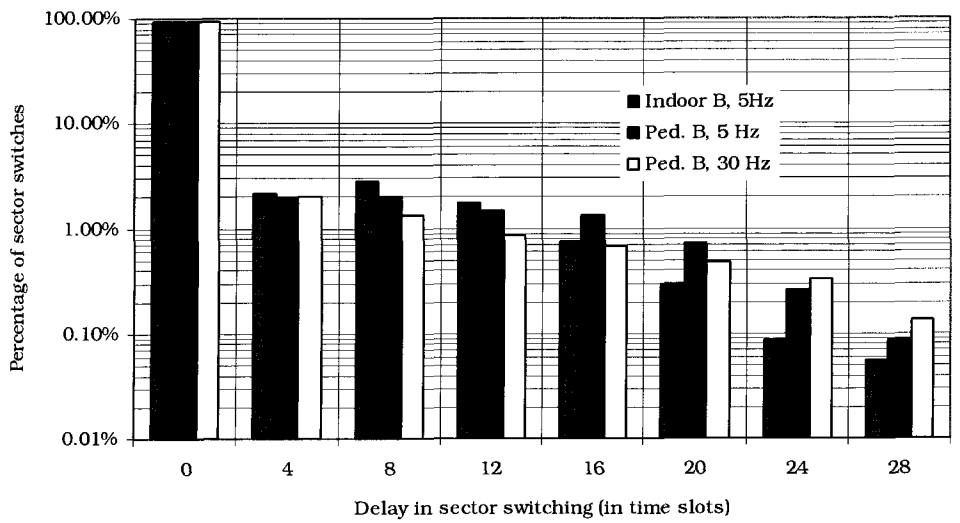


Figure 5.19. The delay in sector switching due to ongoing packet re-transmissions using synchronous re-transmission. $U$=32 users per sector.

## 5.4 Packet Structures with 64-QAM Modulation

In this Section, the average throughput per sector of the SS-OFDM-F/TA system is examined using 64-QAM constellations in the packet format set. Previous packet format sets considered in this thesis used QPSK, 8 PSK, and 16 QAM modulation schemes. Larger constellations such as 64-QAM, or 256 QAM were not considered to avoid having complex receiver structures. In addition, imperfections such as time and frequency offset and phase noise limit the upper bound of the received signal SIR, making the use of large constellation schemes less likely. Signal distortion or clipping due to imperfect non-linear amplification of the signal in the presence of high peak-to-average power ratio (PAPR) in OFDM systems also limit the effectiveness of larger modulation constellations. Regardless of implementation challenges, it is of interest to examine the performance gain by allowing 64-QAM packet structures.

The additional packet structures using the 64-QAM constellation are listed in Table 5.4. These packet structures are used in addition the packet structures listed in Table 5.1 for packet format set $A$, and synchronous re-transmission is considered. System parameters are as listed in Section 5.1, and maximum Doppler shift in the Pedestrian B channel is 5 Hz. The PER curves for these packet structures are given in Appendix B.2. The effect of various symbol amplitudes on the inter-code interference for larger constellation sizes is discussed in Appendix E. The throughput in the Pedestrian B channel (Figure 5.20) increases from 6.3 to 6.85 Mb/s/sector with slow sector selection and $U = 32$ users using 64-QAM, and increased by 8.5 % using fast sector selection. The throughput increase benefits only the top 25% of mobile users in the system (Figure 5.21). The average throughputs for users with generally poorer channel conditions are unchanged.

Table 5.4. Additional Packet structures to packet format set A for 64 QAM

| *Max no. of slots* | *Packet size (bits)* | *SIR at 1% PER (dB)* |
|---|---|---|
| 1 | 4608 | 15.8 |
| 1 | 6144 | 20.3 |

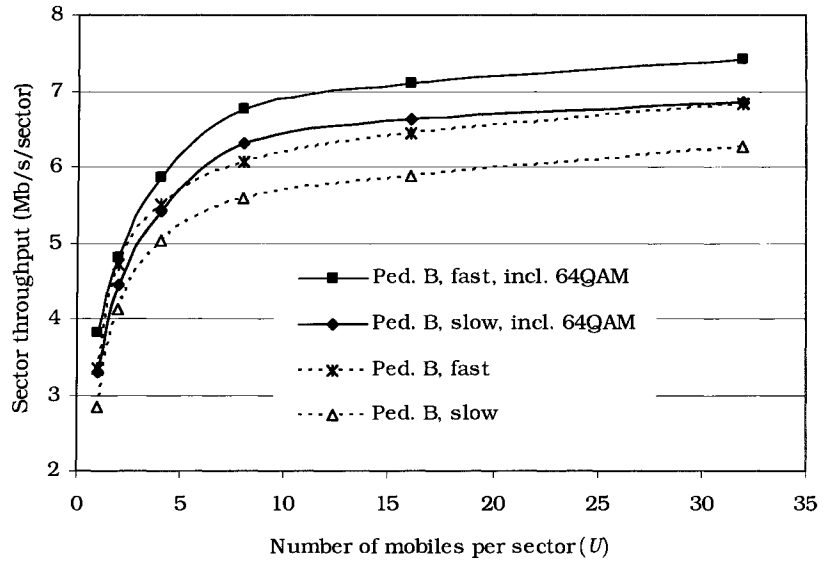


Figure 5.20. The average throughput per sector in the Pedestrian B channel with and without the inclusion of the two 64 QAM packet structures.

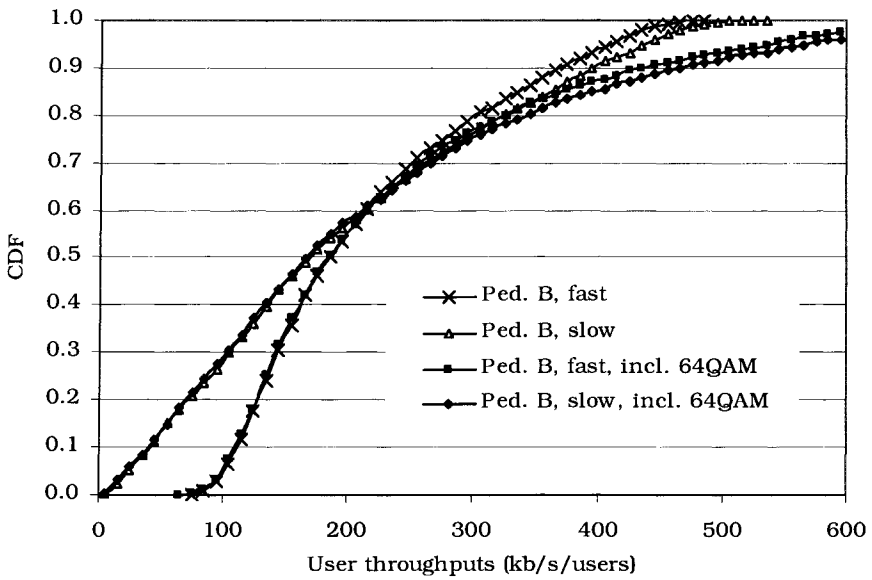


Figure 5.21. The average throughput per sector per user in the Pedestrian B channel with and without the inclusion of the two 64 QAM packet structures.

## 5.5 Quantized SIR feedback

In all previous sections it was assumed that the SIR feedback was continuous, or unquantized. In practical applications the resources on the uplink are limited, so the SIR feedback must be quantized. In this sub-section, decisions based on quantized SIR values are considered. Decisions based on the quantized values include the selection of a mobile to which to transmit in a given sub-band/time slot, packet format selection, and allocation of disjoint groups of sub-bands including the sub-band group formation.

SIR feedback quantization negatively affects the performance of the system, particularly when transmission formats with a low number of re-transmissions are used (Figure 5.22). However, asynchronous re-transmission with 3 dB quantization increments and packet format set $D$ results in the same throughput as synchronous re-transmission with perfect SIR estimates, and only small loss in throughput compared to asynchronous re-transmission with unquantized estimates. These results demonstrate that the system can be implemented with only coarse CSI feedback to the base station, and still retain significant benefit due to multi-user diversity. It can also be noted that in rapidly changing channels such as the Pedestrian B channel with a maximum Doppler shift of 100 Hz, the channel prediction does not have to be overly accurate.

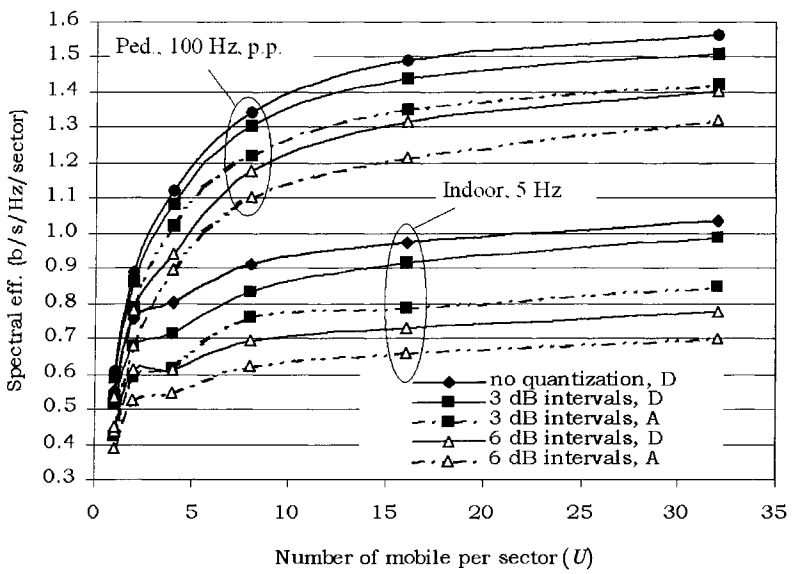


Figure 5.22. Spectral efficiency with quantized SIR feedback in the Indoor B and Pedestrian B channels.

## 5.6 Adaptive Termination with CDM Packet Transmission

In general, this thesis considers the use of all spreading sequences in a sub-band time slot for a single packet transmission or re-transmission. It is also possible to transmit two packets in the same sub-band time slot, to the same user, using code division multiplexing (CDM). If the SIR is sufficiently large at a given time, a larger modulation constellation and only a subset of the spreading sequences can be used for the packet re-transmission. If it is known at the transmitter that using a larger modulation constellation and a only a subset of available spreading codes for the next transmission will be sufficient to successfully complete the packet transmission, then the packet re-transmissions can therefore be *adaptively terminated* (i.e., no further re-transmissions will occur) based on the channel conditions and knowledge of the additional signal energy needed to successfully complete the transmission. The remaining spreading sequences can then be used for another (re)-transmission. This concept was presented in [19][20] for a multi-service, single carrier system. This process requires feedback from the mobile of the extra energy required to successfully complete the transmission. Table 5.5 indicates the possible options.

Table 5.5. Possible formats of packet transmission to be completed using a larger constellation, and formats of the additional packet to be sent in the same time slot/sub-band.

| *Original packet modulation* | *Larger constellation applied* | *Portion of slot resources free for CDM* | *Packet sizes of the additional transmission* | *Constellation of the additional transmission (first slot)* |
|---|---|---|---|---|
| QPSK | 8 PSK | 1/3 | 408, 792 | 8 PSK |
| | 16 QAM | 1/2 | 408, 792, 1560 | QPSK or 16 QAM |
| 8 PSK | 16 QAM | 1/4 | 408, 792 | 16 QAM |

After a mobile is scheduled to receive a re-transmission of a given packet format, the base station can then calculate if the channel conditions can support a transmission with a larger constellation. The link budget for the estimated received SIR per transmission of the packet after the $(i+1)^{th}$ transmission is given by:

$$\hat{\gamma}_{packet}^{(i+1)} = \frac{1}{(\gamma_{pen})(\gamma_{mar})}\hat{\gamma}_m\left(\frac{1}{i+1}\right) + \gamma_{packet}^{(i)}\left(\frac{i}{i+1}\right) \tag{5.3}$$

where $\hat{\gamma}_m$ is the SIR estimate in the $m^{th}$ sub-band, $\gamma_{packet}^{(i)}$ is the average energy per transmission already received by the mobile from $i$ previous packet transmissions, $\gamma_{pen}$ is the SIR penalty incurred by using a larger constellation in the $(i+1)^{th}$ transmission, and $\gamma_{mar}$ is an adaptive margin associated with adaptively terminating transmissions for this packet format. If (5.3) is larger than estimated link level curves for successful packet transmission, then the transmitter will choose to use the larger constellation size and release some code channels for other transmissions. It is important to note that the adaptive margin used in this calculation is similar to the adaptive selection thresholds for packet format selection as described in Section 4.3.3, however, the target failure rate must be significantly lower than 1% in order for the system operation to be stable. In other words, adaptive termination is only used when the predicted success rate is very high. In the simulations for this section, a target adaptive termination failure rate of 0.01% is used. After adaptive termination, the mobile is allocated an additional transmission. The additional transmission may be a new packet transmission or a re-transmission of a packet. The decision is based on the asynchronous re-transmission algorithm used in the system.

Using adaptive termination in order to allow an additional packet transmission by means of code division (Figure 5.23) provided only modest average throughput per sector gains ($< 3\%$). This scheme increased throughput delivered to users with poorer channel conditions, as such users are more likely to select transmission formats with QPSK or 8-PSK constellations. For the case of $U$=32 users, a small increase in average throughput for these users was observed along with a decrease of up to 6% in the total average packet delay per user. The gain in the average throughput per user was more pronounced at $U$=4 users; for example, a nearly 20% (370 to 440 kb/s) gain was observed for the 20$^{th}$ percentile users with $f_D$ =5 Hz (Figure 5.24). Only moderate gains have been observed with this scheme as asynchronous re-transmission and the large number of transmission formats allow for adequate adaptation to the channel. All simulations considered asynchronous re-transmission algorithm MD-ARP-PA (see Section 5.2).

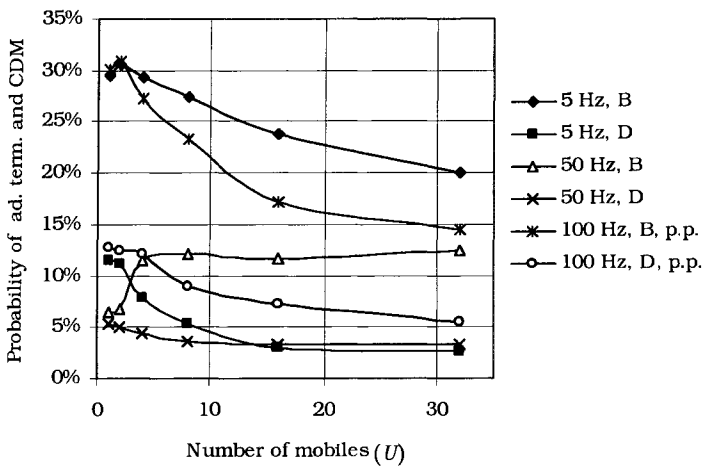


Figure 5.23. The probability of using adaptive termination and CDM of additional packet transmissions in the same sub-band/time slot. The results are for the Pedestrian B channel using packet format sets $B$ and $D$.

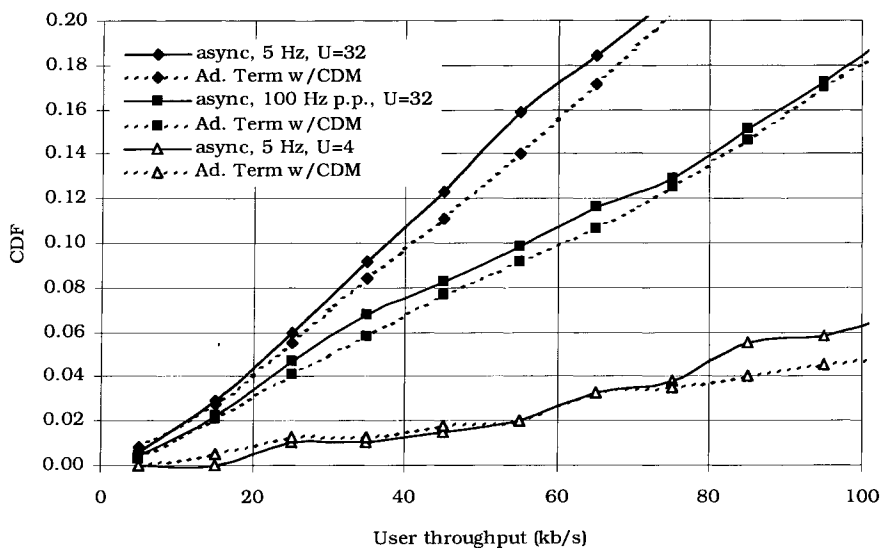


Figure 5.24. The CDF of user throughputs using adaptive termination and CDM of additional packet transmissions for the Pedestrian B channel. Packet format set $B$.

# Chapter 6

# Diversity Combining Options and Low-Complexity MMSE Equalization for SS-OFDM Systems

This chapter compares diversity combining schemes for the downlink of spread spectrum orthogonal frequency division multiplexing (SS-OFDM) systems in frequency selective fading channels. In particular, symbol-level combining after despreading is compared to chip-level combining under maximal ratio combining (MRC) of signals from different diversity branches and minimum mean-square error (MMSE) equalization of spreading sequences. Symbol-level combining takes place after the operations of MMSE equalization and despreading, whereas the operations of equalization and despreading occur after MRC if chip-level combining is used. Chip-level combining combines diversity samples in an efficient manner while reducing inter-code interference (self-interference) that results from the loss of orthogonality of spreading sequences due to a frequency selective channel. This method is shown to be superior to symbol-level combining when the diversity branches are uncorrelated, and when the branches differ only due to subcarrier interleaving. A MMSE equalization method with significantly reduced complexity for partially loaded systems is also presented, based on the premise of chip-level combining. Novel expressions for the bit error rate (BER) of the two methods, as well as the extension of the analysis to partially loaded systems are given. The extensions of chip-level combining and low-complexity equalization of a partially loaded system to an OFDM system with 2-dimensional spreading are also presented. The results are relevant to antenna diversity as well as temporal diversity achieved though re-transmission within an ARQ scheme.

Section 6.1 introduces the topic of diversity combining and describes previous research activities relevant to the findings in this chapter. Section 6.2 of the chapter provides the system description and introduces the analytical method for the case of no diversity. Section 6.3 describes the combining schemes and presents their analysis. The extensions of the work to partially loaded systems and systems with 2-dimensional spreading are discussed in the next two sub-sections (Sections 6.4 and 6.5). Section 6.6 explains the simulation structure and presents the results and their discussion.

## 6.1 Introduction and Existing Literature

Various forms of diversity combining are of significant importance in packet data systems. For example, type II hybrid ARQ with soft packet combining and incremental redundancy is an important performance enhancing technique in delay tolerant packet data systems employing adaptive modulation, as multi-slot packet transmission formats increase the number of effective bit rates, and allow for better adaptation to the channel conditions through earlier termination of re-transmissions. Multiple receive or transmit (or both) antennas create spatial diversity, which may also be exploited through suitable combining.

In frequency selective fading channels, the orthogonal spreading sequences used with SS-OFDM lose their orthogonality, creating inter-code or self-interference, as described in Section 2.2.4. Minimum mean square error (MMSE) equalization partially restores the orthogonality of the spreading sequences. If multiple replicas of a packet are available, it is possible to combine them either before or after equalization and despreading. Combining after equalization and despreading occurs at the symbol level. If combining is done before equalization and despreading, it occurs at the chip level. The latter can result in a large performance benefit due to reduced inter-code interference if properly equalized. Combining and MMSE equalization methods before despreading were also presented in [64]. However, due to the application of non-optimal combining and equalization weights, relatively poor performance was achieved in [63]. A form of diversity combining with MMSE equalization has also been considered in a parallel study [83] to this one, in which blocks of subcarriers are interleaved for each serial re-transmission under an ARQ scheme. In that study, blocks of subcarriers corresponding to a spread data symbol are relocated in frequency for each retransmission, but the interleaving is symbol-wise in frequency (rather than chip/subcarrier-wise as in this chapter) and the simulations focus on systems with equal gain combining (EGC), and spreading in the time domain.

Chip-level diversity combining requires appropriate MMSE equalization of the combined chip samples. Some equalization approaches similar to those in this chapter are presented in [5] in the context of multiple antenna systems. This chapter compares the performance of chip-level combining to symbol-level combining with MMSE equalization, and considers several forms of diversity and provides analytical justification for the results. Cases of independently and identically distributed diversity replicas are considered, as well as, independent subcarrier fading and correlated subcarrier fading within a given signal replica. Further, novel analytical expressions are developed for the bit error rate (BER) of the two combining approaches, and an explanation is given for the difference in their performance. Simulation is used to evaluate performance of turbo-coded systems.

Reference [5] has also found that for partially loaded systems, complex multi-user detection methods, that may involve inversion of large matrices, are required. In this chapter, it is shown that the same performance can be achieved using a simple method similar in complexity to single user detection techniques. The presented approach relies on the observation that some partially loaded systems may be treated as fully loaded systems with multiple diversity replicas. This approach has led to the development of a novel general BER expression for partially loaded systems with or without diversity, which is also presented.

This chapter also considers chip-level combining and MMSE equalization for SS-OFDM systems with spreading in time and frequency. Both fully loaded and partially loaded systems are discussed. SS-OFDM with 2-dimensional spreading and retransmission combining is also discussed in [83], but that work does not consider appropriate chip-level combining and MMSE equalization in both dimensions.

## 6.2 System Description

The downlink of an SS-OFDM system is shown in Figure 6.1, and is similar in form to the system set-up in Chapter 2. For completeness and to introduce the closed form analytical expressions for BER, it is briefly described again in this sub-section. $K$ complex data symbols, $b_0,\ldots,b_k,\ldots,b_{K-1}$ are serial to parallel converted, and are each spread by orthogonal Walsh sequences, $\mathbf{c}_k = [c_{k,0},\ldots,c_{k,l},\ldots c_{k,L-1}]$, $c_{k,l} \in \left\{-1/\sqrt{L}, 1/\sqrt{L}\right\}$, of length $L$. The general case where each of the $K$ symbols is transmitted to a different user is considered in this chapter for simplicity of description by setting $U$=$K$, although this chapter also applies to code-multiplexed signals intended for a single user. The chip sequences are synchronously summed, and the resulting chip stream is serial to parallel

converted to form $L$ chip streams. These $L$ streams are interleaved (which is denoted by $\Pi$) with $M$-1 other groups of $L$ chip streams (from others users, or a different packet), and then mapped onto $N = ML$ subcarriers via an inverse fast Fourier transform (IFFT). For simplicity, only the case of $M$ =1 is considered initially. After addition of a cyclic prefix, the transmitted SS-OFDM symbol is given by:

$$s(t) = \sum_{k=0}^{K-1} \sum_{l=0}^{L-1} b_k c_{k,l} e^{j2\pi lt/T_{sym}}, \quad \text{for } -T_g \le t \le T_{sym} \tag{6.1}$$

The signal is transmitted through a time-varying frequency selective Rayleigh fading channel with additive white Gaussian noise (AWGN). A simple single cell model is considered in this chapter, and hence, no large-scale fading effects are considered. At the input of the receiver, the received signal $r(t)$ during the detection window is given by:

$$r(t) = \sum_{k=0}^{K-1} \sum_{l=0}^{L-1} b_k c_{k,l} h_l e^{j2\pi lt/T_{sym}} + n(t), \quad \text{for } 0 \le t \le T_{sym} \tag{6.2}$$

where $h_l$ is the complex channel gain on the $l^{th}$ subcarrier, and $n(t)$ is the AWGN process. This chapter is only concerned with reception of the signal at a single receiver, and hence the subscript of the user $u$ that was used in previous chapters is dropped from the complex channel gain. It is assumed that the cyclic prefix is longer than the maximum excess delay of the channel so that inter-symbol interference is eliminated.

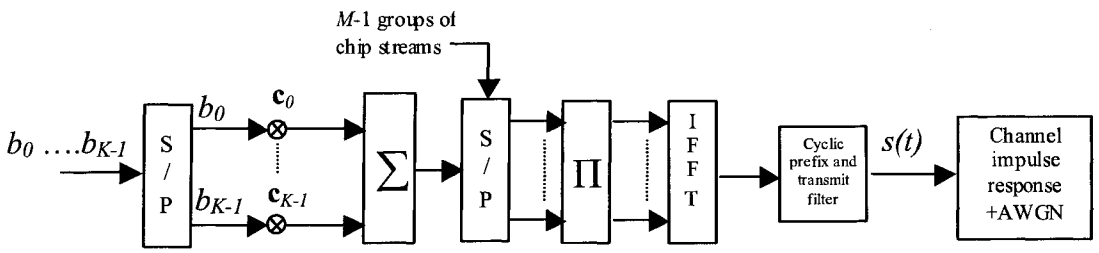


Figure 6.1. SS-OFDM transmitter structure. $\Pi$ denotes the chip stream interleaver.

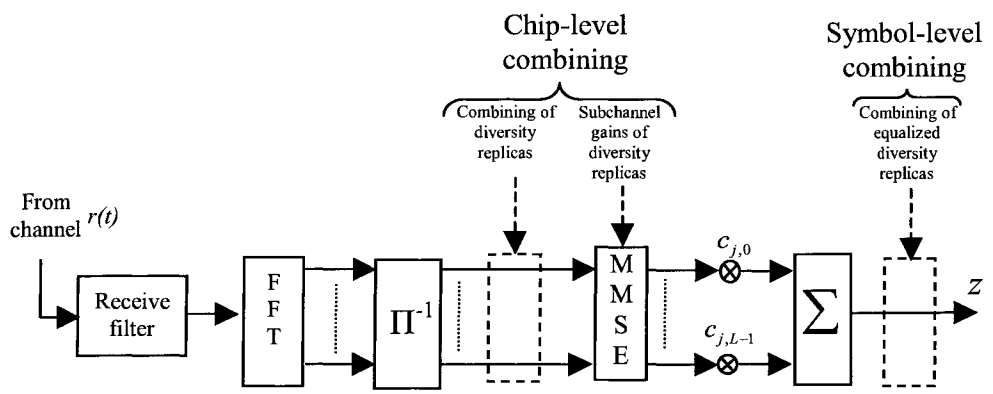


Figure 6.2. Receiver structure; only essential operations for reception of the $j^{th}$ bit are shown.

At the receiver, the received signal is sampled, and then demapped from the subcarriers via an FFT. The $L$ chip streams are despread and the mobile receiver performs MMSE equalization [50] to partially restore the orthogonality between parallel chip streams while minimizing noise amplification. If the system is fully loaded ($K = L$), the MMSE equalization coefficient is given by $g_l = h_l^* / \left( |h_l|^2 + \lambda \right)$, where $1/\lambda = E_s / N_0$, and $E_s$ is the SS-OFDM symbol energy [50]. The partially loaded case will be discussed in Section 6.4. The decision variable for the $j^{th}$ data symbol is given by:

$$z_j = b_j \frac{1}{L} \sum_{l=0}^{L-1} h_l g_l + \sum_{l=0}^{L-1} h_l g_l \sum_{\substack{k=0 \\ k \neq j}}^{K-1} c_{j,l} c_{k,l} b_k + \sum_{l=0}^{L-1} c_{j,l} g_l \eta_l \tag{6.3}$$

where $\eta_l$ is the noise sample on the $l^{th}$ subchannel. The first term of (6.3) is the desired signal, the second term is the inter-code interference and the third term is noise. As in Chapter 2, the signal to interference & noise ratio (SINR) is given by [52]:

$$SINR = \frac{\mu_A^2}{\sigma_A^2 (K-1)/L + \mu_B^2 N_0 / E_s} \tag{6.4}$$

in which $\mu_A$ and $\mu_B$ are the sample means of the random variables $A_l$ and $B_l$, respectively, and $\sigma_A^2$ is the sample variance of $A_l$. The subscripts for the sample means and variance have been simplified in this chapter for ease of presentation. $A_l$ and $B_l$ are given by:

$$A_l = \frac{|h_l|^2}{|h_l|^2 + \lambda} \tag{6.5}$$

$$B_l = \frac{|h_l|^2}{\left( |h_l|^2 + \lambda \right)^2} \tag{6.6}$$

An analytical expression for the BER exists if $L$ is large, and the frequency diversity of the wideband channel is sufficient to assume that the modulated signals on the $L$ subcarriers undergo independent fading after interleaving (this is easier to achieve if $M >> 1$ due to greater available frequency diversity). In this case, $|h_l|^2$ is chi-square distributed (with 2 degrees of freedom) over all $l$, and the sample means and sample variance in (6.4) are replaced by the statistical mean and variance of the random variables $A_l$ and $B_l$. These are given by [52]:

$$\mu_A = E[A_l] = \int_0^\infty \frac{x}{x+\lambda} e^{-x} dx = 1 + \lambda e^{\lambda} \, \mathrm{Ei}(-\lambda) \tag{6.7}$$

$$\sigma_A^2 = E[A_l^2] - E[A_l]^2 \tag{6.8}$$

$$\mu_B = E[B_l] = -1 - (1+\lambda) e^{\lambda} \, \mathrm{Ei}(-\lambda) \tag{6.9}$$

where $E[A_l^2] = 1 + \lambda + (\lambda^2 + 2\lambda)e^{\lambda}\,\mathrm{Ei}(-\lambda)$, and $\mathrm{Ei}(-\lambda) = -\int_{\lambda}^{\infty} \frac{e^{-x}}{x} dx$ is the exponential integral function. The bit error rate of the system using QPSK modulation can be given by [84]:

$$P_b = Q(\sqrt{SINR}) \tag{6.10}$$

using the $Q$ function (which is the area under the tail of a Gaussian distribution).

## 6.3 Soft Combining of Packet Diversity Replicas

In this chapter, multiple receptions of a packet are assumed to be in the form of exact diversity replicas (identical modulation, coding and spreading). Hence, the methods and results of this chapter is most applicable to spatial diversity combining or soft-packet combining within an ARQ scheme, but are also relevant to incremental redundancy schemes with many re-transmissions, in which the same systematic and parity bits are repeated. Note that the packet formats used in Chapter 5 allow for a high level of repetition (see Table B.5).

Two methods for combining diversity replicas are considered. The combining operation can either take place before or after equalization and despreading. Prior to equalization and despreading, chip level information on each subcarrier is available, and after despreading only symbol level information is available as the chips have already been equalized.

### 6.3.1 Symbol-Level Combining

Symbol-level combining is the simplest method, and for applications involving serial diversity replicas requires the least amount of memory ($K$ complex soft symbol samples). In this approach, chip-level equalization and despreading occur first, and then the symbol diversity samples are considered. The MMSE equalization of a given diversity replica in this scheme does not require channel estimates from the other diversity replicas.

The MMSE equalization coefficient for the $t^{th}$ diversity replica is given by $g_{l,t} = |h_{l,t}|^2 / \left(|h_{l,t}|^2 + \lambda\right)$. Symbol level combining is achieved by coherent addition of all despread replicas. Prior to addition, each diversity replica is weighted by its average subchannel gain, $\alpha_t = \frac{1}{L}\sum_{l=0}^{L-1} |h_{l,t}|^2$. Using (6.3) it can be shown that the decision variable for the $j^{th}$ data symbol after symbol-level combining of $T$ diversity replicas is given by:

$$
\begin{aligned}
z_j &= \sum_{t=1}^{T} \alpha_t z_{t,j} \\
&= b_j \frac{1}{L} \sum_{t=1}^{T} \alpha_t \sum_{l=0}^{L-1} h_{l,t} g_{l,t} + \sum_{t=1}^{T} \alpha_t \sum_{l=0}^{L-1} h_{l,t} g_{l,t} \sum_{\substack{k=0 \\ k \neq j}}^{K-1} c_{j,l} c_{k,l} b_k + \sum_{t=1}^{T} \alpha_t \sum_{l=0}^{L-1} c_{j,l} g_{l,t} \eta_{l,t}
\end{aligned} \tag{6.11}
$$

When fading is slow, it may be advantageous to use different interleaving patterns for different serial packet retransmissions (see Section 6.6.2), in which case different subcarriers corresponding to the same chip index are combined.

If $L$ is large, and if there is sufficient frequency diversity in the channel, the average subchannel gain for each diversity replica, $\alpha_t$, will be nearly identical. Hence the combining is a simple coherent addition of symbol-level samples. Assuming that the subchannel gains are independent for each replica, an analytical representation analogous to (6.7)-(6.9) is possible for symbol-level combining with $T$ diversity replicas.

$$
\mu_{A,T} = E[\sum_{t=1}^{T} A_{l,t}] = T\mu_A \tag{6.12}
$$

$$
\sigma_{A,T}^2 = E[(\sum_{t=1}^{T} A_{l,t})^2] - \mu_{A,T}^2 \tag{6.13}
$$

$$
\mu_{B,T} = E[\sum_{t=1}^{T} B_{l,t}] = T\mu_B \tag{6.14}
$$

where $E[(\sum_{t=1}^{T} A_{l,t})^2]$, $A_{l,t}$ and $B_{l,t}$ are given by:

$$
\begin{aligned}
E[(\sum_{t=1}^{T} A_{l,t})^2] &= \sum_{t=1}^{T} E[A_{l,t}^2] + 2\sum_{s=1}^{T} \sum_{t=s+1}^{T} E[A_{l,t} A_{l,s}] \\
&= TE[A_{l,t}^2] + T(T-1)E[A_{l,t}]^2
\end{aligned} \tag{6.15}
$$

$$
A_{l,t} = \frac{|h_{l,t}|^2}{|h_{l,t}|^2 + \lambda} \tag{6.16}
$$

$$
B_{l,t} = \frac{|h_{l,t}|^2}{\left(|h_{l,t}|^2 + \lambda\right)^2} \tag{6.17}
$$

As before, (6.12)-(6.14) can be substituted into (6.4) (with $\mu_A$ replaced by $\mu_{A,T}$, $\mu_B$ replaced by $\mu_{B,T}$, and $\sigma_A^2$ replaced by $\sigma_{A,T}^2$), and subsequently into (6.10) to give an analytical expression for the BER with QPSK modulation. In this expression, $1/\lambda$ is the SINR per diversity replica. It should be noted that the assumption that the average subchannel gains can be considered nearly the same for all diversity replicas is only made to develop the above expressions. In simulations of symbol-level combining $\alpha_t$ is determined separately for each diversity replica.

### 6.3.2 Chip-Level Combining

Alternatively, soft chip samples from each subcarrier can be combined prior to equalization and despreading. Maximum ratio combining (MRC) is used, and it is assumed that the average noise power is the same on all diversity branches. By using MRC, each chip value takes advantage of the channel diversity. Combining several independently faded chip replicas significantly lowers the variance of the equalized chip samples. This small variance results in significantly reduced inter-code interference after MMSE equalization. MRC and MMSE equalization are achieved in one processing step by using the equalization coefficients given by (6.18) for each of the $t$ diversity replicas.

$$g_{l,t} = \frac{h_{l,t}^*}{\sum_{t=1}^{T} \left|h_{l,t}\right|^2 + \lambda} \tag{6.18}$$

The coefficients in (6.18) have been derived by using MRC to combine the chip-level samples, and then determining the equalization coefficients that give the MMSE between transmitted and equalized signals. This derivation is given in Appendix F. The decision variable for the $j^{th}$ symbol is given by substitution of (6.18) into (6.11).

It is apparent from (6.18) that unlike symbol-level combining, chip-level combining as described requires some information from all $T$ diversity replicas in order to equalize a given replica. For the purpose of combining diversity replicas received in serial, the memory requirements are 50% larger than for symbol-level combining if the system is fully loaded ($K = L$) due to the additional $L$ running sums of real chip gains from each diversity replica to form the denominator of (6.18).

As in the previous section, analytical representations analogous to (6.7)-(6.9) are possible for chip-level combining of $T$ diversity replicas under the assumption that subchannel gains for each replica are independent. Under this assumption the $\sum_{t=1}^{T} \left|h_{l,t}\right|^2$ term in (6.18) is a central chi-square random variable with $2T$ degrees of freedom. Hence:

$$\mu_{A,T} = E[A_{l,T}] = \int_0^\infty \frac{\sum_{t=1}^{T} x_t}{\sum_{t=1}^{T} x_t + \lambda} e^{-\sum_{t=1}^{T} x_t} dx_1 \ldots dx_t \ldots dx_T = \frac{1}{(T-1)!} \int_0^\infty \frac{y^T}{y+\lambda} e^{-y} dy \tag{6.19}$$

$$= \frac{1}{(T-1)!} \left( \sum_{t=1}^{T} (-1)^{t-1} \lambda^{t-1} (T-t)! + (-1)^{T+1} \lambda^T e^{\lambda} \, \mathrm{Ei}[-\lambda] \right)$$

$$\sigma_{A,T}^2 = E[(A_{l,T})^2] - E[A_{l,T}]^2 \tag{6.20}$$

$$\mu_{B,T} = E[B_{l,T}] = \int_0^\infty \frac{y}{(y+\lambda)^2}\frac{y^{T-1}}{(T-1)!}e^{-y}dy$$
$$= \frac{(-1)^T\lambda^{T-1}}{(T-1)!}\left\{\sum_{i=2}^{T}\frac{(-1)^i}{i(i-1)}\sum_{j=0}^{i-2}\frac{(T)!}{(T-i)!(i-2-j)!}\lambda^{-j-1} + 1 + (\lambda+T)e^{\lambda}\,\mathrm{Ei}[-\lambda]\right\} \quad (6.21)$$

where $E[(A_{l,T})^2]$, $A_{l,T}$ and $B_{l,T}$ are given by:

$$E[(A_{l,T})^2] = \int_0^\infty \left(\frac{y}{y+\lambda}\right)^2\frac{y^{T-1}}{(T-1)!}e^{-y}dy$$
$$= \frac{(-1)^T\lambda^T}{(T-1)!}\left\{\sum_{i=2}^{T+1}\frac{(-1)^{1+i}}{i(i-1)}\sum_{j=0}^{i-2}\frac{(T+1)!}{(T+1-i)!(i-2-j)!}\lambda^{-j-1} - 1 - (\lambda+T+1)e^{\lambda}\,\mathrm{Ei}[-\lambda]\right\} \quad (6.22)$$

$$A_{l,T} = \frac{\sum_{t=1}^{T}\left|h_{l,t}\right|^2}{\sum_{t=1}^{T}\left|h_{l,t}\right|^2 + \lambda} \quad (6.23)$$

$$B_{l,T} = \frac{\sum_{t=1}^{T}\left|h_{l,t}\right|^2}{\left(\sum_{t=1}^{T}\left|h_{l,t}\right|^2 + \lambda\right)^2} \quad (6.24)$$

Again, (6.19)-(6.21) can be substituted into (6.4) (with $\mu_A$ replaced by $\mu_{A,T}$, $\mu_B$ replaced by $\mu_{B,T}$, and $\sigma_A^2$ replaced by $\sigma_{A,T}^2$), and subsequently into (6.10) to give a closed form expression for the BER with QPSK modulation. This type of chip-level combining is analogous to using longer spreading sequences and MMSE equalization per spreading sequence as described by (6.25), but it is much simpler (see Section 6.4.2 for further discussion).

# 6.4 Application to Partially Loaded Systems

## 6.4.1 Multi-User Detection in Partially Loaded Systems

If the system is not fully loaded ($K < L$), the proper equalization coefficients are different for each spreading sequence [38], $\mathbf{G} = [\mathbf{g}_0,\ldots,\mathbf{g}_k,\ldots,\mathbf{g}_{K-1}]^T$, where the rows are given by $\mathbf{g}_k = [g_{k,0},\ldots,g_{k,n},\ldots,g_{k,N-1}]^T$. Unlike in the fully loaded case, an $LxL$ matrix inversion is required to find the equalization coefficients, and hence, calculation of equalization coefficients for the partially loaded case is significantly more complex. It is convenient to write the modified equalization matrix that includes despreading for the partially loaded case, as in [38]:

$$\mathbf{G}' = [\mathbf{c}_0\mathbf{g}_0,\ldots,\mathbf{c}_k\mathbf{g}_k,\ldots,\mathbf{c}_{L-1}\mathbf{g}_{L-1}]^T = \mathbf{C}\mathbf{H}^*[\mathbf{H}\mathbf{C}\mathbf{A}\mathbf{C}^T\mathbf{H}^* + \mathbf{I}(N_0/E_s)]^{-1} \quad (6.25)$$

where $\mathbf{H}$ is an $LxL$ diagonal matrix with elements $h_{l,l} = h_l$, $\mathbf{C} = [\mathbf{c}^0, \ldots, \mathbf{c}^k, \ldots \mathbf{c}^{L-1}]$ is a Walsh-Hadamard matrix with columns equal to the $L$ spreading sequences, and $\mathbf{I}$ is the identity matrix. The matrix $\mathbf{A}$ is a diagonal matrix with elements $a_{k,k} = 1$ if the $k^{th}$ spreading sequence is in use, and zero otherwise. $\mathbf{C}^T$ is the non-conjugate transpose of the matrix $\mathbf{C}$. Note that while (6.25) has $L$ rows, only those rows corresponding to the $K$ spreading sequences that are actually used are relevant to the analysis. Equation (6.25) gives the multi-user detection (MUD-) MMSE solution for partially loaded systems.

### 6.4.2 Novel Low-Complexity Solution for Partially Loaded Systems

In this sub-section, we propose a simple equalization method that results in the same performance as the complex multi-user detection method for certain cases of partial loading ($K < L$), and can be used as an approximate solution for the other cases. This is achieved by recognizing that certain partially loaded systems are analogous to fully loaded systems with multiple chip-level combined diversity replicas. Furthermore, the analytical expressions given in equations (6.19)-(6.21) for chip-level combining of diversity replicas can be modified to give similar expressions for partially loaded systems ($K < L$).

Consider the set of spreading sequences given by the columns of a 4x4 Walsh-Hadamard matrix:

$$\mathbf{C} = \begin{bmatrix} 1 & 1 & 1 & 1 \\ 1 & -1 & 1 & -1 \\ 1 & 1 & -1 & -1 \\ 1 & -1 & -1 & 1 \end{bmatrix} \tag{6.26}$$

If only the first 2 spreading sequences are in use of this $L = 4$ system, then the system is identical to a fully loaded $L = 2$ system with $T = 2$ diversity replicas, as the last two chips are the same as the first two for both spreading sequences. This can easily be expanded to state that any partially loaded system where the first $K$ sequences are in use, and $K/L = 2^{-r}$ and $r$ is an integer, is the same as a fully loaded system with combining $2^r$ diversity replicas. Applying this observation to (6.18), the equalization coefficient for the $l^{th}$ subcarrier of a partially loaded system becomes

$$g_l = \frac{h_l^*}{\sum_{\upsilon=0}^{L/K-1} \left|h_{l+\upsilon K}\right|^2 + \lambda L/K} \tag{6.27}$$

The performance of a system using (6.27) is identical to that resulting from the application of a substantially more complex processing approach defined by (6.25), as proposed in [38]. Our approach can also be used for any $K \leq L2^{-r}$ as an approximate, low complexity, equalization method. For example, it would be far more efficient to use (6.27) for $K = 510$ and $L$=1024, even though $K/L \neq 2^{-r}$, and suffer a small performance loss rather than solving (6.25). If the $K$ spreading sequences in use are arbitrarily chosen columns from the matrix $\mathbf{C}$, calculation of coefficients required for proper MMSE equalization becomes more complex. In general for (6.27) and the procedure described in this sub-section to apply directly, the $K$ sequences must be from the first $K'$ columns of the Walsh-Hadamard matrix, where $K' = L2^{-\lfloor \log_2(L/K) \rfloor}$.

Equation (6.27) can be modified to account for chip-level combining of $T_p$ identical diversity replicas:

$$g_{l,t} = \frac{h_{l,t}^*}{\sum_{t=1}^{T_p} \sum_{\upsilon=0}^{L/K-1} \left| h_{l+\upsilon K,t} \right|^2 + \lambda L/K} \tag{6.28}$$

Consequently, a relatively simple equalization approach results in system performance equivalent to that achievable with a more complex multi-user detection method [5]. This conclusion holds for any number of combined diversity replicas, and for certain cases of partial loads as discussed above. Again, in cases when the relative partial system load is not exactly a power of ½, the coefficients given by (6.28) can be used for approximate MMSE equalization.

Furthermore, it is possible to find the general expression of the BER for a partially loaded system with $T_p$ diversity replicas. This generalized expression can be found by substituting $\theta$ in (6.19)-(6.21) in place of $T$, where $\theta = T_p L/K = T_p 2^r$. The resulting SINR is then given by:

$$SINR = \frac{\mu_{A,\theta}^2}{\sigma_{A,\theta}^2 (K-1)/K + \mu_{B,\theta}^2 N_0 L/E_s K} \tag{6.29}$$

It should be noted that (6.29) becomes difficult to use at very low SINRs with a high value of $\theta$ due to computational sensitivity. The BER for QPSK is found by substituting (6.29) into (6.10).

Finally, the expression given in (6.29) is valid also for the case of no diversity, and hence, (6.29) with $T_p$=1 applied to (6.10) yields the uncoded BER of an SS-OFDM system with partial loading. This is the same performance that would be found by using the more complex multi-user detection approach defined by (6.25), as proposed in [38].

## 6.5 Extension to Systems with 2-Dimensional Spreading

The work in the previous sections can also be applied to SS-OFDM systems with 2-dimensional spreading. A data symbol can be spread by spreading gains of $L_f$ and $L_m$ in frequency and time respectively, which results in a total spreading gain of $L_f L_m = L$ for the entire data symbol. Spreading in either dimension is achieved with Walsh sequences. In an SS-OFDM system with 2-dimensional spreading each data symbol is spread in frequency over $L_f$ subcarriers, and also spread in time over $L_m$ SS-OFDM symbols. As each SS-OFDM transmission has a time duration of $T_{sym}$ and a cyclic prefix of $T_g$, the total duration of a spread data symbol using 2-dimensional spreading is $(T_{sym} + T_g)L_m$, with a main-lobe bandwidth of $(L_f + 1)/T_{sym}$.

While it is possible to consider successive despreading by first equalizing and despreading in one dimension followed by the other, it is more effective to equalize and despread in both dimensions jointly. Extending the work from the previous sections, chip-level MR combining of $T$ diversity replicas and MMSE equalization in two dimensions are achieved by using the equalization coefficient:

$$g_{l,m,t} = \frac{h^*_{l,m,t}}{\sum_{t=0}^{T-1} \left| h_{l,m,t} \right|^2 + \lambda} \tag{6.30}$$

where $m = [0,1,2,\ldots,L_m - 1]$, $f = [0,1,2,\ldots,L_f - 1]$, $h_{l,m,t}$ is the channel gain of the $l^{th}$ subcarrier and the $m^{th}$ SS-OFDM symbol in the time dimension of spreading for the $t^{th}$ diversity replica. $1/\lambda$ represents the average $E_s / N_0$ of the entire 2-dimensionally spread data symbol.

If the system is partially loaded such that $K_f K_m = K < L = L_f L_m$, proper detection is achieved by applying the multi-user MMSE equalization and detection in a manner similar to that defined by (6.25). The 2-dimensionally spread system is simplified by viewing the spreading matrix as a one-dimensional spreading sequence $\mathbf{c}'_k$ of length $L$, comprised of $L_m$ segments, each of length $L_f$. The $l'$ element of the $k^{th}$ spreading sequence is then given by:

$$c'_{k,l'} = c'_{k_f + k_m L_f, l + mL_f} = c_{k_f,l} c_{k_m,m} \tag{6.31}$$

where $l' = [0,1,\ldots,l + mL_f,\ldots,L-1]$, $k = [0,1,\ldots,k + k_m L_f,\ldots,K-1]$, $c_{k,l}$ is the element at the $l^{th}$ row and $k^{th}$ column of the Walsh-Hadamard matrix. Modifying Equation (6.25),

the analogous equalization and despreading matrix for proper multi-user detection and MMSE equalization for a system with 2-dimensional spreading can be given by:

$$\mathbf{G}'' = \mathbf{C}'\mathbf{H}'^{*}[\mathbf{H}'\mathbf{C}'\mathbf{A}\mathbf{C}'^{T}\mathbf{H}'^{*} + \mathbf{I}(N_0 / E_s)]^{-1} \tag{6.32}$$

where $\mathbf{H}'$ is an $LxL$ diagonal matrix with elements $h_{l',l'} = h_{l'}$, $\mathbf{C}' = [\mathbf{c}'_0,\ldots,\mathbf{c}'_k,\ldots\mathbf{c}'_{L-1}]$ is the spreading matrix with columns equal to the $L$ spreading sequences, and $\mathbf{I}$ is the identity matrix. As in Section 6.4.1, the matrix $\mathbf{A}$ is a diagonal matrix with elements $a_{k,k} = 1$ if the $k^{th}$ spreading sequence is in use, and zero otherwise.

As in Section 6.4, complex multi-user detection defined by (6.32) can be achieved through a simpler method for the cases where $K / L = 2^{-r}$, and $r$ is a positive integer. For this method it is more convenient to examine each dimension separately. If the loading in the frequency domain is $K_f / L_f = 1/2$, then the first $K_f$ subcarriers can be treated as replicas of the next $K_f$ subcarriers, regardless of the loading in the time domain. Hence, partially loading such that $K_f / L_f = 2^{-r_f}$ in the frequency domain can be seen as combining $2^{r_f}$ replicas, regardless of the loading in the time domain. Clearly, it follows that partially loading such that $K_m / L_m = 2^{-r_m}$ in the time domain can be seen as the combining of $2^{r_m}$ replicas, regardless of the loading in the frequency domain. The coefficient for proper MMSE equalization and detection with 2-dimensional spreading and partial loading equal to $K / L = K_m K_f / (L_m L_f) = 2^{-r}$ is given by:

$$g_{l,m} = \frac{h^{*}_{l,m}}{\sum_{\omega=0}^{L_m/K_m-1}\sum_{\upsilon=0}^{L_f/K_f-1}\left|h_{l+\upsilon K_f,m+\omega K_m}\right|^2 + \lambda L_m L_f/(K_m K_f)} \tag{6.33}$$

and for partial loading and $T_p$ diversity replicas, the equalization coefficient becomes:

$$g_{l,m,t} = \frac{h^{*}_{l,m,t}}{\sum_{t=0}^{T_p-1}\sum_{\omega=0}^{L_m/K_m-1}\sum_{\upsilon=0}^{L_f/K_f-1}\left|h_{l+\upsilon K_f,m+\omega K_m,t}\right|^2 + \lambda L_m L_f/(K_m K_f)} \tag{6.34}$$

Similarly to what was mentioned in the previous sub-section, (6.33) gives the identical performance to that when using (6.32) for loading conditions of $K = L2^{-r}$. This approach can also be used for any $K \le L2^{-r}$ as an approximate, low complexity, equalization method.

## 6.6 Simulations and Results

Two frequency selective fading channels are considered in this chapter: (a) a channel with independent Rayleigh fading on each subcarrier, and (b) the ITU Pedestrian B channel [43]. The latter naturally implies correlated subcarrier fading. Only the downlink

of an SS-OFDM system is considered. Independent subchannel fading is a reasonable assumption if the channel is sufficiently frequency selective, and if the number of interleaved groups of $L$ subcarriers is much greater than 1 ($M >> 1$), so that chips of a given spreading sequence are much farther apart than the coherence bandwidth.

The case of combining SS-OFDM symbol diversity replicas that have undergone independent frequency selective fading, and the case where the symbol diversity replicas undergo identical frequency selective fading (Table 6.1) are considered. The case of independent fading of diversity replicas is applicable to describe parallel packet replicas resulting from receive antenna diversity, and also multiple serial packet retransmissions in time. In slowly and very slowly fading channels (e.g. pedestrian and nomadic, respectively), the channel may be virtually the same for all serial transmissions of a packet (static channel), in which case it is appropriate to consider identically faded diversity replicas. In this case we assume that a given subcarrier undergoes the same fading for each diversity replica; however, the channel is still frequency selective as the channel gain on each subcarrier within a replica may be different. For the case of serial transmissions of a packet in slowly fading channel, this chapter also considers the use of transmission specific interleaving patterns so that a given chip is transmitted over a different subcarrier within each temporal diversity replica.

Table 6.1. Applicable scenarios of the diversity branch correlation cases considered

| | *Independent fading of replicas* | *Identical fading without interleaving* | *Identical fading with interleaved subchannel gains* |
|---|---|---|---|
| Serial transmission replicas (ARQ) | Fast fading | Slow fading | Slow fading with replica specific interleaving patterns |
| Parallel transmission replicas (antenna diversity) | Sufficient path diversity | No path diversity (correlated fading at receive antennas) | N/A |

### 6.6.1 Performance in an Uncorrelated Rayleigh Channel

The BER for SS-OFDM with independent fading of diversity replicas and independent Rayleigh fading per subchannel with $T$ replicas is shown in Figure 6.3. The spreading sequence length is $L$=1024, and the system is assumed fully loaded ($K$=$L$) for both simulations and analysis. Chip-level combining is significantly better than combining of symbol samples after despreading even with many diversity replicas, particularly at a

low BER. The gain of the chip combining scheme is still significant even with $T$=16 diversity replicas.

Figure 6.3 also demonstrates the excellent agreement of analytical and simulation results when $L$ is large. Figures 6.4 and 6.5 show the accuracy of the analytical solution in comparison to simulated results with $T$=2 and $T$=8 diversity replicas at a BER = $10^{-2}$ with QPSK modulation. Simulations for combining of serial packet diversity replicas in slow fading conditions (identical frequency selective fading for each replica) with diversity replica specific interleaving patterns are also shown. For $T$=2 diversity replicas, the simulated results approach the analytical ones as the spreading gain $L$ is increased. This occurs because increasing $L$ increases the frequency diversity in the simulated system, and as $L$ increases, the frequency diversity approaches the infinite frequency diversity assumed in the analysis. The simulated results for independently fading diversity replicas are within 0.3 dB of the analytical ones for all values of $L$ with $T = 8$ replicas as the diversity is sufficient even at low $L$ due to a large number of replicas. It can be noted that the performance of symbol-level combining with independent fading per diversity branch and $T = 8$ diversity replicas is better than the analytical result for small $L$. This is because the value of the ratio $(K-1)/L$ is small, resulting in lower inter-code (or self) interference. For symbol combining with identical frequency selective fading for each diversity replica and replica specific interleaving patterns, the performance is poor for low $L$ as the interleaved repetitions add little diversity at the chip level.

At $L = 8$ (Figure 6.5) the simulation results for symbol-level combining of identically faded replicas (static channel) with replica specific interleaving are better than the analytical ones. This is because there is no inter-code interference due to loss of orthogonality of spreading sequences in the simulation model for this case. From the second term of equation (6.11) it can be shown that the inter-code interference is related to the variance of the weighted equalized subchannel gains, $\alpha_t \sum_{l=0}^{L-1} h_{l,t} g_{l,t}$ over all $T$ replicas. The average subchannel gain, $\alpha_t$, is the same for each replica $t$ for the static channel, regardless of $L$. Each chip is transmitted over each of the $L = 8$ subcarriers once (a different subcarrier for each of the $T = 8$ diversity replicas) resulting in the same equalized subchannel gain for all chips of the spreading sequence, and hence there is no inter-code interference for the $L = T = 8$ case. This is not accounted for by the analytical model, which assumes all replicas are independently faded, and therefore also assumes inter-code interference is present. For $L = 2$ and $L = 4$, the frequency diversity

is very limited so the performance is significantly worse than the analytical. For $L$ =16 and $L$=32, inter-code interference is introduced again and the results tend toward the analytical with increasing $L$.

Increasing the number of combined replicas $T$ to infinity reduces the inter-code interference in either the symbol-level or chip-level combining system to zero. Chip-level combining results in a larger reduction of inter-code interference for a given number of replicas than symbol-level combining. Figure 6.6 shows that chip-level combining approaches the BER of an ideal $T$-diversity branch system (with no interference) with fewer combined replicas than symbol-level combining. Uncorrelated subcarrier fading and $N = L$ =1024 subcarriers are assumed. The combined SINR of all $T$ replicas is $E_b / N_0$ = 8 dB.

As described in Section 6.4, proper equalization of partially loaded SS-OFDM systems can be achieved by using a method similar to that described for chip-level combining and equalization of diversity replicas for fully loaded systems. The method proposed in Section 6.4 for equalization of partially loaded systems is significantly simpler than the complex multi-user detection scheme presented in [38] and results in the same performance for certain cases of partial loading. Figure 6.7 shows the relative performance of MMSE equalization using the sub-optimal method employing $g_l = h_l^* \Big/ \left( |h_l|^2 + L\lambda / K \right)$ [52] for all values of $K$ as given in Section 2.2.4, the complex multi-user detection method employing equation (6.25) [38], and the approximate method presented in Section 6.4 of this thesis employing (6.27). Uncorrelated subcarrier fading is assumed at an average $E_b / N_0$ = 8 dB. The system has $N$ = 64 subcarriers. As described earlier, the performance of the scheme presented in this chapter is the same as the multi-user method for values of $K / L = 2^{-r}$, and gives reasonable performance for other values of $K$. This approximate method is particularly effective for $K < L/2$. The greatest relative performance losses in comparison to the multi-user method are for the system loads $K = L2^{-r} + 1$.

Analytical expressions for the BER of a SS-OFDM system with partial loading given by $K / L = 2^{-r}$ are also presented in Section 6.4. It can be noted that the accuracy of the representation for the analytical BER found by using (6.29) in (6.10) with $T_p$ = 1 (partially loaded system with no diversity), can be evaluated from Figures 6.4 and 6.5 if $T$ is replaced by $L$ / $K$.

### 6.6.2 Performance in the ITU Pedestrian B Channel

In general, the results of symbol combining and chip combining assuming independent Rayleigh fading for each subchannel (i.e. uncorrelated subchannels) are somewhat optimistic for typical cellular applications. The performance of the chip-level and symbol-level combining are compared in the ITU Pedestrian B channel [43] with $T$=2 and $T$=8 diversity replicas (Figure 6.8). An SS-OFDM system with $N$=$L$=512 subcarriers is considered, with a symbol duration of $T_{sym}$ = 108.032 μs and a cyclic prefix of $T_g$ = 4 μs, which is longer than the maximum excess delay of the channel. The additional 0.16 dB of energy needed for the cyclic prefix has been omitted from the curves to facilitate comparison to the previous results of the more abstract case of independent subcarrier fading. It can be noted that the curves for independently faded transmission replicas are further to the right (poorer performance) from those in Figure 3. Maximal ratio chip combining followed by MMSE equalization outperforms symbol combining at a BER of $10^{-4}$ by 0.3 dB, 1.8 dB, and 1.9 dB with $T$ = 2, and 2.9 dB, 0.8 dB, and 2.0 dB with $T$ = 8, for identical frequency selective fading of diversity replicas without interleaving, identical fading with diversity replica specific subcarrier interleaving, and independent fading of diversity replicas, respectively.

### 6.6.3 Turbo Coded Packets

As the relative performance difference of the two combining schemes differs at different operating SINRs, it is useful to consider turbo-coded packets. The turbo code parameters are identical to those described in Chapter 4 (see Appendix B.1.1 for further details). Figures 6.9 and 6.10 show the packet error rates (PER) for the two combining methods assuming independent subcarrier fading with $N$ = 1024 subcarriers, turbo code rates of 1/3 and 1/2, a packet size of 1024 bits, and 16 QAM modulation. The combining of $T$ = 2 and $T$ = 8 diversity replicas is considered. It is assumed that a packet is transmitted as an SS-OFDM symbol or set of symbols, during which the channel is virtually constant. The chip-combining scheme outperforms symbol combining by up to 1.3 dB.

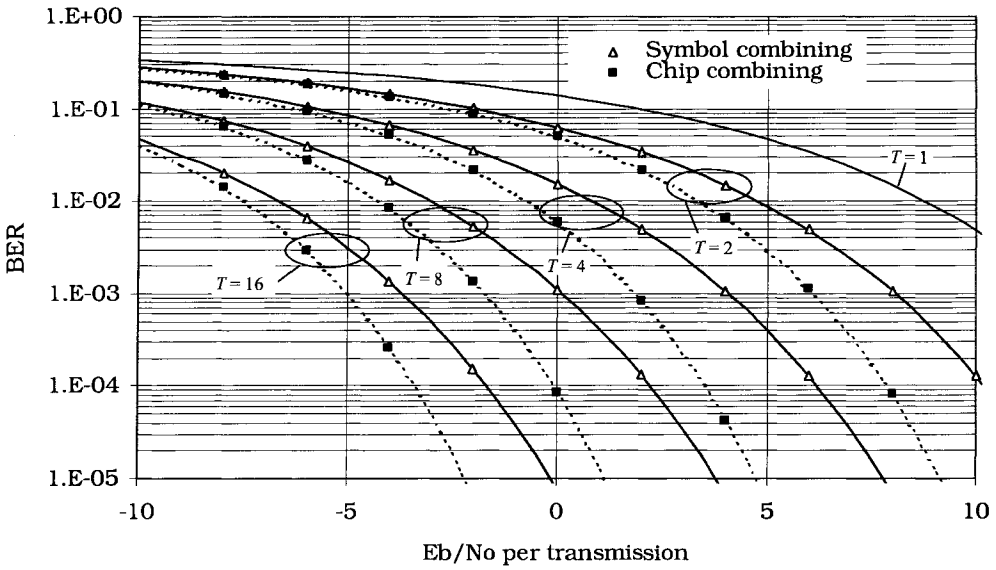


Figure 6.3. BER of SS-OFDM with $T$ diversity replicas. Points are from simulations, solid lines are from equations (6.12)-(6.17) and dashed lines are from equations (6.19)-(6.24). $L = 1024$, and uncorrelated Rayleigh subcarrier fading are assumed.

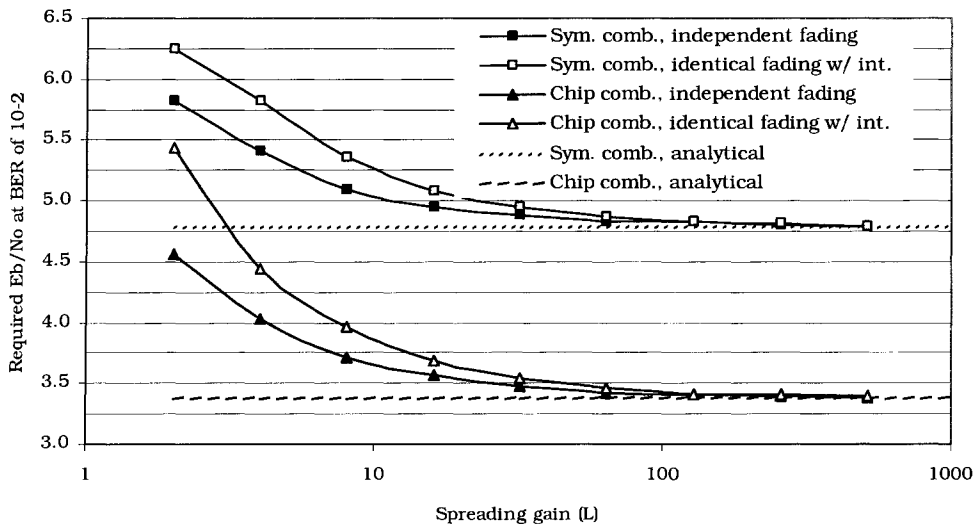


Figure 6.4. Required SINR of the combining options with $T$=2 independent Rayleigh fading diversity replicas, and identically fading serial retransmissions with subcarrier interleaving. Analytical results shown for comparison assume $N$=$L$=1024, and uncorrelated Rayleigh subcarrier fading.

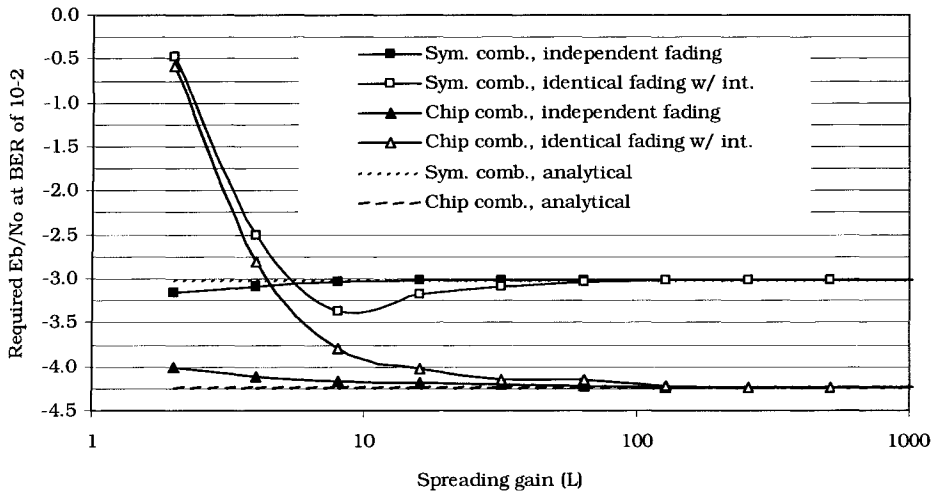


Figure 6.5. Required SINR of the combining options with $T$=8 diversity replicas. Analytical results shown for comparison assume $N$=$L$=1024, and uncorrelated Rayleigh subcarrier fading.

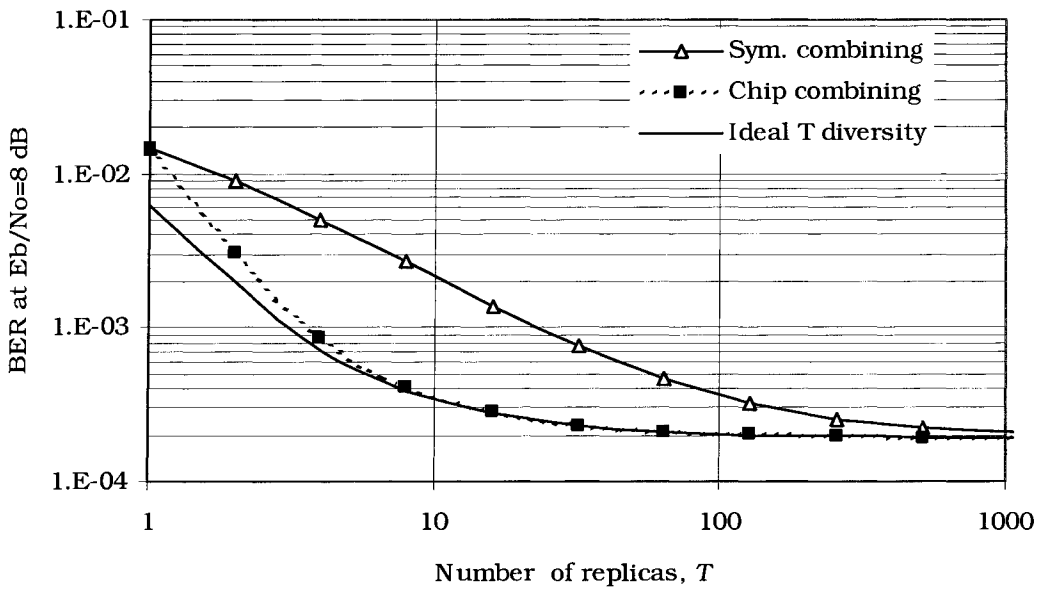


Figure 6.6. BER of chip-level and symbol-level combining compared to an ideal $T$-diversity branch system. $N$=$L$=1024, and uncorrelated Rayleigh subcarrier fading are assumed.

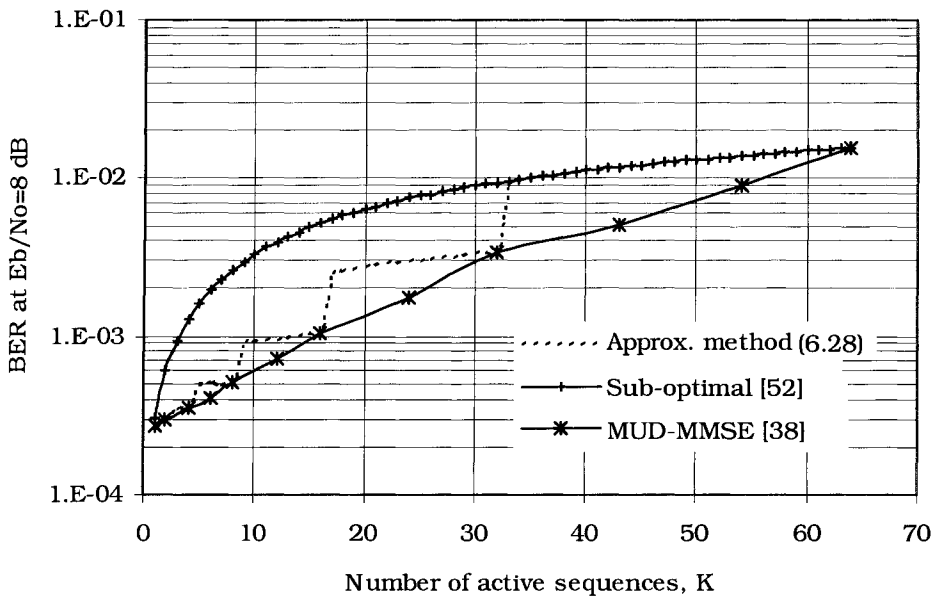


Figure 6.7. BER of the sub-optimal and optimal multi-user detection (MUD) MMSE methods, compared to the method presented in this chapter in Section 6.4.2. $L = 64$, and uncorrelated Rayleigh subcarrier fading are assumed.

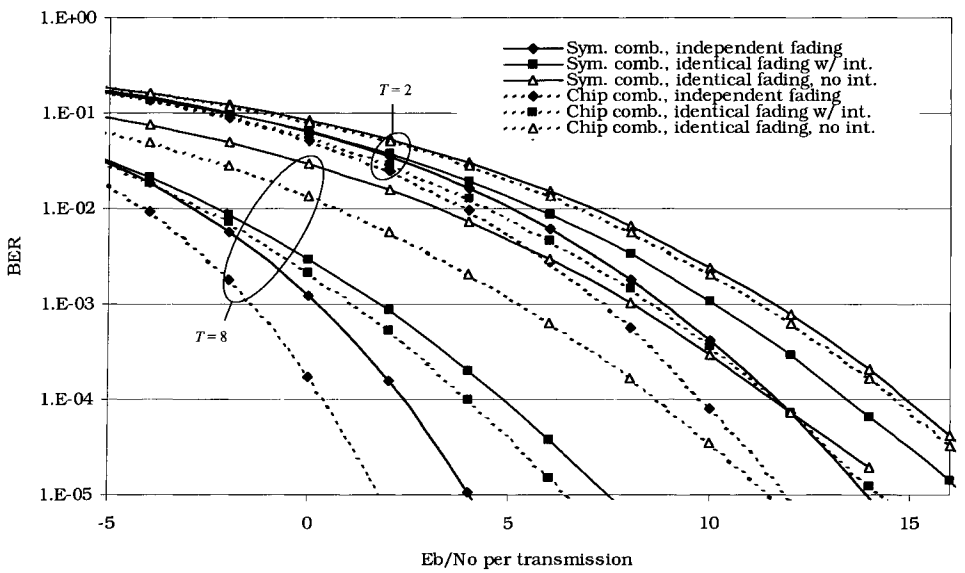


Figure 6.8. BER of the SS-OFDM with $T = 2$ and $T = 8$ diversity replicas for the ITU Pedestrian B channel.

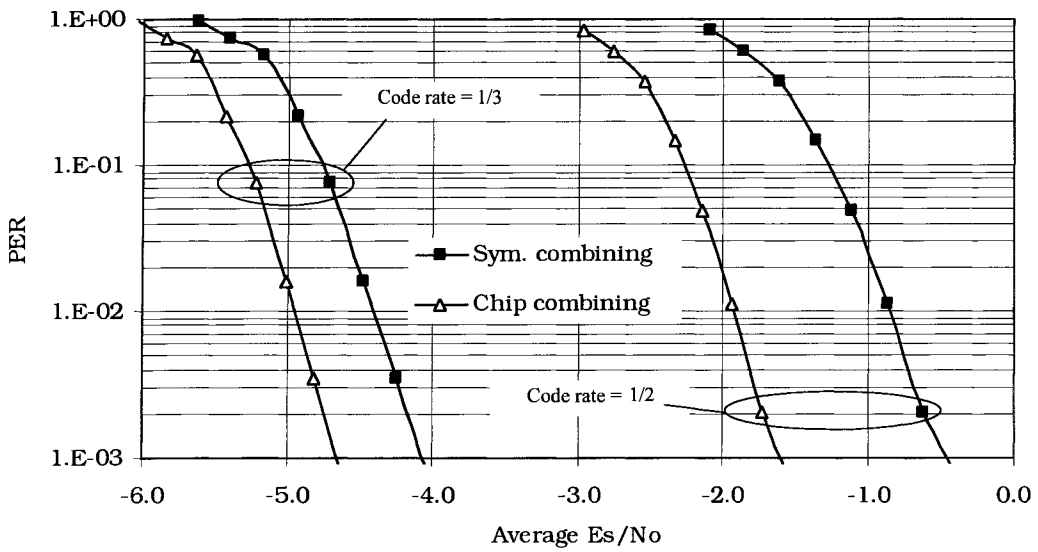


Figure 6.9. Performance with turbo coded packets for $T = 8$ diversity replicas. $L$=1024, and uncorrelated Rayleigh subcarrier fading are assumed.

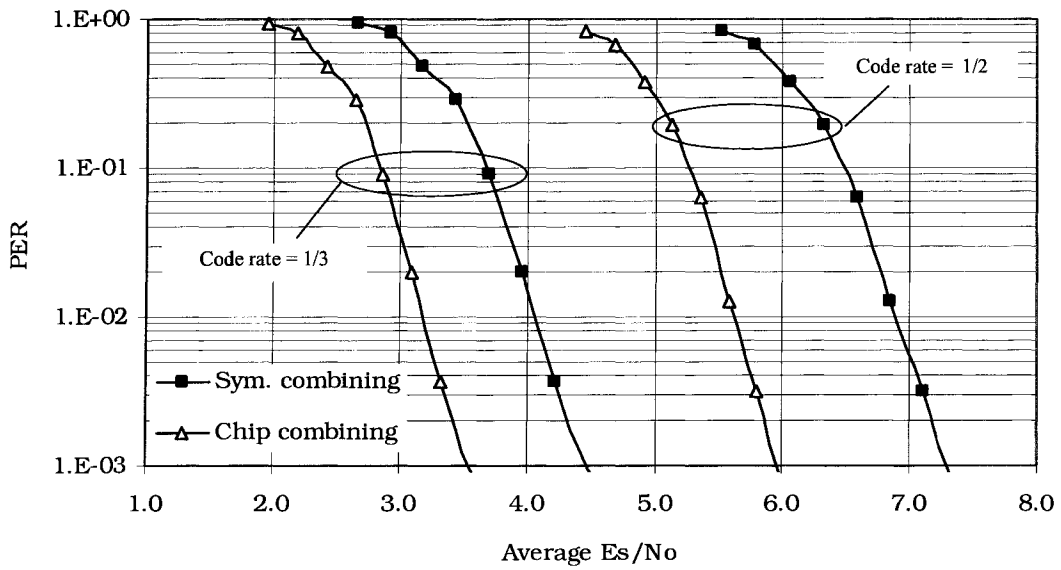


Figure 6.10. Performance with turbo coded packets for $T = 2$ diversity replicas. $L$=1024, and uncorrelated Rayleigh subcarrier fading are assumed.

# Chapter 7

# Conclusions and Future Work

## 7.1 Conclusions

The purpose of this thesis project was to investigate the design of spread spectrum (SS) OFDM systems for the downlink of high throughput cellular data networks. A location dependent radio resource allocation scheme was proposed for conventional SS-OFDM systems. A new SS-OFDM-F/TA cellular packet data system with two-dimensional radio resource allocation was presented, along with adaptive features such as adaptive formation and allocation of groups of disjoint sub-bands and asynchronous re-transmission schemes. Combining schemes for SS-OFDM systems in frequency selective channels were examined, and low-complexity MMSE equalization method was proposed. This section briefly discusses some contributions of this thesis, as well as some of the major findings of the research.

The research in this thesis is very relevant to future wireless cellular systems. As an example of the importance of the research contained in Chapter 4 and 5, many research groups [16][36][44][93][98] including an R&D department of a major cellular systems operator have proposed systems with significant similarities to this work *after* the SS-OFDM-F/TA system proposal in 2001 [74]. In addition, a recent publication proposed a location dependent radio resource allocation scheme for a multi-carrier system [119] with similarities to the system proposed in Chapter 3. The research in Chapter 6 that was first conceived in 2000 [72] but not published until 2005 [79], is also of great importance as other papers which investigated related ideas in 2000 [38], 2002 [64][68], and 2005 [83] failed to arrive at the significant formulations and conclusions developed in this thesis work.

The significance of the topic, namely high throughput SS-OFDM cellular systems, was outlined in Chapter 1. It is envisaged that future mobile cellular systems will employ

multi-carrier transmission due to the features of adaptability, scalability, and inter-symbol interference free communication in multipath channels. The research in this thesis is intended to aid in the development of these next-generation high data rate systems. The basic elements of the downlink of an SS-OFDM system were discussed in Chapter 2. It was shown that the performance advantage of using SS-OFDM systems is most prominent in multipath channels of full system load, and relatively high SNRs.

Chapter 3 presented the inter-cell interference models, and investigated conventional SS-OFDM cellular performance, and proposed a new radio resource allocation method. The interference was shown for synchronous and asynchronous arrivals of interfering transmissions over a frequency selective fading channel. The small-scale fading inter-cell interference models used in this thesis, namely: explicit simulation of ICI components and a composite ICI model were discussed. In the latter, the composite ICI from all sources is modelled a by a single white Gaussian process, where as in the former, each ICI component is explicitly simulated and hence, the short-term ICI is different for different subcarriers due to the effects of the frequency selective channel and also change in time due to small-scale fading. Time dependent (due to mobile motion) large-scale fading effects are applied in both cases. The investigation into SS-OFDM performance indicated an extreme difficulty in transmitting to users near the cell boundary. The cause for this difficultly specific to SS-OFDM systems is lack of an established soft-handoff mechanism and susceptibility to large inter-code interference due to loss of orthogonality of spreading codes. The location dependent rate assignment allocation scheme was a partial remedy to increasing throughput in cell while serving distant users. The system proposed allocating greater resources to users near the transmitter, where transmission conditions are generally more favourable, and limiting the amount of radio resources allocated to distant users. This scheme increases the overall throughput of a cell by allowing many additional transmissions to users relatively near the base station in comparison to traditional equal resource allocation schemes. These additional transmissions require very little of the cell's total transmit power, and hence, the inter-cell and intra-cell interference is virtually unchanged.

The results of Chapter 3 were significant in showing that best effort systems could improve the cellular throughput of SS-OFDM using a type of best-effort resource allocation. Among the shortcomings of the scheme was that it was not restrictive enough in limiting the amount of power used to transmit information to distant users. This was partially because of the very short delay constraint of the circuit switched data. In addition, the system did not incorporate a realistic solution for soft hand-off for users

near the cell boundary. Both of these issues were resolved in the design of the allocation method of SS-OFDM-F/TA discussed in Chapters 4 and 5.

The SS-OFDM-F/TA system considers packet data, which is generally assumed to be somewhat delay-tolerant. Scheduling of users such that only a subset of users receive transmission in any given time slot is a major system improvement as it allows transmitting to distant users only when the channel conditions are favourable. Transmissions to all users in all time slots are of equal power, and hence the desired condition of more equitable power distribution among users of Chapter 3 is assured. In addition, hand-off concerns are alleviated by best serving sector/cell selection. This scheme allows the mobile to periodically ensure that it is receiving transmissions from the most suitable sector/cell antenna. Packet data facilitates this "hard" hand-off method as selection can be done between packet transmissions.

The two-dimensional allocation scheme for the SS-OFDM-F/TA system is presented in Chapter 4. The scheme divides the time-frequency plane into rectangles, and allocates the rectangles to the user with the most favourable channel conditions. In this thesis, proportionally fair scheduling of users is used to govern the allocation process, and hence, a sub-band in a given time slot (which represents the time-frequency rectangle) is allocated to the user with the best channel conditions compared to its average channel conditions. This allocation process is different from previous proposals as radio resources are allocated in both dimensions based on channel conditions, and hence, not every user receives transmission in each time slot nor is any provision made to ensure the minimum data rate of the user with poorest conditions. As the allocation is based on small-scale fading conditions and not on large-scale conditions such as path loss and shadowing, each user is equally likely to be selected by the scheduler over a window that is much longer than the average fade duration of the channel.

The system achieves its objectives by exploiting the adaptability of multi-carrier system to make use of multi-user and frequency diversity, while also maintaining reasonable complexity and allowing for use of spread spectrum techniques and packet data. The sub-bands are chosen narrow enough so that further sub-division would not significantly increase the throughput of the system. Allocation of these sub-bands in time and frequency exploits the multi-user and frequency diversity of the channel. In addition, the grouping of subcarriers into sub-bands significantly reduces the amount of allocation decisions and the feedback of channel state information on the uplink. Spread spectrum can also be used across a given sub-band with minimal performance loss due to inter-code interference, as the subcarrier channel gains within a sub-band are significantly

correlated. The creation of sub-bands facilitates packet data transmission, and the use of spreading across the sub-bands ensures a reliable estimate of the SIR of packet transmissions (provided the estimate is not seriously out-dated), as each code channel within the same sub-band has the same SIR. Adaptive modulation through SIR estimate based packet format selection, and type II hybrid ARQ allow for proper bit loading of each sub-band according the channel conditions. Uniform power allocation across the sub-bands is used to simplify the system, while as noted in Chapter 4 in the presence of multiple users, complex power allocation methods do not improve the system performance significantly. Uniform power allocation also increases the reliability of the SIR estimations in each sub-band by the mobile as the interference power from other cells varies only due to fading, and not due to power allocation or control.

In order to accommodate packets of reasonable size, the allocation of disjoint groups of sub-bands is proposed in Chapter 4. The packet is spread across the group of disjoint sub-bands. It is shown that the SIR across the group of disjoint sub-bands can be accurately estimated from the individual sub-band SIRs. Proper estimation of the sub-band group SIR is important for packet format selection. The optimal allocation algorithm for the formation and allocation of the groups of sub-bands would involve searching through every combination of sub-bands for each user, and then choosing the combinations for transmission in a proportionally fair manner. The computational requirements of this method would be unacceptable, and hence a simple and effective method of formation and allocation is proposed and used. The allocation of disjoint sub-bands significantly increases the sector throughput in highly frequency selective channels.

Vehicular channels are characterized by frequency selective fading and relatively high mobile speeds, which together require narrow sub-bands and short time slot durations. In Chapter 4, the use of disjoint sub-bands is compared to using small packet sizes in terms of throughput, delays and overhead. In highly frequency selective channels, reducing the packet sizes increases the throughput as the system can employ narrower sub-bands. However, using this configuration in a channel where such narrow sub-bands are not needed leads to unnecessary performance loss due to small packet sizes (i.e., loss in turbo coding performance). The sub-band grouping method is shown to be more versatile by producing throughputs the same as or better than for smaller packet size configurations, and not incurring a performance loss when narrow sub-bands are required. The advantage of small packet sizes is decreased packet delay due to a greater number of effective parallel channels in the system; however, the trade-off is an increase in relative

overhead per time slot (over all sub-bands) on the downlink. The allocation of disjoint dub-bands does not require significantly more signalling on the downlink, however the reverse signalling is increased as the SIR of each sub-band must be transmitted to the base station.

Chapter 5 investigates some improvements and performance considerations of the SS-OFDM-F/TA system. A new set of 4 packet formats is used, each of which use shorter packet transmissions sizes and fewer re-transmissions than the IS-856 system to reduce delays. The sub-band size is unchanged as it was determined that it is suitable for 3 out of the 4 channels to be investigated, and the sub-band grouping method proposed in Chapter 4 would adequately exploit the multi-user diversity in the last channel.

In Chapter 5, several asynchronous re-transmission algorithms have been proposed in this thesis. Asynchronous re-transmissions ensure that multi-user diversity is being exploited for each transmission. Asynchronous re-transmission of packets was originally proposed in [19] in a limited sense for a single carrier system. The re-transmission algorithms considered in this work consider many different cases. The improvement of asynchronous re-transmission through parallel allocation of sub-band/packet re-transmission pairs is also proposed. It is found that the minimum delay, absolute re-transmit priority with parallel allocation (MD-ARP-PA) algorithm provides the most favourable delay and throughput performance. Asynchronous re-transmission with a constrained maximum RTI increases the overall throughput of the system by significantly increasing throughput to users with "average" conditions in the cell in comparison to synchronous schemes. This throughput increase is gained while also limiting the packet delays to nearly those of synchronous systems.

As mentioned earlier, no constraints are placed on the minimum data rate per user of the system. The minimum data rate in the system is determined by the average channel conditions of the 'worst' user. It was shown in Section 4.4 that severe shadowing parameters assumed result in poor performance for users with very poor channel conditions. Fast sector selection with a reasonable selection interval of 1 second is proposed to prevent users from enduring very poor channel conditions for extended periods. It is shown in Section 5.3 that fast sector selection increases throughput of the system, increases throughput fairness among users by benefiting the users with the poorest channel conditions, reduces overall packet delays, and significantly reduces packet delays for the poorest users.

The last 3 sections of chapter 5 consider larger modulation constellations, the effect of quantization on SIR feedback, and adaptive termination and code-division

multiplexing (CDM) of packet transmissions. As expected, addition of packet structures using 64 QAM improved the overall sector throughput of the system. However, only users with generally good channel conditions benefited. It is shown that exploiting multi-user diversity is possible with only coarse SIR feedback to the transmitter for radio resource allocation. It was also shown that the adaptive formation and allocation described in Section 4.5 also function with only quantized SIR estimates. The use of adaptive termination and CDM of an additional packet transmission showed that small increases in throughputs to users with very poor channel conditions were possible, however, the total average throughput of the sector was not greatly affected.

In Chapter 6, the chip-level and symbol-level approaches to combining several diversity replicas of an SS-OFDM signal were compared. Diversity replicas arising from antenna diversity or in an ARQ scheme were considered. Novel analytical expressions for the BER have been developed and discussed for diversity combining before and after despreading. These expressions can also be used for partially loaded systems. The results indicate that combining chips prior to equalization and despreading can provide significant gains in comparison to combining equalized symbols. The performance gain due to chip-level combining over symbol-level combining is primarily due to increased reduction of inter-code interference during the combining and equalization processes. The diversity combining scheme considered here is applicable to traditional SS-OFDM schemes in frequency selective fading environments such as those discussed in Chapter 3, or to best-effort systems when the channel estimates are too unreliable for proper sub-band scheduling, and subcarrier interleaving must be used (see Section 4.7, Configuration VII).

A novel low-complexity MMSE equalization scheme for partially loaded systems has also been presented. The low-complexity equalization scheme produces optimal results when the system loading is a power of ½. For these cases, the analytical expressions for the BER of SS-OFDM with partial loading and optimal MMSE equalization can be shown to be variants of the expressions developed for chip-level diversity combining. For other cases of loading, the proposed low-complexity is the same as or significantly better than for other sub-optimal schemes. The application of this scheme to systems with spreading in 2-dimensions is also discussed.

## 7.2 Future Work

The purpose of the SS-OFDM-F/TA system is to provide an innovative multi-carrier solution for 4G wireless cellular systems and beyond. The system utilizes several modern

techniques, but clearly the use of multiple antenna schemes for 4G applications would improve system throughput. Multiple-input multiple-output (MIMO) antenna systems are expected to be a significant part of future best-effort wireless networks as recent work has suggested significant gains in possible throughputs [33]. MIMO systems for high throughput applications are expected to implement a spatial multiplexing approach in order to increase throughput, rather than space-time transmit diversity methods that improve reliability. Given the demonstration of multi-user diversity gain for OFDM-based systems in this thesis, multi-user MIMO-OFDM methods can be expected to achieve significantly higher gains. Of critical concern to this topic are appropriate scheduling algorithms and the form of fed back channel state information to the transmitter. In both cases, there is a need for effective solutions, given the criteria of high throughput with some concept of fairness among users, which address the concerns of complexity and imperfections in system implementation (such as the presence of ISI, etc.). A discussion of multi-user scheduling for MIMO systems in single carrier systems useful for high throughput data systems can be found in [66]. Many early MIMO techniques assumed perfect knowledge of the channel state information at the transmitter in order to achieve significant throughput gains [33], however implementation is unlikely, particularly in the case of OFDM-systems that require CSI from each subcarrier or sub-band. Systems that consider partial CSI feedback have been proposed, such as [67][68] (and references listed therein) which also include sub-optimal methods in order to limit complexity. This also leads to the question of how much multi-user diversity and MIMO gain can be exploited with only a minimal amount of CSI feedback.

Another line of research that is important to this topic is the combining of multiple packet transmissions at the receiver. In Chapter 6, it was shown that inter-code interference can be significantly mitigated by chip-level combining, and proper MMSE equalization of an SS-OFDM system. It should be noted that this technique can be used in any scheme where orthogonal codes are disturbed by different channel gains per chip. In addition this technique can be combined with optimal symbol mapping techniques for multiple transmissions as shown in [92], along with the papers listed in its references. These are important methods as they maximize the diversity gained from the reception of multiple packet replicas, which are common in systems using ARQ schemes similar to that described in this thesis.

# Bibliography


[1] S. Abeta, H. Atarashi, M. Sawahashi, "Forward link capacity of coherent DS-CDMA and MC-CDMA broadband packet wireless access in a multi-cell environment", in *Proceedings of the IEEE Vehicular Technology Conference (VTC 2000 -Fall)*, Boston, MA, October 2000, pp. 2213-2218.

[2] S. Ariyavisitakul, L. F. Chung, "Signal and interference statistics of a CDMA system with feedback power control", *IEEE Transactions on Communications*, vol. 41, no. 11, pp. 1626-1634, November 1993.

[3] B. Arnold, N. Balakrishnan, and M.N. Nagaraja, "*A First Course in Order Statistics*", Wiley, New York, N.Y., 1992.

[4] H. Atarashi, M. Sawahashi, "Variable spreading factor orthogonal frequency and code division multiplexing (VSF-OFCDM)" in *Proceedings of the 3rd International Workshop on Multi-Carrier Spread-Spectrum (MCSS 2001)*, Oberpfaffenhofen, Germany, September 2001, pp. 113-122.

[5] J.-M. Auffray, J.-Y. Baudais, J.-F. Hélard, "STBC MC-CDMA systems: comparison of MMSE single-user and multi-user detection schemes over Rayleigh and MIMO METRA channels", *European Transactions on Telecommunications*, vol. 15, no. 5, pp. 275-281, May-June 2004.

[6] P. Bender, P. Black, M. Grob, R. Padovani, N. Sindhushayana, A. Viterbi, "CDMA/HDR: A bandwidth efficient high speed data service for nomadic users", *IEEE Communications Magazine*, pp. 70-77, July 2000.

[7] J. A. C. Bingham, "Multicarrier modulation for data transmission: an idea whose time has come", *IEEE Communications Magazine*, pp. 5-14, May 1990.

[8] R. Böhnke, R. Stirling-Gallacher, S. Izumi, "BDMA – band division multiple access", the *3rd ACTS Summit,* Rhodes, Greece, June 1998, pp. 467-472.

[9] R. W. Chang, "Synthesis of band-limited orthogonal signals for multichannel data transmission", *Bell Systems Technology Journal*, vol. 45, pp. 1775-1796, December 1966.

[10] R. W. Chang and R. A. Gibby, "A theoretical study of performance of an orthogonal multiplexing data transmission scheme", *IEEE Transactions on Communications Technology,* vol. Com-16, no. 4, pp. 529-540, August 1968.

[11] P. S. Chow, J. M. Cioffi, J. A. C. Bingham, "A practical discrete multitone transceiver loading algorithm for data transmission over spectrally shaped

channels", *IEEE Transactions on Communications,* vol. 43, no. 2/3/4, pp. 773-775, February/March/April 1995.

[12] J. S. Chow, J. C. Tu, and J. M. Cioffi, "A discrete multitone transceiver system for HDSL applications", *IEEE Journal on Selected Areas in Communications,* vol. 9, no. 6, pp. 895-908, August 1991.

[13] J. Chuang *et al*, "High speed wireless data access based on combining EDGE with wideband OFDM", *IEEE Communications Magazine*, pp. 92-98, November 1999.

[14] J. Chuang, N. Sollenberger, "Beyond 3G: wideband wireless data access based on OFDM and dynamic packet assignment", *IEEE Communications Magazine*, pp. 78-87, July 2000.

[15] S. T. Chung, A. Goldsmith, "Adaptive multicarrier modulation for wireless systems", in *Proceedings of the Thirty-Fourth Asilomar Conference on Signals, Systems and Computers*, vol. 2, October 2000, pp. 1603-1607.

[16] B. Classon, P. Sartori, V. Nangia, X. Zhuang, K. Baum, " Multi-dimensional adaptation and multi-user scheduling techniques for wireless OFDM systems", in *Proceedings of the International Conference on Communications (ICC'03)*, Anchorage, Alaska, May 2003, pp. 2251-2255.

[17] E. Costa, H. Haas, E. Shulz, " Optimization of capacity assignment in MC-CDMA transmission systems", in *Proceedings of the 3rd Intl. Workshop on Multi-Carrier Spread-Spectrum (MCSS 2001)*, Oberpfaffenhofen, Germany, September 2001, pp. 217-224.

[18] A. Czylwik, "Comparison between adaptive OFDM and single carrier modulation with frequency domain equalization", in *Proceedings of the IEEE Vehicular Technology Conference (VTC 1997)*, Phoenix, Arizona, May 1997, pp. 865-869.

[19] A. Das, F. Khan, and S. Nanda, "A2IR: an asynchronous and adaptive hybrid ARQ scheme for 3G evolution", in *Proceedings of the IEEE Vehicular Technology Conference (VTC 2001-Spring)*, Rhodes, Greece, May 2001, pp. 628-632.

[20] A. Das, F. Khan, A. Sampath, and H. J. Su," Adaptive, asynchronous incremental redundancy with fixed transmission time intervals (TTI) for HDSPA", in *Proceedings of the International Symposium on Personal, Indoor and Mobile Radio Communications (PIMRC'2002)*, Lisbon, Portugal, September 2002, pp. 1083-1087.

[21] V. M. DaSilva and E. S. Sousa, "Performance of orthogonal CDMA codes for quasi-synchronous communication systems", in *Proceedings of International Conference on Universal Personal Communication (ICUPC'93)*, Ottawa, Canada, October 1993, pp. 995-999.

[22] M. L. Doelz, E. T. Heald, and D. L. Martin, "Binary data transmission techniques for linear systems," in *Proceedings of Institute of Radio Engineers (IRE),* vol. 45, pp. 656-661, May 1957.

[23] R. Elliott, *Scheduling Algorithms for High Throughput Packet Data Service in Cellular Radio Systems*, M.Sc. Thesis, Department of Electrical and Computer Engineering, University of Alberta, Edmonton, AB., Fall 2003.

[24] *Universal Mobile Telecommunications System (UMTS); Selection Procedures for the Choice of Radio Transmission Technologies of the UMTS*, European Telecommunications Standards Institute (ETSI), TR 101 112 v3.2.0, April 1998.

[25] *HIPERLAN Type 2 Functional Specification Part 1 - Physical Layer*, European Telecommunications Standards Institute (ETSI), DTS/BRAN 030003-1, June 1999.

[26] *Digital Video Broadcasting (DVB): Framing Structure, Channel Coding and Modulation for Digital Terrestrial Television*, European Telecommunications Standards Institute (ETSI), EN 300 744 v1.2.1, July 1999.

[27] *Radio Broadcasting Systems: Digital Audio Broadcasting (DAB) to Mobile, Portable and Fixed Receivers*, European Telecommunications Standards Institute (ETSI), EN 300 401 v1.3.3, May 2001.

[28] K. Fazel, "Performance of CDMA/OFDM for mobile communication system", in *Proceedings of International Conference on Universal Personal Communication (ICUPC'93),* Ottawa, Canada, October 1993, pp. 975-979.

[29] K. Fazel, S. Kaiser, *Multi-Carrier and Spread Spectrum Systems*, London. Wiley, 2003.

[30] K. Fazel and L. Papke, "On the performance of convolutionally-coded CDMA/OFDM for mobile communication system", in *Proceedings of the International Symposium on Personal, Indoor and Mobile Radio Communications (PIMRC 1993),* Yokohama, Japan, December 1993, pp. 468-472.

[31] M-H. Fong, Q. Wang, and V. K. Bhargava, "Concatenated orthogonal/PN codes for DS-CDMA systems in a multi-user and multipath fading environment", in *Proceedings of Globecom 1994*, San Francisco, CA, November 1994, pp. 1642-1646.

[32] R.G. Gallagher, *Information Theory and Reliable Communication*, Wiley, New York, NY., 1968.

[33] A. Goldsmith, S. A. Jafar, N.Jindal, S. Vishwanath, "Capacity limits of MIMO channels", *IEEE Journal on Selected Areas of Communications*, vol. 21, no. 5, pp. 684-702, June 2003.

[34] R. Grünheid and H. Rohling, "Adaptive modulation and multiple access for the OFDM transmission technique", *Wireless Personal Communications,* vol. 13, No. 1, pp. 5-13, May 2000.

[35] M. Gudmundson, "Correlation model for shadow fading in mobile radio systems," *Electronics Letters*, vol. 27, No. 23, pp. 2145-2146, November 7, 1991.

[36] Z.–H. Han, Y.–H. Lee, "Opportunistic scheduling with partial channel information in OFDMA/FDD systems", in *Proceedings of the Vehicular Technology Conference (VTC'04-Fall)*, Los Angeles, CA, USA, September 2004, pp. 511-514.

[37] S. Hara, R. Prasad, "Overview of multicarrier CDMA", *IEEE Communications Magazine*, pp. 126-133, December 1997.

[38] J.-F. Hélard, J.-Y. Baudais, J. Citerne, "Linear MMSE detection techniques for MC-CDMA", *Electronics Letters*, vol. 36, no. 7, pp. 665-666, March 2000.

[39] J. M. Holtzman, "CDMA forward link waterfilling power control", in *Proceedings of the Vehicular Technology Conference (VTC2000-Spring)*, Toyko, Japan, May 2000, pp. 1663-1667.

[40] *Telecommunications and Information Exchange Between Systems - LAN/MAN Specific Requirements - Part 11: Wireless MAC and PHY Specifications, High Speed Physical Layer in the 5 GHz Band*, Supplement to IEEE Standard for Information Technology 802.11a, 1999.

[41] *Telecommunications and Information Exchange Between Systems - LAM/MAN Specific Requirements - Part 11: Wireless MAC and PHY Specifications, Amendment 4: Further Higher Data Rate Extension in the 2.4 GHz Band*, IEEE Standard for Information Technology 802.11g, June 2003.

[42] *Initial Contribution on a System Meeting MBWA Characteristics*, IEEE 802.20 Mobile Broadband Wireless Access (MBWA) Contribution, C802.20-03/16, March 2003.

[43] *Guidelines for Evaluation of Radio Transmission Technologies for IMT-2000, International Telecommunication Union*, ITU-R M.1225, Geneva, 1997.

[44] J. Jang, K. B. Lee, "Transmit power adaptation for multiuser OFDM systems", *IEEE Journal on Selected Areas in Communications,* vol. 21, no. 2, pp. 171-178, February 2003.

[45] Y. Jou, "Developments in third generation (3G) CDMA technology", in *Proceedings of the International Symposium on Spread Spectrum Techniques an Applications (ISSSTA 2000)*, Newark, NJ, September 2000, pp. 460-464.

[46] P. Jung, F. Berens, and J. Plechinger, "Joint detection for multi-carrier CDMA mobile radio systems – part 1: system model", in *Proceedings of the International Symposium on Spread Spectrum Techniques an Applications (ISSSTA 1996)*, Mainz, Germany, September 1996, pp. 991-995.

[47] P. Jung, F. Berens, and J. Plechinger, "Joint detection for multi-carrier CDMA mobile radio systems – part 2: detection techniques", in *Proceedings of the International Symposium on Spread Spectrum Techniques an Applications (ISSSTA 1996)*, Mainz, Germany, September 1996, pp. 996-1000.

[48] S. Kaiser, "MC-FDMA and MC-TDMA versus MC-CDMA and SS-MC-MA: performance evaluation for fading channels", in *Proceedings of the International Symposium on Spread Spectrum Techniques an Applications (ISSSTA 1998)*, Sun City, South Africa, September 1998, pp. 115-120.

[49] S. Kaiser, "OFDM-CDMA versus DS-CDMA: performance evaluation for fading channels", in *Proceedings on the International Conference on Communications (ICC'95)*, Seattle, Washington, June 1995, pp. 1722-1726.

[50] S. Kaiser, "On the performance of different detection techniques for OFDM-CDMA in fading channels", in *Proceedings of Globecom 1995*, Singapore, November 1995, pp. 2059-2063.

[51] S. Kaiser, "Trade-off between channel coding and spreading in multi-carrier CDMA systems", in *Proceedings of the International Symposium on Spread Spectrum Techniques an Applications (ISSSTA 1996)*, Mainz, Germany, September 1996, pp. 1366-1370.

[52] S. Kaiser, *Multi-carrier CDMA Mobile Radio Systems - Analysis and Optimization of Detection, Decoding, and Channel Estimation.* Dusseldorf: VDI-Verlag, Fortschrittberichte VDI, series 10, no. 531, 1998, Ph.D. thesis.

[53] S. Kaiser, J. Hagenauer, "Multi-carrier CDMA with iterative decoding and soft-interference cancellation", in *Proceedings of Globecom 1997*, Phoenix, AZ, November 1997, pp. 6-10.

[54] S. Kaiser, L. Papke, "Optimal detection when combining OFDM-CDMA with convolutional and turbo channel coding", in *Proceedings of the International Conference on Communications (ICC'96)*, Dallas, TX., June 1996, pp. 343-348.

[55] I. Kalet, "The multitone channel", *IEEE Transactions on Communications*, vol. 37, no. 2, pp. 119-124, February 1989.

[56] T. Keller, L. Hanzo, "Adaptive orthogonal frequency division multiplexing schemes", in *Proceedings of the ACTS Summit 1998,* Rhodes, Greece, June 1998, pp. 794-799.

[57] T. Keller, L. Hanzo, "Adaptive multicarrier modulation: a convenient framework for frequency-time processing in wireless communications", *IEEE Proceedings*, pp. 611-640, May 2000.

[58] T. Keller, L. Hanzo, "Adaptive modulation techniques for duplex OFDM transmission", *IEEE Transactions on Vehicular Technology,* vol. 49, no. 5, pp. 1893-1906, September 2000.

[59] R. Knopp, P.A. Humblet, "Information capacity and power control in single-cell multiuser communications", in *Proceedings on the International Conference on Communications (ICC'95),* Seattle, WA., June 1995, pp. 331-335.

[60] S. Kondo, L. B. Milstein, "On the use of multicarrier direct sequence spread spectrum systems" in *Proceedings of IEEE Milcom 1993,* Boston, MA, October 1993, pp. 52-56.

[61] S. Kondo, L. B. Milstein, "Performance of multicarrier DS CDMA systems", *IEEE Transactions on Communications,* vol. 44, no. 2, pp. 238-246, February 1996.

[62] Alberto Leon-Garcia, *Probability & Random Processes for Electrical Engineering,* 2nd edition, Addison Wesley 1994.

[63] Y. Li, N. R. Sollenberger, "Clustered OFDM with channel estimation for high rate wireless data", *IEEE Transactions on Communications*, vol. 49, no. 12, pp. 2071-2076, December 2001.

[64] N. Maeda, H. Atarashi, S. Abeta, M. Sawahashi, "Antenna diversity reception appropriate for MMSE combining in frequency domain for forward link OFCDM packet wireless access", in *Proceedings of the International Symposium on Spread Spectrum Techniques and Applications (ISSSTA 2002)*, Prague, Czech Republic, September 2002, pp. 363 – 367.

[65] J. J. Maxey, R. F. Ormondroyd, "Non-coherent differential encoded multi-carrier SS modulation schemes using low-rate orthogonal convolutional coding in frequency selective Rayleigh fading", in *Proceedings of the Vehicular Technology Conference (VTC'97),* Phoenix, Arizona, May 1997, pp. 2045-2049.

[66] D. Mazzarese, *High Throughput Wireless Downlink Packet Data Access with Multiple Antennas and Multi User Diversity*, Ph.D. Thesis, Department of Electrical and Computer Engineering, University of Alberta, Edmonton, AB., Fall 2005.

[67] B. Mielczarek, W. A. Krzymień, "Throughput of realistic multi-user MIMO-OFDM systems", in *Proceedings of the International Symposium on Spread Spectrum techniques and Applications (ISSSTA 2004)*, Sydney, Australia, August-September 2004, pp. 434-438.

[68] B. Mielczarek, W. A. Krzymień, "Flexible channel quantization in multiple antenna systems", in *Proceedings of the IEEE Vehicular Technology Conference (VTC 2005 - Spring)*, Stockholm, Sweden, May-June 2005, pp. 620-624.

[69] A. Morimoto, S. Abeta, M. Sawahashi, "Cell selection based on shadowing variation for forward link broadband OFCDM packet wireless access", in *Proceedings of the Vehicular Technology Conference (VTC'02-Fall)*, Vancouver, B.C., Canada, September 2002, pp. 2071-2075.

[70] K. Miyoshi, A. Matsumoto, C. Wengerter, M. Kasapidis, M. Uesugi, O. Kato, "Constellation rearrangement and spreading code rearrangement for Hybrid ARQ in MC-CDMA", in *Proceedings of Wireless Personal Multimedia Communications (WPMC'02)*, Honolulu, HI., October 2002, pp. 668-672.

[71] S. Nobilet, J.-F. Helard, D. Mottier, "Spreading Sequences Selection for Uplink and Downlink MC-CDMA Systems", in *Proceedings of the 3rd International Workshop on Multi-Carrier Spread-Spectrum (MCSS 2001)*, Oberpfaffenhofen, Germany, September 2001, pp. 123-130.

[72] R. Novak, "Soft-Combining for OFDM-CDMA systems with H-ARQ II", *internal TRLabs memorandum*, October 2000.

[73] R. Novak, W. A. Krzymień, "A cellular multi-service OFDM-CDMA system with spatially-dependent rate assignment", in *Proceedings of Wireless 2000*, Calgary, AB, July 2000, pp. 448-459.

[74] R. Novak, W. A. Krzymień, "A downlink SS-OFDM-F/TA packet data system employing multi-user diversity", in *Proceedings of the 3rd International Workshop on Multi-Carrier Spread-Spectrum (MCSS 2001)*, Oberpfaffenhofen, Germany, September 2001, pp. 181-190.

[75] R. Novak, W. A. Krzymień, "An adaptive downlink spread spectrum OFDM packet data system with two-dimensional radio resource allocation: performance in low-mobility environments", in *Proceedings of Wireless Personal Multimedia Communications (WPMC'02)*, Honolulu, HI, October 2002, pp. 163-167.

[76] R. Novak, W. A. Krzymień, "SS-OFDM-F/TA system packet size and structure for high mobility cellular environments", in *Proceedings of the Vehicular Technology Conference (VTC'03-Spring)*, Jeju, Korea, April 2003, pp. 1438-1444.

[77] R. Novak, W.A. Krzymień, "Packet re-transmission options for the SS-OFDM-F/TA system", in *Proceedings of the 4rd International Workshop on Multi-Carrier Spread-Spectrum (MCSS 2003)*, Oberpfaffenhofen, Germany, September 2003, pp. 89-100.

[78] R. Novak, W. A. Krzymień, "Efficient packet data service in a spread spectrum OFDM cellular system with 2-dimensional radio resource allocation", *European Transactions on Telecommunications*, vol. 15, no. 5, pp. 185-199, May-June 2004.

[79] R. Novak, W. A. Krzymień, "Diversity combining options for spread spectrum OFDM systems in frequency selective channels", in *Proceedings of Wireless Communications and Networking Conference (WCNC'05),* New Orleans, LA, USA, March 2005, pp. 308-314.

[80] R. Novak, W. A. Krzymień, "Diversity combining options and low-complexity MMSE equalization for spread spectrum OFDM systems in frequency selective channels", submitted to *Wireless Personal Communications*, July 2005.

[81] T. Ojanpera J. Skold, J. Castro, L. Girard, A. Klein, "Comparison of multiple access schemes for UMTS", in *Proceedings of the Vehicular Technology Conference (VTC'97),* Phoenix, Arizona, May 1997, pp. 490-494.

[82] S. Parkvall, E. Dahlman, P. Frenger, P. Beming, M. Persson, "The evolution of WCDMA towards higher speed downlink packet access", in *Proceedings of the Vehicular Technology Conference (VTC 2001-Spring)*, Rhodes, Greece, May 2001, pp. 2287-2291.

[83] X. Peng, F. P. S. Chin, A. S. Madhukumar, "Performance studies of a VSF-OFCDM system using a symbol relocated scheme during retransmission", in *Proceedings of Wireless Communications and Networking Conference (WCNC'05),* New Orleans, LA, USA, March 2005, pp. 1138-1143.

[84] J. G. Proakis, *Digital Communications*, McGraw-Hill, New York, NY, 1995.

[85] T. S. Rappaport, *Wireless Communications: Principles and Practice*, 2nd Edition, Prentice Hall, Upper Saddle River, New Jersey, 2002.

[86] C. H. Rentel, W. A. Krzymień, B. Darian, V. Vanghi, R. Elliott, "Comparative forward link traffic channel performance evaluation of HDR and 1xTREME systems", in *Proceedings of the Vehicular Technology Conference (VTC'2002-Spring)*, Birmingham, AL, May 2002, pp. 160-164.

[87] W. Rhee, J. M. Cioffi, "Increase in capacity of multiuser OFDM system using dynamic subchannel allocation", in *Proceedings of the Vehicular Technology Conference (VTC'00-Spring)*, Tokyo, Japan, May 2000, pp. 1085-1089.

[88] H. Rohling, R. Grünheid, "Performance of an OFDM-TDMA mobile communication system", in *Proceedings of the Vehicular Technology Conference (VTC'96),* Atlanta, Georgia, April-May 1996, pp. 1589-1593.

[89] H. Rohling, R. Grünheid, "Performance comparison of different multiple access schemes for the downlink of an OFDM communication system", in *Proceedings of the Vehicular Technology Conference (VTC'97),* Phoenix, Arizona, May 1997, pp. 1365-1368.

[90] A. Ruiz, J. M. Cioffi, S. Kasturia, "Discrete multiple tone modulation with coset coding for the spectrally shaped channel", *IEEE Transactions on Communications,* vol. 40, no. 6, pp. 1012-1029, June 1992.

[91] B. R. Saltzberg, " Performance of an efficient parallel data transmission system", *IEEE Transactions on Communications Technology,* vol. com-15, no. 6, pp. 805-811, December 1967.

[92] H. Samara, Z. Ding, P. M. Hahn, "Symbol mapping diversity design for multiple packet transmissions", *IEEE Transactions on Communications,* vol. 53, no. 5, pp. 810-817, May 2005.

[93] M. Sawahashi, "Broadband packet wireless access beyond IMT-2000", in *Proceedings of IEEE Symposium on Advances in Wireless Communications (ISWC'02)*, Victoria, B.C., September 22-24, 2002, pp. 111-112.

[94] S. Seo, T. Dohi, F. Adachi, "SIR-based transmit power control of reverse link for coherent DS-CDMA mobile radio", *IEICE Transactions on Communications*, vol. E81-B, no. 7, pp. 1508-1516, July 1998.

[95] E. Sourour, M. Nakagawa, "Performance of orthogonal multi-carrier CDMA in nonfading and nonselective fading channels", in *Proceedings of the International Symposium on Spread Spectrum Techniques and Applications (ISSSTA 1994),* Oulu, Finland, July 1994, pp. 203-207.

[96] R. A. Stirling-Gallacher, G. J. R. Povey, "Different coding strategies for OFDM-CDMA", in *Proceedings of the Vehicular Technology Conference (VTC'97),* Phoenix, AZ, May 1997, pp. 845-849.

[97] H.-J. Su, E. Geraniotis, "Power allocation and control for multicarrier systems with soft decoding", *IEEE Journal on Selected Areas in Communications,* vol. 17, no. 10, pp. 1759-1769, October 1999.

[98] A. Svensson, A. Ahlen, A. Brunstrom, T. Ottosson, M. Sternad, "An OFDM Based System Proposal for 4G Downlinks", in *Proceedings of the 4$^{rd}$ Intl. Workshop on*

*Multi-Carrier Spread-Spectrum (MCSS 2003)*, Oberpfaffenhofen, Germany, September 2003.

[99] *Interim Standard: Mobile Station Base Station Compatibility Standard for Dual-Mode Wideband Spread Spectrum Cellular System*, Telecommunications Industry Association, TIA/EIA/IS-95-B, Arlington, VA, November 1995.

[100] *cdma2000 High Speed Packet Data Air Interface Specification*, Telecommunications Industry Association, TIA/EIA/IS-856, Arlington, VA, November 2000.

[101] *Physical Layer Standard for cdma2000 Spread Spectrum Systems,* Telecommunications Industry Association, TIA-IS-2000.2-D, Arlington, VA, March 2004.

[102] L. Tomba, W. A. Krzymień, "Downlink detection schemes for MC-CDMA systems in indoor environments", *IEICE Transactions on Communications,* vol. E79-B, no. 9, pp. 1351-1360, September 1996.

[103] A. Toskala, J. Castro, L. Chalard, S. Hamalainen, K. Kalliojarvi, "Cellular OFDM/CDMA downlink performance in the link and system levels", in *Proceedings of the Vehicular Technology Conference (VTC'97),* Phoenix, Arizona, May 1997, pp. 855-859.

[104] D. N. C. Tse, "Optimal power allocation over parallel Gaussian broadcast channels", in *Proceedings of the International Symposium of Information Theory (ISIT'97)*, Ulm, Germany, June 1997, p. 27.

[105] R. van Nee *et al*, "New high-rate wireless LAN standards", *IEEE Communications Magazine*, pp. 82-88, December 1999.

[106] L. Vandendorpe, "Multitone spread spectrum multiple access communications system in a multipath rician fading channel", *IEEE Transactions on Vehicular Technology* , vol. 44, no. 2, pp. 327-357, May 1995.

[107] P. Viswanath, D. N. C. Tse, R. Laroia, "Opportunistic beamforming using dumb antennas", *IEEE Transactions Information Theory*, vol. 48, no. 6, pp. 1277-1294, June 2002.

[108] A. J. Viterbi, "Very low rate convolutional codes for maximum theoretical performance of spread-spectrum multiple-access channels", *IEEE Journal on Selected Areas in Communications*, vol. 8, no. 4, pp. 641-649, May 1990.

[109] A. J. Viterbi, *CDMA; Principles of Spread Spectrum*, Addison-Wesley, Reading, Massachusetts, 1995.

[110] A. J. Viterbi, R. Pandovani, "Implications of mobile cellular CDMA", *IEEE Communications Magazine*, pp. 38-41, December 1992.

[111] A. M. Viterbi, A. J. Viterbi, "Erlang capacity of a power controlled CDMA system", *IEEE Journal on Selected Areas in Communications*, vol. 11, no. 6, pp. 892-899, August 1993.

[112] S. B. Weinstein and P. M. Ebert, "Data transmission by frequency-division multiplexing using the discrete Fourier transform", *IEEE Transactions on Communications Technology,* vol. com-19, no. 5, pp. 628-634, October 1971.

[113] S. B. Wicker, *Error Control Systems for Communication and Storage*, Prentice-Hall, New Jersey, 1995.

[114] T. J. Willink, P. H. Wittke, "Optimization and performance evaluation of multicarrier transmission", *IEEE Transaction on Communications*, vol. 43, no. 2, pp. 426-440, March 1997.

[115] C. Y. Wong, R. S. Cheng, K. B. Letaief, R. D. Murch, "Multiuser OFDM with adaptive subcarrier, bit, and power allocation", *IEEE Transactions on Communications,* vol. 17, no. 10, pp. 479-483, October 1999.

[116] N. Yee, J. P. Linnartz, and G. Fettweis, "Multi-carrier CDMA in indoor wireless radio networks", in *Proceedings of the International Symposium on Personal, Indoor and Mobile Radio Communications (PIMRC 1993),* Yokohama, Japan, December 1993, pp. 109-113.

[117] N. Yee, J. P. Linnartz, and G. Fettweis, "Multi-carrier CDMA in indoor wireless radio networks", *IEICE Transactions on Communications,* vol. E77-B, no. 7, pp. 900-904, July 1994.

[118] D. Young, N. C. Beaulieu, "The generation of correlated Rayleigh random variates by inverse discrete Fourier transform", *IEEE Transactions on Communications*, vol. 48, no. 7, pp. 1114-1127, July 2000.

[119] S. Yun, S. Y. Park, Y. Lee, E. Alsusa, C. G. Kang, "Spectrum efficient region-based resource allocation with fractional loading for FH-OFDMA cellular systems", *IEE Electronics Letters*, vol. 41, no. 13, pp. 752-754, June 23, 2005.

[120] Y. J. Zhang, K. B. Letaief, "Multiuser subcarrier and bit allocation along with adaptive cell selection for OFDM transmission", in *Proceeding of the International Conference on Communications (ICC '02)*, New York, NY., USA, April-May 2002, pp. 861-865.

[121] Y. J. Zhang, K. B. Letaief, "Multiuser adaptive subcarrier-and-bit allocation with adaptive cell selection for OFDM systems", *IEEE Transactions on Wireless Communications*, vol. 3, no. 5, pp. 1566-1575, September 2004.

[122] A. M. Zoubir, B. Boahash, "The bootstrap and its application in signal processing", *IEEE Signal Processing Magazine,* vol. 15, no. 1, pp. 56-76, January 1988.

# Appendix A

# Channel Models and Fading Envelope Generation

In Chapters 2 through 6, frequency selective Rayleigh fading and ITU channel models are considered. This appendix briefly gives the essential elements of the 6 ITU channel models used. Appendix A.1.1 presents the discrete path channel models that govern the small-scale fading, and Appendix A.1.2 gives the large scale fading parameters for the 6 channel models. In order to implement these channel models, random variable with specific distribution and correlations must be generated. Appendix A.2 gives the method for generating Rayleigh fading values, while the generation of exponential correlated base station-specific shadowing parameter is shown in Appendix A.3.

## A.1 ITU Recommended Channel Models

### A.1.1 Channel Impulse Response Models

The channel impulse response models used in this thesis are taken directly from ITU recommendations [24][43]. The channel models for the $A$ and $B$ channels for the indoor, pedestrian, and vehicular channels are given in Tables A.1, A.2 and A.3, respectively. The $A$ and $B$ channels are assumed to occur randomly. The $B$ channel generally represents the case of a longer delay spread of the channel. In the indoor channel, the A channel is expected to occur 50% of the time, the B channel 45% of the time, and 5% neither will properly represent the channel. In the pedestrian and vehicular channels, the $A$ and $B$ channels have a 40% and 55% chance of occurring, respectively. The pedestrian and vehicular channels use conventional Doppler spectrums, while a flat Doppler spectrum is used for the indoor channels (see Appendix A.2).

Table A.1. Channel impulse response model for the indoor channels.

| *Path no.* | *Indoor A* | | *Indoor B* | |
|---|---|---|---|---|
| | *Relative delay (ns)* | *Average power (dB)* | *Relative delay (ns)* | *Average power (dB)* |
| 1 | 0 | 0.0 | 0 | 0 |
| 2 | 50 | -3.0 | 100 | -3.6 |
| 3 | 110 | -10.0 | 200 | -7.2 |
| 4 | 170 | -18.0 | 300 | -10.8 |
| 5 | 290 | -26.0 | 500 | -18.0 |
| 6 | 310 | -32.0 | 700 | -25.2 |

Table A.2. Channel impulse response model for the pedestrian channels.

| *Path no.* | *Pedestrian A* | | *Pedestrian B* | |
|---|---|---|---|---|
| | *Relative delay (ns)* | *Average power (dB)* | *Relative delay (ns)* | *Average power (dB)* |
| 1 | 0 | 0.0 | 0 | 0.0 |
| 2 | 110 | -9.7 | 200 | -0.9 |
| 3 | 190 | -19.2 | 800 | -4.9 |
| 4 | 410 | -22.8 | 1200 | -8.0 |
| 5 | | | 2300 | -7.8 |
| 6 | | | 3700 | -23.9 |

Table A.3. Channel impulse response model for the vehicular channels.

| *Path no.* | *Vehicular A* | | *Vehicular B* | |
|---|---|---|---|---|
| | *Relative delay (ns)* | *Average power (dB)* | *Relative delay (ns)* | *Average power (dB)* |
| 1 | 0 | 0.0 | 0 | -2.5 |
| 2 | 310 | -1.0 | 300 | 0.0 |
| 3 | 710 | -9.0 | 8900 | -12.8 |
| 4 | 1090 | -10.0 | 12900 | -10.0 |
| 5 | 1730 | -15.0 | 17100 | -25.2 |
| 6 | 2510 | -20.0 | 20000 | -16.0 |

### A.1.2 Path Loss and Shadowing Models

Channel path loss models and shadowing parameters are given in this section. While the entire path loss model is given for use in cellular systems with AWGN such as in Chapter 3, in general, in interference limited systems the loss at the base station is the same for each cell/sector transmitter, so that only the path loss exponent is significant.

### A.1.2.1 Indoor Channels

The path loss model in the indoor channels is given by:

$$\text{Path Loss (dB)} = 37 + 30\log_{10}(D_{mobile}) \tag{A.1}$$

where $D_{mobile}$ is the distance from the base station to the mobile in metres. This model corresponds to a path loss exponent of $\Upsilon = 3$. The shadowing process is exponential correlated with distance as given in Appendix A.3, and has a standard deviation of $\sigma_{shad} = 12$ dB. The decorrelation distance of the process is 5 metres.

### A.1.2.2 Pedestrian Channels

The path loss model in the pedestrian channels is given by:

$$\text{Path Loss (dB)} = 40\log_{10}(D_{mobile}) + 148 \tag{A.2}$$

at a carrier frequency of 2 GHz. This model corresponds to a path loss exponent of $\Upsilon = 4$. The shadowing process is exponential correlated with distance as given in Appendix A.3, and has a standard deviation of $\sigma_{shad} = 10$ dB. The decorrelation distance of the process is 5 metres.

### A.1.2.3 Vehicular Channels

The path loss model in the pedestrian channels is given by:

$$\text{Path Loss (dB)} = 128.1 + 37.6\log_{10}(D_{mobile}) \tag{A.3}$$

at a carrier frequency of 2 GHz, and with base station antenna heights of 15 m. This model corresponds to a path loss exponent of $\Upsilon = 3.76$. The shadowing process is exponential correlated with distance as given in Appendix A.3, and has a standard deviation of $\sigma_{shad} = 10$ dB. The decorrelation distance of the process is 20 metres.

## A.2 Rayleigh Fading Generation

The Rayleigh fading process with specific correlation properties in this thesis are generated by a modified IDFT method as proposed and outlined in [118]. The complex fading channel gains, whose envelope is Rayleigh distributed, is created by generating 2 identical and independently distributed Gaussian $N_{ray}$-length sequences in the frequency domain. Each sequence is multiplied by a filter sequence $F(k)$, corresponding the desired auto-correlation function of the final variates. The two sequences are summed with one being multiplied by the imaginary factor $-j = -\sqrt{-1}$. The summed sequence is then transformed into the time domain by an $N_{ray}$-point IDFT, producing the complex fading process with the desired distribution and auto-correlation properties.

For the pedestrian and vehicular channels, a classic Doppler spectrum is needed. This is defined by the theoretic power spectrum given is by:

$$S(f) = \begin{cases} \dfrac{1}{\pi f_D \sqrt{1-(f_D/f)^2}} & |f| \le f_D \\ 0 & \text{otherwise} \end{cases} \tag{A.4}$$

where $f$ is the carrier frequency (which is approximately 2 GHz in this thesis), and $f_D$ is the maximum Doppler shift of the channel. Equation (A.4) corresponds to an auto-correlation function of $J_0(2\pi f_D \tau)$, where $J_0$ is zeroth order Bessel function of the first kind, and $\tau$ is the shift in time measured in seconds. The corresponding frequency-domain discrete $N_{ray}$-*point* filter given by:

$$F(k) = \begin{cases} 0 & k = 0 \\ \sqrt{\dfrac{1}{2\sqrt{1-\left(\dfrac{k}{N_{ray} f_D}\right)^2}}} & k = 1, 2, \cdots k_m - 1 \\ \sqrt{\dfrac{k_m}{2}\left[\dfrac{\pi}{2} - \tan^{-1}\left(\dfrac{k_m - 1}{\sqrt{2k_m - 1}}\right)\right]} & k = k_m \\ 0 & k = k_m + 1, \cdots N_{ray} - k_m - 1 \\ \sqrt{\dfrac{k_m}{2}\left[\dfrac{\pi}{2} - \tan^{-1}\left(\dfrac{k_m - 1}{\sqrt{2k_m - 1}}\right)\right]} & k = N_{ray} - k_m \\ \sqrt{\dfrac{1}{2\sqrt{1-\left(\dfrac{N_{ray} - k}{N_{ray} f_D}\right)^2}}} & k = N_{ray} - k_m + 1, \cdots, N_{ray} - 1 \end{cases} \tag{A.5}$$

where $k_m = \left\lfloor f_D \left(\dfrac{N_{ray}}{f_s}\right) \right\rfloor$, $\lfloor x \rfloor$ denotes the largest integer less than $x$, and $f_s$ is the sampling frequency used in the simulation. $k_m$ loosely represents the number of unresolvable paths, at frequency offsets less than the maximum Doppler shift, used to create the fading sequence.

In order to generate fading variates with reliable auto-correlation properties, the value of $k_m$ must be sufficiently large; hence for low Doppler shifts and relatively fast channel sampling requirements very large fading sequence, $N_{ray}$ must be generated. This problem was overcome in the project by generating very long sequences to ensure proper auto-correlation properties, and then using only a small segment for a given simulation run so that working array sizes were reasonable. As an example, in the simulations in Chapter 4, the sampling frequency is the inverse of the time slot duration,

$f_s = 1/(1.7925 \text{ ms})$, and the maximum Doppler frequency was 5 Hz. Even though only 22400 samples are required for the 30-second simulation time plus 10-second initialization time. In the simulations, $N_{ray} = 524288$ length fading sequences were generated. It is important to note that new sequences were generated for every simulation run, every path, and every user. Proper normalization of fading sequences is done after each generation (only over the portion that is to be used), and again over the entire channel response.

An example of the auto-correlation function of the generated variates is given in Figure A.1. The flat Doppler spectrum required for the indoor channels is generated in a similar manner, except that the frequency domain filter has a flat response $k_m$ =1 to $N_{ray}$-1 instead of (A.5).

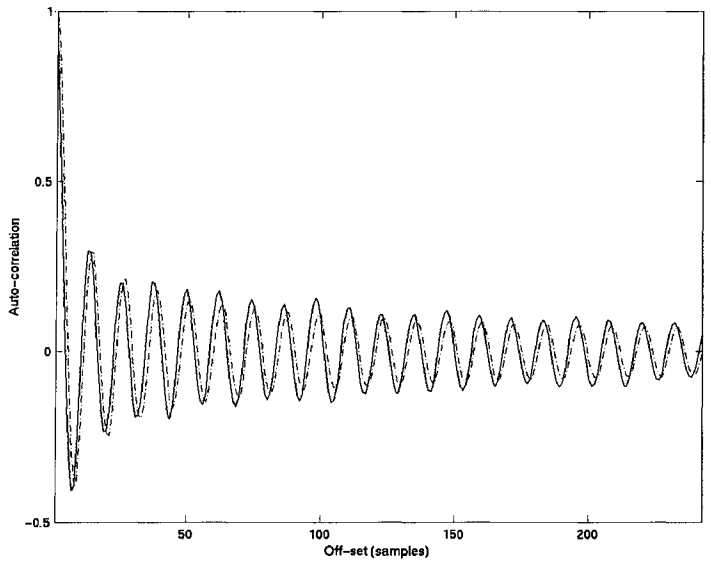


Figure A.1. The auto-correlation function of the generated fading variates (solid line) in comparison to the desired theoretic zeroth order Bessel of the first kind auto-correlation function.

## A.3 Generation of Correlated Shadowing Processes

The distribution of the shadowing processes is log-normal, with standard deviations given in Appendix A.1.2. The auto-correlation function of the shadowing process is exponential with distance according the Gudmundson model [35], and as recommended by the ITU. The auto-correlation is given by:

$$\Gamma(\Delta x) = e^{-\frac{|\Delta x|}{d_{corr}}\ln(2)} \tag{A.6}$$

where $\Delta x$ is the change in mobile position and $d_{corr}$ is the decorrlation distance. The decorrelation distances for the different channel environment are given Appendix A.1.2.

In Chapters 4 and 5 of this thesis, it is also assumed that the cross-correlation of the shadowing processes form different base stations (different cells) is 0.5. Hence, the simulation model requires generating 19 log-normal distributed shadowing processes with a covariance matrix equal to:

$$\mathbf{R} = \sigma_{shad}^2 \begin{bmatrix} 1 & 0.5 & \cdots & 0.5 \\ 0.5 & 1 & \cdots & 0.5 \\ \vdots & \vdots & \ddots & \vdots \\ 0.5 & \cdots & \cdots & 1 \end{bmatrix} \tag{A.7}$$

and with each sequence having an auto-correlation function equal to (A.6). First, 19 log-normal random variable sequences are created. As all values are in dB, the sequence is Gaussian distributed. Each sample of the sequences represents an index in time, corresponding to some sampling time. The sequences are independently filtered in the frequency domain to give the desired auto-correlation function in the time domain. At each sampling time, the values are Gaussian distributed so that the process for generating correlated Gaussian variates given in [62] can be followed. This involves multiplying the column vector of 19 base station shadowing values for a given time index by the 19x19 element matrix $\mathbf{A}_{shad}$, and repeating for each time instant in the sequence. The matrix $\mathbf{A}_{shad}$ is given by:

$$\mathbf{A}_{shad} = \mathbf{P}_{shad}\mathbf{L}_{shad}^{0.5} \tag{A.8}$$

where the columns of $\mathbf{P}_{shad}$ are an orthonormal set of eigenvectors of $\mathbf{R}$, and $\mathbf{L}_{shad}^{0.5}$ is a diagonal matrix with elements equal to the square root of the eigenvalues of $\mathbf{R}$. Clearly, the same matrix $\mathbf{A}_{shad}$ is used for every time index. Finally, the desired sequences are scaled to have the appropriate standard deviations.

After frequency domain filtering, application of $\mathbf{A}_{shad}$ and scaling, the 19 sequences have the desired qualities of auto-correlation and cross-correlation. The auto-correlation functions for several of the 19 sequences generated in a typical simulation are shown in comparison to the function given by (A.6). The covariance matrix of the generated sequences is nearly identical to the covariance matrix given in (A.7). In the simulation the shadowing process is not generated every time slot, and hence, linear interpolation between shadowing sequence samples is used for per time slot samples of the shadowing process. As mentioned for the generation of Rayleigh fading sequences, shadowing sequences significantly longer than needed were generated in order to ensure sequences with reliable auto-correlation.

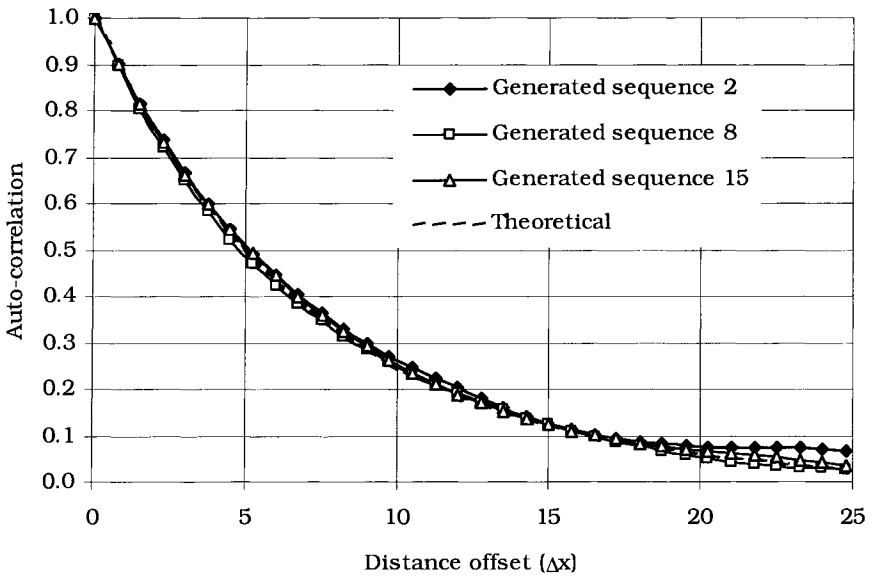


Figure A.2. The auto-correlation functions of 3 generated shadowing processes in comparison the theoretic exponential function. The decorrelation distance is 5 m.

# Appendix B

# Link Level Simulations for SS-OFDM-F/TA Packet Data System Configurations

In the simulations of the SS-OFDM-F/TA packet data system in Chapters 4 and 5, link level results were used extensively in the system level simulation results to produce performance curves in complex cellular environments. The link level simulations consider several turbo coded packet structures in an AWGN environment with appropriate packet structures, turbo coding parameters, and number of re-transmissions of the packet. Slightly different packet structures are used in Chapter 4 than in Chapter 5, so the two chapters are treated separately. Appendix B.1 describes the packet formation and structures for Chapter 4, some of which are the same as those for IS-856 [100], and gives the link level results. Appendix B.2 discusses the assumptions and structures for the packets formats used in Chapter 5, which are based on those suggested for cdma2000 [101], and gives the link level results.

## B.1 Link Level Simulations for Configurations Considered in Chapter 4

### B.1.1 Packet Structures and Coding

In Sections 4.3 through 4.6, packet structures identical to those proposed for IS-856 are used [100]. In Section 4.7, scaled-down versions of these packets are used. As the standard goes into significant detail about the encoding, interleaving, and packet layout, and the process is fairly complex, only a brief summary is given here.

The turbo encoder uses two parallel convolutional encoders, with an interleaver scrambling the data bits prior to entry into the second encoder [100]. Appropriate puncturing patterns are used to generate encoded bit steams of either code rate $r_{turbo} =$ 1/3 or 1/5. In this thesis, rate 1/5 turbo encoding is used for the formats that use a 1024-bit packet size, and rate 1/3 turbo encoding for all others. The last 6 bits of every encoded stream are tail bits appended by the encoder, and hence, the data bits transmitted per packet is *Packet size* – 6 bits. The encoded output is bit scrambled, followed by symbol permuting by a channel interleaver. The encoded chips are then modulated by QPSK, 8 PSK, or 16 QAM modulations.

As mentioned in Section 4.3, the transmission size per sub-band/time slot considered for the majority of Chapter 4 (and given in the IS-856 standard) is 2048 complex symbols, 448 of which are reserved for MAC and pilot signalling. A pre-amble is also considered in the first transmission of each packet format, and hence, less than 1600 complex data symbols are sent in the first transmission. Referencing the packet format set $S_{trans}$= 2048 given in Table 4.4 of Section 4.7, 1024 complex preamble symbols are sent in the first transmission of *Rate* 1, 512 for *Rate* 2, 256 for *Rate* 3, 128 for *Rates* 4 and 6, and 64 for all other rates. Note that the packet structures listed in Table 4.1 are a subset of those listed for the $S_{trans}$= 2048 packet format set given in Table 4.4. A detailed list of the rates for $S_{trans}$= 2048 set is given in Table B.1. The other 2 packet format sets given in Table 4.7 have first-slot preambles that are 4 times and 16 times scaled down versions on those discussed. The preambles are important as they affect the number of bits received after the first transmission, and hence, the ability of the receiver to correctly decode the packet transmission. For the $S_{trans}$=512 and $S_{trans}$=128 packet format sets, the complex symbols per transmission reserved for MAC and plot signalling are also scaled-down to 224 and 112 symbols, respectively.

Finally, it should be noted that the rate 1/2 encoded packets that were used in Section 6.6.3, were achieved be simply using only the first two-thirds of a rate 1/3 encoded packet. The truncation to achieve the rate 1/2 packet is done after symbol permuting [100], and only parity bits are deleted. In Section 6.6.3, no preamble was considered for either the rate 1/3 or rate 1/2 encoded packets.

Table B.1. Details of packet formats considered in Chapter 4.

| *Rate no.* | *No. of transmissions* | *Modulation* | *Code rate (approx.)* | *No. of complete repetitions* | *Data rate (Kb/s/sub-band)* | *Packet size (bits)* | *Preamble (bits)* | *SIR for 1% PER* |
|---|---|---|---|---|---|---|---|---|
| 1 | 16 | QPSK | 1/5 | 9.2 | 35.7 | 1024 | 1024 | -13.5 |
| | 15 | QPSK | 1/5 | 8.6 | 38.1 | 1024 | 1024 | -13.4 |
| | 14 | QPSK | 1/5 | 8.0 | 40.8 | 1024 | 1024 | -13.1 |
| | 13 | QPSK | 1/5 | 7.4 | 43.9 | 1024 | 1024 | -12.8 |
| | 12 | QPSK | 1/5 | 6.8 | 47.6 | 1024 | 1024 | -12.5 |
| | 11 | QPSK | 1/5 | 6.2 | 51.9 | 1024 | 1024 | -12.1 |
| | 10 | QPSK | 1/5 | 5.6 | 57.1 | 1024 | 1024 | -11.7 |
| | 9 | QPSK | 1/5 | 5.0 | 63.5 | 1024 | 1024 | -11.1 |
| | 8 | QPSK | 1/5 | 4.4 | 71.4 | 1024 | 1024 | -10.5 |
| | 7 | QPSK | 1/5 | 3.8 | 81.6 | 1024 | 1024 | -9.9 |
| | 6 | QPSK | 1/5 | 3.2 | 95.2 | 1024 | 1024 | -8.9 |
| | 5 | QPSK | 1/5 | 2.6 | 114.3 | 1024 | 1024 | -8.0 |
| | 4 | QPSK | 1/5 | 2.0 | 142.8 | 1024 | 1024 | -6.9 |
| | 3 | QPSK | 1/5 | 1.4 | 190.4 | 1024 | 1024 | -5.2 |
| | 2 | QPSK | 1/4 | 1.0 | 285.6 | 1024 | 1024 | -2.8 |
| | 1 | QPSK | 1 | 1.0 | 571.3 | 1024 | 1024 | 6.4 |
| 2 | 8 | QPSK | 1/5 | 4.6 | 71.4 | 1024 | 512 | -10.5 |
| | 7 | QPSK | 1/5 | 4.0 | 81.6 | 1024 | 512 | -10.2 |
| | 6 | QPSK | 1/5 | 3.4 | 95.2 | 1024 | 512 | -9.1 |
| | 5 | QPSK | 1/5 | 2.8 | 114.3 | 1024 | 512 | -8.3 |
| | 4 | QPSK | 1/5 | 2.2 | 142.8 | 1024 | 512 | -7.1 |
| | 3 | QPSK | 1/5 | 1.6 | 190.4 | 1024 | 512 | -5.9 |
| | 2 | QPSK | 1/5 | 1.0 | 285.6 | 1024 | 512 | -3.8 |
| | 1 | QPSK | 1/2 | 1.0 | 571.3 | 1024 | 512 | 1.0 |
| 3 | 4 | QPSK | 1/5 | 2.3 | 142.8 | 1024 | 256 | -7.4 |
| | 3 | QPSK | 1/5 | 1.7 | 190.4 | 1024 | 256 | -6.1 |
| | 2 | QPSK | 1/5 | 1.1 | 285.6 | 1024 | 256 | -4.1 |
| | 1 | QPSK | 2/5 | 1.0 | 571.3 | 1024 | 256 | -0.5 |
| 4 | 2 | QPSK | 1/5 | 1.2 | 285.6 | 1024 | 128 | -4.3 |
| | 1 | QPSK | 4/11 | 1.0 | 571.3 | 1024 | 128 | -0.8 |
| 5 | 1 | QPSK | 8/23 | 1.0 | 571.3 | 1024 | 64 | -1.1 |
| 6 | 4 | QPSK | 1/3 | 2.0 | 285.6 | 2048 | 128 | -4.6 |
| | 3 | QPSK | 1/3 | 1.5 | 380.8 | 2048 | 128 | -3.1 |
| | 2 | QPSK | 8/23 | 1.0 | 571.3 | 2048 | 128 | -1.4 |
| | 1 | QPSK | 8/11 | 1.0 | 1142.5 | 2048 | 128 | 3.7 |
| 7 | 2 | QPSK | 16/47 | 1.0 | 571.3 | 2048 | 64 | -1.5 |
| | 1 | QPSK | 16/23 | 1.0 | 1142.5 | 2048 | 64 | 3.4 |
| 8 | 1 | QPSK | 16/23 | 1.0 | 1142.5 | 2048 | 64 | 3.4 |
| 9 | 2 | 8 PSK | 16/47 | 1.0 | 856.9 | 3072 | 64 | 1.5 |
| | 1 | 8 PSK | 16/23 | 1.0 | 1713.8 | 3072 | 64 | 7.1 |
| 10 | 1 | 8 PSK | 16/23 | 1.0 | 1713.8 | 3072 | 64 | 7.1 |
| 11 | 2 | 16 QAM | 16/47 | 1.0 | 1142.5 | 4096 | 64 | 3.3 |
| | 1 | 16 QAM | 16/23 | 1.0 | 2285.1 | 4096 | 64 | 9.1 |
| 12 | 1 | 16 QAM | 16/23 | 1.0 | 2285.1 | 4096 | 64 | 9.1 |

## B.1.2 Link Level Results

The packet structures given in Table 4.4 were simulated in an AWGN channel with proper encoding, interleaving, and preamble and overhead layouts. The packet error rate (PER) curves for each format, and for every possibility of early termination, is simulated. Maximum A Posterori (MAP) turbo decoding is used, and for the cases of multiple re-transmissions, soft-packet combining is considered. Turbo decoding with 8 iterations is implemented in order to ensure effective decoding, without incurring excessive delays. As an example of the trade-off in increased iterations and PER, Figure B.1 shows the PER for *Rate* 7, $S_{trans}$=2048 for up to 20 iterations.

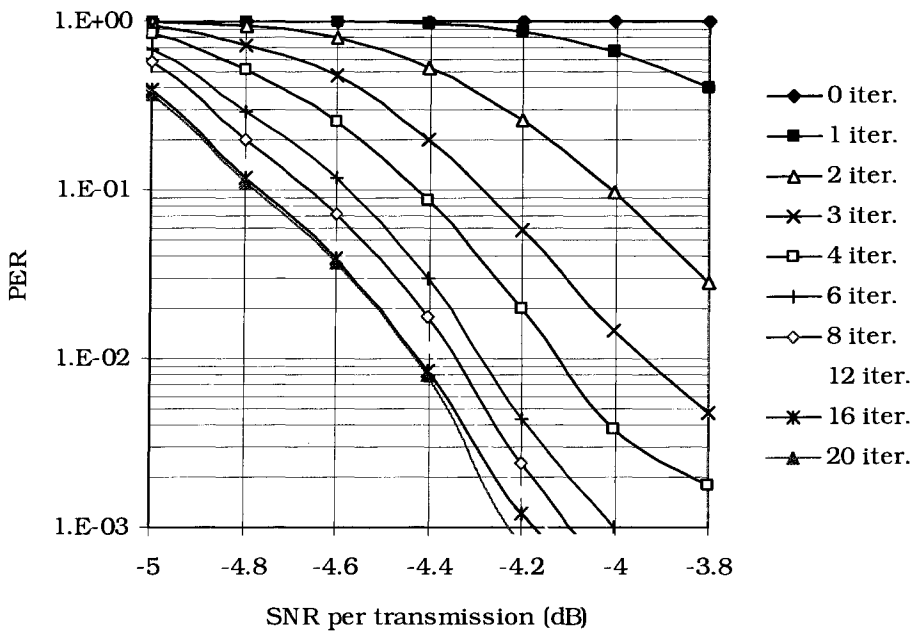


Figure B.1. The PER curves for 2048 bit turbo encoded with 2 transmissions received (1536 symbol first transmission, and 1600 symbol second transmission). 1/3 code rate puncturing pattern. Corresponds to *Rate* 7, $S_{trans}$=2048 on Table 4.4 with 2 slot transmission.

Simply giving the curves for the link level results would require significant space as there are 41 curves per the 3 packet format sets (total of 123) given in Table 4.4. If displayed even on several graphs, the visible resolution would be too low to be useful for future research, and hence, the information has been tabulated in Tables B.2, B.3 and B.4 for ease of reference. *Rates* refer to those listed on Table 4.4. In the system level simulations,

each set of SIR/PER points is appended by a PER of 1.0 (100%) for an SIR that is 0.2 dB lower than the first entry, and a PER of 0 for an SIR that is 0.2 dB greater than the last entry. In order to accurately approximate the PER between link level simulation points for a given SIR, logarithmic interpolation is used (i.e. appears as a straight line on Figure B.1).

Table B.2. Tabulated PER curves for $S_{trans} = 2048$ packet format.

| *Rate* | *Trans.* | | | | | | | | | |
|---|---|---|---|---|---|---|---|---|---|---|
| 1 | 16 | *SIR* | -14.4 | -14.2 | -14.0 | -13.8 | -13.6 | -13.4 | -13.2 | -13.0 | |
| | | *PER* | 0.9839 | 0.6075 | 0.3696 | 0.1229 | 0.0260 | 0.0052 | 0.0012 | 0.0006 | |
| | 15 | *SIR* | -14.2 | -14.0 | -13.8 | -13.6 | -13.4 | -13.2 | -13.0 | -12.8 | -12.6 |
| | | *PER* | 0.9643 | 0.7750 | 0.4819 | 0.2025 | 0.0535 | 0.0092 | 0.0030 | 0.0010 | 0.0002 |
| | 14 | *SIR* | -13.8 | -13.6 | -13.4 | -13.2 | -13.0 | -12.8 | -12.6 | -12.4 | |
| | | *PER* | 0.8841 | 0.6545 | 0.4195 | 0.1242 | 0.0265 | 0.0046 | 0.0008 | 0.0004 | |
| | 13 | *SIR* | -13.6 | -13.4 | -13.2 | -13.0 | -12.8 | -12.6 | -12.4 | -12.2 | -12.0 |
| | | *PER* | 0.9455 | 0.8310 | 0.5714 | 0.2568 | 0.0773 | 0.0142 | 0.0020 | 0.0018 | 0.0002 |
| | 12 | *SIR* | -13.2 | -13.0 | -12.8 | -12.6 | -12.4 | -12.2 | -12.0 | -11.8 | -11.6 |
| | | *PER* | 0.9310 | 0.8611 | 0.5556 | 0.2236 | 0.0659 | 0.0114 | 0.0038 | 0.0008 | 0.0002 |
| | 11 | *SIR* | -12.8 | -12.6 | -12.4 | -12.2 | -12.0 | -11.8 | -11.6 | -11.4 | -11.2 |
| | | *PER* | 0.9167 | 0.7975 | 0.5420 | 0.2112 | 0.0699 | 0.0110 | 0.0020 | 0.0004 | 0.0006 |
| | 10 | *SIR* | -12.4 | -12.2 | -12.0 | -11.8 | -11.6 | -11.4 | -11.2 | -11.0 | -10.8 |
| | | *PER* | 0.9483 | 0.8289 | 0.6471 | 0.2571 | 0.0719 | 0.0202 | 0.0032 | 0.0004 | 0.0006 |
| | 9 | *SIR* | -11.8 | -11.6 | -11.4 | -11.2 | -11.0 | -10.8 | -10.6 | -10.4 | |
| | | *PER* | 0.9322 | 0.7500 | 0.4653 | 0.1657 | 0.0392 | 0.0082 | 0.0020 | 0.0002 | |
| | 8 | *SIR* | -11.4 | -11.2 | -11.0 | -10.8 | -10.6 | -10.4 | -10.2 | -10.0 | -9.8 |
| | | *PER* | 0.9821 | 0.8286 | 0.6731 | 0.3670 | 0.1129 | 0.0254 | 0.0040 | 0.0008 | 0.0006 |
| | 7 | *SIR* | -10.8 | -10.6 | -10.4 | -10.2 | -10.0 | -9.8 | -9.6 | -9.4 | -9.2 |
| | | *PER* | 0.9623 | 0.9836 | 0.7416 | 0.3795 | 0.1479 | 0.0346 | 0.0060 | 0.0024 | 0.0006 |
| | 6 | *SIR* | -9.8 | -9.6 | -9.4 | -9.2 | -9.0 | -8.8 | -8.6 | -8.4 | |
| | | *PER* | 0.8923 | 0.7857 | 0.2847 | 0.1175 | 0.0230 | 0.0046 | 0.0010 | 0.0002 | |
| | 5 | *SIR* | -9.0 | -8.8 | -8.6 | -8.4 | -8.2 | -8.0 | -7.8 | -7.6 | -7.4 |
| | | *PER* | 0.9630 | 0.7470 | 0.5357 | 0.2344 | 0.0511 | 0.0078 | 0.0022 | 0.0002 | 0.0002 |
| | 4 | *SIR* | -7.8 | -7.6 | -7.4 | -7.2 | -7.0 | -6.8 | -6.6 | -6.4 | |
| | | *PER* | 0.9000 | 0.7041 | 0.3633 | 0.1557 | 0.0290 | 0.0054 | 0.0006 | 0.0002 | |
| | 3 | *SIR* | -6.2 | -6.0 | -5.8 | -5.6 | -5.4 | -5.2 | -5.0 | -4.8 | -4.6 |
| | | *PER* | 0.9048 | 0.6837 | 0.3850 | 0.1564 | 0.0270 | 0.0072 | 0.0018 | 0.0006 | 0.0002 |
| | 2 | *SIR* | -3.8 | -3.6 | -3.4 | -3.2 | -3.0 | -2.8 | -2.6 | -2.4 | -2.2 |
| | | *PER* | 0.9091 | 0.6602 | 0.4456 | 0.1466 | 0.0328 | 0.0068 | 0.0014 | 0.0004 | 0.0006 |
| | 1 | *SIR* | 5.5 | 5.7 | 5.9 | 6.1 | 6.3 | 6.5 | 6.7 | 6.9 | 7.1 |
| | | *PER* | 0.9623 | 0.7361 | 0.5000 | 0.2208 | 0.1273 | 0.0509 | 0.0166 | 0.0084 | 0.0032 |
| 2 | 8 | *SIR* | -11.4 | -11.2 | -11.0 | -10.8 | -10.6 | -10.4 | -10.2 | -10.0 | -9.8 |
| | | *PER* | 0.8182 | 0.6701 | 0.3886 | 0.1193 | 0.0268 | 0.0058 | 0.0016 | 0.0004 | 0.0004 |
| | 7 | *SIR* | -10.8 | -10.6 | -10.4 | -10.2 | -10.0 | -9.8 | -9.6 | -9.4 | |
| | | *PER* | 0.8906 | 0.6442 | 0.3692 | 0.1190 | 0.0331 | 0.0050 | 0.0016 | 0.0006 | |
| | 6 | *SIR* | -10.0 | -9.8 | -9.6 | -9.4 | -9.2 | -9.0 | -8.8 | | |
| | | *PER* | 0.8116 | 0.5635 | 0.2396 | 0.0750 | 0.0142 | 0.0042 | 0.0008 | | |
| | 5 | *SIR* | -9.2 | -9.0 | -8.8 | -8.6 | -8.4 | -8.2 | -8.0 | -7.8 | |
| | | *PER* | 0.8592 | 0.5909 | 0.2814 | 0.0833 | 0.0186 | 0.0020 | 0.0014 | 0.0002 | |
| | 4 | *SIR* | -8.2 | -8.0 | -7.8 | -7.6 | -7.4 | -7.2 | -7.0 | -6.8 | |
| | | *PER* | 0.9492 | 0.7816 | 0.3793 | 0.1535 | 0.0361 | 0.0052 | 0.0014 | 0.0004 | |
| | 3 | *SIR* | -6.8 | -6.6 | -6.4 | -6.2 | -6.0 | -5.8 | -5.6 | -5.4 | -5.2 |
| | | *PER* | 0.9231 | 0.6542 | 0.3460 | 0.1535 | 0.0367 | 0.0040 | 0.0032 | 0.0006 | 0.0004 |
| | 2 | *SIR* | -4.8 | -4.6 | -4.4 | -4.2 | -4.0 | -3.8 | -3.6 | -3.4 | -3.2 |
| | | *PER* | 0.8438 | 0.7030 | 0.3724 | 0.1741 | 0.0374 | 0.0078 | 0.0014 | 0.0006 | 0.0002 |
| | 1 | *SIR* | 0.0 | 0.2 | 0.4 | 0.6 | 0.8 | 1.0 | 1.2 | 1.4 | |

| | | | | | | | | | | |
|---|---|---|---|---|---|---|---|---|---|---|
| | | *PER* | 0.9455 | 0.7600 | 0.4177 | 0.1758 | 0.0440 | 0.0094 | 0.0018 | 0.0012 |
| 3 | 4 | *SIR* | -8.2 | -8.0 | -7.8 | -7.6 | -7.4 | -7.2 | -7.0 | -6.8 |
| | | *PER* | 0.6699 | 0.3867 | 0.1583 | 0.0444 | 0.0092 | 0.0020 | 0.0008 | 0.0004 |
| | 3 | *SIR* | -7.0 | -6.8 | -6.6 | -6.4 | -6.2 | -6.0 | -5.8 | -5.6 |
| | | *PER* | 0.8730 | 0.6348 | 0.2943 | 0.0865 | 0.0198 | 0.0024 | 0.0010 | 0.0004 |
| | 2 | *SIR* | -5.0 | -4.8 | -4.6 | -4.4 | -4.2 | -4.0 | -3.8 | -3.6 |
| | | *PER* | 0.8571 | 0.4902 | 0.1875 | 0.0626 | 0.0124 | 0.0034 | 0.0010 | 0.0004 |
| | 1 | *SIR* | -1.2 | -1.0 | -0.8 | -0.6 | -0.4 | -0.2 | 0.0 | 0.2 |
| | | *PER* | 0.8730 | 0.6095 | 0.3807 | 0.1143 | 0.0288 | 0.0054 | 0.0018 | 0.0008 |
| 4 | 2 | *SIR* | -5.2 | -5.0 | -4.8 | -4.6 | -4.4 | -4.2 | -4.0 | |
| | | *PER* | 0.8462 | 0.5809 | 0.1970 | 0.0725 | 0.0180 | 0.0024 | 0.0006 | |
| | 1 | *SIR* | -1.6 | -1.4 | -1.2 | -1.0 | -0.8 | -0.6 | -0.4 | |
| | | *PER* | 0.8406 | 0.5401 | 0.1781 | 0.0481 | 0.0078 | 0.0028 | 0.0014 | |
| 5 | 1 | *SIR* | -2.0 | -1.8 | -1.6 | -1.4 | -1.2 | -1.0 | -0.8 | -0.6 |
| | | *PER* | 0.9077 | 0.6421 | 0.3990 | 0.1447 | 0.0360 | 0.0070 | 0.0024 | 0.0014 |
| 6 | 4 | *SIR* | -5.0 | -4.8 | -4.6 | -4.4 | -4.2 | | | |
| | | *PER* | 0.3495 | 0.0814 | 0.0094 | 0.0020 | 0.0004 | | | |
| | 3 | *SIR* | -3.6 | -3.4 | -3.2 | -3.0 | -2.8 | | | |
| | | *PER* | 0.1254 | 0.0090 | 0.0012 | 0.0010 | 0.0004 | | | |
| | 2 | *SIR* | -2.0 | -1.8 | -1.6 | -1.4 | -1.2 | -1.0 | -0.8 | |
| | | *PER* | 1.0000 | 0.8333 | 0.3852 | 0.0758 | 0.0076 | 0.0008 | 0.0002 | |
| | 1 | *SIR* | 3.0 | 3.2 | 3.4 | 3.6 | 3.8 | 4.0 | 4.2 | 4.4 |
| | | *PER* | 0.8833 | 0.5897 | 0.2640 | 0.0518 | 0.0092 | 0.0030 | 0.0008 | 0.0006 |
| 7 | 2 | *SIR* | -2.0 | -1.8 | -1.6 | -1.4 | -1.2 | -1.0 | | |
| | | *PER* | 0.9254 | 0.6183 | 0.1911 | 0.0234 | 0.0026 | 0.0002 | | |
| 7&8 | 1 | *SIR* | 2.8 | 3.0 | 3.2 | 3.4 | 3.6 | 3.8 | 4.0 | 4.2 |
| | | *PER* | 0.6239 | 0.3012 | 0.0553 | 0.0098 | 0.0030 | 0.0016 | 0.0006 | 0.0004 |
| 9 | 1 | *SIR* | 0.6 | 0.8 | 1.0 | 1.2 | 1.4 | 1.6 | | |
| | | *PER* | 1.0000 | 0.9677 | 0.6929 | 0.2365 | 0.0184 | 0.0004 | | |
| 9&10 | 2 | *SIR* | 6.4 | 6.6 | 6.8 | 7.0 | 7.2 | 7.4 | | |
| | | *PER* | 0.8295 | 0.4468 | 0.1447 | 0.0150 | 0.0025 | 0.0005 | | |
| 11 | 1 | *SIR* | 2.8 | 3.0 | 3.2 | 3.4 | 3.6 | 3.8 | | |
| | | *PER* | 0.9494 | 0.4827 | 0.0685 | 0.0050 | 0.0015 | 0.0015 | | |
| 11&12 | 2 | *SIR* | 8.4 | 8.6 | 8.8 | 9.0 | 9.2 | 9.4 | | |
| | | *PER* | 0.9403 | 0.5621 | 0.1980 | 0.0200 | 0.0030 | 0.0020 | | |

Table B.3. Tabulated PER curves for $S_{trans} = 512$ packet format.

| *Rate* | *Trans.* | | | | | | | | | | |
|---|---|---|---|---|---|---|---|---|---|---|---|
| 1 | 16 | *SIR* | -14.2 | -14.0 | -13.8 | -13.6 | -13.4 | -13.2 | -13.0 | -12.8 | -12.6 |
| | | *PER* | 0.5185 | 0.2951 | 0.2079 | 0.1887 | 0.0667 | 0.0271 | 0.0100 | 0.0042 | 0.0016 |
| | 15 | *SIR* | -14.0 | -13.8 | -13.6 | -13.4 | -13.2 | -13.0 | -12.8 | -12.6 | -12.4 |
| | | *PER* | 0.5481 | 0.4296 | 0.3020 | 0.1949 | 0.0907 | 0.0403 | 0.0143 | 0.0078 | 0.0012 |
| | 14 | *SIR* | -13.6 | -13.4 | -13.2 | -13.0 | -12.8 | -12.6 | -12.4 | -12.2 | -12.0 |
| | | *PER* | 0.5455 | 0.4101 | 0.2566 | 0.1419 | 0.0650 | 0.0286 | 0.0090 | 0.0034 | 0.0008 |
| | 13 | *SIR* | -13.2 | -13.0 | -12.8 | -12.6 | -12.4 | -12.2 | -12.0 | -11.8 | -11.6 |
| | | *PER* | 0.5824 | 0.3395 | 0.1951 | 0.1128 | 0.0529 | 0.0192 | 0.0062 | 0.0022 | 0.0012 |
| | 12 | *SIR* | -13.0 | -12.8 | -12.6 | -12.4 | -12.2 | -12.0 | -11.8 | -11.6 | |
| | | *PER* | 0.6744 | 0.4872 | 0.3218 | 0.1967 | 0.1126 | 0.0606 | 0.0166 | 0.0060 | |
| | 11 | *SIR* | -12.6 | -12.4 | -12.2 | -12.0 | -11.8 | -11.6 | -11.4 | -11.2 | -11.0 | -10.8 |
| | | *PER* | 0.5604 | 0.5340 | 0.3050 | 0.1892 | 0.0966 | 0.0419 | 0.0163 | 0.0062 | 0.0032 | 0.0006 |
| | 10 | *SIR* | -12.0 | -11.8 | -11.6 | -11.4 | -11.2 | -11.0 | -10.8 | -10.6 | -10.4 | -10.2 |
| | | *PER* | 0.5977 | 0.2908 | 0.2424 | 0.1257 | 0.0574 | 0.0243 | 0.0084 | 0.0032 | 0.0006 | 0.0004 |
| | 9 | *SIR* | -11.8 | -11.6 | -11.4 | -11.2 | -11.0 | -10.8 | -10.6 | -10.4 | -10.2 | -10.0 |
| | | *PER* | 0.8030 | 0.6207 | 0.5000 | 0.2372 | 0.1268 | 0.0679 | 0.0370 | 0.0104 | 0.0058 | 0.0018 |
| | 8 | *SIR* | -11.0 | -10.8 | -10.6 | -10.4 | -10.2 | -10.0 | -9.8 | -9.6 | -9.4 | -9.2 |
| | | *PER* | 0.5490 | 0.4104 | 0.1948 | 0.1317 | 0.0688 | 0.0260 | 0.0114 | 0.0014 | 0.0018 | 0.0004 |

| | | | | | | | | | | | | |
|---|---|---|---|---|---|---|---|---|---|---|---|---|
| | 7 | *SIR* | -10.6 | -10.4 | -10.2 | -10.0 | -9.8 | -9.6 | -9.4 | -9.2 | -9.0 | -8.8 |
| | | *PER* | 0.8030 | 0.5758 | 0.4597 | 0.2437 | 0.1339 | 0.0800 | 0.0315 | 0.0114 | 0.0044 | 0.0016 |
| | 6 | *SIR* | -9.8 | -9.6 | -9.4 | -9.2 | -9.0 | -8.8 | -8.6 | -8.4 | -8.2 | -8.0 |
| | | *PER* | 0.6196 | 0.5413 | 0.3618 | 0.1928 | 0.1087 | 0.0654 | 0.0253 | 0.0092 | 0.0032 | 0.0014 |
| | 5 | *SIR* | -9.0 | -8.8 | -8.6 | -8.4 | -8.2 | -8.0 | -7.8 | -7.6 | -7.4 | -7.2 |
| | | *PER* | 0.7612 | 0.6437 | 0.4154 | 0.2652 | 0.1739 | 0.0985 | 0.0378 | 0.0154 | 0.0050 | 0.0020 |
| | 4 | *SIR* | -7.8 | -7.6 | -7.4 | -7.2 | -7.0 | -6.8 | -6.6 | -6.4 | -6.2 | -6.0 |
| | | *PER* | 0.7237 | 0.5806 | 0.4041 | 0.2269 | 0.1373 | 0.0650 | 0.0298 | 0.0106 | 0.0040 | 0.0008 |
| | 3 | *SIR* | -6.0 | -5.8 | -5.6 | -5.4 | -5.2 | -5.0 | -4.8 | -4.6 | -4.4 | -4.2 |
| | | *PER* | 0.5149 | 0.3497 | 0.2085 | 0.1760 | 0.0730 | 0.0281 | 0.0118 | 0.0038 | 0.0014 | 0.0004 |
| | 2 | *SIR* | -3.6 | -3.4 | -3.2 | -3.0 | -2.8 | -2.6 | -2.4 | -2.2 | -2.0 | -1.8 |
| | | *PER* | 0.6180 | 0.3971 | 0.2951 | 0.1517 | 0.0747 | 0.0301 | 0.0122 | 0.0032 | 0.0024 | 0.0006 |
| | 1 | *SIR* | 5.7 | 5.9 | 6.1 | 6.3 | 6.5 | 6.7 | 6.9 | 7.1 | 7.3 | 7.5 |
| | | *PER* | 0.5146 | 0.3910 | 0.2621 | 0.1787 | 0.0929 | 0.0596 | 0.0263 | 0.0169 | 0.0070 | 0.0040 |
| 2 | 8 | *SIR* | -11.4 | -11.2 | -11.0 | -10.8 | -10.6 | -10.4 | -10.2 | -10.0 | -9.8 | -9.6 |
| | | *PER* | 0.6341 | 0.5851 | 0.3273 | 0.2289 | 0.1214 | 0.0696 | 0.0237 | 0.0112 | 0.0036 | 0.0004 |
| | 7 | *SIR* | -10.8 | -10.6 | -10.4 | -10.2 | -10.0 | -9.8 | -9.6 | -9.4 | -9.2 | -9.0 |
| | | *PER* | 0.7465 | 0.5979 | 0.3819 | 0.2590 | 0.1303 | 0.0680 | 0.0347 | 0.0132 | 0.0042 | 0.0008 |
| | 6 | *SIR* | -10.2 | -10.0 | -9.8 | -9.6 | -9.4 | -9.2 | -9.0 | -8.8 | -8.6 | -8.4 |
| | | *PER* | 0.8254 | 0.6136 | 0.5960 | 0.3086 | 0.2045 | 0.0895 | 0.0504 | 0.0244 | 0.0070 | 0.0022 |
| | 5 | *SIR* | -9.2 | -9.0 | -8.8 | -8.6 | -8.4 | -8.2 | -8.0 | -7.8 | -7.6 | -7.4 |
| | | *PER* | 0.6322 | 0.6264 | 0.3735 | 0.1961 | 0.1438 | 0.0641 | 0.0275 | 0.0088 | 0.0026 | 0.0006 |
| | 4 | *SIR* | -8.2 | -8.0 | -7.8 | -7.6 | -7.4 | -7.2 | -7.0 | -6.8 | -6.6 | -6.4 |
| | | *PER* | 0.7857 | 0.5888 | 0.4453 | 0.2965 | 0.1275 | 0.0809 | 0.0308 | 0.0120 | 0.0042 | 0.0012 |
| | 3 | *SIR* | -6.8 | -6.6 | -6.4 | -6.2 | -6.0 | -5.8 | -5.6 | -5.4 | -5.2 | -5.0 |
| | | *PER* | 0.7612 | 0.5591 | 0.4161 | 0.2703 | 0.1417 | 0.0750 | 0.0298 | 0.0122 | 0.0044 | 0.0010 |
| | 2 | *SIR* | -4.8 | -4.6 | -4.4 | -4.2 | -4.0 | -3.8 | -3.6 | -3.4 | -3.2 | -3.0 |
| | | *PER* | 0.7324 | 0.5347 | 0.3893 | 0.2436 | 0.1377 | 0.0649 | 0.0308 | 0.0116 | 0.0032 | 0.0016 |
| | 1 | *SIR* | 0.2 | 0.4 | 0.6 | 0.8 | 1.0 | 1.2 | 1.4 | 1.6 | 1.8 | 2.0 |
| | | *PER* | 0.7051 | 0.4058 | 0.2923 | 0.1662 | 0.1333 | 0.0402 | 0.0164 | 0.0054 | 0.0028 | 0.0004 |
| 3 | 4 | *SIR* | -8.2 | -8.0 | -7.8 | -7.6 | -7.4 | -7.2 | -7.0 | -6.8 | -6.6 | -6.4 |
| | | *PER* | 0.5049 | 0.4309 | 0.2469 | 0.1594 | 0.0895 | 0.0362 | 0.0124 | 0.0036 | 0.0012 | 0.0002 |
| | 3 | *SIR* | -7.0 | -6.8 | -6.6 | -6.4 | -6.2 | -6.0 | -5.8 | -5.6 | -5.4 | -5.2 |
| | | *PER* | 0.6923 | 0.5041 | 0.3836 | 0.2490 | 0.1061 | 0.0451 | 0.0237 | 0.0078 | 0.0036 | 0.0010 |
| | 2 | *SIR* | -5.0 | -4.8 | -4.6 | -4.4 | -4.2 | -4.0 | -3.8 | -3.6 | -3.4 | -3.2 |
| | | *PER* | 0.6625 | 0.4186 | 0.2683 | 0.1923 | 0.0954 | 0.0430 | 0.0169 | 0.0064 | 0.0014 | 0.0016 |
| | 1 | *SIR* | -1.2 | -1.0 | -0.8 | -0.6 | -0.4 | -0.2 | 0.0 | 0.2 | 0.4 | 0.6 |
| | | *PER* | 0.7083 | 0.5806 | 0.3667 | 0.2192 | 0.1383 | 0.0767 | 0.0265 | 0.0098 | 0.0040 | 0.0020 |
| 4 | 2 | *SIR* | -5.0 | -4.8 | -4.6 | -4.4 | -4.2 | -4.0 | -3.8 | -3.6 | -3.4 | -3.2 |
| | | *PER* | 0.5089 | 0.3132 | 0.1640 | 0.1061 | 0.0619 | 0.0243 | 0.0086 | 0.0020 | 0.0004 | 0.0004 |
| | 1 | *SIR* | -1.6 | -1.4 | -1.2 | -1.0 | -0.8 | -0.6 | -0.4 | -0.2 | 0.0 | 0.2 |
| | | *PER* | 0.6279 | 0.4247 | 0.2932 | 0.1612 | 0.0835 | 0.0442 | 0.0180 | 0.0074 | 0.0010 | 0.0006 |
| 5 | 1 | *SIR* | -2.0 | -1.8 | -1.6 | -1.4 | -1.2 | -1.0 | -0.8 | -0.6 | -0.4 | -0.2 |
| | | *PER* | 0.7500 | 0.6429 | 0.4426 | 0.2843 | 0.1869 | 0.1010 | 0.0376 | 0.0148 | 0.0048 | 0.0016 |
| 6 | 4 | *SIR* | -5.0 | -4.8 | -4.6 | -4.4 | -4.2 | -4.0 | -3.8 | -3.6 | | |
| | | *PER* | 0.7000 | 0.5044 | 0.3023 | 0.1473 | 0.0600 | 0.0195 | 0.0042 | 0.0010 | | |
| | 3 | *SIR* | -3.6 | -3.4 | -3.2 | -3.0 | -2.8 | -2.6 | -2.4 | -2.2 | -2.0 | |
| | | *PER* | 0.6404 | 0.5000 | 0.3282 | 0.1506 | 0.0765 | 0.0190 | 0.0060 | 0.0020 | 0.0002 | |
| | 2 | *SIR* | -2.0 | -1.8 | -1.6 | -1.4 | -1.2 | -1.0 | -0.8 | -0.6 | -0.4 | |
| | | *PER* | 0.8871 | 0.7089 | 0.3614 | 0.1969 | 0.0768 | 0.0300 | 0.0086 | 0.0020 | 0.0006 | |
| | 1 | *SIR* | 3.0 | 3.2 | 3.4 | 3.6 | 3.8 | 4.0 | 4.2 | 4.4 | 4.6 | 4.4 |
| | | *PER* | 0.7429 | 0.4961 | 0.3015 | 0.1791 | 0.0711 | 0.0271 | 0.0114 | 0.0044 | 0.0010 | 0.0004 |
| 7 | 2 | *SIR* | -2.0 | -1.8 | -1.6 | -1.4 | -1.2 | -1.0 | -0.8 | -0.6 | -0.4 | |
| | | *PER* | 0.6951 | 0.4878 | 0.3155 | 0.1516 | 0.0619 | 0.0182 | 0.0044 | 0.0012 | 0.0004 | |
| 7&8 | 1 | *SIR* | 2.8 | 3.0 | 3.2 | 3.4 | 3.6 | 3.8 | 4.0 | 4.2 | 4.4 | |
| | | *PER* | 0.5889 | 0.4275 | 0.1792 | 0.0853 | 0.0291 | 0.0088 | 0.0048 | 0.0014 | 0.0002 | |
| 9 | 1 | *SIR* | 1.0 | 1.2 | 1.4 | 1.6 | 1.8 | 2.0 | 2.2 | 2.4 | | |
| | | *PER* | 0.5472 | 0.3009 | 0.1594 | 0.0501 | 0.0082 | 0.0038 | 0.0004 | 0.0002 | | |
| 9&10 | 2 | *SIR* | 6.6 | 6.8 | 7.0 | 7.2 | 7.4 | 7.6 | 7.8 | 8.0 | | |

| | | | | | | | | | | |
|---|---|---|---|---|---|---|---|---|---|---|
| | | *PER* | 0.5810 | 0.2510 | 0.1635 | 0.0551 | 0.0243 | 0.0094 | 0.0034 | 0.0006 |
| 11 | 1 | *SIR* | 2.8 | 3.0 | 3.2 | 3.4 | 3.6 | 3.8 | 4.0 | |
| | | *PER* | 0.8101 | 0.4472 | 0.2249 | 0.0561 | 0.0136 | 0.0038 | 0.0006 | |
| 11&12 | 2 | *SIR* | 8.6 | 8.8 | 9.0 | 9.2 | 9.4 | 9.6 | 9.8 | 10.0 |
| | | *PER* | 0.5446 | 0.2831 | 0.1344 | 0.0426 | 0.0110 | 0.0026 | 0.0008 | 0.0004 |

Table B.4. Tabulated PER curves for $S_{trans} = 128$ packet format.

| *Rate* | *Trans.* | | | | | | | | | | | | | | | |
|---|---|---|---|---|---|---|---|---|---|---|---|---|---|---|---|---|
| 1 | 16 | *SIR* | -14.2 | -14.0 | -13.8 | -13.6 | -13.4 | -13.2 | -13.0 | -12.8 | -12.6 | -12.4 | -12.2 | -12.0 | -11.8 | -11.6 | |
| | | *PER* | 0.4622 | 0.4135 | 0.2872 | 0.1964 | 0.1343 | 0.1011 | 0.0863 | 0.0453 | 0.0259 | 0.0178 | 0.0080 | 0.0052 | 0.0032 | 0.0004 | |
| | 15 | *SIR* | -14.0 | -13.8 | -13.6 | -13.4 | -13.2 | -13.0 | -12.8 | -12.6 | -12.4 | -12.2 | -12.0 | -11.8 | -11.6 | -11.4 | -11.2 |
| | | *PER* | 0.4696 | 0.4180 | 0.2723 | 0.2015 | 0.1704 | 0.1111 | 0.0957 | 0.0518 | 0.0353 | 0.0209 | 0.0130 | 0.0054 | 0.0026 | 0.0016 | 0.0008 |
| | 14 | *SIR* | -13.6 | -13.4 | -13.2 | -13.0 | -12.8 | -12.6 | -12.4 | -12.2 | -12.0 | -11.8 | -11.6 | -11.4 | -11.2 | -11.0 | -10.8 |
| | | *PER* | 0.3969 | 0.3354 | 0.3228 | 0.2118 | 0.1411 | 0.1127 | 0.0660 | 0.0543 | 0.0239 | 0.0152 | 0.0094 | 0.0056 | 0.0026 | 0.0016 | 0.0002 |
| | 13 | *SIR* | -13.2 | -13.0 | -12.8 | -12.6 | -12.4 | -12.2 | -12.0 | -11.8 | -11.6 | -11.4 | -11.2 | -11.0 | -10.8 | -10.6 | -10.4 |
| | | *PER* | 0.4094 | 0.4015 | 0.2271 | 0.1611 | 0.1190 | 0.1035 | 0.0546 | 0.0399 | 0.0198 | 0.0108 | 0.0086 | 0.0036 | 0.0026 | 0.0010 | 0.0004 |
| | 12 | *SIR* | -13.0 | -12.8 | -12.6 | -12.4 | -12.2 | -12.0 | -11.8 | -11.6 | -11.4 | -11.2 | -11.0 | -10.8 | -10.6 | -10.4 | |
| | | *PER* | 0.4344 | 0.3662 | 0.3220 | 0.2961 | 0.1986 | 0.1294 | 0.0837 | 0.0586 | 0.0444 | 0.0171 | 0.0142 | 0.0062 | 0.0020 | 0.0016 | |
| | 11 | *SIR* | -12.6 | -12.4 | -12.2 | -12.0 | -11.8 | -11.6 | -11.4 | -11.2 | -11.0 | -10.8 | -10.6 | -10.4 | -10.2 | -10.0 | -9.8 |
| | | *PER* | 0.4113 | 0.4474 | 0.3605 | 0.2813 | 0.1677 | 0.1181 | 0.0794 | 0.0612 | 0.0380 | 0.0237 | 0.0133 | 0.0042 | 0.0048 | 0.0020 | 0.0012 |
| | 10 | *SIR* | -12.0 | -11.8 | -11.6 | -11.4 | -11.2 | -11.0 | -10.8 | -10.6 | -10.4 | -10.2 | -10.0 | -9.8 | -9.6 | -9.4 | |
| | | *PER* | 0.3688 | 0.3469 | 0.2690 | 0.1505 | 0.1094 | 0.0822 | 0.0749 | 0.0440 | 0.0265 | 0.0145 | 0.0072 | 0.0044 | 0.0016 | 0.0010 | |
| | 9 | *SIR* | -11.8 | -11.6 | -11.4 | -11.2 | -11.0 | -10.8 | -10.6 | -10.4 | -10.2 | -10.0 | -9.8 | -9.6 | -9.4 | -9.2 | -9.0 |
| | | *PER* | 0.4909 | 0.4513 | 0.3953 | 0.3250 | 0.2093 | 0.1608 | 0.1217 | 0.0672 | 0.0497 | 0.0265 | 0.0186 | 0.0098 | 0.0046 | 0.0038 | 0.0012 |
| | 8 | *SIR* | -11.0 | -10.8 | -10.6 | -10.4 | -10.2 | -10.0 | -9.8 | -9.6 | -9.4 | -9.2 | -9.0 | -8.8 | -8.6 | -8.4 | |
| | | *PER* | 0.4113 | 0.3467 | 0.2535 | 0.1884 | 0.1686 | 0.1082 | 0.0802 | 0.0411 | 0.0259 | 0.0157 | 0.0076 | 0.0044 | 0.0018 | 0.0014 | |
| | 7 | *SIR* | -10.6 | -10.4 | -10.2 | -10.0 | -9.8 | -9.6 | -9.4 | -9.2 | -9.0 | -8.8 | -8.6 | -8.4 | -8.2 | -8.0 | -7.8 |
| | | *PER* | 0.4561 | 0.4522 | 0.3901 | 0.2609 | 0.2169 | 0.1800 | 0.1142 | 0.0724 | 0.0556 | 0.0279 | 0.0145 | 0.0080 | 0.0048 | 0.0034 | 0.0020 |
| | 6 | *SIR* | -9.8 | -9.6 | -9.4 | -9.2 | -9.0 | -8.8 | -8.6 | -8.4 | -8.2 | -8.0 | -7.8 | -7.6 | -7.4 | -7.2 | |
| | | *PER* | 0.5313 | 0.5313 | 0.3576 | 0.2464 | 0.2143 | 0.1525 | 0.0967 | 0.0737 | 0.0395 | 0.0259 | 0.0150 | 0.0104 | 0.0046 | 0.0016 | |
| | 5 | *SIR* | -9.0 | -8.8 | -8.6 | -8.4 | -8.2 | -8.0 | -7.8 | -7.6 | -7.4 | -7.2 | -7.0 | -6.8 | -6.6 | -6.4 | -6.2 |
| | | *PER* | 0.5934 | 0.5354 | 0.3942 | 0.2961 | 0.2647 | 0.1408 | 0.1169 | 0.0959 | 0.0470 | 0.0384 | 0.0217 | 0.0108 | 0.0074 | 0.0038 | 0.0016 |
| | 4 | *SIR* | -7.8 | -7.6 | -7.4 | -7.2 | -7.0 | -6.8 | -6.6 | -6.4 | -6.2 | -6.0 | -5.8 | -5.6 | -5.4 | -5.2 | -5.0 |
| | | *PER* | 0.5361 | 0.5152 | 0.4122 | 0.2718 | 0.2120 | 0.1610 | 0.0976 | 0.0622 | 0.0433 | 0.0273 | 0.0180 | 0.0078 | 0.0046 | 0.0022 | 0.0006 |
| | 3 | *SIR* | -6.0 | -5.8 | -5.6 | -5.4 | -5.2 | -5.0 | -4.8 | -4.6 | -4.4 | -4.2 | -4.0 | -3.8 | -3.6 | -3.4 | -3.2 |
| | | *PER* | 0.4513 | 0.3681 | 0.2651 | 0.2656 | 0.1618 | 0.0922 | 0.0750 | 0.0428 | 0.0269 | 0.0153 | 0.0082 | 0.0042 | 0.0018 | 0.0018 | 0.0008 |
| | 2 | *SIR* | -3.6 | -3.4 | -3.2 | -3.0 | -2.8 | -2.6 | -2.4 | -2.2 | -2.0 | -1.8 | -1.6 | -1.4 | -1.2 | -1.0 | -0.8 |
| | | *PER* | 0.5096 | 0.3869 | 0.3269 | 0.1898 | 0.1867 | 0.1289 | 0.0622 | 0.0495 | 0.0379 | 0.0217 | 0.0106 | 0.0056 | 0.0028 | 0.0018 | 0.0012 |
| | 1 | *SIR* | 5.8 | 6.0 | 6.2 | 6.4 | 6.6 | 6.8 | 7.0 | 7.2 | 7.4 | 7.6 | 7.8 | 8.0 | 8.2 | 8.4 | |
| | | *PER* | 0.1395 | 0.1037 | 0.0694 | 0.0429 | 0.0314 | 0.0226 | 0.0123 | 0.0106 | 0.0064 | 0.0034 | 0.0018 | 0.0016 | 0.0010 | 0.0004 | |
| 2 | 8 | *SIR* | -11.4 | -11.2 | -11.0 | -10.8 | -10.6 | -10.4 | -10.2 | -10.0 | -9.8 | -9.6 | -9.4 | -9.2 | -9.0 | -8.8 | |
| | | *PER* | 0.5050 | 0.4545 | 0.3114 | 0.2281 | 0.2062 | 0.1376 | 0.0904 | 0.0993 | 0.0393 | 0.0298 | 0.0172 | 0.0082 | 0.0072 | 0.0016 | |
| | 7 | *SIR* | -10.8 | -10.6 | -10.4 | -10.2 | -10.0 | -9.8 | -9.6 | -9.4 | -9.2 | -9.0 | -8.8 | -8.6 | -8.4 | -8.2 | -8.0 |
| | | *PER* | 0.5778 | 0.3926 | 0.3688 | 0.3252 | 0.2254 | 0.1893 | 0.1279 | 0.0789 | 0.0533 | 0.0261 | 0.0165 | 0.0094 | 0.0068 | 0.0020 | 0.0008 |
| | 6 | *SIR* | -10.2 | -10.0 | -9.8 | -9.6 | -9.4 | -9.2 | -9.0 | -8.8 | -8.6 | -8.4 | -8.2 | -8.0 | -7.8 | -7.6 | -7.4 |
| | | *PER* | 0.6341 | 0.4952 | 0.4160 | 0.2802 | 0.2227 | 0.1622 | 0.1318 | 0.0862 | 0.0477 | 0.0375 | 0.0261 | 0.0142 | 0.0076 | 0.0034 | 0.0020 |
| | 5 | *SIR* | -9.2 | -9.0 | -8.8 | -8.6 | -8.4 | -8.2 | -8.0 | -7.8 | -7.6 | -7.4 | -7.2 | -7.0 | -6.8 | -6.6 | -6.4 |
| | | *PER* | 0.5484 | 0.4771 | 0.3618 | 0.2466 | 0.1953 | 0.1287 | 0.1197 | 0.0565 | 0.0402 | 0.0259 | 0.0142 | 0.0068 | 0.0032 | 0.0022 | 0.0010 |
| | 4 | *SIR* | -8.2 | -8.0 | -7.8 | -7.6 | -7.4 | -7.2 | -7.0 | -6.8 | -6.6 | -6.4 | -6.2 | -6.0 | -5.8 | -5.6 | -5.4 |
| | | *PER* | 0.5361 | 0.4160 | 0.3655 | 0.3193 | 0.2241 | 0.1821 | 0.0952 | 0.0879 | 0.0402 | 0.0278 | 0.0193 | 0.0098 | 0.0046 | 0.0028 | 0.0016 |
| | 3 | *SIR* | -6.8 | -6.6 | -6.4 | -6.2 | -6.0 | -5.8 | -5.6 | -5.4 | -5.2 | -5.0 | -4.8 | -4.6 | -4.4 | -4.2 | |
| | | *PER* | 0.5824 | 0.5152 | 0.3759 | 0.2391 | 0.2075 | 0.1608 | 0.1058 | 0.0755 | 0.0453 | 0.0304 | 0.0189 | 0.0078 | 0.0044 | 0.0026 | |
| | 2 | *SIR* | -4.8 | -4.6 | -4.4 | -4.2 | -4.0 | -3.8 | -3.6 | -3.4 | -3.2 | -3.0 | -2.8 | -2.6 | -2.4 | -2.2 | -2.0 |
| | | *PER* | 0.5667 | 0.4569 | 0.3533 | 0.2536 | 0.1827 | 0.1448 | 0.1069 | 0.0818 | 0.0503 | 0.0293 | 0.0175 | 0.0092 | 0.0056 | 0.0036 | 0.0016 |
| | 1 | *SIR* | 0.2 | 0.4 | 0.6 | 0.8 | 1.0 | 1.2 | 1.4 | 1.6 | 1.8 | 2.0 | 2.2 | 2.4 | 2.6 | 2.8 | |

| | | | | | | | | | | | | | | | | |
|---|---|---|---|---|---|---|---|---|---|---|---|---|---|---|---|---|
| | | *PER* | 0.5258 | 0.3864 | 0.2740 | 0.1992 | 0.1716 | 0.1054 | 0.0662 | 0.0409 | 0.0332 | 0.0203 | 0.0146 | 0.0058 | 0.0032 | 0.0006 |
| 3 | 4 | *SIR* | -8.2 | -8.0 | -7.8 | -7.6 | -7.4 | -7.2 | -7.0 | -6.8 | -6.6 | -6.4 | -6.2 | -6.0 | -5.8 | -5.6 |
| | | *PER* | 0.4643 | 0.3897 | 0.2796 | 0.2190 | 0.1866 | 0.1032 | 0.0705 | 0.0415 | 0.0431 | 0.0161 | 0.0106 | 0.0060 | 0.0036 | 0.0014 |
| | 3 | *SIR* | -7.0 | -6.8 | -6.6 | -6.4 | -6.2 | -6.0 | -5.8 | -5.6 | -5.4 | -5.2 | -5.0 | -4.8 | -4.6 | -4.4 | -4.2 |
| | | *PER* | 0.5361 | 0.4215 | 0.3562 | 0.2714 | 0.1950 | 0.1528 | 0.0931 | 0.0771 | 0.0422 | 0.0222 | 0.0139 | 0.0090 | 0.0040 | 0.0030 | 0.0014 |
| | 2 | *SIR* | -5.0 | -4.8 | -4.6 | -4.4 | -4.2 | -4.0 | -3.8 | -3.6 | -3.4 | -3.2 | -3.0 | -2.8 | -2.6 | -2.4 | -2.2 |
| | | *PER* | 0.5300 | 0.3375 | 0.2928 | 0.2126 | 0.1867 | 0.1086 | 0.0697 | 0.0553 | 0.0356 | 0.0184 | 0.0140 | 0.0056 | 0.0026 | 0.0018 | 0.0006 |
| | 1 | *SIR* | -1.0 | -0.8 | -0.6 | -0.4 | -0.2 | 0.0 | 0.2 | 0.4 | 0.6 | 0.8 | 1.0 | 1.2 | 1.4 | 1.6 | 1.8 |
| | | *PER* | 0.4602 | 0.3910 | 0.2143 | 0.2061 | 0.1360 | 0.1199 | 0.0626 | 0.0396 | 0.0258 | 0.0188 | 0.0086 | 0.0052 | 0.0026 | 0.0016 | 0.0012 |
| 4 | 2 | *SIR* | -5.0 | -4.8 | -4.6 | -4.4 | -4.2 | -4.0 | -3.8 | -3.6 | -3.4 | -3.2 | -3.0 | -2.8 | -2.6 | -2.4 | -2.2 |
| | | *PER* | 0.4180 | 0.2796 | 0.2537 | 0.1521 | 0.1244 | 0.0758 | 0.0510 | 0.0338 | 0.0267 | 0.0138 | 0.0072 | 0.0028 | 0.0022 | 0.0006 | 0.0004 |
| | 1 | *SIR* | -1.6 | -1.4 | -1.2 | -1.0 | -0.8 | -0.6 | -0.4 | -0.2 | 0.0 | 0.2 | 0.4 | 0.6 | 0.8 | 1.0 | 1.2 |
| | | *PER* | 0.4522 | 0.3786 | 0.3881 | 0.2181 | 0.1712 | 0.1066 | 0.0812 | 0.0450 | 0.0359 | 0.0236 | 0.0112 | 0.0048 | 0.0040 | 0.0022 | 0.0012 |
| 5 | 1 | *SIR* | -1.8 | -1.6 | -1.4 | -1.2 | -1.0 | -0.8 | -0.6 | -0.4 | -0.2 | 0.0 | 0.2 | 0.4 | 0.6 | 0.8 | 1.0 |
| | | *PER* | 0.5417 | 0.3784 | 0.3274 | 0.2121 | 0.1383 | 0.1135 | 0.0789 | 0.0402 | 0.0270 | 0.0161 | 0.0096 | 0.0050 | 0.0038 | 0.0020 | 0.0006 |
| 6 | 4 | *SIR* | -5.0 | -4.8 | -4.6 | -4.4 | -4.2 | -4.0 | -3.8 | -3.6 | -3.4 | -3.2 | -3.0 | -2.8 | -2.6 | | |
| | | *PER* | 0.6375 | 0.4696 | 0.4000 | 0.2663 | 0.1966 | 0.1264 | 0.0496 | 0.0309 | 0.0182 | 0.0068 | 0.0038 | 0.0012 | 0.0008 | | |
| | 3 | *SIR* | -3.6 | -3.4 | -3.2 | -3.0 | -2.8 | -2.6 | -2.4 | -2.2 | -2.0 | -1.8 | -1.6 | -1.4 | -1.2 | | |
| | | *PER* | 0.7027 | 0.4135 | 0.3333 | 0.2148 | 0.1980 | 0.1074 | 0.0719 | 0.0307 | 0.0160 | 0.0062 | 0.0040 | 0.0014 | 0.0004 | | |
| | 2 | *SIR* | -1.8 | -1.6 | -1.4 | -1.2 | -1.0 | -0.8 | -0.6 | -0.4 | -0.2 | 0.0 | 0.2 | 0.4 | | | |
| | | *PER* | 0.6092 | 0.4741 | 0.3293 | 0.2210 | 0.1493 | 0.0764 | 0.0377 | 0.0207 | 0.0096 | 0.0046 | 0.0020 | 0.0006 | | | |
| | 1 | *SIR* | 3.0 | 3.2 | 3.4 | 3.6 | 3.8 | 4.0 | 4.2 | 4.4 | 4.6 | 4.8 | 5.0 | 5.2 | | | |
| | | *PER* | 0.4862 | 0.4046 | 0.2619 | 0.2140 | 0.1367 | 0.0703 | 0.0439 | 0.0271 | 0.0151 | 0.0082 | 0.0036 | 0.0010 | | | |
| 7 | 2 | *SIR* | -2.0 | -1.8 | -1.6 | -1.4 | -1.2 | -1.0 | -0.8 | -0.6 | -0.4 | -0.2 | 0.0 | 0.2 | 0.4 | 0.6 | |
| | | *PER* | 0.6235 | 0.4815 | 0.3796 | 0.2653 | 0.2037 | 0.0898 | 0.0641 | 0.0311 | 0.0186 | 0.0074 | 0.0050 | 0.0008 | 0.0010 | 0.0002 | |
| 7&8 | 1 | *SIR* | 2.8 | 3.0 | 3.2 | 3.4 | 3.6 | 3.8 | 4.0 | 4.2 | 4.4 | 4.6 | 4.8 | 5.0 | 5.2 | | |
| | | *PER* | 0.4775 | 0.4309 | 0.2611 | 0.1330 | 0.0693 | 0.0679 | 0.0344 | 0.0188 | 0.0088 | 0.0038 | 0.0020 | 0.0012 | 0.0008 | | |
| 9 | 1 | *SIR* | 1.0 | 1.2 | 1.4 | 1.6 | 1.8 | 2.0 | 2.2 | 2.4 | 2.6 | 2.8 | 3.0 | 3.2 | | | |
| | | *PER* | 0.4865 | 0.3237 | 0.2447 | 0.1375 | 0.0908 | 0.0466 | 0.0195 | 0.0114 | 0.0036 | 0.0018 | 0.0006 | 0.0002 | | | |
| 9&10 | 2 | *SIR* | 6.6 | 6.8 | 7.0 | 7.2 | 7.4 | 7.6 | 7.8 | 8.0 | 8.2 | 8.4 | 8.6 | 8.8 | 9.0 | | |
| | | *PER* | 0.3810 | 0.2345 | 0.2365 | 0.0945 | 0.0673 | 0.0419 | 0.0246 | 0.0172 | 0.0074 | 0.0040 | 0.0030 | 0.0008 | 0.0006 | | |
| 11 | 1 | *SIR* | 2.8 | 3.0 | 3.2 | 3.4 | 3.6 | 3.8 | 4.0 | 4.2 | 4.4 | 4.6 | 4.8 | 5.0 | | | |
| | | *PER* | 0.6235 | 0.5283 | 0.2880 | 0.2086 | 0.0982 | 0.0596 | 0.0220 | 0.0122 | 0.0034 | 0.0020 | 0.0008 | 0.0002 | | | |
| 11&12 | 2 | *SIR* | 8.6 | 8.8 | 9.0 | 9.2 | 9.4 | 9.6 | 9.8 | 10.0 | 10.2 | 10.4 | 10.6 | 10.8 | 11.0 | | |
| | | *PER* | 0.4595 | 0.3957 | 0.2412 | 0.1519 | 0.0792 | 0.0446 | 0.0249 | 0.0120 | 0.0082 | 0.0026 | 0.0016 | 0.0008 | 0.0006 | | |

## B.2 Link Level Simulations for Configurations Considered in Chapter 5

### B.2.1 Packet Structures and Coding

In Chapter 5, the packet structures are based on a subset of structures for cdma2000 [101]. The encoding structure is very similar to the IS-856 turbo encoder, however there are some differences in encoding, interleaving, scrambling, and symbol permuting methods. A turbo code with a specific puncturing pattern to create a code rate of 1/5 is used with a 6-bit tail sequence. The cdma2000 standard [101] goes into significant detail about these methods, so they will not be discussed here.

The packet transmissions in Chapter 5 consist of 1536 complex symbols, 336 of which are reserved for MAC and pilot signalling. No pre-ambles are explicitly considered in these packet structures, and hence, 1200 complex data symbols are sent in every transmission. As Chapter 5 considers asynchronous re-transmissions, a small pre-amble would have to be included in each transmission to have any positive effect. It is assumed that this preamble is contained in the overhead signalling. The packet formats set for Chapter 5 are given in Table 5.1, with modulation constellations in Table 5.2. A more detailed description of the packet formats is given in Table B.5. A single set of link results (consisting of 1 to 8 transmissions) applies to all 4 packet format sets as all consider the same number of data symbols per transmissions.

Table B.5. Details of packet formats considered in Chapter 5.

| | *Modulation* | *Code rate (approx.)* | *No. of complete repetitions* | *Data rate (Kb/s/sub-band)* | *Packet size (bits)* | *SIR for 1% PER* |
|---|---|---|---|---|---|---|
| 8 | QPSK | 1/5 | 9.4 | 37.9 | 408 | -13.1 |
| 7 | QPSK | 1/5 | 8.2 | 43.4 | 408 | -12.5 |
| 6 | QPSK | 1/5 | 7.1 | 50.6 | 408 | -11.9 |
| 5 | QPSK | 1/5 | 5.9 | 60.7 | 408 | -11.1 |
| 4 | QPSK | 1/5 | 4.7 | 75.9 | 408 | -10.0 |
| 3 | QPSK | 1/5 | 3.5 | 101.2 | 408 | -8.8 |
| 2 | QPSK | 1/5 | 2.4 | 151.7 | 408 | -6.9 |
| 1 | QPSK | 1/5 | 1.2 | 303.5 | 408 | -3.7 |
| 8 | QPSK | 1/5 | 4.8 | 73.6 | 792 | -10.5 |
| 7 | QPSK | 1/5 | 4.2 | 84.2 | 792 | -9.9 |
| 6 | QPSK | 1/5 | 3.6 | 98.2 | 792 | -9.1 |
| 5 | QPSK | 1/5 | 3.0 | 117.8 | 792 | -8.4 |
| 4 | QPSK | 1/5 | 2.4 | 147.3 | 792 | -7.3 |
| 3 | QPSK | 1/5 | 1.8 | 196.4 | 792 | -5.9 |
| 2 | QPSK | 1/5 | 1.2 | 294.6 | 792 | -4.0 |
| 1 | QPSK | 1/3 | 1.0 | 589.1 | 792 | -0.7 |
| 8 | QPSK | 1/5 | 2.5 | 145.0 | 1560 | -7.5 |
| 7 | QPSK | 1/5 | 2.2 | 165.8 | 1560 | -7.0 |
| 6 | QPSK | 1/5 | 1.8 | 193.4 | 1560 | -6.1 |
| 5 | QPSK | 1/5 | 1.5 | 232.1 | 1560 | -5.1 |
| 4 | QPSK | 1/5 | 1.2 | 290.1 | 1560 | -4.3 |
| 3 | QPSK | 1/5 | 1.0 | 386.8 | 1560 | -3.4 |
| 2 | QPSK | 1/5 | 1.0 | 580.2 | 1560 | -1.0 |
| 1 | QPSK | 1/3 | 1.0 | 1160.4 | 1560 | 5.0 |
| 8 | 8 PSK | 1/5 | 2.5 | 216.5 | 2328 | -5.0 |
| 7 | 8 PSK | 1/5 | 2.2 | 247.4 | 2328 | -4.5 |
| 6 | 8 PSK | 1/5 | 1.9 | 288.6 | 2328 | -3.7 |
| 5 | 8 PSK | 1/5 | 1.5 | 346.3 | 2328 | -2.7 |
| 4 | 8 PSK | 1/5 | 1.2 | 432.9 | 2328 | -1.8 |
| 3 | 8 PSK | 11/51 | 1.0 | 577.2 | 2328 | -0.9 |
| 2 | 8 PSK | 11/34 | 1.0 | 865.8 | 2328 | 1.7 |
| 1 | 8 PSK | 11/17 | 1.0 | 1731.6 | 2328 | 1.3 |
| 8 | 16 QAM | 1/5 | 2.5 | 287.9 | 3096 | -3.0 |
| 7 | 16 QAM | 1/5 | 2.2 | 329.0 | 3096 | -2.5 |
| 6 | 16 QAM | 1/5 | 1.9 | 383.8 | 3096 | -1.7 |
| 5 | 16 QAM | 1/5 | 1.6 | 460.6 | 3096 | -0.5 |
| 4 | 16 QAM | 1/5 | 1.2 | 575.7 | 3096 | 0.4 |
| 3 | 16 QAM | 20/93 | 1.0 | 767.6 | 3096 | 1.1 |
| 2 | 16 QAM | 10/31 | 1.0 | 1151.5 | 3096 | 3.7 |
| 1 | 16 QAM | 20/31 | 1.0 | 2302.9 | 3096 | 10.5 |
| 8 | 16 QAM | 1/5 | 2.0 | 359.3 | 3864 | -2.0 |
| 7 | 16 QAM | 1/5 | 1.7 | 410.6 | 3864 | -0.9 |
| 6 | 16 QAM | 1/5 | 1.5 | 479.0 | 3864 | -0.2 |
| 5 | 16 QAM | 1/5 | 1.2 | 574.8 | 3864 | 0.5 |
| 4 | 16 QAM | 1/5 | 1.0 | 718.5 | 3864 | 1.1 |
| 3 | 16 QAM | 11/41 | 1.0 | 958.1 | 3864 | 2.6 |
| 2 | 16 QAM | 33/82 | 1.0 | 1437.1 | 3864 | 5.9 |
| 1 | 16 QAM | 33/41 | 1.0 | 2874.2 | 3864 | 13.7 |

## B.2.2 Link Level Results

The packet structures given in Table 5.1 were simulated in an AWGN channel with proper encoding, interleaving, and overhead layouts. The packet error rate (PER) curves for each format, and for every possibility of early termination, is simulated. MAP turbo decoding is used, and for the cases of multiple re-transmissions, soft-packet combining is considered. As before, turbo decoding with 8 iterations is considered.

As there are no explicit pre-ambles per packet format set, the number of link level curves is significantly reduced in comparison to Appendix B.1. Each transmission consists of 1200 complex data symbols, however, in Section 5.6, adaptive termination with CDM of packet transmissions is employed, which results in the need for additional link level results. In addition, factional numbers of transmissions are included for some of the cases that arise in Section 5.6. The PER and SIR information has been tabulated in Table B.6 for all structures and formats listed in Table 5.1. Packet structures for Section 5.4, which considers 64 QAM are also given in Table B.6. As before, each row-pair is appended by a PER of 1.0 (100%) for an SIR that is 0.2 dB lower than the first entry, and a PER of 0 for an SIR that is 0.2 dB greater than the last entry in the system level simulations.

In Section 5.6, SIR penalties are used to approximate the PER curves when using different modulation constellations. After tabulating many cases of varying packet sizes and transmission sizes, 3 appropriate margins were estimated. They are listed in Table B.7, and are used in the simulations for Section 5.6.

Table B.6. Tabulated PER curves for Chapter 5 formats; *A*, *B*, *C* and *D* packet format sets. 64 QAM packet formats are also listed. Each transmission consists of 1200 complex data symbols. Accompanying modulation constellations are given in Tables 5.2 and 5.7.

| *Packet Size* | *Trans. (1200)* | | | | | | | | | | |
|---|---|---|---|---|---|---|---|---|---|---|---|
| 408 | 8 | *SIR* | -14.4 | -14.2 | -14.0 | -13.8 | -13.6 | -13.4 | -13.2 | -13.0 | -12.8 | -12.6 |
| (QPSK) | | *PER* | 0.7761 | 0.6180 | 0.4911 | 0.2333 | 0.1095 | 0.0563 | 0.0152 | 0.0048 | 0.0006 | 0.0002 |
| | 7.5 | *SIR* | -14.2 | -14.0 | -13.8 | -13.6 | -13.4 | -13.2 | -13.0 | -12.8 | -12.6 | -12.4 |
| | | *PER* | 0.9123 | 0.7941 | 0.5089 | 0.3702 | 0.1705 | 0.0833 | 0.0276 | 0.0066 | 0.0010 | 0.0006 |
| | 7 | *SIR* | -13.4 | -13.2 | -13.0 | -12.8 | -12.6 | -12.4 | -12.2 | | | |
| | | *PER* | 0.4255 | 0.2797 | 0.1133 | 0.0502 | 0.0172 | 0.0054 | 0.0010 | | | |
| | 6.5 | *SIR* | -13.4 | -13.2 | -13.0 | -12.8 | -12.6 | -12.4 | -12.2 | -12.0 | -11.8 | -11.6 |
| | | *PER* | 0.8254 | 0.5088 | 0.3372 | 0.1808 | 0.1091 | 0.0333 | 0.0110 | 0.0028 | 0.0008 | 0.0002 |
| | 6 | *SIR* | -13.2 | -13.0 | -12.8 | -12.6 | -12.4 | -12.2 | -12.0 | -11.8 | -11.6 | -11.4 |
| | | *PER* | 0.9310 | 0.6304 | 0.4783 | 0.3333 | 0.1643 | 0.0771 | 0.0231 | 0.0052 | 0.0024 | 0.0002 |

| | | | | | | | | | | | |
|---|---|---|---|---|---|---|---|---|---|---|---|
| | 5.5 | *SIR* | -12.4 | -12.2 | -12.0 | -11.8 | -11.6 | -11.4 | -11.2 | | |
| | | *PER* | 0.5364 | 0.3216 | 0.1423 | 0.0707 | 0.0248 | 0.0054 | 0.0004 | | |
| | 5 | *SIR* | -12.4 | -12.2 | -12.0 | -11.8 | -11.6 | -11.4 | -11.2 | -11.0 | -10.8 |
| | | *PER* | 0.8030 | 0.7534 | 0.4919 | 0.3492 | 0.1641 | 0.0668 | 0.0211 | 0.0060 | 0.0014 |
| | 4.5 | *SIR* | -11.8 | -11.6 | -11.4 | -11.2 | -11.0 | -10.8 | -10.6 | -10.4 | -10.2 |
| | | *PER* | 0.7011 | 0.6000 | 0.3392 | 0.1866 | 0.0946 | 0.0360 | 0.0140 | 0.0014 | 0.0004 |
| | 4 | *SIR* | -11.4 | -11.2 | -11.0 | -10.8 | -10.6 | -10.4 | -10.2 | -10.0 | -9.8 | -9.6 |
| | | *PER* | 0.8689 | 0.6250 | 0.5299 | 0.3450 | 0.1520 | 0.0737 | 0.0262 | 0.0070 | 0.0014 | 0.0006 |
| | 3.5 | *SIR* | -10.8 | -10.6 | -10.4 | -10.2 | -10.0 | -9.8 | -9.6 | -9.4 | -9.2 | -9.0 |
| | | *PER* | 0.7910 | 0.6986 | 0.4345 | 0.2920 | 0.1250 | 0.0512 | 0.0156 | 0.0042 | 0.0014 | 0.0004 |
| | 3 | *SIR* | -9.8 | -9.6 | -9.4 | -9.2 | -9.0 | -8.8 | -8.6 | -8.4 | -8.2 | |
| | | *PER* | 0.5673 | 0.4161 | 0.2463 | 0.1048 | 0.0340 | 0.0108 | 0.0046 | 0.0016 | 0.0002 | |
| | 2.5 | *SIR* | -9.4 | -9.2 | -9.0 | -8.8 | -8.6 | -8.4 | -8.2 | -8.0 | -7.8 | |
| | | *PER* | 0.8793 | 0.6543 | 0.5524 | 0.3316 | 0.1799 | 0.0817 | 0.0255 | 0.0086 | 0.0016 | |
| | 2 | *SIR* | -8.4 | -8.2 | -8.0 | -7.8 | -7.6 | -7.4 | -7.2 | -7.0 | -6.8 | -6.6 |
| | | *PER* | 0.8983 | 0.8286 | 0.5978 | 0.4219 | 0.2671 | 0.1396 | 0.0484 | 0.0172 | 0.0046 | 0.0024 |
| | 1.5 | *SIR* | -6.4 | -6.2 | -6.0 | -5.8 | -5.6 | -5.4 | -5.2 | -5.0 | -4.8 | |
| | | *PER* | 0.5133 | 0.3028 | 0.1639 | 0.0652 | 0.0285 | 0.0096 | 0.0026 | 0.0004 | 0.0002 | |
| | 1 | *SIR* | -4.8 | -4.6 | -4.4 | -4.2 | -4.0 | -3.8 | -3.6 | -3.4 | -3.2 | |
| | | *PER* | 0.6404 | 0.3675 | 0.2174 | 0.1201 | 0.0577 | 0.0134 | 0.0044 | 0.0014 | 0.0008 | |
| | 0.5 | *SIR* | -1.4 | -1.2 | -1.0 | -0.8 | -0.6 | -0.4 | -0.2 | 0.0 | | |
| | | *PER* | 0.9273 | 0.8358 | 0.5351 | 0.2552 | 0.0685 | 0.0090 | 0.0012 | 0.0002 | | |
| 792 | 8 | *SIR* | -11.4 | -11.2 | -11.0 | -10.8 | -10.6 | -10.4 | -10.2 | | |
| (QPSK) | | *PER* | 0.8310 | 0.6563 | 0.3509 | 0.1172 | 0.0297 | 0.0064 | 0.0010 | | |
| | 7.5 | *SIR* | -11.2 | -11.0 | -10.8 | -10.6 | -10.4 | -10.2 | -10.0 | -9.8 | |
| | | *PER* | 0.9508 | 0.8182 | 0.5285 | 0.1986 | 0.0739 | 0.0176 | 0.0024 | 0.0004 | |
| | 7 | *SIR* | -10.8 | -10.6 | -10.4 | -10.2 | -10.0 | -9.8 | -9.6 | -9.4 | |
| | | *PER* | 0.8116 | 0.7241 | 0.2974 | 0.1174 | 0.0318 | 0.0064 | 0.0014 | 0.0002 | |
| | 6.5 | *SIR* | -10.8 | -10.6 | -10.4 | -10.2 | -10.0 | -9.8 | -9.6 | -9.4 | -9.2 |
| | | *PER* | 0.9630 | 0.9636 | 0.7381 | 0.4516 | 0.1948 | 0.0555 | 0.0140 | 0.0030 | 0.0002 |
| | 6 | *SIR* | -10.2 | -10.0 | -9.8 | -9.6 | -9.4 | -9.2 | -9.0 | -8.8 | |
| | | *PER* | 0.8594 | 0.7561 | 0.3901 | 0.2650 | 0.0758 | 0.0146 | 0.0032 | 0.0008 | |
| | 5.5 | *SIR* | -9.8 | -9.6 | -9.4 | -9.2 | -9.0 | -8.8 | -8.6 | -8.4 | |
| | | *PER* | 0.9153 | 0.7901 | 0.4586 | 0.1954 | 0.0591 | 0.0128 | 0.0028 | 0.0002 | |
| | 5 | *SIR* | -9.4 | -9.2 | -9.0 | -8.8 | -8.6 | -8.4 | -8.2 | -8.0 | |
| | | *PER* | 0.8169 | 0.6629 | 0.3153 | 0.1838 | 0.0355 | 0.0082 | 0.0012 | 0.0002 | |
| | 4.5 | *SIR* | -8.8 | -8.6 | -8.4 | -8.2 | -8.0 | -7.8 | -7.6 | -7.4 | |
| | | *PER* | 0.8472 | 0.6596 | 0.3198 | 0.1438 | 0.0332 | 0.0086 | 0.0010 | 0.0002 | |
| | 4 | *SIR* | -8.4 | -8.2 | -8.0 | -7.8 | -7.6 | -7.4 | -7.2 | -7.0 | |
| | | *PER* | 0.8308 | 0.8382 | 0.5631 | 0.3018 | 0.1258 | 0.0299 | 0.0048 | 0.0006 | |
| | 3.5 | *SIR* | -7.8 | -7.6 | -7.4 | -7.2 | -7.0 | -6.8 | -6.6 | -6.4 | |
| | | *PER* | 0.8710 | 0.7791 | 0.3851 | 0.1787 | 0.0437 | 0.0098 | 0.0022 | 0.0004 | |
| | 3 | *SIR* | -6.8 | -6.6 | -6.4 | -6.2 | -6.0 | -5.8 | -5.6 | -5.4 | |
| | | *PER* | 0.7179 | 0.4714 | 0.2470 | 0.0851 | 0.0242 | 0.0056 | 0.0008 | 0.0002 | |
| | 2.5 | *SIR* | -5.8 | -5.6 | -5.4 | -5.2 | -5.0 | -4.8 | -4.6 | -4.4 | |
| | | *PER* | 0.8000 | 0.4643 | 0.2981 | 0.1212 | 0.0293 | 0.0064 | 0.0010 | 0.0004 | |
| | 2 | *SIR* | -5.2 | -5.0 | -4.8 | -4.6 | -4.4 | -4.2 | -4.0 | -3.8 | -3.6 | |
| | | *PER* | 0.9636 | 0.7568 | 0.6019 | 0.3743 | 0.1384 | 0.0403 | 0.0080 | 0.0008 | 0.0004 | |
| | 1.5 | *SIR* | -3.8 | -3.6 | -3.4 | -3.2 | -3.0 | -2.8 | | | |
| | | *PER* | 0.5041 | 0.2331 | 0.0731 | 0.0108 | 0.0026 | 0.0004 | | | |
| | 1 | *SIR* | -1.8 | -1.6 | -1.4 | -1.2 | -1.0 | -0.8 | -0.6 | | |
| | | *PER* | 1.0000 | 1.0000 | 0.8923 | 0.5122 | 0.1183 | 0.0152 | 0.0006 | | |
| | 0.5 | *SIR* | 4.6 | 4.8 | 5.0 | 5.2 | 5.4 | | | | |
| | | *PER* | 1.0000 | 0.8750 | 0.2000 | 0.0036 | 0.0000 | | | | |
| 1560 | 8 | *SIR* | -8.4 | -8.2 | -8.0 | -7.8 | -7.6 | -7.4 | -7.2 | | |
| (QPSK) | | *PER* | 0.9811 | 0.8732 | 0.4689 | 0.1716 | 0.0270 | 0.0030 | 0.0008 | | |
| | 7 | *SIR* | -7.8 | -7.6 | -7.4 | -7.2 | -7.0 | -6.8 | -6.6 | | |
| | | *PER* | 0.9516 | 0.6542 | 0.2871 | 0.0641 | 0.0068 | 0.0008 | 0.0004 | | |
| | 6 | *SIR* | -6.8 | -6.6 | -6.4 | -6.2 | -6.0 | -5.8 | | | |

| | | | | | | | | | | | | |
|---|---|---|---|---|---|---|---|---|---|---|---|---|
| | | *PER* | 0.6602 | 0.2968 | 0.0896 | 0.0138 | 0.0008 | 0.0004 | | | | |
| | 5 | *SIR* | -5.8 | -5.6 | -5.4 | -5.2 | -5.0 | -4.8 | | | | |
| | | *PER* | 0.8095 | 0.5000 | 0.1348 | 0.0288 | 0.0054 | 0.0002 | | | | |
| | 4 | *SIR* | -5.2 | -5.0 | -4.8 | -4.6 | -4.4 | -4.2 | -4.0 | | | |
| | | *PER* | 0.9811 | 0.8657 | 0.5985 | 0.2008 | 0.0411 | 0.0044 | 0.0002 | | | |
| | 3 | *SIR* | -4.2 | -4.0 | -3.8 | -3.6 | -3.4 | -3.2 | | | | |
| | | *PER* | 1.0000 | 0.8125 | 0.2885 | 0.0710 | 0.0088 | 0.0004 | | | | |
| | 2 | *SIR* | -1.8 | -1.6 | -1.4 | -1.2 | -1.0 | -0.8 | | | | |
| | | *PER* | 1.0000 | 1.0000 | 0.8434 | 0.2204 | 0.0098 | 0.0000 | | | | |
| | 1 | *SIR* | 4.2 | 4.4 | 4.6 | 4.8 | 5.0 | 5.2 | | | | |
| | | *PER* | 1.0000 | 1.0000 | 0.9811 | 0.3386 | 0.0012 | 0.0000 | | | | |
| 2328 | 8 | *SIR* | -5.8 | -5.6 | -5.4 | -5.2 | -5.0 | -4.8 | | | | |
| (8PSK) | | *PER* | 1.0000 | 0.7600 | 0.4006 | 0.0781 | 0.0074 | 0.0004 | | | | |
| | 7 | *SIR* | -5.4 | -5.2 | -5.0 | -4.8 | -4.6 | -4.4 | -4.2 | | | |
| | | *PER* | 1.0000 | 0.9429 | 0.5987 | 0.1870 | 0.0288 | 0.0020 | 0.0002 | | | |
| | 6 | *SIR* | -4.8 | -4.6 | -4.4 | -4.2 | -4.0 | -3.8 | -3.6 | | | |
| | | *PER* | 1.0000 | 1.0000 | 0.9683 | 0.6000 | 0.1819 | 0.0268 | 0.0022 | | | |
| | 5 | *SIR* | -3.8 | -3.6 | -3.4 | -3.2 | -3.0 | -2.8 | -2.6 | -2.4 | | |
| | | *PER* | 1.0000 | 1.0000 | 0.9492 | 0.6835 | 0.2758 | 0.0464 | 0.0034 | 0.0002 | | |
| | 4 | *SIR* | -2.8 | -2.6 | -2.4 | -2.2 | -2.0 | -1.8 | -1.6 | -1.4 | | |
| | | *PER* | 1.0000 | 0.9365 | 0.8500 | 0.4150 | 0.1072 | 0.0094 | 0.0008 | 0.0002 | | |
| | 3 | *SIR* | -1.8 | -1.6 | -1.4 | -1.2 | -1.0 | -0.8 | -0.6 | | | |
| | | *PER* | 1.0000 | 0.9831 | 0.6930 | 0.2969 | 0.0370 | 0.0012 | 0.0002 | | | |
| | 2 | *SIR* | 1.2 | 1.4 | 1.6 | 1.8 | 2.0 | | | | | |
| | | *PER* | 0.9531 | 0.4490 | 0.0246 | 0.0004 | 0.0000 | | | | | |
| | 1 | *SIR* | 7.8 | 8.0 | 8.2 | 8.4 | | | | | | |
| | | *PER* | 1.0000 | 0.7941 | 0.0312 | 0.0000 | | | | | | |
| 3864 | 8 | *SIR* | -3.6 | -3.4 | -3.2 | -3.0 | -2.8 | -2.6 | -2.4 | | | |
| (16QAM) | | *PER* | 0.8986 | 0.5044 | 0.1255 | 0.0118 | 0.0038 | 0.0008 | 0.0004 | | | |
| | 7 | *SIR* | -3.4 | -3.2 | -3.0 | -2.8 | -2.6 | -2.4 | -2.2 | -2.0 | -1.8 | -1.6 |
| | | *PER* | 1.0000 | 0.9492 | 0.6972 | 0.2774 | 0.0535 | 0.0048 | 0.0016 | 0.0010 | 0.0008 | 0.0006 |
| | 6 | *SIR* | -2.8 | -2.6 | -2.4 | -2.2 | -2.0 | -1.8 | -1.6 | -1.4 | -1.2 | -1.0 |
| | | *PER* | 1.0000 | 1.0000 | 0.9333 | 0.6667 | 0.2385 | 0.0374 | 0.0038 | 0.0026 | 0.0008 | 0.0004 |
| | 5 | *SIR* | -1.4 | -1.2 | -1.0 | -0.8 | -0.6 | -0.4 | -0.2 | 0.0 | | |
| | | *PER* | 1.0000 | 0.8333 | 0.4673 | 0.1117 | 0.0146 | 0.0016 | 0.0018 | 0.0002 | | |
| | 4 | *SIR* | -0.8 | -0.6 | -0.4 | -0.2 | 0.0 | 0.2 | 0.4 | 0.6 | 0.8 | |
| | | *PER* | 1.0000 | 1.0000 | 0.9474 | 0.6967 | 0.2522 | 0.0431 | 0.0068 | 0.0028 | 0.0008 | |
| | 3 | *SIR* | 0.2 | 0.4 | 0.6 | 0.8 | 1.0 | 1.2 | 1.4 | 1.6 | | |
| | | *PER* | 1.0000 | 0.9655 | 0.7257 | 0.2582 | 0.0330 | 0.0030 | 0.0008 | 0.0002 | | |
| | 2 | *SIR* | 3.2 | 3.4 | 3.6 | 3.8 | | | | | | |
| | | *PER* | 0.9714 | 0.3215 | 0.0142 | 0.0002 | | | | | | |
| | 1 | *SIR* | 10.2 | 10.4 | 10.6 | 10.8 | | | | | | |
| | | *PER* | 0.9167 | 0.0314 | 0.0002 | 0.0000 | | | | | | |
| 4096 | 8 | *SIR* | -2.8 | -2.6 | -2.4 | -2.2 | -2.0 | -1.8 | | | | |
| (16QAM) | | *PER* | 0.8706 | 0.4194 | 0.0724 | 0.0185 | 0.0092 | 0.0056 | | | | |
| | 7 | *SIR* | -1.8 | -1.6 | -1.4 | -1.2 | -1.0 | -0.8 | -0.6 | -0.4 | -0.2 | |
| | | *PER* | 0.7843 | 0.3703 | 0.0847 | 0.0185 | 0.0126 | 0.0050 | 0.0036 | 0.0034 | 0.0008 | |
| | 6 | *SIR* | -1.2 | -1.0 | -0.8 | -0.6 | -0.4 | -0.2 | 0.0 | 0.2 | 0.4 | 0.6 |
| | | *PER* | 1.0000 | 0.8095 | 0.4679 | 0.0962 | 0.0253 | 0.0102 | 0.0054 | 0.0042 | 0.0036 | 0.0020 |
| | 5 | *SIR* | -0.6 | -0.4 | -0.2 | 0.0 | 0.2 | 0.4 | 0.6 | 0.8 | 1.0 | |
| | | *PER* | 1.0000 | 0.9655 | 0.7757 | 0.2457 | 0.0465 | 0.0176 | 0.0084 | 0.0056 | 0.0030 | |
| | 4 | *SIR* | 0.2 | 0.4 | 0.6 | 0.8 | 1.0 | 1.2 | 1.4 | 1.6 | 1.8 | 2.0 |
| | | *PER* | 0.7913 | 0.3442 | 0.0680 | 0.0159 | 0.0116 | 0.0066 | 0.0046 | 0.0044 | 0.0014 | 0.0002 |
| | 3 | *SIR* | 1.6 | 1.8 | 2.0 | 2.2 | 2.4 | 2.6 | 2.8 | 3.0 | 3.2 | 3.4 |
| | | *PER* | 1.0000 | 0.9677 | 0.6538 | 0.1408 | 0.0148 | 0.0070 | 0.0046 | 0.0030 | 0.0016 | 0.0004 |
| | 2 | *SIR* | 5.2 | 5.4 | 5.6 | 5.8 | 6.0 | 6.2 | | | | |
| | | *PER* | 0.7290 | 0.0436 | 0.0020 | 0.0022 | 0.0006 | 0.0004 | | | | |
| | 1 | *SIR* | 13.4 | 13.6 | 13.8 | 14.0 | | | | | | |
| | | *PER* | 1.0000 | 0.6453 | 0.0012 | 0.0000 | | | | | | |

| | | | | | | | | | | | |
|---|---|---|---|---|---|---|---|---|---|---|---|
| 408 | 1/3 | *SIR* | 1.2 | 1.4 | 1.6 | 1.8 | 2.0 | 2.2 | 2.4 | 2.6 | 2.8 |
| (8PSK) | | *PER* | 1.0000 | 0.9048 | 0.7317 | 0.4511 | 0.1833 | 0.0459 | 0.0062 | 0.0014 | 0.0004 |
| 792 | 1/3 | *SIR* | 8.2 | 8.4 | 8.6 | 8.8 | 9.0 | | | | |
| (8PSK) | | *PER* | 0.8814 | 0.2228 | 0.0094 | 0.0002 | 0.0000 | | | | |
| 408 | 2 | *SIR* | -6.4 | -6.2 | -6.0 | -5.8 | -5.6 | -5.4 | -5.2 | -5.0 | -4.8 |
| (16QAM) | | *PER* | 0.4706 | 0.2754 | 0.1756 | 0.0773 | 0.0390 | 0.0136 | 0.0054 | 0.0008 | 0.0004 |
| | 1 | *SIR* | -3.4 | -3.2 | -3.0 | -2.8 | -2.6 | -2.4 | -2.2 | -2.0 | -1.8 | -1.6 |
| | | *PER* | 0.6000 | 0.4184 | 0.3387 | 0.1404 | 0.0845 | 0.0369 | 0.0114 | 0.0044 | 0.0018 | 0.0004 |
| 792 | 2 | *SIR* | -3.4 | -3.2 | -3.0 | -2.8 | -2.6 | -2.4 | -2.2 | | |
| (16QAM) | | *PER* | 0.5882 | 0.2857 | 0.1501 | 0.0578 | 0.0154 | 0.0042 | 0.0006 | | |
| | 1 | *SIR* | -0.4 | -0.2 | 0.0 | 0.2 | 0.4 | 0.6 | 0.8 | 1.0 | |
| | | *PER* | 0.8209 | 0.6154 | 0.4189 | 0.2097 | 0.0788 | 0.0243 | 0.0072 | 0.0008 | |

Table B.7. The SIR penalties, $\gamma_{pen}$, for transmission of a packet using a larger constellation.

| *Original constellation* | *Larger constellation applied* | $\gamma_{pen}$ *(dB)* |
|---|---|---|
| QPSK | 8 PSK | 2.7 |
| QPSK | 16 QAM | 4.7 |
| 8 PSK | 16 QAM | 2.1 |

# Appendix C

# Sector Antenna Radiation Pattern

Sectorized antennas are used in simulations throughout Chapters 4 and 5. The antenna pattern used is from a commercially available antenna with a $65^0$ 3dB beamwidth, and is used for the home sector, and all interfering sectors. The radiation pattern is shown in Figure C.1.

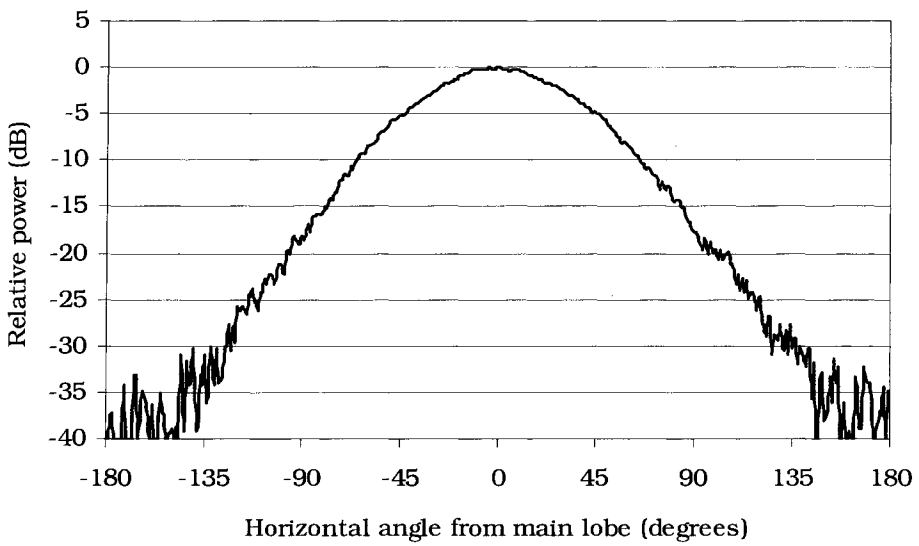


Figure C.1. The horizontal radiation pattern of the sector antennas used in Chapters 4 and 5. Power is normalized to the power of the centre of the main lobe.

# Appendix D

# Determination of Appropriate Sub-band Configurations for SS-OFDM-F/TA

Proper design of the SS-OFDM-F/TA relies on sub-bands that are narrower than the coherence bandwidth of the channel so that the sub-bands are not averaging over the frequency diversity of the channel. This is significant because variation of the received SIR in the sub-bands allows multi-user diversity to be exploited. In addition, the narrower the sub-bands are, the less inter-code interference will be produced as the channel will be nearly flat over the sub-bands. It is important that the sub-bands are only as narrow as required to gain benefits from multi-user diversity and lowered inter-code interference, because systems with many excessively narrow sub-bands waste resources on reverse link signalling for each sub-band, and restrict the packet transmission size leading to an inefficient system.

This appendix determines the appropriate number of sub-bands for a given channel; where the measure of performance will be the gain in the average received SINR during scheduled transmissions due to multi-user diversity and sub-band partitioning in a simple single cell model. This is an appropriate measure as it takes into account the gain due to multi-user diversity given a specific configuration, as well as the inter-code interference in the system. This investigation is conducted for the indoor and pedestrian channels. The vehicular channel design is discussed extensively in Section 4.7.

As in Chapter 4, the average received SINR during scheduled transmissions, $\overline{\gamma}$, with $M$ sub-bands and $U$ users is given by:

$$\overline{\gamma}(U,M) = \mathrm{E}\left[\frac{1}{M}\sum_{m=0}^{M-1}\max_{0\le u<U}\gamma_m^{(u)}\right] \tag{D.1}$$

where $\mathrm{E}[X]$ denotes the expectation of $X$, and it is assumed that long-term fading statistics in each sub-band are identical.

For this investigation, the simple case of $U$ mobiles with identical average $E_s/N_o$= 0 dB are considered. Channel variations are due to Rayleigh fading only. The system configurations are given in Table D.1 for the indoor and pedestrian channels. As this investigation focuses solely on the minimum frequency resolution of the system, the time slot duration is not considered, however, it is assumed that the time slot duration is significantly less than the coherence time of the channel.

Table D.1. System parameters.

| | *Indoor channels* | *Pedestrian channels* |
|---|---|---|
| Bandwidth | 10 MHz | 5 MHZ |
| Main lobe bandwidth | 9.5157 MHz | 4.7486 MHz |
| Subcarriers ($N$) | 256 | 512 |
| Symbol duration ($T_{sym}$) | 27.008 μs | 108.032 μs |
| Cyclic prefix ($T_g$) | 1 μs | 4 μs |

In the Indoor A channel (Figure D.1), it is clear that $M = 4$ is sufficient to exploit the multi-user diversity in the system, given the system parameters. The Indoor B channel, which is shown in Figure 4.2 in Chapter 4, requires $M = 8$ to exploit the multi-user diversity of the channel. Hence, in this thesis the indoor channel is always simulated with $M = 8$ sub-bands so that maximum multi-user diversity is being exploited.

In the Pedestrian A channel (Figure D.2) there is almost no frequency selective fading. $M = 2$ sub-bands is sufficient in this channel, however, as narrower sub-bands are required in the Pedestrian B channel, $M$=4 is generally used in this thesis. The $M$=4 sub-bands correspond to the $M_{eff} = M_n/M_g = 32/8 = 4$ effective sub-bands (or parallel channels) created in the formation of disjoint groups of sub-bands (see Section 4.5). Note that the use of sub-band grouping in general in the Pedestrian channels does not change the performance of the system in the Pedestrian A channel, as there is no loss associated with sub-band grouping in non-selective channels. Allocation of $M = 4$ single sub-bands can be seen as special case of sub-band grouping in which 4 groups of 8 adjacent sub-bands are allocated. Hence, the $M$= 4 system gives the worst-case performance for the (32,8) sub-bands grouping configuration in the Pedestrian A channel, as the formation of sub-band groups is fixed (4 groups of 8 adjacent sub-bands) and not adaptive.

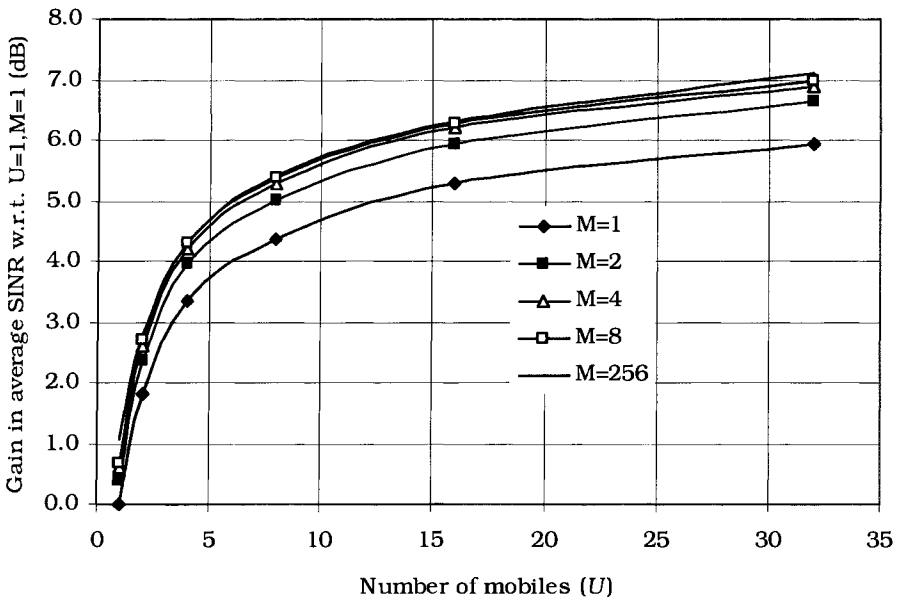


Figure D.1. The normalized gain in average SINR for the Indoor A Channel.

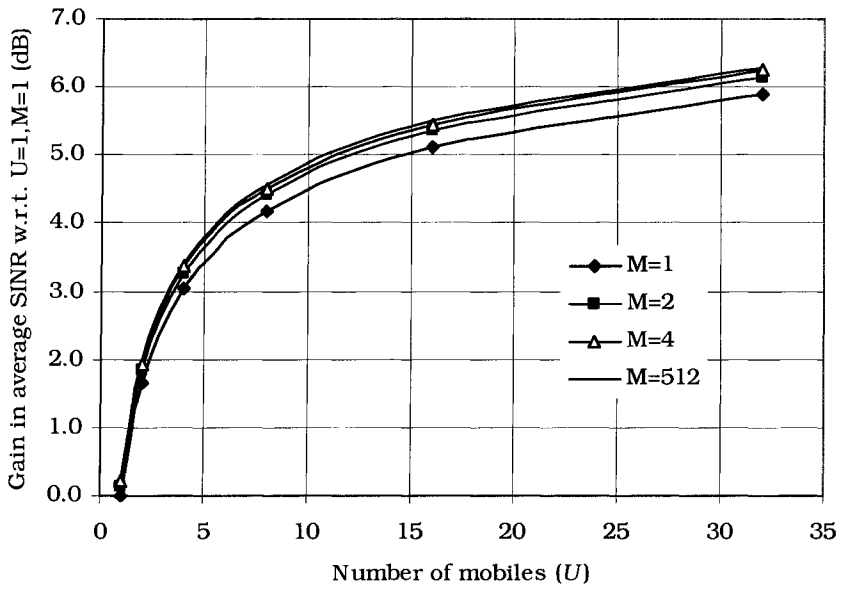


Figure D.2. The normalized gain in average SINR for the Pedestrian A Channel.

# Appendix E

# Inter-code Interference for SS-OFDM-F/TA with QAM Constellations

In the derivation of the inter-code interference and SINR in Section 2.3, and later applied to SS-OFDM-F/TA in Section 4.2, it is assumed that the modulation on each spreading code is the same. Obviously, if a QAM constellation is used, code channels may be modulated by complex symbols with different amplitudes. It can then be postulated whether or not the expression given in (4.3) for the SINR in the $m^{th}$ sub-band can be used with link level results for accurate simulation of system using QAM. This appendix shows that it is acceptable for constellations at least as large as 64 QAM for full loaded systems with $L >> 1$.

The SINR in the $m^{th}$ sub-band as derived in Section 4.2 for QPSK modulation is given by:

$$\gamma_m = \frac{\mu_{A_m}^2}{\sigma_{A_m}^2 \frac{L-1}{L} + \frac{N_0}{E_s}\mu_{B_m}} \tag{E.1}$$

where $A_m$ and $B_m$ are given in (4.4) and (4.5), and the user index $u$ is dropped as only one receiver is considered in this discussion. It can be seen that this expression assumes that all code channels are transmitted at the same energy per symbol. The SINR found in (E.1) can then be compared to link level results for turbo coding and QPSK modulation of a packet in AWGN with the same $E_s / N_0$.

For the case of QAM modulation, the situation is slightly more complex. A more general expression for SINR in QAM systems can be given as:

$$\gamma_m^{(i)} = \frac{E_s^{(i)} \mu_{A_m}^2}{\sigma_{A_m}^2 \frac{\sum_{k=1}^{L-1} E_s^{(k)} - E_s^{(i)}}{\sum_{k=1}^{L-1} E_s^{(k)}} + N_0 \mu_{B_m}} \tag{E.2}$$

where $E_s^{(i)}$ is the energy of the $i^{th}$ complex QAM data symbol, on the $i^{th}$ code channel. Note that the SINR varies with the channel gains, but also with the desired and interfering symbol energies that change due to QAM.

In order to use the QAM link level results in an AWGN environment from Appendix B in system level simulations in a frequency selective channel, it is inherently assumed (from the first term of the denominator in (E.2)) that:

$$\frac{\sum_{k=0}^{L-1} E_s^{(k)} - \max_{0 \le i \le L} E_s^{(i)}}{\sum_{k=0}^{L-1} E_s^{(k)} - \min_{0 \le i \le L} E_s^{(i)}} \approx 1 \tag{E.3}$$

where the "min" and "max" refer to amplitude levels of the given QAM constellation. If $K=L$ is very large, the condition in (E.3) is automatic as the inter-code interference is nearly the same for all symbols as $\sum_{k=0}^{L-1} E_s^{(k)} - E_s^{(i)} \approx \sum_{k=0}^{L-1} E_s^{(k)}$. Generalizing from this statement, if the difference between the largest and smallest symbol energy level for the QAM scheme is quite small compared to $\sum_{\substack{k=0 \\ k \neq i}}^{L-1} E_s^{(k)}$ as described by (E.3), then inter-code interference will be virtually the same for all cases. In this manner, if $L$ is sufficiently large the SINR can be given by:

$$\gamma_m^{(i)}(E_s^{(i)}, E_s^{ave}) = \frac{E_s^{(i)} \mu_{A_m}^2}{\sigma_{A_m}^2 \frac{L-1}{L} E_s^{ave} + N_0 \mu_{B_m}} \tag{E.4}$$

where $E_s^{ave} = \underset{\text{constellation}}{\mathrm{E}} [E_s^{(i)}]$ is the average symbol energy over the entire constellation. It is also important to note that the above discussion only applies to the case of frequency selective fading across the sub-band. If the subchannel gains are the same across the sub-band, the variance of the equalized channel gains, $\sigma_{A_m}^2$, will be zero. Similarly, if the fading across the sub-band is relatively flat, or if the subchannel gains are highly correlated across the sub-bands, the effect of various levels of inter-code interference will be negligible. In addition, if $E_s^{(i)} / N_0$ is sufficiently high, the MMSE becomes closer to a

zero-forcing algorithm as $\lambda = \frac{LN_0}{\sum_{k=0}^{L-1} E_s^{(k)}}$ approaches zero, which reduces the impact of inter-code interference.

In summary, the primary factors that determine whether (E.4) can be used with QAM link level results in AWGN for the SS-OFDM system are the size of $L$, the values of $\sigma_{A_m}^2$, the relationship in (E.3), the $E_s^{(i)}/N_0$, and the probability with which each amplitude level is chosen (which is the property of a given QAM constellation). The relevance of these factors on the performance of the SS-OFDM-F/TA system can be seen by comparing 2 PDFs of the SINRs, namely one SINR that varies with the distribution of channel gains, QAM symbol amplitudes, and the resulting variation of inter-code interference due to both these factors, and the PDF of another SINR that varies with the distribution of channel gains, QAM symbol amplitudes, and the resulting variation of inter-code interference due to equalized channel gain variances only. These two SINRs are given by:

$$\gamma_m(E_s^{(i)}, E_s^{(0)}, \ldots, E_s^{(k)}, \ldots, E_s^{(K-1)}) = \frac{E_s^{(i)}\mu_{A_m}^2}{\sigma_{A_m}^2 \frac{\sum_{k=1}^{K-1} E_s^{(k)} - E_s^{(i)}}{\sum_{k=1}^{K-1} E_s^{(k)}} + N_0\mu_{B_m}} \tag{E.5}$$

$$\gamma_m(E_s^{(i)}, E_s^{ave}) = \frac{E_s^{(i)}\mu_{A_m}^2}{\sigma_{A_m}^2 \frac{K-1}{L} E_s^{ave} + N_0\mu_{B_m}} \tag{E.6}$$

where (E.5) is the proper form of the SINR (relevant to this section), and (E.6) is the SINR model that results from the approximations of the system and link level models used in this thesis.

The comparison of the distributions for (E.5) and (E.6) are given in Figure E.1 for 64 QAM. $L$=$K$=32 is the lowest processing gain considered in this thesis for SS-OFDM-F/TA systems. Independent subcarrier fading is assumed, which corresponds to a worst-case scenario of inter-code interference. Almost 375000 SINR samples were generated for each distribution, where each sample represents the average SINR assuming Gaussian distributed noise and inter-code interference. Figure E.1 clearly shows that for the minimum $L$=$K$=32 case considered in this thesis, the effect of assuming SINRs given by (E.5) instead of (E.6) instead of E.6 results in virtually the same SINR distribution.

It should be noted that the similarities in the distributions shown in Figure E.1 apply only for large groups of symbols over which many SINR realizations occur. As absolute differences between (E.5) and (E.6) of 0.1 dB or more are typical for one QAM symbol,

evaluation of errors for short transmissions (i.e., frame containing only a few symbols) may differ significantly between the 2 models. Figure E.2 shows the square-root of the mean-squared error ($\sqrt{MSE}$) of the average SINR in dB given by (E.6), in comparison to (E.5), for different frame sizes and spreading gains $L$=8 and $L$=32. It is assumed that frames less than $L$ are transmitted entirely within a single SS-OFDM symbol.

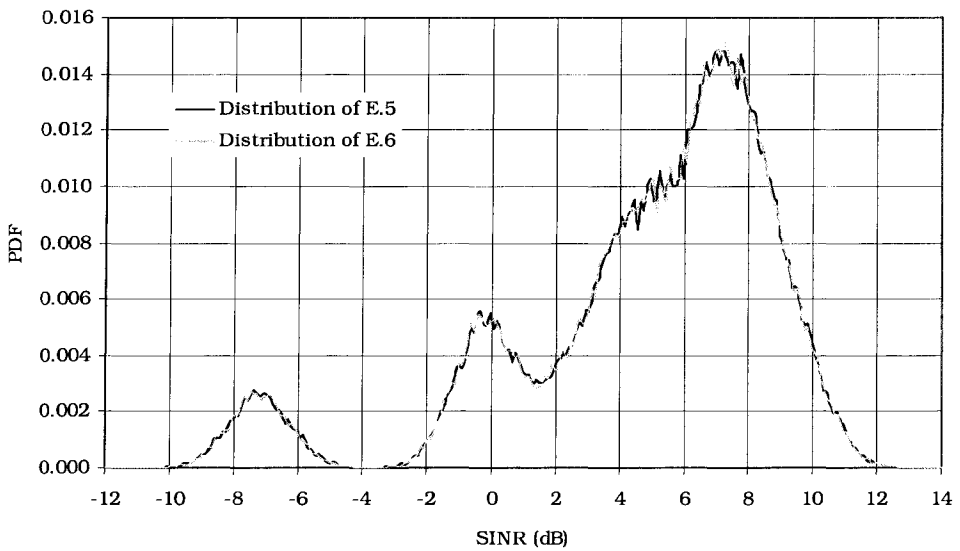


Figure E.1. The distribution of SINRs given by (E.5) and (E.6). $K$=$L$=32 and $E_s/N_0$ = 10 dB. Independent subcarrier fading is assumed.

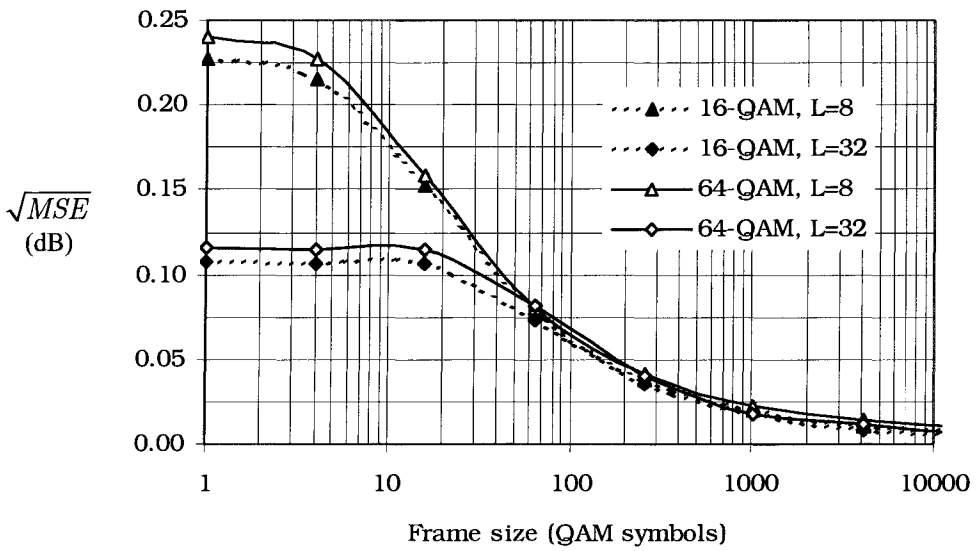


Figure E.2. The $\sqrt{MSE}$ of the approximate model for the SINR of a QAM symbol for spreading gains of $L$=8 and $L$=32; $E_s/N_0$ = 10 dB. Independent subcarrier fading is assumed.

# Appendix F

# Derivation of MMSE Equalization Coefficient Formula for Chip-Level MRC of Diversity Replicas

In Chapter 6, Equation (6.18) gives the appropriate closed form expression for a tap gain coefficient for minimum mean-squared error (MMSE) equalization under chip-level MR combining. In this appendix, it is explicitly shown that (6.18) is indeed the proper coefficient to jointly perform MR combining of chips, and then perform proper MMSE equalization of the combined chip sequence.

In Chapter 2, the general formula for the MMSE coefficients for a single SS-OFDM symbol are given in (2.9), and is used in Chapter 2, 3, 4 and 5. This is a special case of the final result given in this Appendix, in which there is only one diversity replica (i.e., $T = 1$).

The mean-squared error is given by

$$J = E\left[|\varepsilon|^2\right] = E\left[s - \hat{s}\right]^2 \tag{F.1}$$

For the system in Chapter 6, the fully loaded ($K$=$L$) SS-OFDM signal prior to sub-carrier mapping is given by:

$$s = \sum_{k=0}^{L-1}\sum_{l=0}^{L-1} b_k c_{k,l} \tag{F.2}$$

and the estimate of the signal for the $t^{th}$ diversity replica at the receiver after subcarrier demapping is given by

$$\hat{s}_t = \sum_{k=0}^{L-1} b_k c_{k,l} g_{l,t} h_{l,t} + g_{l,t}\eta_{l,t} \tag{F.3}$$

In Section 6.3, the information transmitted on the $l^{th}$ subcarriers for the $t^{th}$ and $(t+1)^{th}$ diversity replicas are identical. The symbol energy of each transmission is $E_s$.

Maximal ratio combing (MRC) of the chips on the $l^{th}$ subcarriers, followed by equalization by $g'_{l,t} = g'_{l,t+1}$, gives the mean squared error:

$$
\begin{aligned}
J &= E\left[\left|\varepsilon_l\right|^2\right] = E\left[\left|s_{l,t} - \sum_{t'=t}^{t+1} h^*_{l.t}\hat{s}_{l,t'}\right|^2\right] \\
&= E\left[\left|\sum_{k=0}^{L-1} c_{k,l}b_k - \sum_{k=0}^{L-1} c_{k,l}b_k h_{l.t}g'_{l,t}h^*_{l,t} - g'_{l,t}\eta_{l,t}h^*_{l,t} - \sum_{k=0}^{L-1} c_{k,l}b_k h_{l.t+1}g'_{l,t+1}h^*_{l,t+1} - g'_{l,t+1}\eta_{l,t+1}h^*_{l,t+1}\right|^2\right] \\
&= E\left[\left|\sum_{k=0}^{L-1} c_{k,l}b_k - \sum_{k=0}^{L-1} c_{k,l}b_k g'_{l,t}\left|h_{l,t}\right|^2 - \sum_{k=0}^{L-1} c_{k,l}b_k g'_{l,t+1}\left|h_{l,t+1}\right|^2 - g'_{l,t}\eta_{l,t}h^*_{l,t} - g'_{l,t+1}\eta_{l,t+1}h^*_{l,t+1}\right|^2\right] \\
&= E\left[\left|\sum_{k=0}^{L-1} c_{k,l}b_k - \sum_{k=0}^{L-1} c_{k,l}b_k g'_{l,t}\left(\left|h_{l,t}\right|^2 + \left|h_{l,t+1}\right|^2\right)\right|^2\right] + E\left[\left|g'_{l,t}\eta_{l,t}h_{l,t}\right|^2\right] + E\left[\left|g'_{l,t+1}\eta_{l,t+1}h_{l,t+1}\right|^2\right]
\end{aligned}
\tag{F.4}
$$

Note that the expectation over all data modulated, normalized spreading sequences is simply the data symbol energy, $E\left[\left|\sum_{k=0}^{L-1} c_{k,l}b_k\right|^2\right] = \left|\sum_{k=0}^{L-1} b_k\right|^2 / L = E_s$. Furthermore, the mean of $\sum_{k=0}^{L-1} c_{k,l}b_k$ is zero, and hence:

$$
\begin{aligned}
J &= \left|1 - g'_{l,t}\left|h_{l,t}\right|^2 - g'_{l,t}\left|h_{l,t+1}\right|^2\right|^2 E_s + \left|g'_l\right|^2\left(\left|h_{l,t}\right|^2 + \left|h_{l,t+1}\right|^2\right)N_0 \\
&= \begin{pmatrix} 1 - g'_{l,t}\left|h_{l,t}\right|^2 - g'_{l,t}\left|h_{l,t+1}\right|^2 - 1 + \left|g'_{l,t}\right|^2\left|h_{l,t}\right|^4 + \left|g'_{l,t}\right|^2\left|h_{l,t+1}\right|^2\left|h_{l,t}\right|^2 \\ -1 + \left|g'_{l,t}\right|^2\left|h_{l,t+1}\right|^4 + \left|g'_{l,t}\right|^2\left|h_{l,t+1}\right|^2\left|h_{l,t}\right|^2 \end{pmatrix} E_s \\
&\quad + \left|g'_l\right|^2\left(\left|h_l\right|^2 + \left|h_{l,t+1}\right|^2\right)N_0
\end{aligned}
\tag{F.5}
$$

The value of $g'_{l,t}$ for which (F.5) is minimized is found by:

$$
\begin{aligned}
&\frac{\partial E[|\varepsilon|^2]}{\partial\left|g'_{l,t}\right|} = 0 \\
&\quad = \left(-\left|h_{l,t}\right|^2 - \left|h_{l,t+1}\right|^2 + 2\left|g'_{l,t}\right|\left|h_{l,t}\right|^4 + 2\left|g'_{l,t}\right|\left|h_{l,t+1}\right|^4 + 4\left|g'_{l,t}\right|\left|h_{l,t}\right|^2\left|h_{l,t+1}\right|^2\right) \\
&\quad + 2\left|g'_{l,t}\right|\left(\left|h_{l,t}\right|^2 + \left|h_{l,t+1}\right|^2\right)N_0 / E_s
\end{aligned}
\tag{F.6}
$$

Solving for $g'_{l,t}$, the MMSE coefficient becomes

$$g'_{l,t} = \frac{\left|h_{l,t}\right|^2 + \left|h_{l,t+1}\right|^2}{(2\left|h_{l,t}\right|^4 + 2\left|h_{l,t+1}\right|^4 + 4\left|h_{l,t+1}\right|^2\left|h_{l,t}\right|^2) + (2\left|h_l\right|^2 + 2\left|h_{l,t+1}\right|^2)N_0 / E_s}$$
$$= \frac{1/2}{(\left|h_{l,t}\right|^2 + \left|h_{l,t+1}\right|^2) + N_0 / E_s} \tag{F.7}$$

In equation (F.7), the factor of ½ can be dropped as it is simply a scalar multiple that affects both diversity replicas equally, and does not impact the equalization in any way. Note that the SNR in the denominator of the coefficient is the SNR per transmission, and not for both diversity replicas. Replacing the SNR per transmission by $\lambda = N_0 / E_s$, the single-tap per subcarrier equalizer coefficient is given by:

$$g'_{l,t} = \frac{1}{(\left|h_{l,t}\right|^2 + \left|h_{l,t+1}\right|^2) + \lambda} \tag{F.8}$$

The MRC operation can be combined with the MMSE equalization, so the multiplication of the $l^{th}$ subcarrier by $g_{l,t}$ for the $t^{th}$ transmission, and by $g_{l,t+1}$ for the $(t+1)^{th}$ transmission is all that is required, as implied in (6.18). The extension of this derivation to multiple re-transmissions is easily achieved, and hence, the equalization coefficient for chip-level MRC of diversity replicas, followed by appropriate MMSE equalization is given by:

$$g_{l,t} = \frac{h^*_{l,t}}{\sum_{t=0}^{T-1}\left|h_{l,t}\right|^2 + \lambda} \tag{F.9}$$

# Appendix G

# Multi-cell Simulation Statistical Significance Assessment

This thesis has used extensive simulations to evaluate the performance of the SS-OFDM-F/TA system. It is necessary to investigate the statistical significance of these large simulations. In this section the reproducibility of the results is examined. The simulation structure contains two parts: the link level PER simulations and the system level simulations. The confidence intervals for each part can be determined by using the bootstrap principle [122], which is described in detail below.

The *bootstrap method* utilizes resampling of a given data set with replacement in order to estimate the reproducibility of the mean value. For example, given a specific set of $N_{data}$ values, the mean is given by $\mu_{data}$. In order to determine the confidence intervals for the result $\mu_{data}$, $N_{boot}$ sets of $N_{data}$ samples are taken from the original data with replacement to create $N_{boot}$ bootstrapped sets of data, from which $N_{boot}$ bootstrapped sample means are found. The confidence intervals of the mean of the original $N_{data}$ values can then be found from the distribution of the $N_{boot}$ bootstrapped sample means. It is convenient to consider the distribution of the *deviations about the mean*, rather then the distribution of the actual means in this section. Figure G.1 shows the CDF of the deviations of the $N_{boot} = 1000$ bootstrapped sample means, sampled from the $N_{data} = 100$ system simulation runs for Configuration I in the Vehicular A channel (as discussed in Section 4.7). The confidence intervals are readily determined from the CDF of the deviations about the mean and are shown on the figure.

The reproducibility of the total average throughput per cell can be determined by combining variances of the system and link level results, and approximating the distribution of deviations about the mean throughput as Gaussian. The distribution of the deviations from the mean for the entire link/system simulation can be considered

Gaussian as long as the link and system level distributions of deviations from the mean can also be approximated as Gaussian. It is shown that this is the case in the following two sections, and hence, the standard deviation of the *deviations about the mean* for the $N_{boot}$ is recorded for the link and system level simulations so that they can be combined in the final section to estimate the confidence intervals for the entire simulation method.

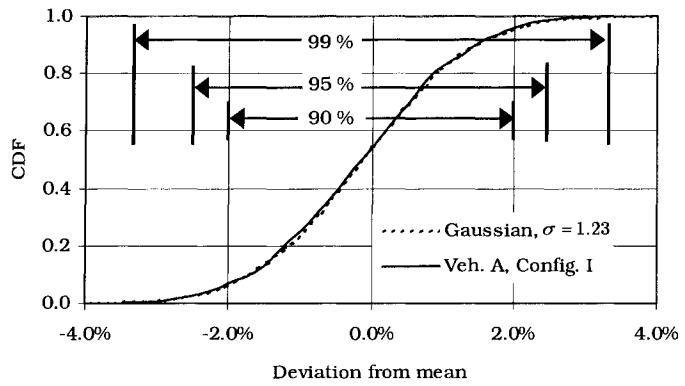


Figure G.1. The distribution of the deviations of the means of the bootstrapped sets. The comparison to a Gaussian distribution is also shown.

The following three sections determine the confidence intervals and standard deviations of the bootstrapped means for the link and system level simulation segments, and then approximate the overall reproducibility of the results. This appendix focuses specifically on the average cell throughput results presented in Chapters 4 and 5 of this thesis.

# G.1 Link Level Simulations

As described in Section 4.3, the link level results determine the packet error rate curves (PER) for each packet format, and number of re-transmissions, used in this thesis. Each point of a curve was the result of a minimum of 5000 trials. It is useful to approximate the accuracy of these simulations in order to approximate the reproducibility of the results from the entire simulation model. As the PER 1% is the operating target of the system level simulations, it can be estimated that the reproducibility of the link level simulations at 1% PER should be determined.

As per the discussion of the bootstrap method, the distribution of the deviations of the means of the 1000 bootstrapped sample sets for the PER is recorded. The confidence intervals at a PER of 1 % are given in Table G.1.

Table G.1 Confidence intervals for link level simulations of 5000 frames at a PER of 1%.

| Confidence Intervals at 1% PER (x $10^{-2}$) | | |
|---|---|---|
| 99% | 95% | 90% |
| {0.66, 3.4} | {0.74, 2.6} | {0.78, 2.2} |

The primary concern of this section is to find the effect of the inaccuracies of link level simulations on the final throughput value of the entire cellular simulation. The standard deviation of the PER bootstrapped means is related to the throughput of the cellular system by first plotting the mean $PER(1 \pm \sigma_{PER})$ for each curve (see Figure G.2). As an approximation, the standard deviation of the PER is related to the standard deviation of the SIR values via these curves. From the value of $\sigma_{SIR}$, an approximate value for the resulting standard deviation in throughput must be estimated. From the expression of maximum spectral efficiency given by (4.1), the maximum relative increase in throughput $d[C/B]$, due to a relative increase in SIR $d\gamma$ is given by ($P_i = 1$):

$$d[C/B] = \frac{\log_2(1+\gamma d\gamma)}{\log_2(1+\gamma)} \leq d\gamma \tag{G.1}$$

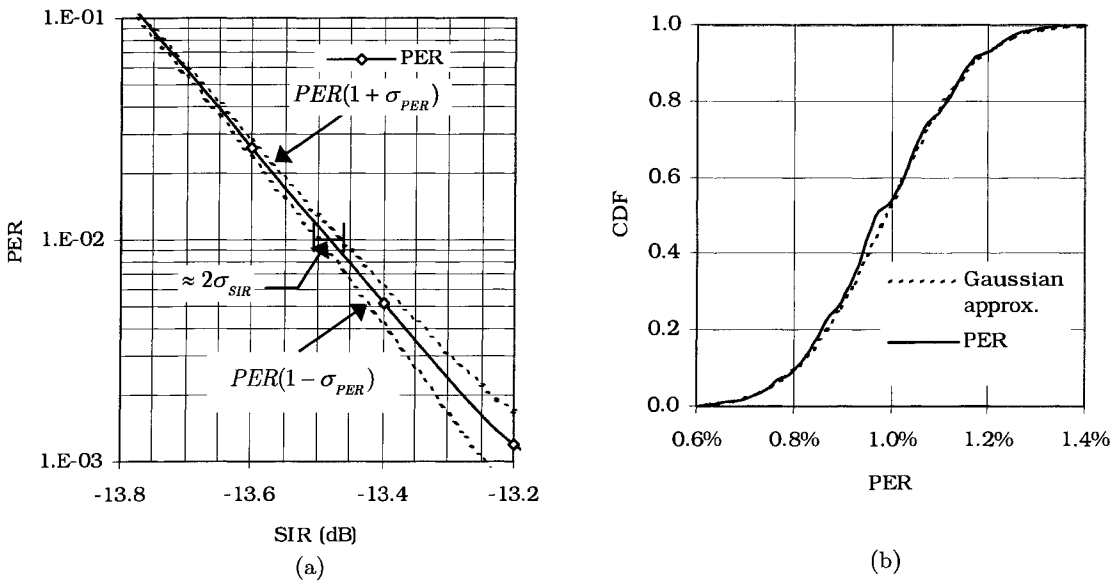


Figure G.2. The estimation of the standard deviation of $\sigma_{SIR}(dB)$ from the link level PER curves (a) and the comparison of the deviation of the bootstrapped PER means to a Gaussian distribution (b); $S_{trans}$= 2048 symbols and 16 transmissions.

For the purpose of determining the worst case based on (G.1), a linear relationship between the relative change in SIR and the resulting relative change in throughput is assumed such that $\sigma_{SIR}(dB) \approx \sigma_{link}(dB)$. The link level standard deviation is expressed as a percentage by $\sigma_{link}(\%) = 100\{10^{[\sigma_{link}(dB)/10]} - 1\}$.

The standard deviation of the PER depends on the packet structure, format and number of re-transmissions. In terms of this analysis, the worst case (lowest slope on Figure G.2) occurs for the smallest packet size and the maximum number of transmissions. The resulting $\sigma_{link}$ values are given in Table G.2 for these cases (see Appendix B for packet structure details).

Table G.2. Link level confidence intervals standard deviations for different packet structures.

| | $\sigma_{SIR}$ | $\sigma_{link}$ |
|---|---|---|
| Chapter 4 | | |
| $S_{trans}$= 2048 | 0.03 dB | 0.69 % |
| $S_{trans}$= 512 (Vehicular only) | 0.04 dB | 0.93 % |
| $S_{trans}$= 128 (Vehicular only) | 0.05 dB | 1.16 % |
| Chapter 5 | 0.03 dB | 0.69 % |

## G.2 System Level Simulations

The system level simulations include modelling of shadowing, random mobile positions, multi-user selection, sub-bands allocation, transmission and re-transmissions of packets. The system level simulations determine the mean cell/sector throughput as the average of 100 runs, or 60 runs in the vehicular model analysis in Section 4.7. The reproducibility of the results in this thesis can be found via the bootstrap method [122]. 1000 sets of values are sampled with replacement from the 100 (or 60 in the vehicular case) simulation runs' values of the mean throughput. The mean of each 1000 sample bootstrapped set is compared to the average throughput. The 90, 95 and 99% confidence intervals can then be readily determined from the CDF of the deviation of the bootstrapped means, as was shown in Figure G.1. Tables G.3 and G.4 list the confidence intervals for some of the significant system level simulations used in this thesis. As this thesis is primarily concerned with multi-user cases, the results for $U = 32$ and $U = 8$ simulations are shown. Clearly the results for 32 users are more reliable. In addition, the indoor results are less reproducible due to the higher probability of a user suffering an outage for an extended period than in the pedestrian environment.

Table G.3. System level simulation confidence intervals for cases considered in Chapter 4

| | *Confidence intervals (% of mean) U=32* | | | *Confidence Intervals (% of mean) U=8* | | |
|---|---|---|---|---|---|---|
| | 99 % | 95 % | 90 % | 99 % | 95 % | 90 % |
| Indoor A | {-3.0, 3.0} | {-2.3, 2.2} | {-1.9, 1.8} | {-5.9, 6.2} | {-4.7, 4.7} | {-3.9, 4.1} |
| Indoor B | {-2.9, 2.9} | {-2.3, 2.2} | {-1.8, 1.8} | {-5.8, 5.8} | {-4.9, 4.6} | {-4.1, 3.8} |
| Pedestrian A | {-1.7 1.8} | {-1.3, 1.4} | {-1.1, 1.2} | {-5.0, 5.1} | {-3.6, 3.6} | {-3.0, 2.9} |
| Ped. B (4,1) | {-2.2, 2.5} | {-1.7, 1.6} | {-1.4, 1.4} | {-4.1, 4.6} | {-3.4, 3.6} | {-2.9, 3.1} |
| Ped, B (32,8) | {-1.8, 2.1} | {-1.4, 1.5} | {-1.1, 1.2} | {-3.9, 4.5} | {-3.0, 3.6} | {-2.6, 2.8} |
| Vehicular A | | | | | | |
| Config. I | {-3.3, 2.4} | {-2.3, 2.4} | {-2.0, 2.0} | {-6.1, 7.1} | {-5.0, 5.3} | {-4.3, 4.5} |
| Config. III | {-2.2, 2.5} | {-1.8, 1.7} | {-1.6, 1.5} | {-6.0, 6.7} | {-4.8,4.6} | {-4.0, 3.6} |
| Config. IV | {-2.8, 2.7} | {-2.2, 2.1} | {-2.8, 2.7} | {-6.5, 6.8} | {-5.0, 4.7} | {-4.2, 3.9} |
| Config. V | {-2.6, 2.6} | {-1.9, 2.0} | {-1.7, 1.7} | {-6.5, 7.1} | {-5.2, 5.7} | {-4.3, 4.6} |
| Config. VII | {-4.1, 3.7] | {-3.1, 3.0} | {-2.6, 2.6} | {-7.2, 7.6} | {-5.1, 5.7} | {-4.6, 4.5} |
| Vehicular B | | | | | | |
| Config. I | {-3.0, 3.1} | {-2.3, 2.2} | {-1.9, 1.8} | {-7.2, 6.5} | {-5.1, 5.5} | {-4.4, 4.4} |
| Config. III | {-2.6, 2.8} | {-1.9, 2.0} | {-1.6, 1.7} | {-6.5, 6.2} | {-5.1, 4.8} | {-4.2, 3.9} |
| Config. IV | {-2.8, 2.6} | {-2.1, 2.1} | {-1.7, 1.9} | {-6.4, 6.8} | {-4.9, 5.0} | {-4.3, 4.2} |
| Config. V | {-2.9, 2.9} | {-2.1, 2.2} | {-1.7, 1.8} | {-6.3, 6.7} | {-5.0, 5.3} | {-4.4, 4.3} |
| Config. VII | {-3.7, 3.7} | {-3.0, 2.7} | {-2.5, 2.3} | {-7.6, 6.6} | {-5.4, 5.4} | {-4.6, 4.5} |

Table G.4. System level simulation confidence intervals for cases considered in Chapter 5

| | *Confidence intervals U=32* | | | *Confidence Intervals U=8* | | |
|---|---|---|---|---|---|---|
| | 99 % | 95 % | 90 % | 99 % | 95 % | 90 % |
| Indoor B | | | | | | |
| sync., D | {-2.5, 2.6} | {-2.0, 1.8} | {-1.7, 1.6} | {-7.6, 7.2} | {-5.2, 6.1} | {-4.6, 4.9} |
| async., D | {-2.3, 2.8} | {-2.0, 2.0} | {-1.8. 1.8} | {-7.0, 8.7} | {-5.5, 5.9} | {-4.6, 5.0} |
| async., fast, B | {-1.6, 1.8} | {-1.3, 1.3} | {-1.0, 1.1} | {-4.6, 4.4} | {-3.4, 3.3} | {-2.9, 2.7} |
| Ped. B, (32,8) | | | | | | |
| sync., A | {-2.3, 2.7} | {-1.9, 1.9} | {-1.6, 1.6} | {-5.8, 5.7} | {-4.2, 4.4} | {-3.6, 3.8} |
| sync., D | {-2.3, 2.5} | {-1.9, 1.8} | {-1.6, 1.6} | {-5.2, 5.2} | {-4.1, 4.4} | {-3.5, 3.7} |
| async., A | {-2.4, 2.9} | {-1.7, 1.9} | {-1.6, 1.6} | {-4.8, 5.5} | {-3.9, 4.1} | {-3.3, 3.4} |
| async., D | {-2.2, 2.2} | {-1.8, 1.7} | {-1.3, 1.5} | {-4.8, 5.1} | {-4.0, 4.0} | {-3.3, 3.4} |
| async., D, 30 Hz | {-1.9, 1.7} | {-1.4, 1.4} | {-1.3, 1.2} | {-3.9, 4.2} | {-3.0, 3.2} | {-2.6, 2.8} |
| async., D, 50 Hz | {-1.9, 1.9} | {-1.5, 1.4} | {-1.2, 1.2} | {-3.8, 4.7} | {-3.1, 3.3} | {-2.7, 2.6} |
| async., A, 100 Hz, p.p. | {-1.8, 1.9} | {-1.4, 1.5} | {-1.2, 1.3} | {-5.2, 6.0} | {-4.2, 3.8} | {-3.5, 3.2} |
| async., D, 100 Hz, p.p. | {-1.6, 1.8} | {-1.3, 1.3} | {-1.1, 1.1} | {-5.4, 4.9} | {-3.9, 4.1} | {-3.2, 3.4} |
| async., fast, B | {-1.6, 1.8} | {-1.3, 1.3} | {-1.0, 1.1} | {-4.6, 4.4} | {-3.4, 3.3} | {-2.9, 2.7} |
| async., D, 30 Hz, RTI =10 | {-1.8, 2.2} | {-1.5, 1.5} | {-1.2, 1.2} | {-4.0, 3.7} | {-3.0, 3.0} | {-2.6, 2.4} |
| async., D, 6 dB quant. intervals | {-2.6, 2.8} | {-2.0, 1.9} | {-1.7, 1.6} | {-6.4, 5.9} | {-4.7, 4.8} | {-4.0, 4.1} |
| async., B, Ad. Term. | {-2.9, 2.7} | {-2.1, 2.0} | {-1.7, 1.6} | {-4.8, 5.2} | {-3.6, 4.1} | {-3.1, 3.3} |

## G.3 Multi-Cell Simulation Reproducibility

The total statistical significance of the multi-cell simulations can be estimated using results from the previous two sections. The deviation about the mean throughput for the entire simulation can be given by Gaussian distribution with variance equal to the sum of the variances of the link level deviation and the system level deviation:

$$\sigma_{total} = \sqrt{\sigma_{link}^2 + \sigma_{system}^2} \tag{G.2}$$

The component standard deviations are given in Table G.5. The confidence intervals for the worst cases (based on the relevant standard deviations) in this thesis are given in Table G.6.

Table G.5. Standard deviations of the throughput for the total multi-cell simulation

| | *Standard Deviations of Means (%) U=32* | | | *Standard Deviation of Mean (%) U=8* | | |
|---|---|---|---|---|---|---|
| | $\sigma_{system}$ | $\sigma_{link}$ | $\sigma_{total}$ | $\sigma_{system}$ | $\sigma_{link}$ | $\sigma_{total}$ |
| **Chapter 4** | | | | | | |
| Indoor A | 1.14 | 0.69 | 1.33 | 2.41 | 0.69 | 2.51 |
| Ped. B (4,1) | 0.84 | 0.69 | 1.09 | 1.77 | 0.69 | 1.90 |
| Vehicular A | | | | | | |
| Config. I | 1.23 | 0.69 | 1.41 | 2.63 | 0.69 | 2.72 |
| Config. III | 0.93 | 1.16 | 1.49 | 2.37 | 1.16 | 2.64 |
| Config. IV | 1.09 | 0.69 | 1.29 | 2.57 | 0.69 | 2.67 |
| Config. VII | 1.55 | 0.69 | 1.70 | 2.83 | 0.69 | 2.91 |
| **Chapter 5** | | | | | | |
| Indoor B, async | 1.02 | 0.69 | 1.23 | 2.90 | 0.69 | 2.98 |
| Ped. B | | | | | | |
| sync., A | 0.98 | 0.69 | 1.20 | 2.20 | 0.69 | 2.31 |
| async., D, 6 dB | | | | | | |
| quant. inter. | 1.03 | 0.69 | 1.24 | 2.47 | 0.69 | 2.56 |
| async., B, | | | | | | |
| Ad. Term. | 1.06 | 0.69 | 1.26 | 1.95 | 0.69 | 2.07 |

Table G.6. Reproducibility for specified confidence levels for the worst cases

| | *Confidence (% of mean) U=32* | | | *Confidence (% of mean) U=8* | | |
|---|---|---|---|---|---|---|
| | 99 % | 95 % | 90 % | 99 % | 95 % | 90 % |
| **Chapter 4** | | | | | | |
| Indoor A | ± 3.4 | ± 2.6 | ± 2.2 | ± 6.5 | ± 4.9 | ± 4.1 |
| Ped. B (4,1) | ± 2.8 | ± 2.1 | ± 1.8 | ± 4.9 | ± 3.7 | ± 3.1 |
| Vehicular A | | | | | | |
| Config. I | ± 3.6 | ± 2.8 | ± 2.3 | ± 7.0 | ± 5.3 | ± 4.5 |
| Config. III | ± 3.8 | ± 2.9 | ± 2.5 | ± 6.8 | ± 5.2 | ± 4.3 |
| Config. IV | ± 3.3 | ± 2.5 | ± 2.1 | ± 6.9 | ± 5.2 | ± 4.4 |
| Config. VII | ± 4.4 | ± 3.3 | ± 2.8 | ± 7.5 | ± 5.7 | ± 4.8 |
| **Chapter 5** | | | | | | |
| Indoor B, async | ± 3.2 | ± 2.4 | ± 2.0 | ± 7.7 | ± 5.8 | ± 4.9 |
| Ped. B | | | | | | |
| sync., A | ± 3.1 | ± 2.4 | ± 2.0 | ± 5.9 | ± 4.5 | ± 3.8 |
| async., D, 6 dB quant. inter. | ± 3.2 | ± 2.4 | ± 2.0 | ± 6.6 | ± 5.0 | ± 4.2 |
| async., B, Ad. Term. | ± 3.2 | ± 2.5 | ± 2.1 | ± 5.3 | ± 4.1 | ± 3.4 |